DISS. ETH NO. 27118

Region of Attraction Analysis of Uncertain Equilibrium Points and Limit Cycles

with Application to Airborne Wind Energy Systems

A thesis submitted to attain the degree of

DOCTOR OF SCIENCES of ETH ZURICH

(Dr. sc. ETH Zurich)

presented by

Eva Laura Ahbe

MSc, Ruprecht-Karls-Universität Heidelberg, Germany
born on 28. November 1988
citizen of Germany and Hungary

accepted on the recommendation of

Prof. Dr. Roy S. Smith, examiner (ETH Zurich, Switzerland)
Prof. Dr. John Lygeros, co-examiner (ETH Zurich, Switzerland)
Prof. Dr. Lorenzo Fagiano, co-examiner (Politecnico di Milano, Italy)

2020

ISBN 978-3-907234-34-1
DOI 10.3929/ethz-b-000461553

To my parents

Acknowledgements

First and foremost, I would like to express my gratitude to Prof. Roy Smith for giving me the opportunity to pursue my PhD at the Automatic Control Laboratory (IfA). I am deeply thankful for his continuous support, invaluable expertise and encouraging guidance which at the same time allowed me a great deal of freedom to follow my research interests during my PhD. His passion for periodic systems and stochastic problems have inspired and motivated me throughout these years.

I would like to thank my first co-examiner, Prof. John Lygeros for agreeing to serve on my PhD committee. His expertise in the field of control have always deeply impressed me. I found that Prof. Lygeros, together with Prof. Smith, Prof. Florian Dörfler and Prof. Maryam Kamgarpour, created an outstanding academic environment at IfA and I have counted myself lucky every day for the possibility to be part of it. My appreciation also goes to my second co-examiner, Prof. Lorenzo Fagiano, for his availability to referee this PhD. Prof. Fagiano's work in the field of Airborne Wind Energy (AWE) has always been an inspiration to me and I feel honored to have him on my committee.

Little did I know about what was waiting for me when I applied for a position within the EU's Innovative Training Network AWESCO, but I soon came to appreciate the opportunity far beyond of what I could have imagined. In this regard, I would like to give my thanks to all the PI's for investing their time and effort to provide us with numerous instructive workshops, summer schools and conferences over the years. They brought us right to the heart of the AWE community and greatly supported us in our contributions to the field. In this regard, I am especially thankful to Prof. Colin Jones, for introducing me to the sum-of-squares techniques during my first secondment at EPFL. My sincerest thanks also go to my colleague ESRs in AWESCO for all the inspiring, creative and motivating times we spent together during the many meetings.

Many colleagues at IfA have contributed to making these PhD years truly rewarding. I am deeply grateful to Dr. Andrea Iannelli for his collaboration both in the works on stochastic systems and projects on system identification. He always had his door open for a brainstorming and discussion about the newest ideas and results, during which he provided me with most valuable feedback. I would further like to thank Dr. Tony Wood for the collaboration on the AWE topics. He always took the time to answer my many questions about kite systems and discuss control approaches. My diving into the AWE field in the first year was also greatly facilitated by Dr. Henrik Hesse and his expertise on

aerodynamics, for which I am very grateful. I would further like to thank Samuel Balula for the collaboration on the Paramotor student projects and for his catching enthusiasm for hardware. Special thanks go to Dr. Annika Eichler for making the sharing of an office truly enjoyable, to Dr. Yvonne Stürz for sharing the ups and downs of a PhD, and to Irina Subotic for the many fun conversations both in person and virtually during the Covid lockdown.

Many thanks also go to Dr. Mathias Hudoba de Badyn, Dr. Suli Zou, Dr. Sandro Merkli, Dr. Tobias Sutter, Dr. Ben Flamm, Dr. Goran Banjac, Dr. Adrian Hauswirth, Dr. Paul Bechat, Dr. Alex Liniger, Mohammad Khosravi, Angeliki Kamoutsi, Anil Parsi, and Lukas Ortmann, Miguel Picallo Cruz, Nicoló Pagan, Andrea Martinelli, Pier Giuseppe Sessa, Yin Mingzhou and Sandeep Menta for the fruitful, enjoyable discussions, their readiness to help, and their collaboration in the TA assignments. My heartfelt thanks also go to Sabrina Baumann and Tanja Turner for their continuous support even beyond the expected and making IfA run so smoothly.

The AWE topic gave various chances for collaborations with other Laboratories at ETH. I would like to thank Dr. Thomas Stastny and Manuel Dangel for their collaboration on the Easyglider project, and Dr. Urban Fasel together with the Ftero guys for sharing their kite model and their knowledge in the field.

I would also like to express my heartfelt gratitude to Prof. Ken Caldeira and Prof. Thomas Leistner for their support in getting me on this PhD journey.

Finally, I would not have gotten here without the unconditional love and support of my family, Stephan, Zsuzsanna, Dora, and my partner Claudio, for which I find myself without words that could truly express my gratitude.

Eva Ahbe
Zurich, October 2020

Abstract

Guaranteeing reliability of a system's operation is a challenge in many engineering applications. A measure for the reliability is given by the set of all initial conditions from which a perturbed system converges back to the desired operating point. This set is referred to as *region of attraction* (ROA). The task of obtaining information on its size depends highly on the kind of system under consideration and is posing an ongoing stream of new challenges to the field. In this thesis, we consider various classes of nonlinear systems for which we propose theoretical conditions and their efficient algorithmic implementation to obtain an inner estimate of the ROA of their equilibrium. The computational verification of the conditions is based on results from real algebraic geometry and on *sum-of-squares* (SOS) programming techniques.

The first class of system consists of stochastic systems with finite second moment, for which we consider uncertainty dependent equilibrium points. The framework of *Polynomial Chaos Expansion* (PCE) is used on the stochastic system to represent it by a higher-dimensional set of deterministic equations. We first show how the equilibrium point of the deterministic formulation relates to an uncertainty-dependent stochastic equilibrium point. A connection between the boundedness of the moments of the stochastic system and the Lyapunov stability of the PCE system is then derived with corresponding notions of the ROA. We show how this connection can be leveraged to recover an inner estimate of the ROA of the stochastic system from the ROA of the PCE system. From a first optimization program, which implements the Lyapunov stability arguments, an inner estimate of the ROA of the PCE system is obtained. Based on this result and user specifications on the moments for the initial conditions, a second program employs the shown connection to provide the corresponding ROA of the stochastic system. The developed method is then applied to the problem of controller synthesis where the aim is to design a stochastic state feedback controller which maximizes the ROA of the closed-loop stochastic system. An optimization program is proposed and implemented to obtain feedback gains and the corresponding maximized ROA estimate.

Stable periodic solutions characterize the second class of systems considered in this thesis. Deterministic systems as well as systems affected by bounded affine parametric uncertainty, which have stable limit cycles are considered. The analysis is facilitated in both cases by a transformation to transverse coordinates defined on a moving orthonormal system which is similar to the concept of moving Poincaré maps. For the transformation we first consider the classical approach and then proceed by proposing a

novel construction of a moving coordinate system with improved well-definedness properties. For deterministic system we formulate conditions for an inner estimate of the ROA based on Lyapunov theory. Due to the location of the limit cycle being affected by the uncertainty, contraction methods are employed to derive conditions on the *region of contraction* (ROC) in the uncertain case. We demonstrate by several examples the various features of the approaches developed in this thesis, and show how improved estimates compared to existing methods are obtained. As a third class of systems with limit cycles, we consider stochastic systems with finite second moment and periodic behavior. An approach to analyze the stability of limit cycles of this class of systems is proposed which connects stochastic orbital stability with the transverse contraction of the system's PCE representation.

The optimization problems for the ROA and ROC analysis methods are formulated in the form of generalized SOS programs. The algorithms are outlined and the collection of the scripts containing the implementation of the methods is provided.

The application of the analysis methods for limit cycle systems is demonstrated by the example of Airborne Wind Energy systems, which are an emerging renewable energy technology. Being on the verge of commercialization, measures for the reliability of their operation experience a growing demand. We consider the system in the crosswind flight phase and verify regions, in which the employed flight controller is guaranteed to stabilize the system model, by applying the methods developed in this thesis.

Zusammenfassung

Die Gewährleistung der Zuverlässigkeit des Systembetriebs ist in vielen technischen Anwendungen eine Herausforderung. Ein Maß für die Zuverlässigkeit ist die Menge aller Anfangsbedingungen, unter denen ein gestörtes System zum gewünschten Betriebspunkt zurückkonvergiert. Diese Menge wird als *region of attraction* (ROA) bezeichnet. Die Aufgabe, Informationen über seine Größe zu erhalten, hängt in hohem Maße von der Art des betrachteten Systems ab und stellt das Forschungsfeld kontinuierlich vor neue Herausforderungen. In dieser Arbeit betrachten wir verschiedene Klassen nichtlinearer Systeme, für die wir theoretische Bedingungen und ihre effiziente algorithmische Implementierung vorschlagen, um eine innere Schätzung der ROA ihres Gleichgewichtpunktes zu erhalten. Die rechnerische Überprüfung der Bedingungen basiert auf Ergebnissen der realen algebraischen Geometrie und auf *sum-of-squares* (SOS) Programmiertechniken.

Die erste Klasse von Systemen besteht aus stochastischen Systemen mit endlichem zweiten Moment, für die wir unsicherheitsabhängige Gleichgewichtspunkte betrachten. Die Methodik zur Unsicherheitsdarstellung namens *Polynomial Chaos Expansion* (PCE) wird auf das stochastische System angewendet, um es durch einen höherdimensionalen Satz deterministischer Differentialgleichungen darzustellen. Wir zeigen zunächst, wie sich der Gleichgewichtspunkt der deterministischen Formulierung auf einen unsicherheitsabhängigen stochastischen Gleichgewichtspunkt bezieht. Ein Zusammenhang zwischen der Begrenztheit der Momente des stochastischen Systems und der Lyapunov-Stabilität des PCE -Systems wird dann mit entsprechenden Begriffen für die ROA abgeleitet. Wir zeigen, wie diese Verbindung genutzt werden kann, um eine innere Schätzung der ROA des stochastischen Systems aus der ROA des PCE-Systems zu gewinnen. Aus einem ersten Optimierungsprogramm, das die Lyapunov-Stabilitätsargumente implementiert, wird eine innere Schätzung der ROA des PCE-Systems erhalten. Basierend auf diesem Ergebnis und den Benutzerspezifikationen für die Momente der Anfangsbedingungen verwendet ein zweites Programm die gezeigte Verbindung, um das entsprechende ROA des stochastischen Systems zu berechnen.

Die entwickelte Methode wird dann auf das Problem der Reglersynthese angewendet, bei dem das Ziel darin besteht, einen stochastischen Zustandsrückkopplungsregler zu entwerfen, der die ROA des stochastischen Systems mit geschlossenem Regelkreis maximiert. Ein Optimierungsprogramm wird vorgeschlagen und implementiert, um Rückkopplungsgewinne und die entsprechende maximierte ROA-Schätzung zu erhalten.

Stabile periodische Lösungen charakterisieren die zweite Klasse von Systemen, die in

dieser Arbeit betrachtet werden. Es werden sowohl deterministische Systeme als auch Systeme mit begrenzter affiner parametrischer Unsicherheit berücksichtigt, die stabile Grenzzyklen aufweisen. Die Analyse wird in beiden Fällen durch eine Transformation in Querkoordinaten erleichtert, die auf einem sich bewegenden orthonormalen System definiert sind, das dem Konzept der bewegten Poincaré-Abbildungen ähnlich ist. Für die Transformation betrachten wir zunächst den klassischen Ansatz und schlagen dann eine neuartige Konstruktion eines sich bewegenden Koordinatensystems mit verbesserten Wohldefiniertheitseigenschaften vor. Für das deterministische System formulieren wir Bedingungen für eine innere Schätzung der ROA basierend auf der Lyapunov-Theorie. Aufgrund des Ortes des Grenzzyklus, der von der Unsicherheit beeinflusst wird, werden Kontraktionsmethoden verwendet, um im unsicheren Fall Bedingungen für die sogenannte *region of contraction* (ROC) abzuleiten. Wir demonstrieren anhand mehrerer Beispiele die verschiedenen Merkmale der in dieser Arbeit entwickelten Ansätze und zeigen, wie verbesserte Schätzungen im Vergleich zu bestehenden Methoden erhalten werden. Als dritte Klasse von Systemen mit Grenzzyklen betrachten wir stochastische Systeme mit endlichem zweiten Moment und periodischem Verhalten. Es wird ein Ansatz zur Analyse der Stabilität von Grenzzyklen dieser Systemklasse vorgeschlagen, der die stochastische Orbitalstabilität mit der transversalen Kontraktion der PCE-Darstellung des Systems verbindet.

Die Optimierungsprobleme für die Analysemethoden der ROA und der ROC werden in Form von verallgemeinerten SOS-Programmen formuliert. Die Algorithmen werden beschrieben und die Sammlung der Skripte, die die Implementierung der Methoden enthalten, wird bereitgestellt.

Die Anwendung der Analysemethoden für Grenzzyklus-Systeme wird am Beispiel von Airborne Wind Energy-Systemen demonstriert, bei denen es sich um eine aufstrebende Technologie für erneuerbare Energien handelt. Mit der baldigen Kommerzialisierung der Technologie werden die Maßnahmen zur Zuverlässigkeit ihres Betriebs zunehmend nachgefragt. Wir betrachten das System in der Seitenwindflugphase und verifizieren Regionen, in denen der eingesetzte Flugregler das Systemmodell garantiert stabilisiert, indem wir die in dieser Arbeit entwickelten Methoden anwenden.

Notation

Acronyms

AWE	Airborne Wind Energy
BMI	Bilinear matrix inequality
class-MOC	Classical MOC
CPA	Center point algorithm
cp-MOC	Center point MOC
LC	Limit cycle
LMI	Linear matrix inequality
LQR	Linear Quadratic Regulator
MC	Monte-Carlo
MOC	Moving orthonormal coordinate system
PCE	Polynomial Chaos Expansion
PSD	Positive semidefinite
ROA	Region of attraction
ROC	Region of contraction
SDP	Semidefinite program
SOS	Sum-of-squares

Symbols

Symbols

$\mathbb{N}$, $\mathbb{N}_0$	set of natural numbers, including zero
$\mathbb{R}$, $\mathbb{R}^n$, $\mathbb{R}^{n\times m}$	set of real numbers, real valued n-dimensional vectors, real valued $n \times m$-dimensional matrices
$\mathbb{R}[x]$, $\mathbb{R}[x]_{\leq r}$	ring of n-variate polynomials with real coefficients, total degree at most $r \in \mathbb{N}_0$
$\Sigma[x]$	set of all sum-of-squares polynomials in x
$\Sigma^{n\times n}[x]$	set of all matrix sum-of-squares in x of dimension $n \times n$
$\mathbb{S}^n$	set of symmetric matrices of size $\mathbb{R}^{n\times n}$
$\mathcal{C}^d(\mathbb{R}, \mathbb{R}^n)$	space of continuous functions taking $\mathbb{R} \to \mathbb{R}^n$, with continuous derivatives up to order d
$\mathcal{L}_l$	Lebesgue space, $1 \leq l \leq \infty$
Θ	sample space in the reals
$\mathcal{F}$	σ-algebra of Θ
μ	non-negative probability measure
$\langle\cdot,\cdot\rangle$, $\langle\cdot,\cdot\rangle_{\mathcal{L}_2(\mu)}$	inner product in the $\mathcal{L}_2$ space with respect to μ
$\mathbb{E}$	expectation in the $\mathcal{L}_2$ sense
$M_P(\xi)$	P-th moment of a random variable ξ, i.e. $\mathbb{E}[\lvert\xi\rvert^P]$, $1 \leq P < \infty$
λ, $\lambda(M_P)$	probability distribution, with P given moments
$\mathcal{U}(a, b)$	uniform distribution over the range $[a, b]$, $-\infty < a < b < \infty$
$A \succ 0$ ($\succeq 0$)	square matrix A is positive (semi-) definite
A^T	transpose of matrix A
$\mathrm{v}(x)$, $\mathrm{v}(x)_r$	monomial vector in x, up to degree r
V	Lyapunov function
$\partial(g(x))$	degree of a polynomial $g(x)$ in x (x is omitted if context unambiguous)
$\mathbb{I}, \mathbb{I}_n$	identity matrix, of dimension $n \times n$
dist	distance measured in an arbitrary norm
$\lVert\cdot\rVert$	Euclidean norm
$:=$	equal by definition
$\parallel$	parallel
$\nparallel$	not parallel
$\sim$	element from probability distribution
$\bar{(\cdot)}$	indicates a PCE coefficient or a variable dependent on such
$\bar{(\cdot)}_i$	indicates a the i-th PCE coefficient (scalar or vector valued) of the expansion series
$\bar{y}_0$	vector of mean modes (zeroth PCE coefficients) of the random variable $y \in \mathbb{R}^m$, i.e., $[\bar{y}_{1_0}, ..., \bar{y}_{m_0}]^T \in \mathbb{R}^m$

$\bar{y}_J$	vector of variance modes (PCE coefficients 1 to $p+1$) of the random variable $y \in \mathbb{R}^m$, i.e., $\bar{y}_{1_1}, ..., \bar{y}_{m_1}, ..., \bar{y}_{1_p}, ..., \bar{y}_{m_p}]^T \in \mathbb{R}^{m \cdot p}$
$\bar{y}$	vector of all stochastic modes (PCE coefficients) of the random variable $y \in \mathbb{R}^m$, i.e., $[\bar{y}_0, \bar{y}_J]^T \in \mathbb{R}^{m \cdot (p+1)}$

Other notation

The important distinction between the *true* region of attraction, respectively contraction, and an *inner estimate* of it is made by indicating the true regions with a asterisk superscript, i.e., $\mathcal{R}^*$, $\bar{\mathcal{R}}^*$, $\mathcal{Z}^*$, $\bar{\mathcal{Z}}^*$, and the inner estimates of the respective regions as the same calligraphic letter without the asterisk, i.e.,$\mathcal{R}$, $\bar{\mathcal{R}}$, $\mathcal{Z}$, $\bar{\mathcal{Z}}$.

The term *estimate* in this work always refers to an *inner estimate*, where for the sake of brevity the reference to *inner* is frequently dropped.

The term *region* is used within its mathematical definition of an open, simply-connected and non-empty subset of $\mathbb{R}^d$, where d is the appropriate dimension.

Contents

CHAPTER 1

Introduction

A fundamental property of a nonlinear system consists in its behavior, such as stability, instability and convergence, being dependent on the state of the system. This gives rise to the definition of a *region of attraction* (ROA) as the set of initial conditions in the state space from which trajectories converge to an equilibrium of the system contained in this region. The equilibrium can thereby be given by an attracting equilibrium point or a limit set such as a stable limit cycle. Numerous ways to estimate, compute or analytically derive the ROA have been investigated [Zub61; GTV85; Kha02; Che11; CA15]. Obtaining information on the ROA has not only been a fascinating and challenging topic in nonlinear system analysis but is also of significant importance in many control applications. An example is readily provided by considering the control system of an aircraft [CSB11]. How far can the system's states, such as angle of attack and pitch, be perturbed before the controller fails to return the aircraft to the trim state? Since this question equally represents a measure of safety, the answer to it is decisive for the aircraft's fielding. Attaining knowledge of the ROA is also of vital importance to power grids, in particular its transient stability, which denotes its ability to maintain synchronous operation when subject to disturbances. Knowing the region of operating conditions from which a post fault system can still return to the equilibrium point is of immense importance to engineers as the region can be translated into an estimate on the maximum amount of time they have to clear the contingency before failure of the system [GTK14]. These examples show how the size of the ROA can act as a measure of the robustness of the system with respect to perturbations in the initial conditions. As such, the ROA defines the part of the state space in which a system can be safely operated.

The challenge of obtaining information on the size the ROA varies greatly with the particular class of system. While for certain types of systems theoretical achievements were successful in providing criteria for the exact shape of the ROA [Zub61; CHW88], those criteria are often difficult to apply to practical problems, either because of computational constraints or due to lack of information. It has thus been of wide interest to develop practically useful methods which trade in dispensable exact characterization of

the ROA for approximations with tractable computations.

The most commonly employed methods descend from Lyapunov stability theory. The underlying idea in these approaches is to find a continuously differentiable function that is positive in a region of the state space which includes the equilibrium point, and has negative derivative with respect to the trajectories of the system. If these conditions hold for all states within a sublevel set of that function, then the sublevel set has been shown to be inside of the true ROA of the equilibrium point [Lya92]. This Lyapunov approach often extends to the aim of finding a Lyapunov function verifying a largest possible sublevel set in order to obtain less conservative estimates of the ROA.

Lyapunov methods are popular for ROA analysis for various reasons, including their exceedingly well-established theory, the often clear, elegant and concise equations involved and the versatility of the approach. The theory has been extended from the deterministic continuous case to many other system classes such as time-varying, periodic, controlled, hybrid and discrete time systems [Kha02; BCN91].

For nonlinear systems, the Lyapunov conditions present sufficient conditions for asymptotic stability. A plethora of analytical and numerical approaches have been developed with the aim of constructing or computing a Lyapunov function for a given system. In the past 20 years a numerical method in the field of polynomial optimization has gained popularity for the computation of Lyapunov functions [PPW04; Che+05; TP08; TPS08; Che11; AM19a]. This method is based on the formulation of semialgebraic set conditions as *sum-of-squares* (SOS) programs which can be efficiently posed as *semidefinite programs* (SDPs) and thus solved as convex optimization problems.

A drawback of Lyapunov arguments is given by the fact that their applicability hinges on the knowledge of the equilibrium's location. This is of particular concern for uncertain and stochastic systems whose equilibria are often dependent on the uncertainty. In more recent years, the use of contraction methods for the stability analysis of these systems has emerged [LS98; APS08; MS14]. Contraction methods analyze stability by considering the rate of change of an incremental distance between any two neighboring trajectories of a system. If for a region, which contains an equilibrium, the rate of change of this distance is negative then all trajectories are contracting and are shown to eventually converge to the equilibrium. Other than being contained in the region, no further information on the location of the considered equilibrium is required. In analogy to the term 'region of attraction', the term 'region of contraction' has been coined for this method.

In this thesis we employ Lyapunov and contraction arguments to propose analysis methods for the ROA of various classes of systems. These include 1. autonomous and controlled stochastic systems in the form of second order random processes with uncertainty-dependent equilibrium points; 2. deterministic systems with limit cycles; 3. systems affected by parametric uncertainty with limit cycles; and 4. stochastic systems in the form of second order random processes with limit cycles.

The stability analysis of stochastic systems is an active field of research which has gained momentum with the development of computational analysis methods, such as Monte Carlo simulations. While the ROA of a deterministic system is clearly defined, the definition of an attractive region of uncertain system can vary. For stochastic systems a definition of the ROA can be derived from the type of stochastic stability under consideration. A widely used notion for the ROA of uncertain systems is that of a 'robust' ROA, which is the intersection of the ROAs obtained for each possible realization of the uncertainty. As it thus relates to the worst case, this notion is suitable for uncertainties with uniform distributions but less so for other distributions where the worst case is not of practical interest or exploiting the statistical information available gives less conservative results. In this work we present an approach for the stability analysis of a class of stochastic systems and provide a corresponding definition of a ROA, both of which make use of *Polynomial Chaos Expansion* (PCE).

PCE is a spectral method for uncertainty quantification and consists in polynomial approximations applicable to second order random processes, which are stochastic systems with finite second moments. The expansion results in a higher-dimensional deterministic representation of the stochastic system [Sul15; LK10]. We derive conditions for such a stochastic system to converge to an uncertain equilibrium point by considering its PCE representation, and propose computationally efficient algorithms from which inner estimates of the ROA can be obtained. The approach is further extended for controller synthesis.

Systems with periodic behavior represent many processes of the real world, and understanding their stability is often crucial. Due to the time-varying nature of a periodic system trajectory, the analysis of its attracting region poses a more complex problem than the analogous problem for equilibrium points, even when the system is deterministic. In this work we consider both the case of deterministic systems and uncertain systems which have a stable limit cycle. In order to obtain an inner estimate of the periodic orbit's ROA we derive conditions based on Lyapunov and contraction arguments for the system in transverse coordinates. These coordinates are defined within a moving orthonormal system and are conceptually similar to moving Poincaré maps [Poi99; Hal80]. Using the classical approach as well as a novel construction of the moving orthonormal coordinates, we show in numerical implementations a more efficient analysis compared to the previously proposed methods can be achieved.

In order to cast the various stability conditions derived for the different classes of systems into computationally efficient algorithms, we focus on polynomial representations of the systems. This makes the verification of the conditions amenable to the above mentioned SOS programming techniques. Along with derivations and explanations of these algorithms we provide a comprehensive collection of the scripts which contain their implementation.

The methods proposed in this thesis are illustrated by various examples covering each

considered class of system. As a case study, the ROA analysis of limit cycles is applied to the model of a controlled *Airborne Wind Energy* (AWE) system. AWE systems are a new renewable energy technology that aims at extracting power from high-altitude winds by using flying vehicles which are tethered to the ground. Guaranteeing reliable operation is a crucial problem among the wide range of challenges the technology still has to overcome before its commercialization. Similarly to the first example mentioned for the ROA above, the information on the ROA of the controlled kite systems allows to understand from which initial conditions the flight controller is capable of bringing the perturbed system back to a desired reference trajectory, and thus provides a measure of safety.

1.1 Literature review

This section provides an overview of the literature which is most relevant to the work presented in this thesis. This overview is not exhaustive and is further supported by additional review of thematically specific literature at the beginning of each chapter.

1.1.1 Verification of polynomial positivity and sum-of-squares programs

A computationally tractable test for a polynomial function to be globally nonnegative was proposed in [Par00] by posing conditions on the existence of a SOS decomposition of the polynomial. These conditions are based on a Positivstellensatz and can be tested by semidefinite programming. In real algebraic geometry a Positivstellensatz characterizes positive polynomials on a semialgebraic set defined by polynomial equations and inequalities with real coefficients. Being the real analogue to Hilbert's Nullstellensatz [Hil93] for the complex space, several versions of the Positivstellensatz with varying assumptions have been proposed. The Positivstellensatz of Stengle [Ste74] states that, for a system of polynomial equations and inequalities, either there exists a solution in the reals, or there exists a certain polynomial identity which certifies that no solution exists. [Par00] shows how a hierarchy of sufficient conditions for the existence of this polynomial identity can be formulated to certify the emptiness of a semialgebraic set. Each condition essentially represents a test of a polynomial to be decomposable into a SOS. By formulating a set containment problem as a question of set emptiness, the Positivstellensatz reveals its applicability in the form of a generalized S-procedure.

Ever since its introduction in 2000, the relaxation of a semialgebraic set emptiness condition into the, semidefinite programming verifiable, question of the existence of a SOS decomposition has been widely applied: SOS techniques are employed for nonlinear system and stability analysis [PP02; PP05a; TP08; TPS08; VA17; JP19; ISM19] and

control applications [JW+05; PPW04; PL03; CSB11], with a comprehensive overview of applications of SOS programming in these fields found in [Che11]. An overview of business applications is presented in [Hal19], with further examples in [AM19b]. SOS programming techniques have been extended to account for matrix polynomials in [APS08; SH06]. The verification of stability regions along trajectories, also referred to as 'funnels', of feedback controlled robotic systems, was obtained from SOS programming in [Ted+10; TMT11; Man+11; MCT14; MT17]. In order to apply the SOS methods to non-polynomial systems polynomial approximation techniques are explored in [WYL14; Che09; PP05b]. In [SB10], quasiconvex optimization problems with a bilinear term in the SOS constraints are considered, and a solution converging to global optimality which is based on bisection is shown. The authors introduce the term *generalized SOS program* for these problems. Since we consider similar types of bilinear constraints in this work, we adopt this term with a rigorous definition of its meaning in this context provided in Chapter 2.

Several Matlab toolboxes, e.g., SOSTOOLS [Pap+13], SPOTless [Meg13], or the SOS toolbox in Yalmip [Lof09], have been developed to facilitate the solving of an SOS program as an SDP.

Since the efficient computation of a semidefinite program is still limited to low dimensions, more tractable alternatives to SOS programming to test polynomial positivity were recently presented in [AM19b]. These alternatives are called DSOS for the approach based on linear programs, and SDSOS for the alternative employing second-order cone programs. The application of DSOS/SDSOS to control problems is demonstrate in [MAT14]. Current research in these alternatives focuses on quantifying and tractably reducing their conservativeness [AH17; AHA19].

In this thesis we employ the semidefinite relaxations based on Stengle's Positivstellensatz as outlined above. For completeness, we mention an approach to certify global polynomial nonnegativity based on a different Positivstellensatz, namely Putinar's [Put93]. The approach, introduced in [Las01], uses the theory of moments from which converging linear matrix inequality hierarchies are constructed to optimize over semialgebraic sets. The two optimization approaches can be viewed as dual to each other.

1.1.2 Region of attraction analysis

The methods to analyse the ROA can be divided into two classes, of which the first contains methods by which the exact (or true) size of the ROA is obtained, and the second contains all methods aiming at an approximation or inner estimate of the ROA. The applicability of exact methods is largely dependent on the kind of system under consideration. For planar deterministic systems, geometric methods can often be used, e.g., when the system has an unstable limit cycle encircling a stable equilibrium point. The exact ROA in this case is obtained in the form of the either numerically or analyti-

cally obtained limit cycle trajectory [Kha02]. In [CHW88], a method for finding the true ROA for a class of nonlinear autonomous systems is proposed. The method is based on the topological properties of the ROA and requires a determination of the stable manifold of an equilibrium point which quickly becomes computationally expensive with increasing state dimension. Based on Lyapunov theory, Zubov's method [Zub61] provides conditions for the exact ROA of a dynamical system based on the solution to a partial differential equation, which needs to be available. Zubov's method was generalized to perturbed [CGW01] and stochastic systems [CL06]. For many classes of system, the exact methods are either computationally prohibitively expensive, or require information which is not available.

In [GTV85; CA15] an early and more recent overview of various exact and estimating methods is presented. Among the methods for estimating the ROA, Lyapunov theory represents the most common approach. In fact, all references on stability analysis mentioned in the literature review of SOS techniques in Section 1.1.1 are based on Lyapunov arguments. In [TVG96] quadratic Lyapunov functions are considered where an estimate of the ROA is obtained by solving a suitable convex optimization problem. While the search for quadratic Lyapunov functions is often the computationally least expensive and theoretically most lean approach, the obtained estimates tend to be very conservative. A method combining Lyapunov theory, trajectory simulation and topological properties of the ROA is proposed in [LN00]. While being able to return close-to-exact estimates of the ROA for a broad class of systems, the method requires a global Lyapunov function to be available.

Other approaches to estimating the ROA, which are not based on Lyapunov theory, are, for instance, found in viability theory. In [CMS01] an algorithm based on the viability kernel and differential inclusion arguments is proposed from which inner and outer estimates of the ROA are obtained.

Reachability analysis has gained popularity, in particular for the analysis of transient stability in power systems. In [JKE10; KBF16] the ROA is analyzed in the form of a backward reachable set which is used for control of power system transients. This backwards reachable set is computed by numerically solving the Hamilton–Jacobi–Isaas partial differential equation backwardly in time. In [EGHA17] forward reachable sets are investigated, promising a computationally less expensive alternative to the backwards reachable set analysis.

In general, the aptitude of a particular approach to estimate the ROA crucially depends on the class of system under consideration, with the decision for a method being often inevitably connected to choosing a point on the trade-off curve between computational cost and conservativeness of the estimate.

1.1.3 Generalized Polynomial Chaos Expansion

The expansion of a Gaussian random variable by orthogonal polynomials from the Hermite basis functions was introduced by Wiener [Wie38]. Wiener also coined the term 'Polynomial Chaos' in which 'Chaos' was the commonly used name for 'stochastic process' at the time. This approach was later called the 'Wiener-Hermite Polynomial Chaos Expansion'. In [CM47] the authors showed that any second order random process, a class of systems which includes most processes of the real world [XK02], can be approximated by a Hermite polynomial basis with the solution being convergent in the $\mathcal{L}_2$ sense. The dependence of the expansion's convergence rate on the choices of basis functions was investigated in [XK02] where the authors show the connection of the dependence to the Askey scheme. The extension of the Wiener Polynomial Chaos to other polynomial basis and probability measures is called the 'Generalized PCE' and has been explored in [Xiu+02; XK03; LSK04], among others. Since in this thesis we only consider the latter, we omit the 'generalized' in the following.

Due to limited computation power, the application of PCE to engineering problems did not start to gain popularity until decades after its introduction by Wiener with the seminal work by [GS91]. Having been mostly considered for modeling of fluid dynamics and the stochastic differential equations, PCE arrived in the control community even later in time with [NB03]. Ever since then, PCE has been used, among others, for uncertainty analysis of chemical and biotechnical processes [NB03], for stability analysis [HT06; FB09; Luc+17], for state and parameter estimation [LX09], and for the design of various stochastic controllers in the field of optimal control including model predictive control [FB08; FK12; KB13; BM16]. In [Kim+13] a comprehensive overview of various applications also in other fields can be found.

Since any practical use of PCE entails the truncation of an infinite series, the accuracy of the truncated expansion has been subject to various studies [FG04; Deb+05; FKN11; Müh+18]. As the expansion series is $\mathcal{L}_2$-convergent for second order random processes, truncations at low orders are in general sufficient to keep the error introduced by the truncation small and represent the original system sufficiently well [Sul15; XK02]. Investigations to quantify this statement can be found, e.g., in [FG04], where the authors consider various Gaussian and non-Gaussian stationary stochastic processes and develop metrics for assessing the accuracy of the PCE truncation. An analysis of the effect of the truncation order and investigation of various undesired effects that truncated systems can exhibit can be found, e.g., in [Luc+17]. The authors consider linear systems and propose error bounds for the first two moments which can be used to design controllers that are robust to the truncation error. A worst-case bound on the approximation error between the PCE and the true stochastic variable is derived via a set membership approach in [FKN11]. In [Müh+18] exact error descriptions for the approximation are provided and bounds are formulated, which enable the computation of a truncated PCE

expansion with user defined error tolerance.

Detailed layouts of PCE and the involved numerical methods can be found in [Sul15; LK10; Xiu10].

1.2 Outline and contribution

This thesis can be divided into three main parts which are each dedicated to a certain class of systems. The first part considers stochastic systems with equilibrium points for both autonomous and feedback controlled systems. Periodic orbits of deterministic, uncertain and stochastic systems are the focus of the second part. The application of the developed analysis methods to Airborne Wind Energy systems is presented in the third part. In more detail, the chapters of this thesis are outlined as follows.

Chapter 2 A brief presentation of essential definitions and mathematical prerequisites which are relevant for all or most of the following chapters is given. The material in this chapter has been previously published and is included here for reference and completeness. Further chapter-specific preliminary material is included in the corresponding chapters with the due references provided.

Chapter 3 The first part of this chapter focuses on the ROA analysis for equilibrium points of autonomous stochastic systems which represent second order random processes. This enables the consideration of uncertain parameters coming from any $\mathcal{L}_2$-bounded probability distribution. In contrast to most existing approaches we further allow the equilibrium point to be subject to uncertainty. The framework of PCE is used to represent the stochastic system through deterministic equations in a higher dimensional state space. The analysis of the stochastic equilibrium point as well as its ROA are then performed by taking advantage of the deterministic nature of the PCE system and exploiting the connection of its stability to the stability of the true system. The second part of the chapter applies the results of the first to feedback controlled stochastic systems. The aim is to design a control law such that the ROA of the equilibrium point of the closed loop system is maximized. The design procedure enables to adhere to input constraints.

The contributions of Chapter 3 are summarized in the following.

1. We show how the equilibrium set of the stochastic system corresponds to an equilibrium point of the PCE system and derive a connection between the moment boundedness of the stochastic equilibrium point and the local asymptotic stability of its PCE representation.

2. Employing Lyapunov arguments, we formulate conditions from which an inner estimate of the ROA of the PCE system is obtained. While the Lyapunov conditions are well-established criteria for the ROA, their application for the ROA of the PCE systems is novel. Based on this PCE estimate, we present criteria which allow to recover an inner estimate of the stochastic ROA.

3. Using results from real semialgebraic geometry we propose optimization programs which implement the conditions for the PCE ROA as well as recover the stochastic ROA estimate.

4. We propose a stochastic nonlinear state feedback law and and provide an optimization program for its design which simultaneously maximizes the ROA of the closed loop system's equilibrium point. The design process of the stochastic controller accounts for input constraints. In order to incorporate the input constraints into the control design we derive polynomial formulations for the constraints.

Chapter 4 For the analysis of limit cycles we use a framework similar to Poincaré maps provided by a transformation to a transverse coordinate system. The chapter starts by presenting the conventional transformation law and proposing an improved formulation targeting the well-definedness of the transformation. Deterministic orbits are then considered and their ROA is analyzed using Lyapunov arguments for the system in transverse coordinates. Moving on to periodic orbits of systems with polytope bounded affine uncertainties reveals the challenge of uncertain locations of the orbit. Because Lyapunov methods are in general unavailable to such systems, the system is analyzed for its transverse contraction in the neighborhood of the uncertain orbit. This results in estimates of its ROA which is then referred to as *region of contraction* (ROC). Finally, considering stochastic systems in the form of second order random processes, the PCE framework is applied to represent and formulate deterministic contraction criteria.

The contributions of Chapter 4 are summarized in the following.

1. The classical construction of a *moving orthonormal coordinate system* (MOC) as presented in [Hal80] is prone to large variations in the size of the region for which the coordinate transformation is well-defined. These variations pose a limitation to the maximum size of a verifiable ROA estimate in the framework of transverse coordinates. Motivated by this shortcoming, we propose a novel MOC and derive its construction. A classification of the systems to which the transformation can be applied is provided. By deriving the well-definedness properties of the novel MOC its benefits over the classical MOC are shown. These consist of analytically obtainable knowledge of the well-defined regions and flexibility in the choice of the parameters influencing the region sizes. The examples of its application to ROA and ROC analysis demonstrate its ability to verify significantly larger estimates.

2. Existing conditions for an inner estimate of the ROA of a deterministic periodic orbit for a system in transverse coordinates are employed to formulate a computationally efficient algorithm. For this method we propose several algorithmic options consisting of different forms of cost functions, variability in the choice of Lyapunov function degree, and related constraints. A comprehensive comparison of the algorithmic options and choices of MOC is presented in which a general benefit of the proposed, more flexible cost functions is revealed.

3. Previously formulated criteria for a deterministic system to be transversely contracting are extended to uncertain systems and completed by invariance criteria. As such they pose conditions for an inner estimate of the ROC. Two algorithms are proposed from which an inner estimate of the ROC, respectively the allowed variation of the uncertainty bounds, is maximized.

4. A connection between the orbital stability of a stochastic orbit and the orbital stability of the orbit of the system's PCE representation is proposed. Transverse contraction criteria are formulated which verify a region to be an inner estimate of the ROC of the stochastic limit cycle.

Chapter 5 Airborne Wind Energy is an emerging renewable energy technology consisting of crosswind-flying tethered kites. In this chapter we first briefly present this technology and some of the challenges it is facing related to the autonomous operation. Since the kite is controlled to follow a periodic motion we use the analysis tools presented in the previous chapter to obtain an estimate of the ROA for a deterministic closed loop kite model. We then allow uncertainty to affect selected parameters of the model and analyze the ROC of the closed loop uncertain system. While the kite model serves as a more involved example to demonstrate the application of the analysis methods, the fact that it is controlled requires the development of a transverse controller. The presentation of the controller as well as the simulation of the closed loop system are included in this chapter.

The contributions of Chapter 5 are summarized in the following.

1. We propose a transverse state feedback controller which is based on the transformation of the system to transverse coordinates and the estimated size of the ROA. Due to the formulation in transverse coordinates the time dependence of a trajectory following control problem is removed, which renders the transverse controller in the form of a static state feedback law.

2. Inner estimates of the ROA of the nominal and uncertain closed-loop kite system are provided and validated in simulation. The analysis is not coupled to a particular controller and can thus be applied to other closed-loop kite system models.

Chapter 6 The ROA and ROC analysis methods developed in the previous chapters are implemented in a generalized form in a collection of Matlab scripts. Chapter 6 provides a brief description of the analysis tools in the scripts and highlights some aspects with the aim of facilitating user experience when applying the tools to a system of interest. All scripts are written by the author, are open source and available at `https://github.com/evaahbe/roa-analysis-tools.git`.

Chapter 7 This chapter provides conclusions on the work presented in this thesis and offers an outlook to future research.

1.3 Publications

The articles submitted or published during the author's time as doctoral candidate involved close collaboration with a number of colleagues. The following list is split in two parts with the first part showing the articles appearing in this thesis and the second listing the contributions that are indirectly or unrelated to this work.

Appearing in this thesis

Chapter 3 is based on the following publications.

[AIS20b] E. Ahbe, A. Iannelli, and R. S. Smith. "Region of attraction analysis of nonlinear stochastic systems using Polynomial Chaos Expansion". In: *Automatica* (2020), to appear.

[Ahb+20] E. Ahbe, P. Listov, A. Iannelli, and R. S. Smith. "Feedback control design maximizing the region of attraction of stochastic systems using Polynomial Chaos Expansion". In: *IFAC World Congress*. 2020, to appear.

Chapter 4 and Chapter 5 are based on results published in the following papers.

[AIS20a] E. Ahbe, A. Iannelli, and R. S. Smith. "Local contraction analysis of stochastic systems with limit cycles". In: *IEEE Conference on Decision and Control*. 2020, to appear.

[AWS18b] E. Ahbe, T. A. Wood, and R. S. Smith. "Transverse contraction-based stability analysis for periodic trajectories of controlled power kites with model uncertainty". In: *IEEE Conference on Decision and Control*. 2018, pp. 6501–6506.

[AWS18a] E. Ahbe, T. A. Wood, and R. S. Smith. "Stability verification for periodic trajectories of autonomous kite power systems". In: *IEEE European Control Conference*. 2018, pp. 46–51.

[AWS17] E. Ahbe, T. A. Wood, and R. S. Smith. "Stability Certificates for a Model-Based Controller for Autonomous Power Kites". In: *Book of Abstracts of the International Airborne Wind Energy Conference (AWEC 2017)*. 2017, p. 86.

Chapter 6 is based on all the above mentioned publications as it presents the computational implementation of the algorithms developed therein.

Other works

The following contributions are related to Airborne Wind Energy systems but are not presented in this thesis.

[Sta+19] T. Stastny, E. Ahbe, M. Dangel, and R. Siegwart. "Locally power-optimal nonlinear model predictive control for fixed-wing airborne wind energy". In: *American Control Conference*. 2019, pp. 2191–2196.

[Woo+18] T. A. Wood, H. Hesse, M. Polzin, E. Ahbe, and R. S. Smith. "Modeling, Identification, Estimation and Adaptation for the Control of Power-Generating Kites". In: *IFAC PapersOnLine* 51.15 (2018), pp. 981–989.

[Woo+17] T. A. Wood, E. Ahbe, H. Hesse, and R. S. Smith. "Predictive Guidance Control for Autonomous Kites with Input Delay". In: *IFAC World Congress* 50.1 (2017), pp. 13276–13281.

The following paper is the result of the author's Master thesis work.

[AC17] E. Ahbe and K. Caldeira. "Spatial distribution of generation of Lorenz's available potential energy in a global climate model". In: *Journal of Climate* 30.6 (2017), pp. 2089–2101.

The following open source application was published by the author within the course of the AWE related research.

[AS17] E. Ahbe and R. S. Smith. *Airborne Wind Energy Trajectory Analysis Application*. 2017. URL: https://github.com/evaahbe/AWE_tool.

CHAPTER 2

Mathematical Preliminaries

In this chapter some of the mathematical concepts are presented which are used throughout the thesis. While polynomials and *sum-of-squares* (SOS) programming are relevant to Chapters 3-6 the framework of *Polynomial Chaos Expansion* (PCE) is fundamental to Chapter 3 and parts of Chapter 4. The concepts and results presented here are either standard in the literature or have been previously published.

2.1 Polynomials and sum-of-squares programming

In this section we introduce polynomials and the semialgebraic set constraints-based programming technique enabled by SOS polynomials.

2.1.1 Polynomials

Let $x^\alpha = x_1^{\alpha_1} \cdots x_n^{\alpha_n}$ denote the monomial in the variables $x = [x_1, ..., x_n]^T$ with exponent vector $\alpha := [\alpha_1, ..., \alpha_n]^T$ of nonnegative integer entries. The degree of a monomial is given by $\partial(x^\alpha) = \sum_{i=1}^n \alpha_i$ and the monomial vector $\mathrm{v}(x)$ of degree r has entries given by all monomials of degrees $\leq r$. The cardinality of the set of monomials in the vector $\mathrm{v}(x)$ is given by $d = \binom{n+r}{r}$.

Definition 2.1. *(Polynomial) A n-variate polynomial $g(x)$ of degree r with coefficients in the field k is the finite linear combination of monomials*

$$g(x_1, ...x_n) = \sum_\alpha c_\alpha x^\alpha, \quad c_\alpha \in k, \tag{2.1}$$

where the sum is over the finite number of n-tuples in α such that $\partial(x^\alpha) \leq r$.

In this work we consider polynomials with real coefficients c_α in real fields, e.g., $k = \mathbb{R}^n$, and denote the ring of all such polynomials by $\mathbb{R}[x]_{\leq r}$, where the subscript is omitted if it is not specified.

When all monomials in (2.1) have the same degree, the polynomial $g(x)$ is called a *homogeneous* polynomial.

2.1.2 Sum-of-squares program

A fundamental question throughout this thesis will be the one of polynomial positivity. This translates into the aim to certify that a real valued polynomial function is globally nonnegative, i.e.,

$$g(x_1, ..., x_n) \geq 0, \quad \forall x_1, ..., x_n \in \mathbb{R}. \tag{2.2}$$

A sufficient condition for (2.2) to hold is if $g(x)$ can be written as a *sum-of-squares* (SOS).

Definition 2.2 (SOS polynomial)**.** *A polynomial $g(x)$ is called a SOS if there exists a decomposition consisting of the sum of squared terms q_i,*

$$g(x) = \sum_i q_i(x)^2. \tag{2.3}$$

The set of SOS polynomials in the variable x with coefficients in $\mathbb{R}$ is denoted by $\Sigma[x]$.

Note that while clearly all SOS polynomials are *positive semidefinite* (PSD), not all PSD polynomials are also SOS. The gap, however, seems small [Rez00].

The following result provides a necessary and sufficient condition for $g(x)$ to be SOS, which can be efficiently exploited in computational implementations discussed further below.

Theorem 2.1 (Theorem 1, [Par04])**.** *A polynomial $g(x)$ is SOS if and only if it can be written as a quadratic form,*

$$g(x) = \mathrm{v}(x)^T Q \mathrm{v}(x), \tag{2.4}$$

with $Q \in \mathbb{S}^d$ and $Q \succeq 0$.

In this context, Q is often also referred to as *Gram matrix*. If $g(x)$ has n-variables and degree r, then $\mathrm{v}(x)$ can always be chosen such that $\partial(\mathrm{v}) \leq r/2$. In general, due to the algebraic dependence of the variables $x_1, ..., x_n$, the matrix Q in Theorem 2.1 is not unique. Matching the coefficients of (2.3) and (2.4) imposes linear constraints on Q, in addition to the positive semidefiniteness constraint. A SOS program is thus defined as follows:

Definition 2.3 (SOS program, [SB10])**.** *A sum-of-squares program is an optimization problem with a linear cost and affine SOS constraints on the decision variables.*

$$\begin{aligned} \min_u \quad & c^T u \\ \text{subject to} \quad & a_k(x, u) \in \Sigma[x], \quad k = 1, ..., K, \end{aligned} \tag{2.5}$$

where $u \in \mathbb{R}^l$ are the decision variables and K is the number of polynomials. The polynomials $\{a_k\}$ are of the form

$$a_k(x, u) := a_{k,0}(x) + a_{k,1}(x)u_1 + ... + a_{k,m}(x)u_m. \tag{2.6}$$

In its structure, the constraints in the SOS program, i.e., the problem of finding a $Q \succ 0$, is equivalent to testing the feasibility of a *semidefinite program* (SDP) in the standard primal form.

Definition 2.4 (Semidefinite program)**.** *A SDP is a convex optimization problem of the (primal) form*

$$\begin{aligned} \min_{U} \quad & \operatorname{tr}(CU) \\ \text{subject to} \quad & \operatorname{tr}(A_i U) = b_i, \\ & U \succeq 0, \end{aligned} \tag{2.7}$$

where $U \in \mathbb{S}^d$ is the decision variable, $b \in \mathbb{R}^m$, C, $A_i \in \mathbb{S}^d, i = 1, ..., m$, are given matrices, and $\operatorname{tr}(\cdot)$ denotes the trace of a matrix.

In this work we consider problems which consist in SOS program-like optimizations extended to include constraints with bilinear terms in the decision variables. In reference to [SB10], we call these problems *generalized sum-of-squares programs*.

Definition 2.5 (Generalized SOS program)**.** *A generalized SOS program is an optimization problem with a convex objective function and affine as well as bilinear SOS constraints.*

$$\begin{aligned} \min_{u,v} \quad & h(u) \\ \text{subject to} \quad & a_k(x,u) \in \Sigma[x], \quad k = 1, ..., K, \\ & d_j(x,v) \in \Sigma[x], \quad j = 1, ..., J, \\ & z_t(x,u) d_j(x,v) \in \Sigma[x], \quad t = 1, ..., T, \end{aligned} \tag{2.8}$$

where $u \in \mathbb{R}^l$, $v \in \mathbb{R}^o$ are the decision variables and K, JT the number of respective polynomials. The polynomials $\{a_k\}$, $\{d_j\}$, and $\{z_t\}$ are of the form (2.6).

Generalized SOS programs can be solved by directly tackling the bilinearities via a bilinear matrix inequality (BMI) solver, such as PENLAB [FKS13]. Alternatively, they can be solved by an iterative procedure in which in each step alternatingly one term in the bilinearity is fixed and the optimization is performed on the other. This results in a series of SOS programs and thus in a series of convex optimizations. If there is a single bilinear term, the problem has been shown to be quasiconvex for which the global optimum can be obtained via bisection of the bilinearly appearing decision variable [SB10].

2.1.3 Semialgebraic set containment problems

The problem of certifying (2.2) is extended to a more general problem by considering a system of polynomial inequalities $f_j \leq 0$, inequations $g_l \neq 0$ and equalities $h_k = 0$. Additionally, the aim can be to optimize a polynomial or algebraic quantity over the feasible set of the polynomial constraints system. Solving such an optimization problem

exactly is in general np-hard. Using the following results from real algebraic geometry, however, enables computationally tractable relaxations of the problem.

Positivstellensatz

Theorem 2.2 (Positivstellensatz, Theorem 4.4.2, [BCR98]). *Let the polynomial inequalities $(f_j)_{j=1,...,J}$, inequations $(g_l)_{l=1,...,L}$, and equalities $(h_k)_{k=1,...,K}$ be finite families of polynomials in $\mathbb{R}[x]$. Then, the following properties are equivalent:*

1. *The set*

$$\left\{ x \in \mathbb{R}^n \;\middle|\; \begin{array}{ll} f_j(x) \geq 0, & j = 1, ..., J \\ g_l(x) \neq 0, & l = 1, ..., L \\ h_k(x) = 0, & k = 1, ..., K \end{array} \right\}, \tag{2.9}$$

   is empty.

2. *There exist $f \in P$, $g \in M$, $h \in O$ such that $f + g^2 + h = 0$.*

The algebraic quantities P, M and O are thereby given by

$$P := \text{cone}(f_1, ..., f_J) = \{f \,|\, s_0 + \sum_a s_a f_a + \sum_{a,b} s_{ab} f_a f_b + ..., \;\; s_0, s_a, s_{ab} \in \Sigma[x]\},$$
$$M := \text{monoid}(g_1, ..., g_L) = \{g_1^{m_1} \cdot \cdots \cdot g_L^{m_L} \,|\, m_1, ..., m_L \in \mathbb{N}_0\},$$
$$O := \text{ideal}(h_1, ..., h_K) = \{h \,|\, h = \sum_{k=1}^{K} q_k h_k, \;\; q_k \in \mathbb{R}[x]\}.$$

Theorem 2.2 provides *certificates*, i.e., formal refutations, in form of the SOS multipliers s_0, s_a, s_{ab}, the integer exponent multiplier $m_1, ..., m_L$, and the indefinite polynomial multiplier q_k for a semialgebraic set to be empty. The degree, or, respectively, the integer value of the multiplier certificates is not prescribed by the Positivstellensatz and can be arbitrarily high.

Theorem 2.3 ([Par00]). *Consider a system of polynomial equalities and inequalities of the form (2.9). Then, the search for bounded degree Positivstellensatz refutations can be done using semidefinite programming. If the degree bound is chosen to be large enough, then the SDPs will be feasible, and the certificates obtained from its solution.*

This theorem follows directly from Theorem 2.1 and the structure of SDPs as given in Definition 2.4.

Set containment conditions from Positivstellensatz

The Positivstellensatz can be applied to formulate semialgebraic set containment conditions. This is particularly useful for applications in which the feasible set can be formulated by polynomial constraints. The Positivstellensatz results in S-procedure-like arguments. While the standard S-procedure [BV04] provides necessary and sufficient conditions for the set containment problem of quadratic forms, the criteria of the Positivstellensatz provide sufficient conditions for the set containment problem involving polynomials of arbitrary degree sets. For this reason the criteria for this particular case are also referred to as *generalized S-procedure*, and have been proposed as such in, among others, [Par00; JW03; TP08; TP09; IML19b].

Lemma 2.1 (Set containment condition)**.** *Given* $\{f_j\}_{j=0}^{J} \in \mathbb{R}[x]$, $h \in \mathbb{R}[x]$ *and* $g \in \mathbb{R}[x]$, *the set containment*

$$\{x \in \mathbb{R}^n \mid f_1 \geq 0, \ldots f_J \geq 0, h = 0, g \neq 0\} \subseteq \{x \in \mathbb{R}^n \mid f_0 \geq 0\}, \tag{2.10}$$

is certified if there exist SOS multipliers $s_1, \ldots, s_J \in \Sigma[x]$, *an indefinite multiplier* $q \in \mathbb{R}[x]$ *and an integer multiplier* $m \in \mathbb{N}_0$ *such that*

$$f_0(x) - \sum_{j=1}^{J} s_j(x) f_j(x) - q(x)h(x) - g^{2m} \in \Sigma[x]. \tag{2.11}$$

Additional inequations and equality constraints can be added in (2.10) by simple addition of the corresponding terms.

For any fixed degree of the multipliers s_j, q, Lemma 2.1 represents sufficient conditions. Since Theorem 2.2 presents a hierarchy of sufficient conditions with respect to the multiplier degrees, choosing higher degrees for the multipliers in (2.11) can potentially certify larger sets contained in f_0.

2.1.4 Matrix sum-of-squares

In Chapter 4 optimization problems are considered which involve inequality constraints on matrices with polynomial entries. These types of constraints can be included in SOS programs by relaxing the PSD constraints to *matrix* SOS constraints.

Definition 2.6 (Matrix SOS, [APS08])**.** *A symmetric matrix with polynomial entries,* $F(x) \in \mathbb{S}^{n \times n}$, *is called a matrix SOS if for a vector of new indeterminants* $y = [y_1, \ldots, y_n]^T$ *the scalar polynomial* $y^T F(x) y$ *is an SOS polynomial in* $\Sigma[x, y]$.

The set of SOS matrices in x is denoted by $\Sigma^{n \times n}[x]$.

2.1.5 Set volume maximization

Consider the set $\Omega = \{x \in \mathbb{R}^n \,|\, g(x) \leq 1\}$, where $g(x) = \mathrm{v}(x)^T Q \mathrm{v}(x)$, $Q \in \mathbb{S}^n$, $Q \succeq 0$. In the problems considered in this work the issue will arise to find matrices Q which maximize the volume of a set such like Ω.

- Case $\partial(g) = 2$:
  The volume of Ω is inversely proportional to the determinant of Q. The geometric mean of the eigenvalues of Q is a monotonic function of its determinant and presents a concave (and, by negation, convex) expression. By using the geometric mean of the eigenvalues of Q as the objective function to minimize for, the volume of Ω is maximized.

  $$\max \mathrm{vol}(\Omega) \longrightarrow \max_{Q} \quad -\det(Q)^{1/n}. \tag{2.12}$$

  More details and proofs can be found in [JP19].

- Case $\partial(g) \geq 4$:
  There is no direct convex relationship to the volume of Ω in this case. However, by using a surrogate set in the form of the sublevel set of a quadratic form (such as in the first case) which is constrained to lie withing Ω, the volume of Ω can be maximized indirectly by maximizing the volume of the surrogate set. Let $b(x) = x^T B x$ and $\mathcal{B} = \{x | \, b(x) \leq 1\}$.

  $$\begin{aligned} \max \mathrm{vol}(\Omega) \longrightarrow \max_{Q,B} \quad & -\det(B)^{1/n} \\ \text{subject to} \quad & \mathcal{B} \subseteq \Omega. \end{aligned} \tag{2.13}$$

2.2 Random variables and Polynomial Chaos Expansion

Polynomial Chaos Expansion (PCE) is a spectral method for uncertainty quantification in which a stochastic variable or process is expanded with respect to an appropriate orthogonal basis in the Lebesgue space. This method can be applied to stochastic processes with finite second moment, also called second order processes. In contrast to the more simple to implement but computationally expensive *Monte-Carlo* (MC) methods, the PCE of a stochastic quantity, once constructed, directly leads to its distribution. The following sections first provide some relevant definitions before presenting the spectral expansion method of PCE.

2.2.1 Probability spaces and random variables

Let Θ be a sample space and $\mathcal{F}$ a σ-algebra of the subsets in Θ. Then the pair $(\Theta, \mathcal{F})$ is a *measurable space*. A measure μ defined on $(\Theta, \mathcal{F})$ is called a probability measure if it is nonnegative and $\mu(\Theta) = 1$. The triple $(\Theta, \mathcal{F}, \mu)$ with μ being a probability measure denotes a probability space.

Definition 2.7 (Random variable, [Sul15]). *Let $(\Theta, \mathcal{F})$ and $(\mathcal{Y}, \mathcal{G})$ be measurable spaces. A function $f : \Theta \to \mathcal{Y}$ generates a σ-algebra on Θ by $\sigma(f) := \sigma(\{[f \in E] \,|\, E \in \mathcal{G}\})$ and f is called a measurable function if $\sigma(f) \subseteq \mathcal{F}$. That is, f is measurable if the pre-image $f^{-1}(E)$ of every $\mathcal{G}$-measurable subset E of $\mathcal{Y}$ is an $\mathcal{F}$-measurable subset of Θ. A measurable function whose domain is a probability space is called a random variable.*

Definition 2.8 (Stochastic process, [Sul15]). *Let S be any set and let $(\Theta, \mathcal{F}, \mu)$ be a probability space. A function $U : S \times \Theta \to \mathcal{X}$ such that each $U(s, \cdot)$ is a random variable is called an $\mathcal{X}$-valued stochastic process on S.*

Definition 2.9 (Lebesgue space, [Sul15]). *Let $(\Theta, \mathcal{F}, \mu)$ be a measure space (i.e., μ is any measure, not necessarily a probability measure). For $1 \leq l \leq \infty$, the $\mathcal{L}_l$ space (Lebesgue space) is defined by*

$$\mathcal{L}_l(\Theta, \mu; \mathbb{K}) := \{f : \Theta \to \mathbb{K} \,|\, f \text{ is measurable and } ||f||_{\mathcal{L}_l(\mu)} \text{ is finite}\}. \tag{2.14}$$

For $1 \leq l < \infty$, the norm is defined by the integral expression

$$||f||_{\mathcal{L}_l(\mu)} := \left(\int_\Theta |f(x)|^l d\mu(x)\right)^{1/l}, \tag{2.15}$$

and for $l = \infty$ it is defined by the essential supremum.

As PCE considers stochastic variables with finite second moment, the focus in this work will be on the $\mathcal{L}_2$ space which is a complete square-integrable space and thus a Hilbert space. The inner product in the $\mathcal{L}_2$ space is denoted by $\langle \cdot, \cdot \rangle_{\mathcal{L}_2(\mu)}$ (where the $\mathcal{L}_2$-subscript will frequently be dropped), and represents integration, i.e., expectation, with respect to μ. Expectation in the $\mathcal{L}_2$ sense is further indicated by $\mathbb{E}$.

The generalized PCE enables the expansion of any random variable, vector or stochastic process $U \in \mathcal{L}_2(\Theta, \mu)$ in terms of elementary μ-orthogonal functions. These μ-orthogonal functions $\xi_i : \Theta_i \to \mathbb{R}, i = 1, ..., d$ compose independent entries of a $\mathbb{R}^d$-valued random variable ξ which is called the *stochastic germ*. The support of ξ is given by the measurable rectangle $\Theta = \Theta_1 \times ... \times \Theta_d \subseteq \mathbb{R}^d$, and the distribution of ξ on Θ by $\mu = \mu_1 \otimes ... \otimes \mu_d$. For clarity of presentation in this work we consider one-dimensional stochastic germs ξ, i.e., $\Theta \subseteq \mathbb{R}$. All methods presented in this thesis can be applied to higher-dimensional stochastic germs in a straight-forward but notation and computation-wise increasingly complex manner.

2.2.2 Orthogonal polynomial bases

For a given probability space, an orthogonal polynomial basis is defined as follows.

Definition 2.10 (Orthogonal polynomial basis)**.** *Let μ be a nonnegative measure on Θ. A set of polynomials $\mathcal{Q} = \{\Phi_i | i \in \mathbb{N}\} \subseteq \mathbb{R}[x]$ is called an orthogonal basis of polynomials if for each $i \in \mathbb{N}$, $\partial(\Phi_i) = i$, $\Phi_i \in \mathcal{L}_2(\Theta, \mu)$ and*

$$\langle \Phi_i(\xi), \Phi_j(\xi) \rangle = \int_\Theta \Phi_i(\xi)\Phi_j(\xi) d\mu(\xi) = \gamma_i \delta_{ij}, \tag{2.16}$$

where

$$\gamma_i := \langle \Phi_i(\xi), \Phi_i(\xi) \rangle. \tag{2.17}$$

are (non-negative) normalization constants of the basis.

The orthogonal polynomial basis is constructed using a normalization such that $\Phi_0 = 1$.

For certain polynomial bases the weighting function of the orthogonality relationship of the polynomial basis is identical to the probability function of a classical probability distribution. Table 2.1 shows examples of these orthogonal polynomials and their associated probability distributions.

Table 2.1: Examples of orthogonal polynomial bases of the Askey-scheme and their associated probability distributions.

Polynomial basis	Probability distribution
Hermite	Gaussian
Legendre	Uniform
Jacobi	Beta
Laguerre	Gamma
Charlier	Poisson
Krawtchouk	Binomial
Hahn	Hypergeometric

2.2.3 Polynomial Chaos Expansion

Even though the Hermite-polynomial basis expansion will yield an $\mathcal{L}_2$-convergent approximation of any random function belonging to the $\mathcal{L}_2$ space, particular choices of bases depending on the kind of random distribution can render higher rates of convergence. If the polynomial basis is chosen, such that its weighting function is identical to the probability function of the random variable under consideration, then the expansion in the corresponding polynomial basis is converging with an exponential rate (in the $\mathcal{L}_2$-sense). Table 2.1 provides examples of these $\mathcal{L}_2$-optimal pairings. For any complete orthogonal basis $\{\Phi_i\}_{i \in \mathbb{N}_0}$ of the Hilbert space $\mathcal{L}_2(\Theta, \mu)$ the PCE is then defined as follows.

Definition 2.11 (Polynomial Chaos Expansion series)**.** *Let $y(\xi) \in \mathcal{L}_2(\Theta, \mu)$ be a square-integrable vector-valued random variable in $\mathbb{R}^m$, $m \in \mathbb{N}$. The PCE of $y(\xi)$ with respect to the stochastic germ ξ is the expansion of $y(\xi)$ in the orthogonal basis $\{\Phi_i\}_{i=0}^p$*

$$y(\xi) = \sum_{i=0}^{p} \bar{y}_i \Phi_i(\xi) \in \mathbb{R}^m, \tag{2.18}$$

with vector valued PCE coefficients $\bar{y}_i \in \mathbb{R}^m$, $\bar{y}_i = [\bar{y}_{1_i}, ..., \bar{y}_{m_i}]^T$, which are obtained from, e.g, the Galerkin projection

$$\bar{y}_i = \frac{\langle y(\xi), \Phi_i(\xi) \rangle}{\gamma_i}. \tag{2.19}$$

With $p \to \infty$ the series in (2.18) becomes an exact expansion of $y(\xi)$.

The coefficients $\{\bar{y}_i\}_{i \in \mathbb{N}_0}$ can be obtained by computing the integral in equation (2.19) for each component of y. In general, there are several numerical approaches to computing the PCE coefficients consisting of intrusive methods (e.g., Galerkin projection) and non-intrusive methods (e.g., collocation methods).

PCE of moments

The statistical moments of a random variable $y(\xi) \in \mathbb{R}^m$ can be retrieved from the PCE coefficients of the expansion in the $\mathcal{L}_2$-optimal basis. With the notation in (2.18), the P-th moment, where $1 \leq P < \infty$, can be obtained from

$$\begin{aligned} \mathbb{E}[|y(\xi)|^P] &= \sum_{i=0}^{p} \sum_{jj=0}^{p} \cdots \sum_{P=0}^{p} \bar{y}_i \bar{y}_j \cdots \bar{y}_P \langle \Phi_i(\xi) \Phi_j(\xi) \cdots, \Phi_P(\xi) \rangle \\ &=: \bar{M}_P(\bar{y}). \end{aligned} \tag{2.20}$$

In particular, for the first moment, i.e., the mean $\Lambda \in \mathbb{R}^m$ of $y(\xi) \in \mathbb{R}^m$, equation (2.20) results in

$$\Lambda(y(\xi)) := \mathbb{E}[y(\xi)] = \langle y(\xi), \Phi_0 \rangle = \bar{y}_0. \tag{2.21}$$

For the variance $\sigma^2 \in \mathbb{R}^n$ of $y(\xi)$ follows

$$\sigma^2 := \mathbb{E}[|y(\xi) - \mathbb{E}[y(\xi)]|^2] = \sum_{j=1}^{p} \bar{y}_j^2 \gamma_j, \tag{2.22}$$

and for the covariance matrix $\Xi \in \mathbb{R}^{m \times m}$ of $y(\xi)$

$$\Xi(y(\xi)) := \sum_{j=1}^{p} \bar{y}_j \bar{y}_j^T \gamma_j, \tag{2.23}$$

where, in particular, for each entry of the matrix it is that

$$\Xi_{kl} = \sum_{j=1}^{p} \bar{y}_{k_j} \bar{y}_{l_j} \gamma_j. \tag{2.24}$$

with $\bar{y}_{k_j}, \bar{y}_{l_j}$ representing the j-th PCE coefficients of the k-th, respectively l-th, component of the random variable $y \in \mathbb{R}^m$.

Motivated by equations (2.21) and (2.22) for the mean and variance of a random variable $y \in \mathbb{R}^m$, the PCE coefficients in

$$\bar{y}_0 = [\bar{y}_{1_0}, ..., \bar{y}_{n_0}]^T \in \mathbb{R}^m, \tag{2.25}$$

are called the *mean modes*, and PCE coefficients

$$\bar{y}_J := [\bar{y}_{1_1}, ..., \bar{y}_{m_1}, ..., \bar{y}_{1_p}, ..., \bar{y}_{m_p}]^T \in \mathbb{R}^{m \cdot p}, \tag{2.26}$$

are called the *variance modes*. Together, they present the *stochastic modes*, denoted by

$$\bar{y} := [\bar{y}_0, \bar{y}_J]^T \quad \in \mathbb{R}^{m(p+1)}. \tag{2.27}$$

PCE of stochastic polynomial ODEs

Applying the PCE to a stochastic dynamical system (3.1) results in a deterministic representation of the system at the expense of an increased state dimension. More precisely, by expanding the random variables up to the truncation order p and projecting the resulting expansion onto each of the p basis functions, the n-dimensional stochastic system is represented by a $n \cdot (p+1)$-dimensional deterministic system. The expansion is demonstrated for an example system where $n = 1$.

$$\dot{x}(t, \xi) = a(\xi) x^3(t, \xi). \tag{2.28}$$

Expanding (2.28) gives

$$\sum_{i=0}^{p} \dot{\bar{x}}_i(t) \Phi_i(\xi) = \sum_{j=0}^{p} \sum_{k=0}^{p} \sum_{l=0}^{p} \sum_{m=0}^{p} \bar{a}_j \bar{x}_k(t) \bar{x}_l(t) \bar{x}_m(t) \Phi_j(\xi) \Phi_k(\xi) \Phi_l(\xi) \Phi_m(\xi). \tag{2.29}$$

Projecting (2.29) onto the q-th basis polynomial results in q deterministic differential equations

$$\sum_{i=0}^{p} \dot{\bar{x}}_i(t) \langle \Phi_i(\xi), \Phi_q(\xi) \rangle = \sum_{j=0}^{p} \sum_{k=0}^{p} \sum_{l=0}^{p} \sum_{m=0}^{p} \bar{a}_j \bar{x}_k(t) \bar{x}_l(t) \bar{x}_m(t) \langle \Phi_j(\xi) \Phi_k(\xi) \Phi_l(\xi) \Phi_m(\xi), \Phi_q(\xi) \rangle. \tag{2.30}$$

This expression motivates the introduction of a tensor notation, where

$$T_{ij..q} = \frac{\langle \Phi_i(\xi) \Phi_j(\xi) \cdots, \Phi_q(\xi) \rangle}{\gamma_q}, \tag{2.31}$$

is called the rank-r Galerkin tensor, where r is the monomial degree of the term in the summation. It is a sparse tensor where the entries are function of the chosen polynomial basis functions. As such, the entries are constant. Even though size of the tensor increases rapidly with increasing polynomial degree and truncation order, computing the tensor is a one-time cost. It can be computed once offline and then stored for dynamic computations. Using the tensor notation in (2.31), equation (2.30) results in

$$\dot{\bar{x}}_q(t) = \sum_{j=0}^{p}\sum_{k=0}^{p}\sum_{l=0}^{p}\sum_{m=0}^{p} \bar{a}_j \bar{x}_k(t)\bar{x}_l(t)\bar{x}_m(t)T_{jklmq}. \tag{2.32}$$

The polynomial basis for the PCE of (2.28) is often chosen according to the $\mathcal{L}_2$-optimal basis for ξ. While the PCE for a second order random process such as (2.28) can be performed in any basis as given by Definition 2.10, the convergence of the expansion will be faster or slower depending on the choice. This translates into the truncation order p which is needed to represent the system sufficiently accurately by the expansion, with slower convergence implying larger p.

2.3 Function definitions

Various definitions around functions, which are relevant for this thesis are provided in the following.

Definition 2.12 (Lipschitz continuous function)**.** *A function $f : D \to \mathbb{R}$ with domain $\mathcal{D} \subseteq \mathbb{R}^n$ is Lipschitz continuous if there exists a constant $L > 0$, such that for all x, $y \in \mathcal{D}$, the following holds.*

$$\|f(x) - f(y)\| \leq L\|x - y\|. \tag{2.33}$$

Definition 2.13 (Well-definedness)**.** *A relation $f : X \to Y$ is well-defined (i.e., a function), if $f \subseteq X \times Y$, the domain of f is X, and further for every (x_1, y_1), $(x_2, y_2) \in f$:*

$$x_1 = x_2 \implies y_1 = y_2. \tag{2.34}$$

Definition 2.14 (Kernel)**.** *Let $F : V \to W$ be a linear transformation between the vector spaces V, W. The kernel of F, also referred to as the null space of F, is the set of all vectors such that*

$$\ker(F) = \{v \in V \mid Fv = 0\}. \tag{2.35}$$

where 0 denotes the zero vector in W.

CHAPTER 3

Region of Attraction Analysis of Equilibrium Points of Stochastic Systems

The numerous ways in which uncertainty can manifest itself and affect a system makes generalized approaches to *region of attraction* (ROA) analysis particularly challenging. This has caused a multitude of system and uncertainty specific analysis methods to be proposed instead [CGW01; Che04b; TD14; Ber+16; VA17]. A class of uncertain systems commonly considered has two characteristic properties: firstly, the equilibrium point of the system is independent of the uncertainty, and secondly, the uncertainty comes from a uniform distribution over a finite and known range [TP09; Top+10; ISM19; IML19b]. While these characteristics allow for well-established methods, such as Lyapunov arguments to be used for the analysis, most systems of the real world are not captured by them as they are affected by uncertainty with stochastic nature and the equilibrium point's location is dependent on the uncertainty.

In the first part of this chapter we aim for systems which are not equipped with these two restricting characteristics. We do this by considering the class of stochastic nonlinear systems represented by second order processes for which we present an approach to analyze the ROA. This class of systems allows to take into account uncertainty coming from any $\mathcal{L}_2$-bounded distribution, i.e., distributions with finite second moment. Moreover, the method is derived such that it can explicitly account for systems whos equilibrium points are dependent on the uncertainty. The stochastic system is represented by a higher-dimensional set of deterministic equations obtained from a the *Polynomial Chaos Expansion* (PCE) of the stochastic dynamics. By deriving a connection firstly between the equilibria of the two system representations and secondly between the moment stability of the stochastic system and the asymptotic stability of the PCE system we arrive at a notion of the ROA of the stochastic equilibrium point on the basis of the ROA the PCE equilibrium point. More precisely, the ROA is obtained in terms of the region of initial conditions with specified moment properties for which trajectories almost surely converge to the equilibrium set of the stochastic system. The moment properties of the initial condition consist of, for example, a fixed variance in the initial state, and can

be specified by the user. Using Lyapunov stability conditions on the PCE system we propose an optimization program to compute an inner estimate of the ROA of the PCE equilibrium point. Based on the derived notion of the ROA of the stochastic equilibrium point an optimization program is proposed to efficiently compute an inner estimate of the stochastic ROA from the results of the PCE ROA.

Based on the results of the first part of the chapter, the second part turns to the problem of designing of feedback controllers for stochastic systems which are second order processes. The aim in the control design is to enlarge the ROA of the operating point which poses two major challenges. Firstly, means to measure the size of the ROA are required in order to quantify the attractive region. And secondly, conditions on the controller need to be formulated in a way such that an increase of the attractive properties of the system is obtained. The first challenge of efficiently measuring the size of the ROA is tackled by using the results presented in the first part of the chapter. The second challenge is followed up by developing computationally tractable conditions for the controller to increase the ROA. As second order processes are considered the proposed control design explicitly takes into account the statistical information available on the uncertainty, thus potentially allowing for less conservative results compared to standard robust approaches. Moreover, the enforcing of input constraints in the design of the feedback controller is enabled. An optimization program is proposed which efficiently implements the controller design.

This chapter is structured as follows. In Section 3.1 an overview of related works in the field is provided. The class of stochastic systems and its PCE representation as well as the definition of its equilibrium set together with a definition of its ROA are presented in Section 3.2.1. In Section 3.2.2 the notions of moment stability and Lyapunov stability for the two systems are presented and the their connection is derived. The algorithms of the optimization programs for the computation of the ROAs are presented in Section 3.2.4. Section 3.2.5 illustrates the application and various features of these algorithms by two examples. In Section 3.3.1 the feedback control design problem and the considered system class is presented. Criteria for the ROA of the controlled PCE equilibrium point are presented in Section 3.3.2 and details on the feedback control design within the framework of PCE are provided in Section 3.3.3. The optimization program for the controller design and the algorithm of its implementation are detailed in Section 3.3.4, followed by two illustrative examples in Section 3.3.5. The chapter ends with conclusions presented in Section 3.4.

3.1 Related work

For uncertain systems the analysis of the ROA is a particularly active field of research. [CGW01; Che04b; TP09; Top+10; TD14; Ber+16; VA17; ISM19; IML19b]. The type

of uncertainty and its appearance in the dynamical equations is often pivotal for the choice of the analytical approach. The stability of the class of commonly considered uncertain systems for which the equilibrium point of the system is independent of the uncertainty, and for which the uncertainty comes from a uniform distribution is most often analyzed using Lyapunov methods [Che04b; TP09; Top+10; IML19b]. In these methods an estimate of the ROA is obtained in the form of the sublevel set of a Lyapunov function. Optimization programs are often used to extend the approach with the aim of finding a Lyapunov function verifying a largest possible sublevel set. For systems where the uncertainty itself is parametric and polytope-bounded, parameter-dependent as well as common and composite Lyapunov functions have been investigated in, e.g., [Top+10; Che04b; ISM19].

The ROA analysis in the case of uncertainty-dependent equilibria, however, is not directly amenable to the use of Lyapunov functions, as standard Lyapunov methods require knowledge of the equilibrium's location. To tackle this problem, an equilibrium-independent version of the ROA was proposed in [ISM18] where the ROA was formulated as a function of a new coordinate representing the deviation of the state relative to the equilibrium point. As such, the approach admits the use of Lyapunov methods, however, it is still limited to uncertainties from uniform distributions. A more general approach for ROA analysis is provided by contraction methods which carry the benefit of inherently not requiring knowledge on the equilibrium state. Contraction of uncertain systems was studied, e.g. in [AWS18b] for polytope-bounded parametric uncertainty and in [BS19], [PTS09] for Itô stochastic differential equations. Contraction methods often pose, however, numerically more complex problems compared to Lyapunov analysis as they consider the differential system. Furthermore, while contraction analysis gives conclusions about the contractive behaviour of a system it in general does not provide information on the state of the (stochastic) equilibrium. Their advantage, thus, has to be carefully weighted against their drawbacks with regard to the system under consideration. In particular for the analysis of limit cycles, contraction methods can provide a useful tool, which will be a focus in both Chapter 4 and 5.

When considering stochastic systems, there is no classically unique notion of the ROA in the way there is for the deterministic case. For stochastic systems a definition of the ROA can be derived from the type of stochastic stability under consideration. An overview of the different definitions of stochastic stability is provided, e.g., in [Kha12; Koz69]. A widely used notion for the ROA of uncertain systems is that of a 'robust' ROA, which is the intersection of the ROAs obtained for each realization of the uncertainty. As it thus relates to the worst case, this notion is suitable for uncertainties with uniform distributions but less so for other distributions where the worst case is not of practical interest or exploiting the statistical information available gives less conservative results. A probabilistic ROA of an uncertainty-independent equilibrium point was investigated for Ito-stochastic system via Lyapunov functions in [GH18]. In [ST12] 'safe sets' of a

controlled system with quantified failure probabilities were considered and computed with a supermartingale approach.

While PCE techniques have become established tools in uncertainty quantification, their use in stability and control is still sparse [Kim+13] and mostly focused on linear systems. Stability analysis of linear stochastic systems via PCE using Lyapunov inequalities was previously performed in [FB09] and [Luc+17]. In [HT06], the evolution of the stochastic modes resulting from the PCE was used to obtain information on the stability of a nonlinear system. A more generalized approach for polynomial systems using Lyapunov arguments is briefly presented in [FB08], however the method proposed therein can only be used to certify global stability properties.

Using feedback control to increase the size of the ROA can be particularly desirable when uncertainties affect the system and exert a detrimental effect on the ROA. The task, in particular measuring the ROA, becomes significantly more complex in the case of uncertain systems. While the computation of inner estimates of the ROA was proposed for systems with uniformly distributed uncertainty [TP09; IML19b; VA17], none of these methods include a control design aiming at enlarging the ROA. On the other hand, for the class of *deterministic* polynomial systems with affinely appearing control inputs, such feedback controllers which aim at enlarging the ROA have been previously proposed, e.g., in [JW+05; Che04a; MAT13]. In these studies, both the feedback gains as well as the size of an inner estimate of the ROA are obtained by formulating Lyapunov arguments in an optimization problem which aims to maximize the size of the ROA.

3.2 ROA analysis for uncertain equilibrium points of stochastic systems

3.2.1 Stochastic systems and equilibrium sets

The system class considered in the following are polynomial continuous time second order random processes of the form

$$\dot{x}(t,\xi) = f(x(t,\xi), a(\xi)), \tag{3.1}$$

where $x(\cdot,\xi) \in \mathcal{L}_2(\Theta,\mu;\mathbb{R}^n)$ is the random state variable, $a(\xi) \in \mathcal{L}_2(\Theta,\mu;\mathbb{R}^m)$ is an uncertain parameter given by a random variable, and ξ is the one-dimensional stochastic germ as defined in Section 2.2.1. To avoid overloading on notation we drop the $\mathcal{L}_2$ reference, as the general stochastic variable considered here is assumed to be $\mathcal{L}_2$-bounded, and only specify if needed. E.g., $x(\xi) \in \mathcal{L}_2(\Theta,\mu;\mathbb{R}^n)$ will simply be written $x(\xi) \in \mathbb{R}^n$. The stochastic dynamics, $f : \mathbb{R}^n \times \mathbb{R}^m \to \mathbb{R}^n$, are polynomial in x and a.

Assumption 3.1. *The support of the random variable $\xi \in \mathcal{L}_2(\Theta,\mu)$ is finite.*

Assumption 3.1 holds for most practical applications. In the case that uncertainty distributions with typically infinite support, such as Gaussian distributions, are considered, [HT06] showed that the support can be limited with in practice negligible approximation error.

System (3.1) is considered to have an uncertainty-dependent attractive equilibrium point $x_{\text{EP}}(\xi)$. More precisely, for each realization of the uncertainty ξ the system converges to a different equilibrium point $x_{\text{EP}}(\xi)$. The set described by all such equilibrium points will be of central importance in this section and is formally defined as follows.

Definition 3.1 (Equilibrium set)**.** *The equilibrium set is the set given by the evaluation of $x_{EP}(\xi) \in \mathcal{L}_2(\Theta, \mu; \mathbb{R}^n)$ for each realization of the uncertainty, and is denoted by*

$$\mathcal{I} = \{x \in \mathbb{R}^n \mid f(x, a(\xi)) = 0,\ \xi \in \mathcal{L}_2(\Theta, \mu)\}. \tag{3.2}$$

Stochastic ROA

Let $\psi(t, x_{\text{ini}}(\xi), \xi)$ denote the uncertainty-dependent solution of (3.1) at time t with initial condition $x_{\text{ini}}(\xi)$, where the initial state is also allowed to be random, i.e. $x(t = 0) = x_{\text{ini}}(\xi)$. Note that for simplicity of notation we consider the same stochastic germ for the initial state as for the independent random variable. The ROA of the equilibrium set $\mathcal{I}$ is then defined as follows.

Definition 3.2 (Stochastic ROA of $\mathcal{I}$)**.** *The ROA of the equilibrium set $\mathcal{I}$ of a system (3.1) is defined as the set*

$$\mathcal{R}^* = \{x_{ini} \in \mathbb{R}^n \mid \mathbb{P}[\lim_{t\to\infty} \text{dist}(\psi(t, x_{ini}(\xi), \xi), \mathcal{I}) = 0] = 1\}, \tag{3.3}$$

where $\mathbb{P}$ denotes probability, and dist *is the distance measured in a chosen norm (e.g., the Euclidean norm).*

PCE system representation

Using the PCE framework presented in Section 2.2, the PCE representation of system (3.1) is denoted by

$$\dot{\bar{x}} := \bar{f}(\bar{x}), \tag{3.4}$$

where $\bar{x} \in \mathbb{R}^{n(p+1)}$ is the vector of PCE coefficients of the p-truncated expansion series, and $\bar{f} : \mathbb{R}^{n(p+1)} \to \mathbb{R}^{n(p+1)}$ refers to the dynamics resulting from the PCE of the stochastic dynamics in (3.1). We will frequently refer to (3.4) simply as *PCE system*.

Regarding the truncation order p of the expansion series the commonly made assumption is introduced.

Assumption 3.2. *The truncation order p is chosen such that the PCE system (3.4) accurately represents the stability properties of the stochastic system (3.1).*

3.2.2 Stability of stochastic systems

The aim in the following is to analyze the stability properties of the equilibrium set $\mathcal{I}$ (3.2) of a stochastic system by means of the PCE system (3.4). In order to draw conclusions from the stability properties of the PCE system on the stability of the stochastic system, a connection between the stability behavior of both systems needs to be established. This requires the introduction of suitable notions of stability for both systems.

Relationship of equilibria

Before turning to the notions of stability we first show the relationship between the equilibria of (3.1) and (3.4).

Lemma 3.1. *The stochastic system* (3.1) *has an equilibrium set* $\mathcal{I}$ *as defined in* (3.2) *if and only if the PCE system has an equilibrium point,* $\bar{x}_{EP} \in \mathbb{R}^{n(p+1)}$.

Proof. Let $f(x_{\mathrm{EP}}(\xi)) = 0$. The PCE of $f(x_{\mathrm{EP}}(\xi))$ is $\bar{f}(\bar{x}_{\mathrm{EP}})$, where $x_{\mathrm{EP}}(\xi) = \sum_{i=0}^{p} \bar{x}_{\mathrm{EP}i}\Phi_i(\xi)$ from (2.18). Assume $\bar{x}_{\mathrm{EP}}$ was not an equilibrium of $\bar{f}$, i.e. $\bar{f}(\bar{x}_{\mathrm{EP}}) \neq 0$. Then there exists a $t > 0$, $\bar{\psi}(t, \bar{x}_{\mathrm{EP}}) = \bar{x}(t) \neq \bar{x}_{\mathrm{EP}}$. However, $\bar{\psi}(t, \bar{x}_{\mathrm{EP}})$ is the PCE of $\psi(t, x_{\mathrm{EP}})$, and, by equation (3.2), $\psi(t, x_{\mathrm{EP}}(\xi)) = \psi(0, x_{\mathrm{EP}}(\xi)) = x_{\mathrm{EP}}(\xi)$, so $\bar{\psi}(t, \bar{x}_{\mathrm{EP}}) = \bar{x}_{\mathrm{EP}}$. This argument holds both ways, and thus $f(x_{\mathrm{EP}}(\xi)) = 0 \Leftrightarrow \bar{f}(\bar{x}_{\mathrm{EP}}) = 0$. □

The equilibrium set can be obtained numerically by explicit computation of the expansion $x_{\mathrm{EP}}(\xi) = \sum_{i=0}^{p} \bar{x}_{\mathrm{EP}i}\Phi_i(\xi)$. Using equation (2.20) for a known $\mathcal{L}_2$-optimal basis, the equilibrium set can further be expressed in terms of its moments,

$$\mathcal{I} = \{x \in \mathbb{R}^n \,|\, x \in x_{\mathrm{EP}}(\xi) \sim \lambda(\bar{M}_P(\bar{x}_{\mathrm{EP}}))\}. \tag{3.5}$$

Due to Lemma 3.1 the task of analyzing the stability of the uncertainty-dependent equilibrium point of the stochastic system converts to the well-known problem of analyzing the stability of an equilibrium point of a deterministic system. Moreover, it emphasizes the important aspect that an equilibrium point of the PCE system not only corresponds to an equilibrium set of the stochastic system but also contains the statistical information of the set. Note that the location of $\bar{x}_{\mathrm{EP}}$ can be easily obtained by simulating a trajectory of (3.4) with initial state in the region of interest.

Remark 3.1. If the variance modes of $\bar{x}_{\mathrm{EP}}$ are zero, i.e., $\bar{x}_{\mathrm{EP}J} = 0$, then the stochastic system has an uncertainty-independent equilibrium point located at $x_{\mathrm{EP}} = \bar{x}_{\mathrm{EP}0}$. The equilibrium set $\mathcal{I}$ thus only contains one element. Moreover, if all stochastic modes are zero, $\bar{x}_{\mathrm{EP}} = 0$, then also $x_{\mathrm{EP}} = 0$.

Based on this relationship between the equilibria a connection is proposed between certain stability notions which are specified for each system in the following.

P-th moment boundedness and stability

Among the various concepts of stability for stochastic system we focus on P-th moment boundedness and stability of stochastic systems where definitions as found in, e.g., [Kha12], [WM04], [Kha02].

Definition 3.3 (Moment stability)**.** *The solutions of* (3.1) *are called ultimately bounded in the P-th moment if there exists a constant $c > 0$ such that for any $b > 0$ there exists a $T = T(b) > 0$ such that*

$$|x_{ini}| < b \;\rightarrow\; \mathbb{E}[|x(t,\xi)|^P] < c, \quad \forall t \geq T. \tag{3.6}$$

Further, if there is only one element in $\mathcal{I}$ then let this element, without loss of generality, be the zero point. This zero point is called

- *stable in the P-th moment, if for each $\epsilon > 0$, there exists a $\delta > 0$ such that*

$$|x_{ini}| < \delta \;\rightarrow\; \mathbb{E}[|x(t,\xi)|^P] < \epsilon, \quad \forall t \geq 0, \tag{3.7}$$

- *asymptotically stable in the P-th moment, if it is P-th moment stable and, further,*

$$|x_{ini}| < \delta \;\rightarrow\; \mathbb{E}[|x(t,\xi)|^P] \to 0 \text{ as } t \to \infty. \tag{3.8}$$

We now define a suitable notion of stability for the PCE system. As we are interested in equilibrium points of (3.4) and, further, (3.4) is deterministic, we use stability in the sense of Lyapunov.

Definition 3.4 (Lyapunov stability)**.** *The equilibrium point $\bar{x}_{EP}$ of* (3.4) *is locally stable if for each $\epsilon > 0$ there exists a $\delta > 0$ such that*

$$|\bar{x}_{ini}| < \delta \Rightarrow |\bar{x}(t) - \bar{x}_{EP}| < \epsilon, \quad \forall t > 0. \tag{3.9}$$

Further, $\bar{x}_{EP}$ is locally asymptotically stable if it is locally stable and δ can be chosen such that

$$|\bar{x}_{ini}| < \delta \Rightarrow |\bar{x}(t) - \bar{x}_{EP}| \to 0 \text{ as } t \to \infty. \tag{3.10}$$

Utilizing both presented notions of stability and the equilibria relationship established in Lemma 3.1 we find the following result for the stochastic system.

Theorem 3.1. *Let the system* (3.4) *with $\bar{f} : \bar{D} \to \bar{D} \subseteq \mathbb{R}^{n\cdot(p+1)}$ be the PCE of the stochastic system* (3.1)*. If the equilibrium point $\bar{x}_{EP} \in \bar{D}$ is locally asymptotically stable then the solutions of* (3.1) *are ultimately bounded in the P-th moment in a neighborhood of $\mathcal{I}$. If, further, $\bar{x}_{EP}$ represents a $\mathcal{I}$ containing a single point, then* (3.1) *is locally asymptotically stable in the P-th moment.*

Proof. If $\bar{x}_{\mathrm{EP}}$ is an equilibrium point of (3.4) then every trajectory $\bar{x}(t)$ in a neighborhood of $\bar{x}_{\mathrm{EP}}$ will eventually converge to $\bar{x}_{\mathrm{EP}}$. As all components $\bar{x}_i(t)$ in this case converge to a finite value, so does every term in the expression in (2.20) and thus $\mathbb{E}[|x(t,\xi)|^P]$ will eventually converge to a finite value, which is given by inserting $\bar{x}_{\mathrm{EP}}$ into the right hand side of equation (2.20). The ultimate boundedness of the P-th moment as defined in (3.6) follows. If the equilibrium point $\bar{x}_{\mathrm{EP}}$ represents an $\mathcal{I}$ consisting of a single point then this implies that $\bar{x}_{\mathrm{EP}\,J} = 0$ (cf. Remark 3.1). Thus, every component of $\bar{x}_J(t)$ will converge to zero and every component of $\bar{x}_0(t)$ will converge to $\bar{x}_{\mathrm{EP}0}$ as $t \to \infty$. Assuming, without loss of generality, $\bar{x}_{\mathrm{EP}0} = 0$, it follows that equation (2.20) converges to zero and thus equation (3.8) holds. □

Theorem 3.1 allows to obtain information about the behavior of the stochastic system by analyzing the local stability properties of an equilibrium point $\bar{x}_{\mathrm{EP}}$ of the PCE system. Since the PCE system is deterministic, this connection opens up the possibility of analyzing stability of stochastic systems using deterministic criteria.

Remark 3.2. Note that the reverse of the statement in Theorem 3.1 is not true: ultimately bounded solutions of the stochastic system (3.1) do not imply a convergence of the components $\bar{x}(t)$ to constant values. One example for this is readily provided by systems with a stable limit cycle. The trajectories in a neighborhood of the limit cycle converge to the limit cycle and thus are locally ultimately bounded, however the PCE coefficients $\bar{x}_i(t)$ do not converge to an equilibrium point but instead remain ultimately bounded to a set as well. This will further be explored in Chapter 4.

In the following, criteria for the attractive region of $\bar{x}_{\mathrm{EP}}$ are formulated.

3.2.3 PCE-based region of attraction analysis

In this section we first define the ROA of an equilibrium point $\bar{x}_{\mathrm{EP}}$ of the PCE system and state the criteria with which an inner estimate of it can be obtained. We then show how this ROA estimate translates to an inner estimate of $\mathcal{R}^*$, the ROA of the stochastic system.

The ROA of the PCE system

Let the exact ROA of $\bar{x}_{\mathrm{EP}}$ be defined by the set

$$\bar{\mathcal{R}}^* = \{\bar{x}_{\mathrm{ini}} \in \mathbb{R}^{n\cdot(p+1)} \mid \lim_{t\to\infty} \mathrm{dist}(\bar{\psi}(t,\bar{x}_{\mathrm{ini}}),\bar{x}_{\mathrm{EP}}) = 0\}, \tag{3.11}$$

where $\bar{\psi}(t,\bar{x}_{\mathrm{ini}})$ denotes the solution of the PCE system at time t with initial state $\bar{x}_{\mathrm{ini}}$. An inner estimate of $\bar{\mathcal{R}}^*$, denoted by $\bar{\mathcal{R}}$, is then obtained from the following arguments.

Theorem 3.2. *Let $\bar{D} \subset \mathbb{R}^{n\cdot(p+1)}$ be a compact domain containing $\bar{x}_{EP}$ and let V be a continuously differentiable function $V(\bar{x}) : \bar{D} \to \mathbb{R}$. For a scalar $\beta > 0$ let $\Omega_{V_\beta} = \{\bar{x} \in \bar{D} \,|\, V(\bar{x}) \leq \beta\}$ be the β-sublevel set of V. If V satisfies*

$$V(\bar{x}) > 0 \quad \forall \bar{x} \in \Omega_{V_\beta} \backslash \{\bar{x}_{EP}\}, \qquad V(\bar{x}_{EP}) = 0, \tag{3.12}$$

$$\dot{V}(\bar{x}) = \frac{\partial V}{\partial \bar{x}} \bar{f}(\bar{x}) < 0 \quad \forall \bar{x} \in \Omega_{V_\beta} \backslash \{\bar{x}_{EP}\}, \tag{3.13}$$

then V is a Lyapunov function and every trajectory $\bar{x}_{ini}$ starting in Ω_{V_β} will converge to $\bar{x}_{EP}$ as $t \to \infty$. Thus, the set $\bar{\mathcal{R}} = \{\bar{x}_{ini} \in \bar{D} | \bar{x}_{ini} = \bar{x},\ \forall \bar{x} \in \Omega_{V_\beta}\}$ is an inner estimate of $\bar{\mathcal{R}}^*$.

The proof utilizes standard Lyapunov arguments and is shown in Appendix A.1.

In the following, the connection of $\bar{\mathcal{R}}$ to the stability properties of the original stochastic system is drawn.

Stochastic ROA retrieved from PCE coefficients

Theorem 3.2 presents a criterion for a set $\bar{\mathcal{R}}$ to be an inner estimate of the PCE system's ROA (3.11), where $\bar{\mathcal{R}}$ is expressed in terms of the PCE coefficients. We now provide the means to infer information about $\mathcal{R}^*$, the ROA of the equilibrium set $\mathcal{I}$ of the stochastic system, from $\bar{\mathcal{R}}$. More precisely, we show how the inner estimate $\bar{\mathcal{R}}$ translates into an inner estimate $\mathcal{R}$ of the stochastic ROA $\mathcal{R}^*$. Recalling the expression (3.3) for the ROA of the equilibrium set $\mathcal{I}$ of a stochastic system, the following arguments can be made.

Lemma 3.2. *Let $\bar{\mathcal{R}}$ be an inner estimate of the ROA of $\bar{x}_{EP}$, $\bar{\mathcal{R}} \subseteq \bar{\mathcal{R}}^*$. Then the set*

$$\mathcal{R} = \{x_{ini} \in \mathbb{R}^n \,|\, x_{ini}(\xi) \sim \lambda(\bar{M}_P(\bar{x}_{ini})), \forall \bar{x}_{ini} \in \bar{\mathcal{R}}\}, \tag{3.14}$$

is a subset of the ROA of x_{EP}, $\mathcal{R} \subseteq \mathcal{R}^*$.

Proof. We first establish the relationship between $x_{\text{ini}}(\xi)$ and $\bar{x}_{\text{ini}} \in \bar{\mathcal{R}}$. The PC coefficients $\bar{x}_{\text{ini}} \in \bar{\mathcal{R}}$ represent the stochastic variables $x_{\text{ini}}(\xi)$ by the relation (2.18), such that any $x^\sharp_{\text{ini}}(\xi) \in \mathcal{R}$ is given by $x^\sharp_{\text{ini}}(\xi) = \sum_{i=0}^{p} \bar{x}_{\text{ini}}{}^\sharp_i \Phi_i(\xi)$. For this $x^\sharp_{\text{ini}}(\xi)$, from equation (2.20) the moments are given by $M_P(x^\sharp_{\text{ini}}) = \bar{M}_P(\bar{x}_{\text{ini}}{}^\sharp)$. This reasoning holds for all $x_{\text{ini}} \in \mathcal{R}$.
We now turn to prove $\mathcal{R} \subseteq \mathcal{R}^*$. Recall, that from Theorem 3.2 we have $\bar{x}_{\text{ini}} \in \bar{\mathcal{R}} \implies \lim_{t\to\infty} \bar{\psi}(t, \bar{x}_{\text{ini}}) = \bar{x}_{\text{EP}}$. Let further $\bar{x}(t) = \bar{\psi}(t, \bar{x}_{\text{ini}})$ and $x(t, \xi) = \psi(t, x_{\text{ini}}(\xi), \xi)$. With equation (2.20) and the results from Theorem 3.1, it follows that if $\bar{x}_{\text{ini}} \in \bar{\mathcal{R}}$ then

$$\begin{aligned}
\mathbb{E}[|x(t,\xi)|^P] &= \sum_{i=0}^{p} \cdots \sum_{P=0}^{p} \bar{x}_i(t) \cdots \bar{x}_P(t) \langle \Phi_i \cdots, \Phi_P \rangle, \\
&\xrightarrow{t\to\infty} \sum_{i=0}^{p} \cdots \sum_{P=0}^{p} \bar{x}_{\text{EP}i} \cdots \bar{x}_{\text{EP}P} \langle \Phi_i \cdots, \Phi_P \rangle = \mathbb{E}[|x_{\text{EP}}(\xi)|^P],
\end{aligned} \tag{3.15}$$

where $1 \leq P < \infty$ and for a given $x_{\text{EP}}(\xi)$ and P the term $\mathbb{E}[|x_{\text{EP}}(\xi)|^P]$ is a constant. So far, we have shown the moment convergence of a random variable $x_{\text{ini}}(t,\xi) \in \mathcal{R}$. It remains to show that from this follows $\lim_{t\to\infty} \mathbb{P}[\text{dist}(\psi(t, x_{\text{ini}}(\xi),\xi),\mathcal{I}) = 0] = 1$ almost surely. To this end, recall Assumption 3.1, thus Θ is bounded. Now, assume there is a subset $\Theta^\dagger \subset \Theta$ for which $\xi^\dagger \in \Theta^\dagger : \text{dist}(x(t,\xi^\dagger),\mathcal{I}) \not\to 0$ as $t \to \infty$. Consider first the case where $x(t,\xi^\dagger) \to \infty$ as $t \to \infty$. Then

$$\begin{aligned}\mathbb{E}[|x(t,\xi)|^P] &= \int_\Theta |x(t,\xi)|^P d\mu(\xi) \\ &= \int_{\Theta^\dagger} |x(t,\xi^\dagger)|^P d\mu(\xi^\dagger) + \int_{\Theta^{\dagger C}} |x(t,\xi^{\dagger C})|^P d\mu(\xi^{\dagger C}),\end{aligned} \tag{3.16}$$

where $\xi^{\dagger C} \in \Theta^{\dagger C}$ and $\Theta^{\dagger C}$ denotes the complement of $\Theta^\dagger$, such that $\Theta^{\dagger C} \cup \Theta^\dagger = \Theta$. The first term in equation (3.16) and by that the P-th moment of $x(t,\xi)$ will, however, tend to infinity as t goes to infinity, unless the elements in $\Theta^\dagger$ have μ-measure zero. Consider now the case where $\text{dist}(x(t,\xi^\dagger),\mathcal{I}) \to c$ as $t \to \infty$, where $0 < c < \infty$ is a constant. In order to not contradict (3.15) with the expression in (3.16) we find that either $x(t,\xi^\dagger) = x(t,\xi)$ for all $\xi^\dagger = \xi$, but this implies $\text{dist}(x(t,\xi^\dagger),\mathcal{I}) \to 0$ as $t \to \infty$, or $\mu(\xi^\dagger) = 0$. Hence, from moment convergence follows the almost sure convergence of $x(t,\xi)$ to $\mathcal{I}$, such that $\lim_{t\to\infty} \mathbb{P}[\text{dist}(\psi(t, x^\dagger_{\text{ini}}(\xi),\xi),\mathcal{I}) = 0] = 1$ for all $x_{\text{ini}} \in \mathcal{R}$ and thus $\mathcal{R} \subseteq \mathcal{R}^*$. □

If Assumption 3.1 does not hold and ξ has infinite support then almost sure convergence of trajectories from moment convergence cannot be concluded. In that case, based on the proof above the meaning of the computed region $\mathcal{R}^*$ would change and could now be characterized as the region for which the moments of all trajectories starting in $\mathcal{R}^*$ converge to the moments of $\mathcal{I}$.

3.2.4 Algorithms to compute a ROA estimate

In the following we present two algorithms based on *sum-of-squares* (SOS) programs by which $\bar{\mathcal{R}}$ and $\mathcal{R}$ can be computed. The first algorithm returns the set $\bar{\mathcal{R}}$ as an inner estimate of the ROA of the PCE system's equilibrium point. The second algorithm uses $\bar{\mathcal{R}}$ as well as user-specified fixed variance levels and computes the corresponding inner estimate of the stochastic ROA, $\mathcal{R}$. In order to make the following implementations generalizable, a coordinate shift is introduced, similar to the one proposed in [ISM18]. The shift is

$$\bar{z} = \bar{x} - \bar{x}_{\text{EP}}, \tag{3.17}$$

and it is such that the analyzed system is centered around the zero point. Note that while in [ISM18] $\bar{x}_{\text{EP}}$ is not known because it depends on the uncertainty, in this formulation $\bar{x}_{\text{EP}}$ is deterministic and obtained by simulation of the PCE system, as mentioned in Section 3.2.2.

Algorithm 1: Computing $\bar{\mathcal{R}}$

A ROA estimate of the PCE equilibrium is obtained by finding a Lyapunov function which satisfies the conditions stated in Theorem 3.2. Recall that the PCE system is polynomial in the PCE coefficients. Using polynomial Lyapunov functions, the conditions in Theorem 3.2 then result in polynomial form. This enables the reformulation of the conditions in Theorem 3.2 as semialgebraic set containment conditions imposed on the Lyapunov function. Applying Theorem 2.3 and Lemma 2.1 presented in Section 2.1.3, the conditions are cast in the form of a generalized SOS program which can efficiently be checked by a series of *semidefinite programs* (SDPs).

The aim of the algorithm is to maximize the set $\bar{\mathcal{R}}$ represented by the sublevel set Ω_{V_β} of the Lyapunov function. Using

$$V(\bar{z}) = \mathrm{v}(\bar{z})^T Q_V \mathrm{v}(\bar{z}), \quad Q_V \succ 0, \tag{3.18}$$

the set Ω_{V_β} is formulated as the sublevel set $\Omega_{V_{\beta=1}} = \{\bar{z} \,|\, V(\bar{z}) \leq 1\}$ where β is fixed to 1 as optimizing over β is redundant when optimizing over Q_V. It has been previously observed [JW+05; TP06; AWS18a] that higher degree functions V have the potential to verify larger estimates of the ROA. In order to have the required convex measure for the set $\bar{\mathcal{R}}$ we use a quadratic surrogate set $\mathcal{B} = \{\bar{z} \,|\, b(\bar{z}) \leq 1\}$ to maximize over, where $b(\bar{z}) := \bar{z}^T B \bar{z}$ and $B \succ 0$. This surrogate set is constrained to lie inside $\bar{\mathcal{R}}$, with further details as presented in Section 2.1.5.

The set containment conditions for the $\bar{\mathcal{R}}$ maximization problem then result as follows.

$$\{\bar{z} \in \mathbb{R}^n \,|\, V(\bar{z}) > 0,\, \bar{z} \neq 0\} \subseteq \{\bar{z} \in \mathbb{R}^n \,|\, 1 - V(\bar{z}) \geq 0\}, \tag{3.19}$$

$$\{\bar{z} \in \mathbb{R}^n \,|\, 1 - V(\bar{z}) \geq 0,\, \bar{z} \neq 0\} \subseteq \{\bar{z} \in \mathbb{R}^n \,|\, \dot{V}(\bar{z}) < 0\}, \tag{3.20}$$

$$\{\bar{z} \in \mathbb{R}^n \,|\, 1 - b(\bar{z}) \geq 0\} \subseteq \{\bar{z} \in \mathbb{R}^n \,|\, 1 - V(\bar{z}) \geq 0\}. \tag{3.21}$$

Applying the procedure demonstrated by Lemma 2.1 and adding the objective function according to the outline in Section 2.1.5, results in the following optimization problem in the form of a generalized SOS program.

$$\min_{Q_V, s_1, s_2, B} \quad \det(B)^{1/n(p+1)} \tag{3.22a}$$

subject to

$$V(\bar{z}) - l(\bar{z}) \in \Sigma[\bar{z}], \tag{3.22b}$$

$$-\dot{V}(\bar{z}) - s_1(\bar{z})(1 - V(\bar{z})) - l(\bar{z}) \in \Sigma[\bar{z}], \tag{3.22c}$$

$$-s_2(\bar{z})(1 - b(\bar{z})) - (1 - V(\bar{z})) \in \Sigma[\bar{z}], \tag{3.22d}$$

$$s_1(\bar{z}),\, s_2(\bar{z}) \in \Sigma[\bar{z}] \tag{3.22e}$$

$$B \succ 0. \tag{3.22f}$$

where the multipliers s_1 and s_2 are the SOS multipliers resulting from the Positivstellensatz arguments 2.2. Once obtained for a bounded degree, they certify the inequality constraints in (3.19)-(3.21) to hold. The term $l(\bar{z})$ is an even polynomial with small fixed coefficients (e.g., $l(\bar{z}) = 10^{-4}\bar{z}^T\bar{z}$), which is used to enforce the inequation constraint $\bar{z} \neq 0$ in (3.19) and (3.20). Due to the chosen structure of the Lyapunov function (3.18), which directly results in global positivity, the set containment condition (3.19) reduces to the simpler condition given in (3.22b).

The generalized SOS program (3.22) is bilinear in the coefficients of the multipliers s_1, respectively s_2 and Q_V, respectively B, which prevents its direct solution as an SDP. However, by an iterative approach the problem is turned into a series of SDPs (cf. Sectino 2.1.2). Algorithm 3.1 provides an outline of the computational implementation. The procedure is initialized by linearizing the PCE dynamics (3.4) around $\bar{z} = 0$,

$$\bar{A} = \left.\frac{\partial \bar{f}(\bar{x})}{\partial \bar{x}}\right|_{\bar{z}=0}, \tag{3.23}$$

and solving the matrix Lyapunov equation,

$$\bar{A}^T Q + Q\bar{A} + H = 0, \tag{3.24}$$

for a given $H \succ 0$. If $\bar{x}_{\text{EP}}$ is a asymptotically stable equilibrium point, the obtained Q is positive definite. The function $V_{\text{ini}}(\bar{x}) = \bar{x}^T Q \bar{x}$ then provides an initial Lyapunov function. The matrix Q is scaled by a $c > 0$ using bisection until constraints (3.22c) and (3.22e) are feasible. The initialization finishes with choosing an initial matrix B such that (3.22d) and (3.22e) are feasible. Then an iteration over two steps follows. In Step 1, the Lyapunov function and surrogate set are fixed and a feasibility test is solved to find the SOS multipliers. Since in this step the constraints (3.22c) and (3.22d) are independent of each other the multiplier search can be performed separately for each constrained and potentially parallelized for speed up. In Step 2, the multipliers are fixed to the obtained values in Step 1 and the optimization problem (3.22) is solved to find a Lyapunov function for which the surrogate set $\mathcal{B}$ can be maximized. The two steps are iterated until the relative increase in the set $\mathcal{B}$ falls below a predefined threshold (convCrit_B in Algorithm 3.1). The problem in each of the two steps is an SOS program, hence it is convex and can be solved as an SDP.

Algorithm 2: Recovering $\mathcal{R}$ from $\bar{\mathcal{R}}$

We propose an approach in form of an optimization problem in which the set $\mathcal{R}$, as given by Lemma 3.2 for initial conditions with specified stochastic properties, can be recovered from the set $\bar{\mathcal{R}}$. In particular, the program shows how to obtain a maximized inner estimate $\mathcal{R}$ of the true ROA $\mathcal{R}^*$ from a given set $\bar{\mathcal{R}}$. The set $\mathcal{R}$ is given by *stochastic* variables x, whose statistical properties are given by all possible states of the

Algorithm 3.1 Maximize ROA estimate of $\bar{x}_{\mathrm{EP}}$

Input: p, $\partial(s_1)$, $\partial(s_2)$, $\partial(V)$, $\mathrm{convCrit}_B$
Output: V, $\bar{\mathcal{R}}$
procedure MAXROAESTIMATE
    $\bar{f}(\bar{x}) \xleftarrow{\text{PCE}} f(x,a)$
    $\bar{f}(\bar{z}) \xleftarrow{\text{shift}} \bar{f}(\bar{x})$

    Initialization:
    $Q_{V\,\mathrm{ini}} \leftarrow c \cdot Q$, solution of (3.24), scaled by $c > 0$ until (3.22c), (3.22e) feasible
    choose a $B \succ 0$ small enough such that (3.22d), (3.22e) is feasible

    Iteration:
    $k \leftarrow 0$
    repeat
        $k \leftarrow k + 1$
        Step 1:
            $s_1 \leftarrow$ fix Q_V, B, solve (3.22c),(3.22e)
            $s_2 \leftarrow$ fix Q_V, B, solve (3.22d),(3.22e)
        Step 2:
            Q_V, $B \leftarrow$ fix s_1, s_2, solve (3.22a)-(3.22d), (3.22f)
    until $\det(B)_{k-1} - \det(B)_k < \mathrm{convCrit}_B$

PCE coefficients contained in $\bar{\mathcal{R}}$. In the set $\bar{\mathcal{R}}$, the mean modes $\bar{x}_0$ and the variance modes $\bar{x}_J$ can be traded off, allowing for a wide range of statistical properties of x_{ini} being represented by $\bar{\mathcal{R}}$.

In order to obtain a set $\mathcal{R}$ of the stochastic system in the x_{ini} variables, one of the two statistical properties, either the mean or the covariance, of the initial states can be fixed and the set $\mathcal{R}$ obtained in terms of the other. We here choose to fix the covariance of the initial states x_{ini} to a specified level, which is denoted by $\hat{\Xi}$, and compute $\mathcal{R}$ in terms of the mean of x_{ini}. The $\mathcal{R}$ obtained in this way will be denoted by $\mathcal{R}_0$ in the following. Since $\Lambda(x_{\text{ini}}) = \bar{x}_{\text{ini}0}$ for x_{ini} distributed with stochastic germ ξ (equation (2.21)), the set $\mathcal{R}_0$ is given by

$$\mathcal{R}_0 = \{\bar{x}_{\text{ini}0} \in \mathbb{R}^n \mid \bar{x}_{\text{ini}} = \bar{x},\ \bar{x} \in \bar{\mathcal{R}},\ \sum_{j=1}^{p} \bar{x}_j \bar{x}_j^T \gamma_j = \hat{\Xi}\}. \tag{3.25}$$

Note that as defined in (2.27), $\bar{x} = [\bar{x}_0, \bar{x}_J]^T$.

The set $\mathcal{R}_0$ can be computed from a given $\bar{\mathcal{R}}$ by the following optimization problem. Let $\mathcal{R}_0$ hereby be represented by the 1-sublevel set of the polynomial function $\mathcal{R}_0 := \{\bar{x}_{\text{ini}0} \,|\, \mathrm{v}(\bar{x}_0)^T Q_0\, \mathrm{v}(\bar{x}_0) \leq 1\}$. The aim is to maximize $\mathcal{R}_0$ inside $\bar{\mathcal{R}}$ while keeping the size of the polynomials in (2.23), representing the covariance of the initial states x_{ini}, fixed.

$$\max_{Q_0} \quad \text{vol}(\mathcal{R}_0) \tag{3.26a}$$

$$\text{subject to} \tag{3.26b}$$

$$\mathrm{v}(\bar{x}_{\text{ini}})^T Q_V\, \mathrm{v}(\bar{x}_{\text{ini}}) \leq 1, \tag{3.26c}$$

$$\sum_{j=1}^{p} \bar{x}_{\text{ini}j} \bar{x}_{\text{ini}j}^T \gamma_j = \hat{\Xi}, \tag{3.26d}$$

$$\mathrm{v}(\bar{x}_{\text{ini}0})^T Q_0 \mathrm{v}(\bar{x}_{\text{ini}0}) \leq 1, \tag{3.26e}$$

$$Q_0 \succ 0, \tag{3.26f}$$

$$\mathcal{R}_0 \subseteq \bar{\mathcal{R}}, \tag{3.26g}$$

where Q_V is the optimizer of (3.22). Note that (3.26d) is a matrix equality constraint with polynomial entries. Since $\hat{\Xi}$ is a symmetric matrix, equation (3.26d) results in $\frac{n(n+1)}{2}$ scalar constraints. As $\partial(\mathcal{R}_0) = \partial(V)$, a convex surrogate set and the corresponding objective function are introduced, as outlined in Section 2.1.5, to tractably maximize $\mathcal{R}_0$ for $\partial(\mathcal{R}_0) > 2$. In this case the surrogate set consists of a quadratic sublevel set in terms of the mean modes, $\mathcal{B}_0 = \{\bar{x}_{\text{ini}} | \, \bar{x}_{\text{ini}0}^T B_0 \bar{x}_{\text{ini}0} \leq 1\}$, constrained to remain within $\mathcal{R}_0$. As a result from this procedure the following constraints are added to program (3.26), which as such give a convex optimization of a lower bound on the volume of $\mathcal{R}_0$.

$$\bar{x}_{\text{ini}0}^T B_0 \bar{x}_{\text{ini}0} \leq 1, \tag{3.27a}$$

$$B_0 \succ 0, \tag{3.27b}$$

$$\mathcal{B}_0 \subseteq \mathcal{R}_0. \tag{3.27c}$$

The constraints in (3.26) and (3.27) are polynomial and can, with the same procedure as in the previous subsection for constraints (3.19)-(3.21), first be reformulated to set containment constraints and then to the following generalized SOS program.

$$\max_{s_1,s_2,h_{11}\ldots h_{nn},Q_0,B_0} \quad \det(B_0)^{1/n} \tag{3.28a}$$

subject to:

$$-s_1(\bar{x}_{\text{ini}})(1-\text{v}(\bar{x}_{\text{ini}0})^T Q_0 \text{v}(\bar{x}_{\text{ini}0})) + (1-\text{v}(\bar{x}_{\text{ini}})^T Q_V \text{v}(\bar{x}_{\text{ini}}))+ \\ + \sum_{l=1,k\geq l}^{n} h_{lk}(\bar{x}_{\text{ini}})(\hat{\Xi}_{lk} - \bar{x}_{\text{ini}l_J}^T \Gamma \bar{x}_{\text{ini}k_J}) \quad \in \Sigma[\bar{x}_{\text{ini}}], \tag{3.28b}$$

$$-(1-\bar{x}_{\text{ini}0}^T B_0 \bar{x}_{\text{ini}0}) s_2(\bar{x}_{\text{ini}0}) + (1-\text{v}(\bar{x}_{\text{ini}0})^T Q_0 \text{v}(\bar{x}_{\text{ini}0})) \quad \in \Sigma[\bar{x}_{\text{ini}0}], \tag{3.28c}$$

$$s_1(\bar{x}_{\text{ini}}) \quad \in \Sigma[\bar{x}_{\text{ini}}], \tag{3.28d}$$

$$s_2(\bar{x}_{\text{ini}0}) \quad \in \Sigma[\bar{x}_{\text{ini}0}], \tag{3.28e}$$

$$B_0 \succ 0, \quad Q_0 \succ 0. \tag{3.28f}$$

The vector $\bar{x}_{\text{ini}d_J} := [\bar{x}_{\text{ini}d_1}, ..., \bar{x}_{\text{ini}d_p}]^T$ contains the variance modes of the d-th dimension with $d = 1, ..., n$ and $\Gamma = \text{diag}[\gamma_1, ..., \gamma_p]$. The sum in the second term of (3.28b) represents the scalar equality constraints given by the matrix equality in (3.26d). The polynomials s_1, s_2 are the SOS multipliers, resulting from the Positivstellensatz arguments 2.2, which certify the inequality constraints. The polynomials h_{lk} are indefinite multipliers certifying the equality constraints. The highest monomial degree in $\text{v}(\bar{x}_{\text{ini}0})$ is chosen to be equal to the highest monomial degree of $\text{v}(\bar{x}_{\text{ini}})$ in $V(\bar{x}_{\text{ini}})$. As the constraint (3.28c) involves only the $\bar{x}_{\text{ini}0}$ coordinates, the associated multiplier s_2 contains polynomial terms only in $\bar{x}_{\text{ini}0}$.

Remark 3.3. In the case of $\hat{\Xi} = 0$, i.e., the covariance in the initial state is fixed to zero, $\mathcal{R}_0$ can be obtained directly from the computed estimate $\bar{\mathcal{R}}$ by setting all terms containing variance modes to zero as shown in Algorithm 3.2. This requires no additional optimization problem to be solved.

The program (3.28) has bilinear terms in the SOS multipliers and B_0, respectively Q_0. As for the case of program (3.22), we solve (3.28) iteratively as outlined in Algorithm 3.2. For a nonzero $\hat{\Xi}$, the algorithm is initialized by scaling a unit matrix taken for Q_0 by using bisection until the constraints (3.28b) and (3.28d) are feasible. A feasible initial B_0 is found from a unit matrix scaled by a variable larger than the previous scaling variable for Q_0. Similar to Algorithm 3.1 the algorithm then consists in two steps in which the first finds multipliers for a fixed B_0 and Q_0 by solving a feasibility test, and the second maximizes the size of $\mathcal{B}_0$ over Q_0 while keeping the multipliers fixed. This algorithm terminates after a relative increase in B_0 has fallen below a specified convergence criteria (convCrit_{B_0} in Algorithm 3.2).

Remark 3.4. If $\partial(V) = 2$ then the optimization can be performed to directly minimize

Algorithm 3.2 Maximize $\mathcal{R}_0$ as ROA estimate in terms of the mean modes.

Input: $\partial(s_i)$, $\hat{\Xi}$, convCrit_{B_0}, Q_V result from Algorithm 3.1
Output: Q_0, $\mathcal{R}_0$
procedure MAXSTOCHASTICROAESTIMATE
    Initialization:
    if $\hat{\Xi} = 0$ **then**
        $Q_0 \leftarrow \mathrm{v}(\bar{x}_{\text{ini}0})^T Q_0 \mathrm{v}(\bar{x}_{\text{ini}0}) = \mathrm{v}(\bar{x}_{\text{ini}})^T Q_V \mathrm{v}(\bar{x}_{\text{ini}})\Big|_{\bar{x}_{\text{ini}\,J}=0}$
    else
        $Q_{0\text{ini}} \leftarrow c_1 \cdot \mathbb{I}$, bisect on $c_1 > 0$ until (3.28b), (3.28d) feasible
        $B_{0\text{ini}} \leftarrow c_2 \cdot \mathbb{I}$, for a $c_2 > c_1$ such that (3.28c), (3.28e) feasible
        Iteration:
        $k \leftarrow 0$
        repeat
            $k \leftarrow k + 1$
            Step 1:
                s_1, $h_{11}...h_{nn} \leftarrow$ fix Q_0, B_0, solve (3.28b), (3.28d)
                $s_2 \leftarrow$ fix Q_0, B_0, solve (3.28c), (3.28e)
            Step 2:
                Q_0, $B_0 \leftarrow$ fix s_1, s_2, $h_{11}...h_{nn}$, solve (3.28a)- (3.28c),(3.28f)
        until $\det(B_0)_{k-1} - \det(B_0)_k < \text{convCrit}_{B_0}$

$\det(Q_0)^{1/n}$ without using the surrogate set (cf. Section 2.1.5). This removes the constraints (3.28c) and (3.28e) from the algorithm.

Remark 3.5. The complementary problem of maximizing the allowed covariance in the initial conditions for a fixed mean can be done by inserting the desired fixed matrix Q_0 and moving $\hat{\Xi}$ into the objective. The objective then consists of the convex expression $\det(\hat{\Xi})^{1/n}$ and the resulting problem can be solved without the use of a surrogate set and its associated constraints.

3.2.5 Illustrative examples

The application of the proposed analysis method is illustrated by an uncertain Van-der-Pol system and by the dynamics investigated in [ISM18]. Both dynamics are affected by uncertainty in form of a random variable with a uniform distribution. While the first example locally converges to the zero point for all realizations of the random variable, the dynamics of the second example have an uncertainty-dependent attractive equilibrium point.
A uniform distribution between the boundary values u and v is denoted by $\mathcal{U}(u, v)$. The choice of a uniform distribution is motivated here by the possibility to compare the results to previous studies. However, any other $\mathcal{L}_2$-distribution can be considered using the methods presented. Considering other distributions only requires the computation of the Galerkin tensor (2.31) for the associated polynomial basis.
The numerical results were computed using the collection of scripts which are presented in more detail in Chapter 6, where further details on the numerical implementation can be found.

Uncertain Van-der-Pol dynamics

In the first example, we consider

$$\begin{aligned} \dot{x}_1 &= -x_2, \\ \dot{x}_2 &= -a(\xi)(1 - x_1^2)\, x_2 + x_1, \end{aligned} \tag{3.29}$$

where $a(\xi) \sim \mathrm{Unif}(0.7, 1.3)$ is a random variable depending on the stochastic germ $\xi \sim \mathrm{Unif}(-1, 1)$. Based on this stochastic germ we use the Legendre polynomial basis for the PCE of the dynamics which is the basis associated with uniform probability distributions (see Table 2.1). We expand the dynamics (3.29) in the Legendre basis to obtain the PCE coefficient dynamics

$$\begin{aligned} \dot{\bar{x}}_{1_q} &= \bar{x}_{2_q}, \\ \dot{\bar{x}}_{2_q} &= -\sum_{i,j=0}^{p} \bar{a}_i \bar{x}_{2_j} T_{ijq} + \sum_{i,j,k,l=0}^{p} \bar{a}_i\, \bar{x}_{1_j} \bar{x}_{1_k} \bar{x}_{2_l} T_{ijklq} + \bar{x}_{1_q}. \end{aligned} \tag{3.30}$$

The dynamics (3.30) have an equilibrium point $\bar{x}_{\text{EP}} = 0$ and thus the equilibrium set $\mathcal{I}$ consists of the zero point which shows that the system (3.29) has an uncertainty-independent equilibrium point at $x_{\text{EP}} = 0$. This equilibrium point is locally stable for $a > 0$ and for any fixed $a > 0$ the true region of attraction is given by the unstable limit cycle encircling the equilibrium point which can be obtained by simulation.
The truncation order for a PCE needs to be decided such that Assumption 3.2 is satisfied. This can be achieved by simulating the dynamics of the PCE system for a high truncation order and a range of initial conditions in the region of interest. Since the stochastic modes are convergent with increasing truncation order there will be an order for which the contribution from the higher stochastic modes can in practice be considered negligible. The truncation order is thus chosen such that only the significant modes are captured. In this example, the significance of the first five stochastic modes has been investigated by simulating the dynamics (3.30) for a range of initial conditions in the region of interest. Figure 3.1 shows the evolution of the modes starting from the deterministic initial condition $x_{\text{ini}} = [1, 1.5]$. The figure demonstrates how the stochastic modes for $p > 3$ are practically negligible. Consequently, the truncation was set to $p = 3$ which results in a total of $p + 1 = 4$ modes per dimension.

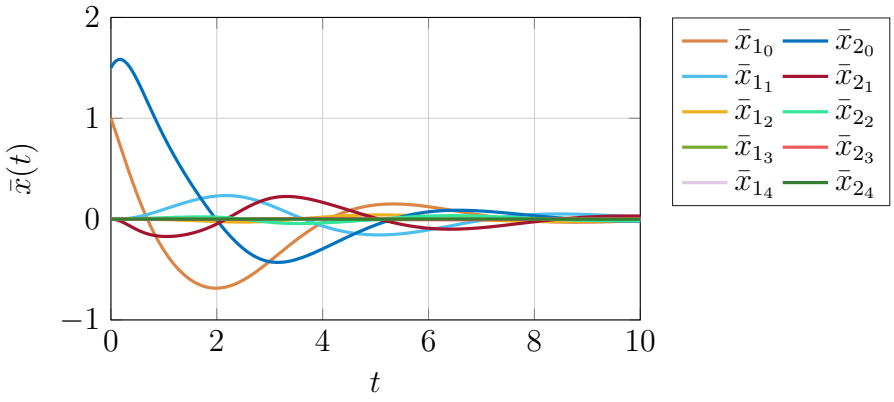

Figure 3.1: Evolution of the stochastic modes in (3.30) starting from the deterministic location $x_{\text{ini}} = [1, 1.5]^T$. All modes eventually converge to zero, which is the equilibrium point of the system.

The set $\bar{\mathcal{R}}$ is computed from the optimization program (3.22) for $\partial(V) = 4$, and the results are used to compute the ROA estimate $\mathcal{R}_0$ as in (3.28) for different values of fixed variance on the initial condition. To this end a diagonal covariance matrix $\hat{\Xi}$ with equal diagonal entries is chosen. The results are presented in Figure 3.2 (right plot). As expected, the $\mathcal{R}_0$ in terms of the initial state of the mean modes decreases with increasing size of variance in the initial state. Additionally, for comparison of different Lyapunov function degrees, the $\mathcal{R}_0$ estimate with zero initial variance for a quadratic V was computed. It can be seen in Figure 3.2 (left plot) how the higher degree V returns larger estimates of the ROA in this case. In each of the cases considered here,

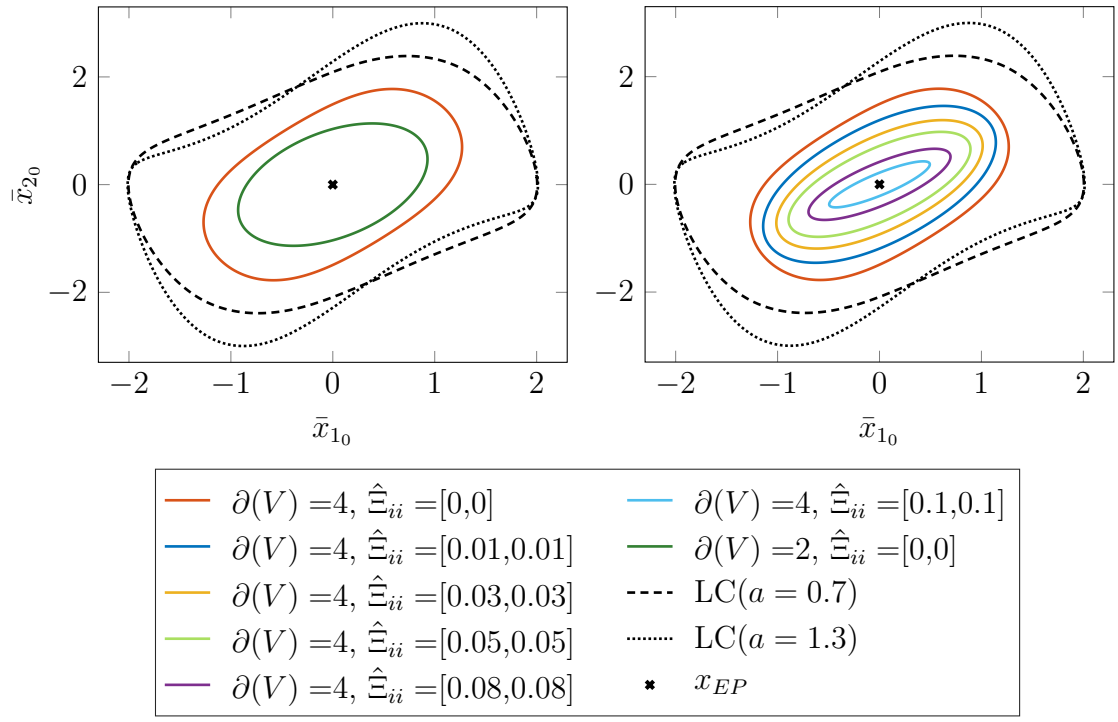

Figure 3.2: *Left plot:* Estimates of $\mathcal{R}_0$ obtained from various degrees of Lyapunov functions V. The set $\mathcal{R}_0$ is chosen in terms of the initial mean states for the case of zero variance on the initial state. *Right plot:* Estimates of $\mathcal{R}_0$ in terms of the initial mean states for various cases of fixed variance on the initial state. In each case an equal variance in both initial coordinate states is considered. The results are obtained from a quartic V. The black dashed and dotted lines show the Van-der-Pol limit cycle trajectory for the extreme values of the uniform distribution of $a(\xi)$. In this example their intersection provides the true ROA of the system, and thus give an indication on the conservativeness associated with the computed inner estimates.

the multiplier degrees were set to $\partial(s_1) = 4$, $\partial(s_2) = 2$ in Algorithm 3.1, and $\partial(s_1) = 0$, $\partial(s_2) = 2$ and $\partial(h) = 2$ in Algorithm 3.2. Both plots in Figure 3.2 further indicate the true ROA of the stochastic system which in this particular example consists of the intersection set encircled by the two limit cycles resulting from using the extreme realizations of the uncertainty to simulate the system.

Dynamics with uncertainty dependent equilibria

In the second example we consider the following uncertain dynamics studied in [ISM18]

$$\begin{aligned} \dot{x}_1 &= -x_2 - \frac{3}{2}x_1^2 - \frac{1}{2}x_1^3 + a(\xi), \\ \dot{x}_2 &= 3x_1 - x_2 - x_2^2, \end{aligned} \tag{3.31}$$

where $a(\xi) \sim \text{Unif}(0.9, 1.1)$ is a random variable depending on the stochastic germ $\xi \sim \text{Unif}(-1, 1)$. This system has two equilibrium points whose location is uncertainty-dependent, and of which one is stable and the other unstable. Using the Legendre polynomial basis, we expand the system similarly to the first example and simulate sample trajectories of the PCE system in order to determine the significant modes as well as the exact location of the stable equilibrium point. In order to decide on the truncation order the same procedure was conducted as in the previous example of the Van-der-Pol. Figure 3.3 shows an example simulation of the stochastic modes of the PCE dynamics. The plot reveals that choosing $p = 2$ captures the significant modes, as well as the location of the equilibrium point, which is found at $\bar{x}_{\text{EP}} = [0.4086,\ 0.7145,\ 0.0369,\ 0.0456,\ \text{-}4.9635\text{e-}04,\ \text{-}0.0012]^T$ for the truncated system.

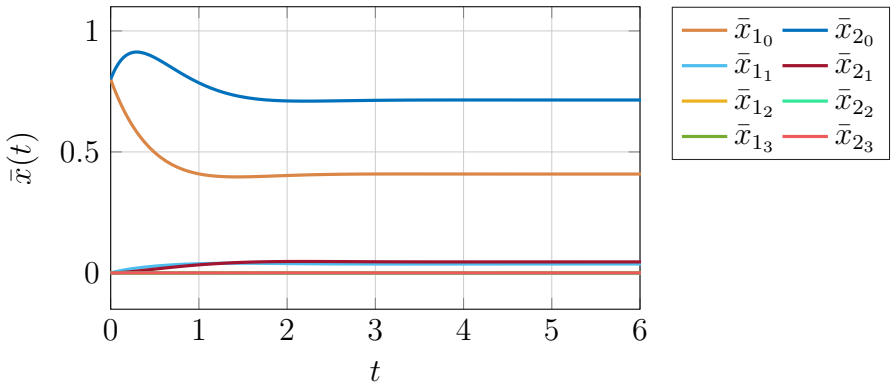

Figure 3.3: Evolution of the stochastic modes in (3.31) starting from the deterministic location $x_{\text{ini}} = [0.8, 0.8]^T$. The simulation reveals the coordinates of the attractive equilibrium point $\bar{x}_{\text{EP}}$ which correspond to the limit values of each coefficient.

As the PCE system has a non-zero equilibrium point, we can numerically obtain from the coefficients the equilibrium set $\mathcal{I}$ of the stochastic system from (2.18). The right plot in Figure 3.4 illustrates this set by showing how trajectories from three different initial states converge to a different equilibrium point for different values of uncertainty. As in the first example, the ROA estimate is computed from (3.22) for a quartic V and the results are used to obtain the ROA $\mathcal{R}_0$ in terms of the mean modes for zero variance on the initial state, as described in Remark 3.3. The multiplier degrees were set to $\partial(s_1) = 4$, $\partial(s_2) = 2$ in Algorithm 3.1.

The $\mathcal{R}_0$ result is shown in the left plot of Figure 3.4. The comparison with the ROA estimates in [ISM18] shows that the approach proposed here provides similar sized estimates of the ROA. To validate the results, we ran a *Monte-Carlo* (MC) simulation of the stochastic system (3.31) for 1000 initial conditions on the boundary of the $\mathcal{R}_0$ for each of 20 realizations of the uncertainty covering the full range of the distribution and confirmed their convergence to the equilibrium set. For illustration, three examples of a MC simulation starting at the boundary of the ROA and using each 8 realizations of the

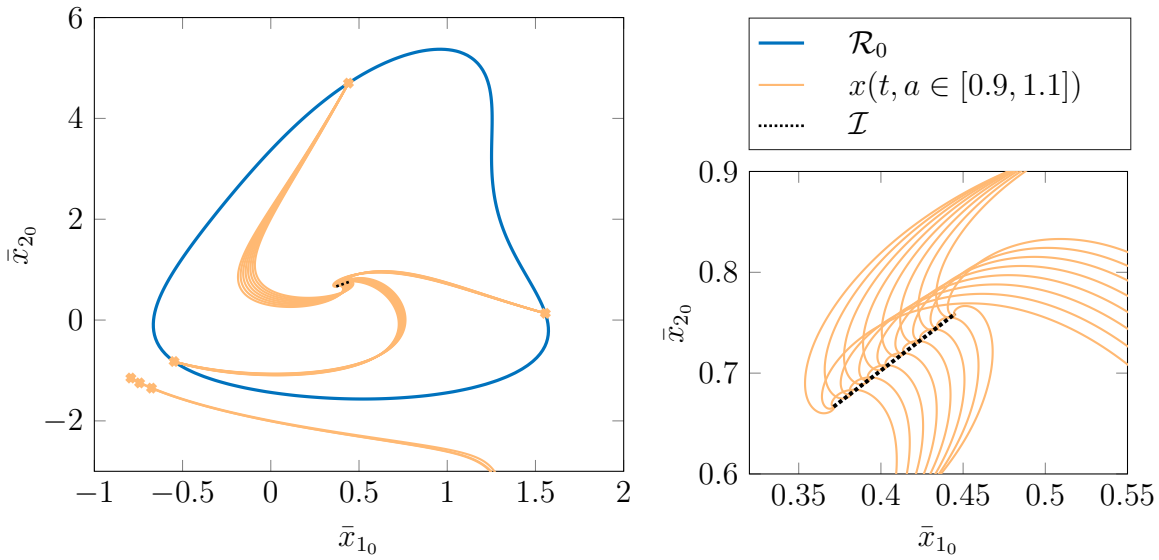

Figure 3.4: *Left plot:* $\mathcal{R}_0$ estimate obtained for the uncertainty-dependent x_{EP} of (3.31). For three initial conditions on the boundary of $\mathcal{R}_0$, a MC simulation of trajectories $x(t)$ of the system for a range of realizations of $a(\xi) \sim \text{Unif}(0.9, 1.1)$ is shown. Note that coming from a MC simulation, these trajectories are deterministic (obtained by sampling random values of the uncertainties in the stochastic dynamics); as for deterministic variables the mean equals the nominal value, $x_{\text{nom}} = \Lambda(x_{\text{nom}})$, the trajectories are plotted here in the mean coordinates $\bar{x}_0$. For the three closest detected initial states with diverging trajectories the worst-case result of the MC simulation is plotted.
Right plot: Close up of the converging trajectories in the left plot. Depending on the realization of uncertainty the trajectories of the system (3.31) converge to different equilibrium points, which together present the equilibrium set as given by Lemma 3.1.

random variable over the distribution range are shown. The true ROA for this system is unknown. In order to obtain an upper bound on the conservativeness of $\mathcal{R}_0$ we search for diverging trajectories by performing MC simulations for a range of initial conditions located in the neighborhood outside of $\mathcal{R}_0$. The closest diverging trajectories found with the chosen sampling grid are shown in Figure 3.4.

3.3 ROA analysis for equilibrium points of feedback controlled stochastic systems

3.3.1 Feedback controlled stochastic systems

In this chapter we turn to the feedback control design for stochastic systems with the objective of maximizing the ROA of the closed loop system. The systems under consideration are continuous time second order random processes with affine input,

$$\dot{x}(t,\xi) = f(x(t,\xi), a(\xi)) + g(x(t,\xi), a(\xi))u(t,\xi), \tag{3.32}$$

where $x \in \mathbb{R}^n$ is the random state variable[1], $u \in \mathbb{R}^l$ is a random input variable, $a \in \mathcal{L}_2(\Theta, \mu; \mathbb{R}^m)$ is a random variable representing the parametric uncertainty, and $f : \mathbb{R}^n \times \mathbb{R}^m \to \mathbb{R}^n$, $g : \mathbb{R}^n \times \mathbb{R}^m \to \mathbb{R}^{n\times l}$ are polynomial functions in x and a. Similar as in Section 3.2.1, we impose Assumption 3.1 to hold, and further, the initial state of (3.32) is random, $x(t=0) = x_{\text{ini}}(\xi)$, with dependence on the same stochastic germ.

The control law is based on the state feedback policy,

$$u(t,\xi) = Kh(x(t,\xi)), \tag{3.33}$$

where $h(x(t,\xi)) : \mathbb{R}^n \to \mathbb{R}^k$ is a vector with entries consisting of polynomials of the components of $x(t,\xi)$, and $K \in \mathbb{R}^{l\times k}$ is the feedback gain matrix. The objective of the feedback control is to stabilize the system around an equilibrium point x_{EP}, whose location can be dependent of the uncertainty affecting the system. As in the previous section, an equilibrium set $\mathcal{I}$ as in Definition 3.1 is thus considered.

Let the closed loop system be denoted by

$$\dot{x}_{\text{cl}} = f_{\text{cl}} = f(x(t,\xi), a(\xi)) + g(x(t,\xi), a(\xi))Kh(x(t,\xi)), \tag{3.34}$$

and let $\psi_{\text{cl}}(t, \xi, x_{\text{ini}}(\xi))$ denote the solution of (3.34) at time t with initial condition $x_{\text{ini}}(\xi)$.

Stochastic ROA of feedback-controlled equilibrium point

The region of attraction of the equilibrium set $\mathcal{I}$ of the closed loop system (3.34) is defined similarly to the definition of the stochastic ROA for autonomous systems in Section 3.2.1.

Definition 3.5 (Stochastic ROA of $\mathcal{I}$)**.** *The ROA of the equilibrium set $\mathcal{I}$ of a feedback controlled system (3.34) is defined as the set of initial conditions*

$$\mathcal{R}^* = \{x_{ini} \in \mathbb{R}^n \,|\, \mathbb{P}[\lim_{t\to\infty} d(\psi_{cl}(t,\xi,x_{ini}), \mathcal{I}) = 0] = 1\}, \tag{3.35}$$

where $\mathbb{P}$ denotes probability, and dist *is the distance measured in a norm of choice.*

[1] Again, the simplified notation introduced in Section 3.2.1 is used.

PCE representation of the controlled stochastic system

Using the PCE framework presented in Section 2.2, the PCE representation of system (3.32) is denoted by

$$\dot{\bar{x}} := \bar{f}(\bar{x}) + \bar{g}(\bar{x})\bar{u}, \tag{3.36}$$

where $\bar{x} \in \mathbb{R}^{n(p+1)}$, $\bar{u} \in \mathbb{R}^{l(p+1)}$ are the vector of PCE coefficients of state x and input u, and $\bar{f}, \bar{g} : \mathbb{R}^{n(p+1)} \times \mathbb{R}^{l(p+1)} \to \mathbb{R}^{n(p+1)\times l(p+1)}$ the PCE system dynamics.

Assumption 3.2 is also assumed to hold for the PCE system (3.36).

3.3.2 Stability connection between PCE and feedback-controlled stochastic system

As shown in Section 3.2, an estimate of the ROA of the equilibrium set $\mathcal{I}$ of a stochastic system can be obtained from an estimate of the ROA of the equilibrium point $\bar{x}_{\mathrm{EP}}$ of the PCE system. The objective of the control design presented in the following, is to obtain a control law maximizing the ROA of the stochastic system. This is achieved by aiming at maximizing the ROA of the PCE system. We introduce a version of Theorem 3.2 which now gives an inner estimate of the ROA of the controlled PCE system (3.36).

Theorem 3.3. *Let $\bar{D} \subset \mathbb{R}^{n\cdot(p+1)}$ be a compact domain containing $\bar{x}_{EP}$. If there exists a continuously differentiable function $V(\bar{x}) : \bar{D} \to \mathbb{R}$ such that*

$$V(\bar{x}) > 0 \quad \forall \bar{x} \in \bar{D}\backslash\{\bar{x}_{EP}\}, \qquad V(\bar{x}_{EP}) = 0, \tag{3.37}$$

$$\dot{V}_{cl}(\bar{x}) = \frac{\partial V(\bar{x})}{\partial \bar{x}} \bar{f}_{cl}(\bar{x}) < 0 \quad \forall \bar{x} \in \bar{D}\backslash\{\bar{x}_{EP}\}, \tag{3.38}$$

then $\bar{x}_{EP}$ is asymptotically stable and $V(\bar{x})$ is a Lyapunov function of the system (3.36). If these conditions are satisfied for all $\bar{x}$ in a sublevel set

$$\bar{\mathcal{R}} = \{\bar{x} \in \bar{D} \,|\, V(\bar{x}) \leq \beta\}, \tag{3.39}$$

where β is a positive scalar and $\bar{\mathcal{R}} \subseteq \bar{D}$, then $\bar{\mathcal{R}}$ is an inner estimate of the ROA of $\bar{x}_{EP}$.

With an obtained set $\bar{\mathcal{R}}$ an inner estimate of the ROA of (3.35) can be retrieved from Lemma 3.2 for a fixed variance on the initial conditions, as outlined in Section 3.2.4.

3.3.3 Feedback control design

The stochastic controller (3.33) is considered with the aim of obtaining a state feedback law maximizing the ROA. The approach offers flexibility in choosing the explicit expression of the state function $h(x(t,\xi))$ which is a vector of desired polynomials in $x(t,\xi)$.

Stochastic state feedback law

We use the stochastic state feedback law (3.33) and focus on the design of the gain matrix K as well as the state vector $h(x(t,\xi))$. A linear version of this feedback law has been used in [FB09] for the design of a *Linear Quadratic Regulator* (LQR). Since in this work we are dealing with nonlinear systems, the control law can contain polynomials in the state vector.

As the control design proposed here considers the PCE of the closed loop system, the control law (3.33) needs to be expanded. Note that by considering the PCE system in the control design task, the stochastic information on x is directly exploited in the computation of K. Expanding the control law (3.33) in the PCE framework as in equation (2.18) results in

$$\bar{u}_{i_j} = \gamma_j^{-1} \langle K_i h(x), \Phi_j(\xi) \rangle, \tag{3.40}$$

where $i = 1, ..., l$, $j = 0, ..., p$ and K_i is the i-th row vector of K. Note that the dimension of K depends only on the dimension of the stochastic input and the stochastic vector $h(x)$, and is independent on the truncation order p of the PCE.

Remark 3.6. There are other possibilities for feedback laws, e.g., where the input is considered deterministic, or where K is a random variable (see, e.g., [FB09]). The approach proposed here can be used for other feedback laws as well, however in applications these laws require knowledge of the current probability density function of the state vector. While for linear systems there exist well-established state estimation techniques providing the probability density of the state, estimates of the probability density are harder to obtain for uncertain nonlinear systems. Thus, we limit our focus to the stochastic state feedback law.

Remark 3.7. In this work we are assuming that x_{EP} is a locally stable (uncertainty-dependent) equilibrium point and the control design only aims at maximizing the ROA. The approach also remains valid in principle if x_{EP} is unstable. This is done by first stabilizing x_{EP} with standard techniques (e.g., feedback linearization) and then applying the design scheme proposed here to increase the ROA of the stabilized system.

Input constraints

For the stochastic control law, input limits can be imposed with the aim of obtaining a controller which maximizes the certified ROA while respecting the system's physical constraints. As the analysis deals with PCE systems, the constraints need to be expressed in terms of PCE coefficients. Let the constraints on the stochastic input be

$$u^L \leq u(t,\xi) \leq u^U. \tag{3.41}$$

Due to the stochastic nature of u, the constraints are expressed in terms of the statistical properties of the input, which are provided by the PCE. More precisely, we consider

the mean with the addition of one standard deviation of the control input[2], given by equations (2.21) and (2.22) applied to the stochastic signal u, and constrain these to remain within specified limits. This results in

$$\begin{aligned} u^L &\leq \bar{u}_0 - \sigma, \\ u^U &\geq \bar{u}_0 + \sigma, \end{aligned} \tag{3.42}$$

with

$$\sigma_i := \left(\sum_{j=1}^{p} \bar{u}_{i_j}^2 \gamma_j \right)^{\frac{1}{2}}, \tag{3.43}$$

for each component $i = 1, .., l$ in of the input u. Note that due to the square root, equation (3.42) does not result in a polynomial expression. As the design method proposed here hinges on both the constraints to be in polynomial form and the matrix K to only appear linearly, we introduce the following relaxation of (3.42). Since γ_j is positive by definition, each term in the summation in (3.43) is positive and thus the following holds

$$\left(\sum_{j=1}^{p} \bar{u}_j^2 \gamma_j \right)^{\frac{1}{2}} \leq \sum_{j=1}^{p} |\bar{u}_j| \gamma_j^{\frac{1}{2}}. \tag{3.44}$$

The right-hand side of (3.44) provides an upper bound on the standard deviation of u. By considering the maximum negative and maximum positive realizations of $\bar{u}_j$ separately, the right-hand side of (3.44) can be expressed as two polynomial constraints, which will be explained in more detail in the following section.

Remark 3.8. Note that if the uncertainty distribution has finite support (as assumed here and is usually the case in control applications) then the constraints in (3.42) impose hard constraints on the input. In the more general case of uncertainty distribution with infinite support the constraint violations cannot be excluded due to the tails of the distributions. In that case the constraints as formulated here would have primarily the effect of penalizing the input magnitude.

3.3.4 Algorithm for computing K while maximizing ROA

In this section we show how the stochastic control law (3.33) is computed such that the ROA of the closed loop system (3.34) is maximized. Outlines of the algorithmic implementation of the computations are provided for both unconstrained and constrained input cases.

[2]The addition of two or three standard deviations could be equally well considered

Maximizing ROA over K

Leveraging the stability criteria stated in Theorem 3.3, the following nonlinear optimization problem can be formulated for the computation of the matrix K and concurrent maximization of the PCE ROA inner estimate $\bar{\mathcal{R}}$.

$$\max_{V(\bar{x}),K} \quad \text{vol}(\bar{\mathcal{R}}(\bar{x})) \tag{3.45a}$$

$$\text{subject to} \quad V(\bar{x}) > 0,\, V(0) = 0, \tag{3.45b}$$

$$\dot{V}_{\text{cl}} = \frac{\partial V(\bar{x})}{\partial \bar{x}} \bar{f}_{\text{cl}}(\bar{x}, K) < 0, \tag{3.45c}$$

$$u^L \leq \bar{u}(\bar{x}, K) \leq u^U, \tag{3.45d}$$

where we use $V = \text{v}(\bar{x})^T Q_V \text{v}(\bar{x})$ with $\text{v}(\bar{x})$ being the vector of monomials in $\bar{x}$ up to a chosen degree, and $\bar{\mathcal{R}}$ as defined in (3.39). Constraint (3.45d) is only present if there are input constraints.

Algorithmic implementation

All constraints in the optimization program (3.45) are polynomial. Similar to the algorithmic approach chosen in the previous chapter in Section 3.2.4 we use the results of the Positivstellensatz presented in Section 2.1.3 and formulate the constraints in (3.45) as semialgebraic set containment conditions. Using Lemma 2.1 the conditions are then turned into a generalized SOS program. In order to obtain a convex expression for the cost function, also here a surrogate set as explained in Section 2.1.5 is employed. In this case, the surrogate set consists in a quadratic form $b(\bar{x}) := \bar{x}^T B \bar{x}$ with the sublevel set $\mathcal{B} = \{\bar{x} | \, b(\bar{x}) \leq 1\}$. By imposing the constraint $\mathcal{B} \subseteq \bar{\mathcal{R}}$, maximizing over the volume of $\mathcal{B}$ leads to a maximization of $\bar{\mathcal{R}}$. The stochastic input constraint (3.42) is represented through the upper bound in (3.44). For the implementation of the absolute value in a polynomial constraint, additional steps are required which are presented in the following. For a computed K, let c_j be the maximum absolute value of the j-th term in the right hand side of (3.44) over all $\bar{x}$ in the sublevel set β of V. Then the input constraint (3.42) can be written as

$$u^L \leq \bar{u}_0(t) - \sum_{j=1}^{p} c_j, \quad u^U \geq \bar{u}_0(t) + \sum_{j=1}^{p} c_j. \tag{3.46}$$

For clarity of presentation a single input u is considered. Also, the sublevel set size β is fixed to 1 as optimization over β is redundant with optimizing over Q_V. Assuming without loss of generality $\bar{x}_{\text{EP}} = 0$ (see the shift proposed in (3.17)), we obtain the

following optimization program.

$$\max_{V,K,B,s_i,c_j} \quad -\det(B)^{1/n(p+1)} \tag{3.47a}$$

$$\text{subject to} \quad V(\bar{x}) - l(\bar{x}) \in \Sigma[\bar{x}], \tag{3.47b}$$

$$-s_1(\bar{x})(1-b(\bar{x})) - (1-V(\bar{x})) \in \Sigma[\bar{x}], \tag{3.47c}$$

$$-\dot{V}_{\text{cl}}(\bar{x},K) - s_2(\bar{x})(1-V(\bar{x})) - l(\bar{x}) \in \Sigma[\bar{x}], \tag{3.47d}$$

$$-s_3(\bar{x})\left(\bar{u}_0(\bar{x},K) + \sum_{j=1}^{p} c_j - u^U\right) - s_4(\bar{x})(1-V(\bar{x})) \in \Sigma[\bar{x}], \tag{3.47e}$$

$$-s_5(\bar{x})\left(u^L - \left(\bar{u}_0(\bar{x},K) - \sum_{j=1}^{p} c_j\right)\right) - s_6(\bar{x})(1-V(\bar{x})) \in \Sigma[\bar{x}], \tag{3.47f}$$

$$\text{for each } j: \quad s_7(\bar{x})(c_j - \bar{u}_j(\bar{x},K)\gamma_j^{\frac{1}{2}}) - s_8(\bar{x})(1-V(\bar{x})) \in \Sigma[\bar{x}], \tag{3.47g}$$

$$s_9(\bar{x})(c_j + \bar{u}_j(\bar{x},K)\gamma_j^{\frac{1}{2}}) - s_{10}(\bar{x})(1-V(\bar{x})) \in \Sigma[\bar{x}], \tag{3.47h}$$

$$s_{i,i=1,\dots(6+4p)}(\bar{x}) \in \Sigma[\bar{x}], \tag{3.47i}$$

where the multipliers $s_i(\bar{x}), i = 1,..,(6+4p)$ are the SOS polynomials certifying the solution of the program to adhere to the constraints (cf. Lemma 2.1). Similarly, the terms $l(\bar{x}) = \epsilon \bar{x}^T \bar{x}$, $\epsilon \ll 1$, in (3.47b) and (3.47d) which guarantee that $\bar{x} = 0$ is not included in the constrained set. Constraint (3.47c) ensures the containment of the surrogate set in the sublevel set of the Lyapunov function. The constraints (3.47e)-(3.47h) enforce the input constraints on the computation of K and $\bar{\mathcal{R}}$. Note that for each PCE coefficient of u there are two additional constraints (3.47g)-(3.47h), leading to four additional multipliers and thus making the total amount of multipliers dependent on the truncation order p. In the implementation, the variables c_j are 'measures' of the maximum absolute values of both the positive and negative values of $\bar{u}_j\gamma_j^{\frac{1}{2}}$ over all $\bar{x}$ in $\bar{\mathcal{R}}$ and add, respectively subtract, them from the mean value $\bar{u}_0$. Constraints (3.47e)-(3.47f) then ensure (3.46). In the case of no input constraints the optimization program only includes (3.47a)-(3.47d) and (3.47i).

The optimization (3.47) is a generalized SOS program due to bilinearly appearing decision variables in the terms containing both V and s_i, b and s_i, c_j and s_i, V and K, and K and s_i. To circumvent the bilinearities and obtain convex constraints, similar to the algorithms in Section 3.2.4, an iterative scheme is proposed consisting of an iterative loop over three steps. A pseudocode of the iteration steps is shown in Algorithm 3.3. The program returns both the matrix K as well as the corresponding ROA estimate $\bar{\mathcal{R}}$. The algorithm is initialized by finding a suitable Lyapunov function, e.g., from the linearization of the system around $\bar{x}_{\text{EP}}$ with $K = 0$, solving the Lyapunov equation (3.24), and scaling the result appropriately. An initial surrogate set size is obtained by choosing an initial diagonal B-matrix with entries sufficiently large. The initial K can be taken as a matrix with small nonzero or with zero entries. The iteration over the three steps is then

concerned with maximizing the surrogate set, i.e., the ROA estimate, while searching for appropriate K values. In particular, Step 1 consists in finding multipliers for the current Q_V, B and K. Since for fixed Q_V, K and B each of the constraints (3.47c)-(3.47h) is independent of the others, the multipliers s_i can be found by solving a feasibility test separately for each constraint. In Step 2, the obtained s_i are fixed together with Q_V and B and K is optimized for while allowing the c_j to vary. In Step 3 the surrogate set volume is maximized over Q_V while the multipliers, K and c_j are fixed. Note, that in the case of no constraints on the input, constraints (3.47e)-(3.47i) including the variables c_j are omitted from Steps 1-3. The iteration terminates when a predefined convergence criteria on the size of the surrogate set (convCrit_B in Algorithm 3.3) is reached.

Algorithm 3.3 Find control to maximize ROA

Input: p, $\partial(s_i)$, $\partial(V)$, convCrit_B, $h(\cdot)$, u^L/u^U
Output: K ,V
procedure MAXROAESTIMATE
    $\bar{f}_{\text{cl}}(\bar{x}, K) \xleftarrow{\text{PCE}} f(x, a, u)$
    Initialization:
    set $K = 0$
    $Q_{V\,\text{ini}} \leftarrow Q$, solution of (3.24) with $\bar{A} = \frac{\partial \bar{f}(\bar{x})}{\partial \bar{x}}\Big|_{\bar{x}_{\text{EP}}}$
    choose B small enough such that (3.47c) is feasible
    $K_{\text{ini}} \leftarrow \ll 1$ (or zero)
    Iteration:
    $k \leftarrow 0$
    repeat
        $k \leftarrow k + 1$
        Step 1: $s_i \leftarrow$ fix Q_V, B, K, c_j, solve (3.47c)-(3.47i)
        Step 2: K, $c_j \leftarrow$ fix Q_V, s_i, solve (3.47d)-(3.47h)
        Step 3: Q_V, $B \leftarrow$ fix s_i, K, c_j, solve (3.47)
    until $\det(B)_{k-1} - \det(B)_k < \text{convCrit}_B$

Recovering $\mathcal{R}$ from $\bar{\mathcal{R}}$

Algorithm (3.3) returns $\bar{\mathcal{R}}$ which describes a set in terms of the PCE coefficients $\bar{x}$. In order to obtain from $\bar{\mathcal{R}}$ an inner estimate $\mathcal{R}$ of the true ROA of the stochastic system, $\mathcal{R}^*$, the optimization program proposed in Section 3.2.4 is used. This program computes $\mathcal{R}$ from the $\bar{\mathcal{R}}$ estimate by specifying the stochastic properties of the initial conditions. In the following examples we set the variance of the initial state to zero and thus $\mathcal{R}$ is obtained in terms of the mean of the initial state. As mentioned in Remark 3.3, this

gives the computation of $\mathcal{R}$ directly from the Lyapunov sublevel set representing $\bar{\mathcal{R}}$ by setting all PCE coefficients of the variance modes in $\bar{\mathcal{R}}$ to zero.

3.3.5 Illustrative examples

We demonstrate the proposed control design on two examples. Both stochastic systems are open loop stable and a feedback control will be used to enlarge the ROA. In order to benchmark our approach, we compare it, firstly, with the ROA estimate computed for the open loop system. The open loop ROA estimate is thereby obtained from applying the ROA computations outlined in Section 3.2.4. Secondly, we compare our approach with one of the few available PCE based control algorithms which consists in a LQR control design proposed in [FB09] for the PCE of a *linear* stochastic systems. For the LQR control the example dynamics presented here are linearized around their equilibrium point and the feedback law "stochastic state feedback with constant deterministic gain" in [FB09], Sec. 5.2.2, is applied. The control design proposed therein results in a *bilinear matrix inequality* (BMI). This is solved here using PENLAB [FKS13] which returns the LQR values for the gain matrix. In order to obtain the ROA of the LQR controlled system, the open loop ROA computations are applied to the LQR controlled closed loop system.
Note that in contrary to the illustrative results shown in the previous Section 3.2.5, the $\mathcal{R}$ results in this section are shown in the original x coordinates. This is because for the examples shown here a zero variance on the initial condition is assumed. Since in the case of zero variance the initial states are deterministic, it follows that the mean equals just the deterministic value, $x_{\text{det}} = \bar{x}_0$.

The numerical results were computed using the collection of scripts which are presented in Chapter 6, where further details on the numerical implementation can be found.

2D stochastic dynamics

The first example considers the dynamical system from [Che04a], p. 146, with modifications to introduce uncertainty,

$$\begin{aligned} \dot{x}_1 &= -x_1 + x_2 - a(\xi)(x_1^2 + x_2^3) + x_1 u, \\ \dot{x}_2 &= -2x_2 - a(\xi)x_1^2 + u, \end{aligned} \tag{3.48}$$

where $a(\xi)$ is a random variable coming from a uniform distribution, $a(\xi) \sim \mathcal{U}(0.8, 1.2)$ with $\xi \sim \mathcal{U}(-1, 1)$. The Legendre polynomials, associated with uniform distributions, are used for the PCE. The closed loop system is analyzed and compared for two choices

of h which differ in the degree of the polynomial entries,

$$\begin{aligned} h_{(1)} &= [x_1, x_2]^T, \quad &\longrightarrow \quad K_{(1)} \in \mathbb{R}^2 \\ h_{(2)} &= [x_1, x_2, x_1^2, x_1x_2, x_2^2]^T, \quad &\longrightarrow \quad K_{(2)} \in \mathbb{R}^5. \end{aligned} \tag{3.49}$$

In this example the input is unconstrained. In order to decide on a truncation order of the PCE we simulate the evolution of the stochastic modes of the system for a large p starting from various initial conditions in the region of interest and then set p such that it captures the significant modes. Here, $p = 2$, i.e., there are three significant modes for each state dimension, which results in a six-dimensional deterministic system. The equilibrium point is uncertainty independent.

Figure 3.5 (left plot) shows the ROA estimates $\mathcal{R}$ for open loop dynamics and the closed loop systems using $h_{(1)}$. The estimates are computed for both cases for a quadratic and quartic Lyapunov function to compare the effect of its order. It can be seen that the feedback control is able to largely increase $\mathcal{R}$ compared to the uncontrolled system. Further, for both open and closed loop system the higher order Lyapunov function results in a larger ROA estimate.

Figure 3.5 (right plot) provides a comparison of the $\mathcal{R}$ estimates obtained for the control law (3.33) with each $h_{(1)}$ and $h_{(2)}$ as in (3.49), and the LQR. A quadratic Lyapunov function was considered in each case. The controllers based on (3.33) result in significantly larger ROA estimates than the LQR. It is stressed that these improvements on the ROA are mainly due to the fact that a nonlinear control design formulation is employed, rather than due to the adoption of a polynomial basis for h. This is shown by the case of $h_{(1)}$ which is a linear state vector and significantly outperforms the LQR. The $\mathcal{R}$ estimate for the LQR controlled system found for this example shows an improvement over the $\mathcal{R}$ estimate for the open loop system. It is, however, small compared to the nonlinear controllers. Note that since the BMI has, in general, local optima and the obtained solution depends on the initialization, the LQR-$\mathcal{R}$ results shown here are not unique results. In each of the cases considered here, the multiplier degrees were set to $\partial(s_1) = 2$ and $\partial(s_2) = 4$.

Short period aircraft dynamics

The second example consists of the 2-D aircraft short period dynamics from [CSB11]. While in this reference the dynamics are nominal, two uncertain parameters affecting the nonlinear part of the system are considered here. With x_1 representing the angle of attack (in radians) and x_2 the pitch rate (in radians/seconds), the dynamics are given

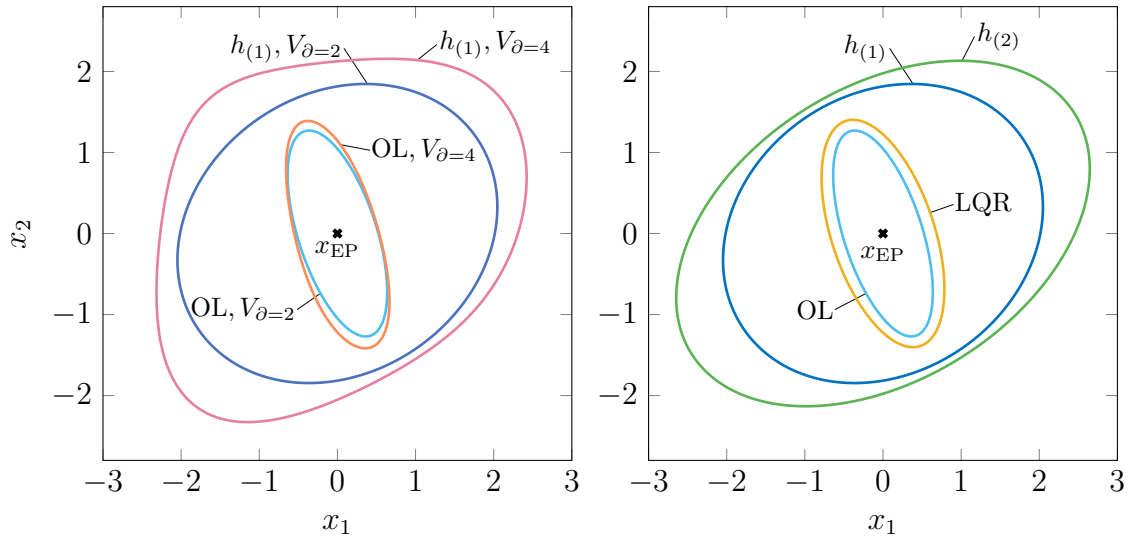

Figure 3.5: *Left plot:* $\mathcal{R}$ estimates obtained for the open loop (OL) and closed loop system using the state feedback vector $h_{(1)}$ in (3.33). The estimates were computed using each a quadratic ($V_{\partial=2}$) and a quartic ($V_{\partial=4}$) Lyapunov function. *Right plot:* $\mathcal{R}$ estimates for the open loop (OL), LQR controlled and the two closed loop systems for each state feedback vector $h_{(1)}$ and $h_{(2)}$. The results are obtained from a quadratic V.

by

$$\begin{aligned}\dot{x}_1 &= a_1(\xi)(-1.492x_1^3 + 4.239x_1^2 + 0.003x_1x_2 + 0.006x_2^2) - \\ &\quad - 3.236x_1 + 0.923x_2 + (-0.317 + 0.240x_1)u, \\ \dot{x}_2 &= a_2(\xi)(-7.228x_1^3 + 18.36x_1^2 + 1.103x_2^3) - \\ &\quad - 45.34x_1 - 4.372x_2 + (-59.99 + 41.5x_1)u,\end{aligned} \tag{3.50}$$

where $a_1(\xi) \sim \mathcal{U}(0,2)$ and $a_2(\xi) \sim \mathcal{U}(0.5,1.5)$, with $\xi \sim \mathcal{U}(-1,1)$, are random variables from a uniform distribution. The input u represents the elevator deflection (in radians). A truncation order of $p = 2$ is found to capture the significant modes. Further, the vector $h = [x_1, x_2]^T$ is chosen for the control law (3.33). The equilibrium point of this system is uncertainty independent.

The dynamics (3.50) in their nominal form with $a_1 = 1$, $a_2 = 1$, are open loop stable. To investigate the effects of uncertainty and feedback control on the stability of the system, first the ROA for both the nominal open loop dynamics, OL$_n$-$\mathcal{R}$, and the stochastic open loop dynamics, OL$_s$-$\mathcal{R}$, were computed. Figure 3.6 reveals a significant decrease of the ROA of the stochastic system compared to the nominal. Algorithm 3.3 was then used to compute the closed loop system's ROA (CL-$\mathcal{R}$), and the corresponding gains where no input constraints were considered. Figure 3.7 shows the ROA estimates OL$_n$-$\mathcal{R}$, OL$_s$-$\mathcal{R}$, and CL-$\mathcal{R}$. The results for CL-$\mathcal{R}$ reveal that the controller is able to stabilize the stochastic closed loop system such that the feedback not only counteracts the uncertainty but further enlarges the ROA. For two initial conditions x_{ini}^a and x_{ini}^b,

with x^a_{ini} located outside of OL$_s$-$\mathcal{R}$ and inside OL$_n$-$\mathcal{R}$, and x^b_{ini} located outside OL$_n$-$\mathcal{R}$ and inside CL-$\mathcal{R}$ a MC simulation was run for 5 realizations of each a_1 and a_2 over the range of their distributions. The MC simulation was thereby performed for both the open loop stochastic system (x_{ol}) and the closed loop system (x_{cl}). The trajectories exemplify the destabilizing effect of the uncertainty on the system and the ability of the controller to stabilize the system for all realizations of the uncertainty.

In the left plot of Figure 3.8, the result of a MC simulation of the closed loop system states and input for an initial condition inside CL-$\mathcal{R}$ for 10 realizations of each a_1 and a_2 over the range of their distributions is shown. The plot reveals input magnitudes exceeding by far the physical limits of ± 0.5 rad for the elevator deflection. We thus impose the constraints $-0.5 \text{ rad} \leq u(\xi, t) \leq 0.5$ rad and recalculate both the $\mathcal{R}$ estimate and resulting feedback gains from Algorithm 3.3. Figure 3.9 shows the estimates OL$_s$-$\mathcal{R}$, CL$_{u\in\mathbb{R}^l}$-$\mathcal{R}$ for the input unconstrained CL system, CL$_{u^L\leq u\leq u^U}$-$\mathcal{R}$ for the input constrained CL system and additionally the CL-$\mathcal{R}$ obtained for the LQR controlled system for comparison as in the previous example.

The comparison of CL$_{u\in\mathbb{R}^l}$-$\mathcal{R}$ and CL$_{u^L\leq u\leq u^U}$-$\mathcal{R}$ shows how the ROA estimate shrinks for the constrained case relative to the unconstrained. In this example the ROA estimate found for the LQR controlled (naturally unconstrained) system is able to increase the ROA largely beyond OL$_s$-$\mathcal{R}$, it is however still significantly smaller than CL$_{u\in\mathbb{R}^l}$-$\mathcal{R}$. The right plot in Figure 3.8 illustrates how the constrained input for the same initial condition and range of uncertainties as for the unconstrained input (left plot) now remains within the prescribed bounds for all realizations of the uncertainty over the given range.

In all computations of the ROA estimates without input constraints, the degrees of the multiplier were set to $\partial(s_1) = 4$, $\partial(s_2) = 2$. These multiplier degrees were kept for the case with input constraints, where additionally $\partial(s_{3,5,7,9}) = 2$ and $\partial(s_{4,6,8,10}) = 0$.

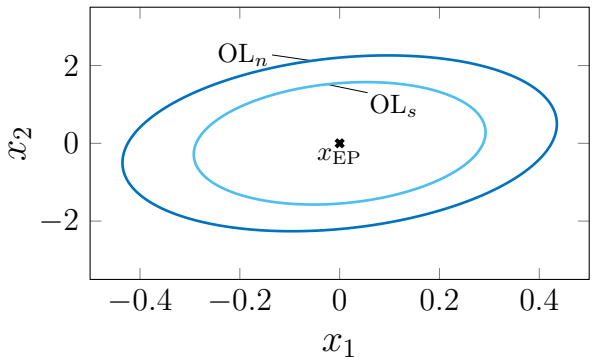

Figure 3.6: $\mathcal{R}$ estimates obtained for the nominal open loop (OL$_n$) and stochastic open loop (OL$_s$) system, revealing the detrimental effect of the uncertainty on the *ROA* of the system (3.50), computed from a quadratic V.

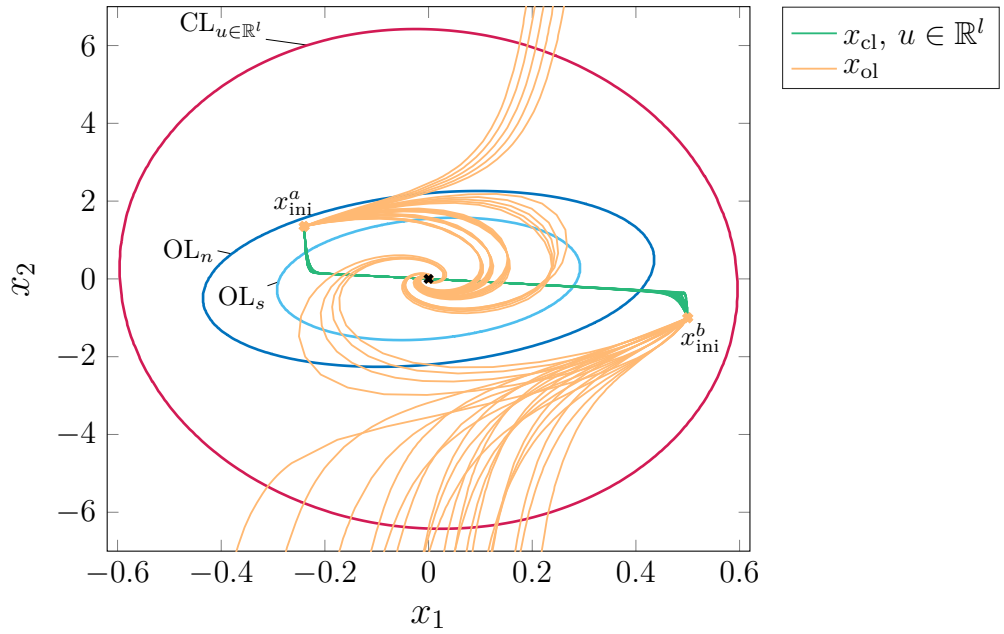

Figure 3.7: $\mathcal{R}$ estimates obtained for the nominal open loop (OL_n), stochastic open loop (OL_s) and unconstrained closed loop ($\mathrm{CL}_{u\in\mathbb{R}^l}$) system, computed from a quadratic V. Trajectories obtained from a MC simulation of the OL_s and CL system for each 5 realizations of $a_1 \sim \mathcal{U}(0,2)$ and $a_2 \sim \mathcal{U}(0.5,1.5)$ are shown for two initial conditions x^a_{ini} and x^b_{ini}. According to the fact that both x^a_{ini} and x^b_{ini} being located outside of OL_s-$\mathcal{R}$, for certain realizations of a_1 and a_2 diverging trajectories are found. As they are, however, located inside of $\mathrm{CL}_{u\in\mathbb{R}^l}$-$\mathcal{R}$, the unconstrained controller is able to stabilize the trajectories for all realizations of a_1 and a_2.

3.4 Conclusions

In the first part of this chapter we present a method to compute inner estimates of the ROA of stochastic nonlinear systems. The proposed method is applicable to a broad class of system consisting of second order random processes which are affected by uncertainties coming from any $\mathcal{L}_2$-distribution and which are further allowed to have uncertainty-dependent equilibria. The analysis is enabled by using PCE through which a stochastic ordinary differential equation is converted into a deterministic one. Using suitable stability notions in the form of moment boundedness and Lyapunov stability, it is shown how the ROA analysis of the PCE system offers direct information on the attractive behavior of the stochastic system for which a notion of a ROA is derived. A numerical implementation for obtaining inner estimates of the ROA when the PCE system has a polynomial expression are provided via SOS optimization. The application to two examples taken from the literature shows that the proposed approach provides estimates of the ROA which are comparable to literature results obtained with less general

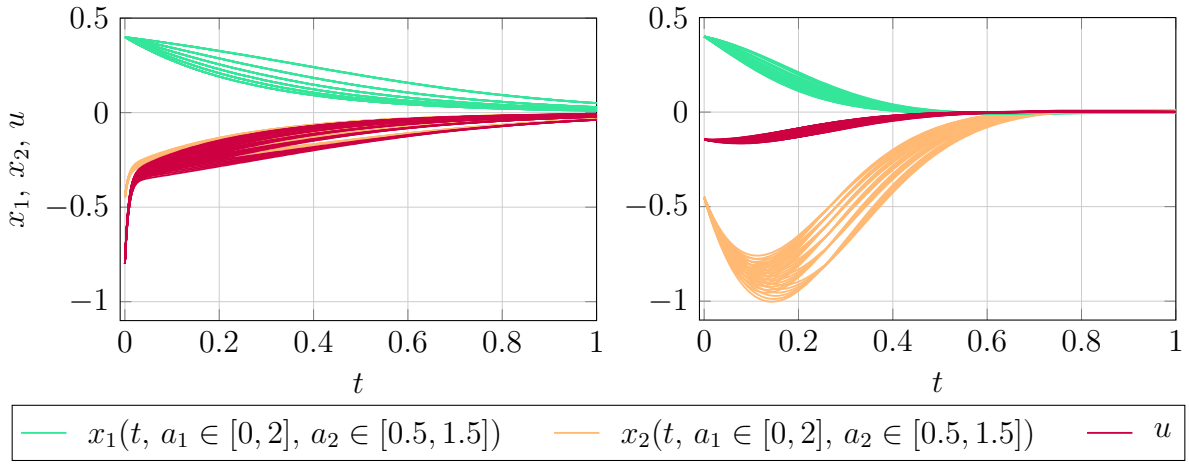

Figure 3.8: *Left plot:* Closed loop system trajectories of the states and input starting from the deterministic initial condition $x = [0.4; -0.45]$ and for 10 different uncertainty realizations of each uncertain parameter a_1, a_2 covering the whole range of both distributions (resulting in 100 trajectories per plotted quantity). The feedback gains resulted from unconstrained input computations. The time axis zero point has a slight offset to better visualize the evolution at the starting point.
Right plot: Same simulation configuration as in the left plot, but here using the feedback gains resulting from input constraints at $u^L = -0.5$ rad, $u^U = 0.5$ rad.

methods.

An extension of the developed method in the first part is presented in the second where a method to obtain feedback gains which maximize an inner estimate of the ROA of a stochastic closed loop system is proposed. To this end, the PCE framework is employed to represent the stochastic equations by higher dimensional deterministic ones. The control design is based on Lyapunov stability for deterministic systems where the resulting stability conditions are verified via SOS programs. We demonstrate by two examples the various features of the control design and the corresponding ROA estimates which result from the proposed method. For the second example, which consists in the short period aircraft dynamics, the comparison with the (non-stochastic) literature confirms the prowess of the approach developed in this thesis to address the nonlinear design objective of maximizing the ROA. Moreover, the proposed approach offers flexibility in choosing the stochastic feedback law and imposing input constraints.

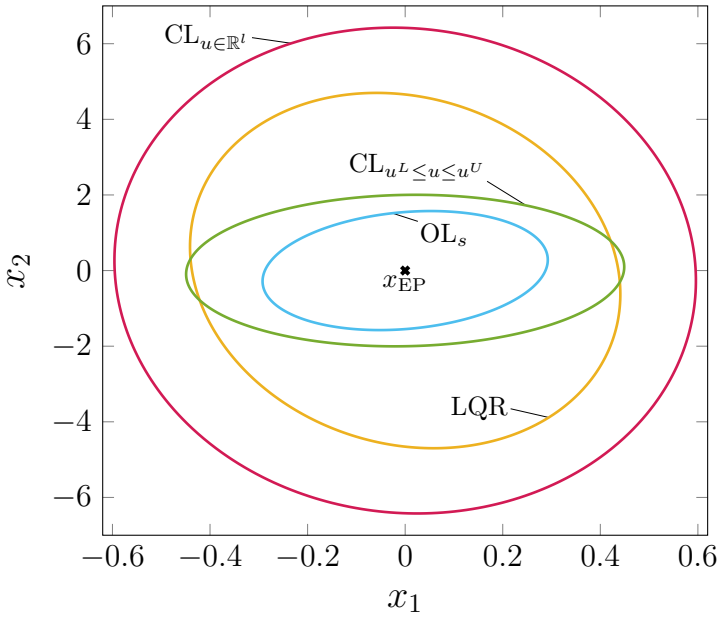

Figure 3.9: $\mathcal{R}$ estimates for the stochastic open loop (OL_s), unconstrained ($\mathrm{CL}_{u\in\mathbb{R}^l}$) and constrained ($\mathrm{CL}_{u^L\leq u\leq u^U}$) closed loop, and the LQR controlled system, computed from a quadratic V.

CHAPTER 4

Region of Attraction Analysis of Periodic Orbits

Systems which exhibit periodic solutions represent a wide range of processes of the real world and are subject to research in, e.g., robotics, power systems, biology, and aerospace. Periodic solutions which are stable and attracting nearby solutions are of particular interest for, e.g., legged locomotion [Man+11; TBM17], oscillatory behavior of power systems [RH05], population evolution models [CF06], flutter in aeroelastic plants [BPM06], power generating kites [ADS13; Sch18], to name a few.

This chapter is concerned with the analysis of the region in which trajectories converge to a periodic orbit, also referred to as limit cycle[1]. The approach of the analysis depends on the class of system, of which three different ones are considered here. These are deterministic systems, systems affected by affine parametric uncertainty, and stochastic systems in the form of second order processes. For the first two system classes, the approaches are based on a transformation to a *moving orthonormal coordinate system* (MOC). The MOC provides a moving Poincaré maps-like tool allowing to formulate criteria of orbital stability in the form of asymptotic stability conditions based on Lyapunov arguments. The coordinates obtained by the transformation are referred to as transverse coordinates and essentially consist in the splitting of the dynamics into a $(n-1)$-dimensional part transversal to the evolution of the systems and a scalar part normal to the first. While the construction of this MOC has been introduced since the 1960's [Ura67], most implementation of it are limited to the classical approach of maps consisting of hyperplanes which are orthogonal to the flow of the system [Hal80; HC94; Leo06; Man11; FS12].

In this work we derive a novel construction of a MOC which surpasses the well-definedness constraints of the classical transformation. In particular, our MOC allows to analytically obtain and flexibly modify the regions in which the transformation is

[1] In the strict sense a periodic orbit refers to any closed trajectory in the state space of a system, while the term 'limit cycle' implies a ω-limit set or α-limit set property of an orbit. Since we here analyze exclusively attracting orbits we will use the two names interchangeably.

well-defined. Based on the transformation to transverse coordinates we propose analysis methods for the attractive region. For deterministic systems the location of the orbit is usually known, which allows for Lyapunov stability arguments to be applied. The Lyapunov conditions represent sufficient conditions and their verification can be hard in general. Limiting the scope to polynomial systems we propose computationally efficient algorithms to test these sufficient conditions and obtain Lyapunov functions verifying inner estimates of the *region of attraction* (ROA) of the limit cycle. Different algorithmic options are proposed to increase the estimates of the ROA obtained from the optimization.

For uncertain systems, the location of the orbit depends usually on the realization of the uncertainty. In order to obtain an inner estimate of the region in which trajectories of the system converge to the uncertain orbit, contraction criteria are employed to analyze a transverse contracting behavior. In contrast to the Lyapunov condition, contraction methods do not require knowledge of the limit set. We propose algorithms for obtaining a maximized estimate of the *region of contraction* (ROC) as well as maximizing the allowed size of the uncertainty polytope for a fixed sized region inside the ROC.

The analysis of contracting regions for periodic orbits of stochatic system is approached by using *Polynomial Chaos Expansion* (PCE). By applying PCE to stochastic systems with limit cycles we allow to consider uncertainties coming from a wide range of probability distributions as opposed to most existing approaches which employ robust control-based deterministic approaches. We explore on the limitations of the expansion and leverage the accuracy of PCE in representing the combined temporal and spatial statistics of limit cycles. Based on these findings a connection between the periodic behavior of both the stochastic and the PCE system representations is drawn. This allows the analysis of the attractive regions of the stochastic system's limit cycle by considering the PCE representation. By exploiting the deterministic nature of the PCE system, we show how transverse contraction of the PCE representation translates to transverse contraction of the original stochastic system.

The chapter is outlined as follows. An overview of related work is provided in Section 4.1. A general class of systems with periodic solutions together with the relevant definitions of orbital stability and ROA of periodic orbits is presented in Section 4.2. In Section 4.3 the *classical MOC* (class-MOC) is explained first, which is then followed by the derivation of the *center point MOC* (cp-MOC). Section 4.4 presents the conditions on the ROA of deterministic orbits and provides the algorithms for the computational verification of the conditions. The contraction criteria and their algorithmic implemention which result in a ROC estimate for uncertain systems are presented in Section 4.5. The analysis of stochastic orbits is presented in Section 4.6. The chapter is finalized by conclusions presented in Section 4.7.

4.1 Related work

The stability analysis of periodic solutions has a long history, with Poincaré maps [Poi99] presenting the most well-known and established analysis tool. Using Poincaré maps the problem of orbital stability of a periodic solution is reduced to the stability of a fixed point of the map [Wig03]. In [Hal80], the concept of such maps was extended to consider moving orthonormal systems along the periodic trajectory, similar to moving Poincare maps. Based on earlier results presented in [Ura67], the moving orthonomal system is used in [Hal80] to divide the dynamics into a transversal part confined to a $(n-1)$-dimensional subspace representing a hyperplane transversal to the flow of the system at any given time, and a scalar part which is normal to the hyperplane. The straight-forward and most common choice of hyperplanes are those perpendicular to the system flow. Thus here referred to as *classical MOC* (class-MOC), this MOC has been used, e.g., in [HC94] for constructing periodic quadratic Lyapunov functions for exponentially stable orbits, in [Gie09] for the analysis of the ROA of periodic orbits in $n \geq 3$ dimensions based on Borg's criterion, and in [Leo06] for formulating generalized criteria for orbital stability in the sense of Zhukovski. For the control of various classes of nonlinear systems including hybrid and underactuated systems the class-MOC has been applied, e.g., in [Man+11; FS12; CH95]. An MOC not based on the classical choice of orthogonal hyperplanes has been proposed in [Man11], where a nonlinear optimization program aiming at maximizing the well-defined region of the transformation is proposed for the construction of the MOC. Similarly, in [TBM17] an application-specific choice of MOC was proposed which reduces the computational load of the transformation and resulting transverse equations.

Apart from the above mentioned works employing transverse coordinates, methods to analyze the ROA of deterministic orbits are proposed in [Gie04] where sufficient conditions based on Floquet theory and Lyapunov functions for a set to belong to the ROA of a limit cycle are presented. In [Gon05] linear matrix inequality conditions that guarantee asymptotic stability in a region around a limit cycle for the class of piecewise linear systems are provided.

Attractive regions of uncertain orbits have been significantly less considered in comparison. In [HS19] robust sets in a state-action space are obtained from viability theory for limit cycles of systems representing legged locomotion. In [IML19a] two methods based on describing functions and integral quadratic constraints are proposed to analyze the stability of limit cycles of an aeroelastic plant. One of the reasons contributing to the relatively sparse coverage of this research is that, in general, the location of the periodic orbit of an uncertain system depends on the realization of the uncertainty. This excludes the use of well-established Lyapunov arguments for the analysis of the attractive region as these methods would require the knowledge of the location of the limit cycle.

An approach for stability analysis which does not require the information on the limit cycle location is given by contraction methods [LS98; APS08; FS14]. For limit cycle systems, a weaker form of contraction which is required to hold only in a $(n-1)$-dimensional subspace transversal to the system is proposed in [MS14]. This is called transverse contraction and has been studied for deterministic continuous as well as hybrid systems in [GH13; MS14; TM14].

With respect to limit cycles, PCE has been used to investigate the statistical properties of stochastic periodic orbits [PB04; BPM06]. While in [PB04] the authors have found PCE to accurately represent the spatial statistics of stochastic systems with limit cycles for short time horizons, the limitations of PCE for analyzing the purely spatial statistics of limit cycles such as peak amplitude variations are revealed.

4.2 General systems with periodic orbits

In this section relevant notions for deterministic as well as uncertain systems with limit cycle are introduced in a general form.

Consider a continuous time system of the form

$$\dot{x} = f(x, \vartheta) = f_0(x) + f_d(x, \vartheta), \tag{4.1}$$

where $x \in \mathbb{R}^n$ is the state variable and $\vartheta \in \Theta$ is an uncertain variable belonging to a known compact set $\Theta \subset \mathbb{R}^m$. The function $f : \mathbb{R}^n \times \mathbb{R}^m \to \mathbb{R}^n$ is Lipschitz continuous in x, ϑ. The nominal dynamics are represented by $f_0 : \mathbb{R}^n \to \mathbb{R}^n$ and the dynamics affected by the uncertainty are given by $f_d : \mathbb{R}^n \times \mathbb{R}^m \to \mathbb{R}^n$, where $f_d(x, 0) = 0$, $\forall x$. Both $f_0(x)$ and $f_d(x, \vartheta)$ are assumed to have continuous partial derivatives with respect to x. For simplicity of demonstration we will assume (4.1) to be a polynomial in x and ϑ. For non-polynomial systems the results of this section can be applied to a polynomial approximation of the systems, e.g., coming from a Taylor expansion.

The system (4.1) is considered to have a periodic solution, referred to as periodic orbit or *limit cycle* (LC), which is in general dependent on the realization of the uncertainty $\vartheta \in \Theta$.

We will frequently consider time intervals, where we use the notation $\mathcal{I}_T := [0, T]$ for closed intervals, and $\mathcal{I}_T^\circ := [0, T)$ for half-open intervals.

Definition 4.1 (Periodic orbit)**.** *Let $\psi(x_{ini}, \vartheta^\dagger, t)$ denote the flow of the system (4.1) with initial condition x_{ini} and for a particular realization $\vartheta^\dagger \in \Theta$. A periodic orbit $\Gamma_{\vartheta^\dagger}$ is defined by a solution $\omega(t, \vartheta^\dagger) = \psi(x_{ini}, \vartheta^\dagger, t)$ which satisfies $\omega(0, \vartheta^\dagger) = \omega(T_{\vartheta^\dagger}, \vartheta^\dagger)$ with the period given by the minimum nontrivial $T_{\vartheta^\dagger} > 0$,*

$$\Gamma_{\vartheta^\dagger} = \{x \in \mathbb{R}^n | x = \omega(t, \vartheta^\dagger),\, t \in \mathcal{I}_{T_{\vartheta^\dagger}}\}. \tag{4.2}$$

Due to the stated properties of (4.1) the periodic solution $\omega(t, \vartheta)$ depends continuously on the uncertain variable ϑ[2]. The nominal orbit Γ_0, i.e., the set given by the periodic solution $\omega_0(t)$ obtained for $\vartheta = 0$, is assumed to be known throughout this chapter. When an analytic solution of the nominal periodic trajectory $\omega_0(t)$ does not exist a solution can be obtained numerically by simulation of the nominal dynamics[3].

The union of the periodic orbits for all realizations of $\vartheta \in \Theta$ is denoted by

$$\Gamma := \bigcup_{\vartheta \in \Theta} \Gamma_\vartheta, \tag{4.3}$$

and is in the following referred to as the *periodic orbit set* of (4.1).

4.2.1 Local stability of periodic orbits

The focus in this chapter is on systems for which the trajectories locally converge to the periodic orbits $\Gamma_\vartheta \in \Gamma$ for all realizations of $\vartheta \in \Theta$. Unlike equilibrium points for which asymptotic stability is defined by the convergence of all trajectories to one single point, trajectories of a system which converge to a periodic orbit will not converge to a single point but instead to a set, within which they will remain apart. Thus, the notion of *asymptotic orbital stability* can be defined instead and is found, related to nominal systems, e.g., in [Hal80]. We extend this definition for a general uncertain system (4.1) with periodic orbit set (4.3).

Definition 4.2 (Orbital stability)**.** *Let $K \subseteq \mathbb{R}^n$ be a region with $\Gamma \subset K$. The periodic orbit set Γ is called asymptotically orbitally stable if it is stable and attractive. It is stable if $\forall \epsilon > 0$, there is a $\delta > 0$ such that $\forall x_{ini} \in K$ with $\operatorname{dist}(x_{ini}, \Gamma) < \delta$ we have that $\operatorname{dist}(\psi(x_{ini}, \vartheta, t), \Gamma) < \epsilon$, $\forall t > 0$ and $\forall \vartheta \in \Theta$, and it is further attractive if there is a $\delta > 0$ such that $\forall x_{ini} \in K$ with $\operatorname{dist}(x_{ini}, \Gamma) < \delta$ we have $\lim_{t\to\infty} \operatorname{dist}(\psi(x_{ini}, \vartheta, t), \Gamma) = 0$, $\forall \vartheta \in \Theta$.*

If there is only one periodic orbit in the set Γ, e.g., Γ_0 in the nominal case when $\vartheta = 0$, then the periodic orbit itself is called asymptotically orbitally stable.

4.2.2 Region of attraction of periodic orbits

With Definition 4.2, the *region of attraction* (ROA) of a periodic orbit set Γ is defined as

$$\mathcal{R}^* := \{x_{\text{ini}} \in \mathbb{R}^n \mid \lim_{t\to\infty} \operatorname{dist}(\psi(x_{\text{ini}}, \vartheta, t), \Gamma) = 0, \forall \vartheta \in \Theta\}, \tag{4.4}$$

which is the set of initial conditions for which a system is converging to Γ.

[2] cf. Theorem VI.4.1, [Hal80]

[3] This is possible since we consider attractive limit cycles, and if the simulation is started in a neighborhood of the periodic solution.

4.3 Moving transverse coordinate system

In this section the analysis tool consisting of a *moving orthonormal coordinate system* (MOC) along a deterministic periodic orbit is presented. To this end, the nominal orbit Γ_0 is considered. First, the classical implementation of a MOC as introduced by [Hal80] is shown. Based on Hale's results for the existence of a MOC we then derive an improved MOC which overcomes well-definedness limitations of the former.

The basic idea behind using an MOC in the stability and ROA analysis of a periodic orbit (4.2) is to decompose the dynamics of the system in the neighborhood of Γ into two parts: The first part contains the dynamics on a hyperplane transversal to the trajectory of the limit cycle, and the second part represents the dynamics in the direction of the normal to the hyperplane. The hyperplanes and the transformation operator are constructed for Γ_0 and are a function of the scalar variable used to parameterize the orbit, which here is chosen as τ. The two parts of the decomposed dynamics are then described by two separate sets of coordinates, given by $\tau \in \mathcal{I}_{T_0}$ and $\rho \in \mathbb{R}^{n-1}$, which will be referred to as *transverse coordinates*.

4.3.1 Transformation to a moving orthonormal coordinate system

Let $\tau \in \mathcal{I}_{T_0}$ be the variable used to parametrize the orbit Γ_0,

$$\Gamma_0 = \{x \in \mathbb{R}^n \,|\, x = \omega_0(\tau),\ \tau \in \mathcal{I}_{T_0}\}, \tag{4.5}$$

such that any solution of $f_0(t)$ on Γ_0 (i.e., $x(0) \in \Gamma_0$) defines a function $\tau(t)$, $-\infty < t < \infty$ for which

$$\left.\frac{d\tau}{dt}\right|_{\omega_0(t)} = 1. \tag{4.6}$$

Then, the following results from [Hal80] establish the existence and the construction of a MOC.

Lemma 4.1 (Lemma IV.1.1,[Hal80])**.** *If $n \geq 3$ and $v(\tau)$ is a unit vector in $\mathbb{R}^n$ which has period T_0 and satisfies a Lipschitz condition, then there exists a unit vector ζ^* (independent of τ) such that*

$$v(\tau) \neq \pm\zeta^*, \quad \forall\tau. \tag{4.7}$$

The proof uses the fact that the curve described by any such $v(\tau)$ is rectifiable on a sphere in $\mathbb{R}^n$ and thus covers a set of measure zero. Therefore there always exists a vector ζ^* which is not on this curve or its reverse. A detailed proof can be found in [Hal80].

Remark 4.1. The reason for excluding the case $n = 2$ in Lemma 4.1 lies in the fact that a vector ζ^* is not needed for the construction of a MOC for a 2-dimensional system. This can be seen in the constructive proof of the following theorem which is shown in Appendix A.2.

In [Hal80] the function $v(\tau)$ is taken to be the normalized tangential vector along the flow of system on Γ_0,

$$v(\tau) = \frac{f_0(\omega_0(\tau))}{\|f_0(\omega_0(\tau))\|_2}. \tag{4.8}$$

An MOC with construction based on $v(\tau)$ as in (4.8) has been considered in [HC94; Leo06; Man11] and we will further refer to this MOC as the *classical MOC* (class-MOC).

Using the vector ζ^* from Lemma 4.1 and the function $v(\tau)$ as given in (4.8), the existence of the class-MOC is shown in [Hal80] as follows.

Theorem 4.1 (Theorem VI.1.1., [Hal80])**.** *If $\omega_0 \in \mathcal{C}^p(\mathbb{R}, \mathbb{R}^n)$, $p \geq 2$, $\omega_0(\tau + T_0) = \omega_0(\tau)$, $T_0 > 0$, $\frac{d\omega_0(\tau)}{d\tau} \neq 0$, $0 \leq \tau < T_0$, and Γ_0 is defined in (4.5), then there is a moving orthonormal system along Γ_0 which is $\mathcal{C}^{p-1}(\mathbb{R}, \mathbb{R}^n)$.*

The proof of this theorem as provided in [Hal80] demonstrates the construction of the MOC and is therefore included in Appendix A.2.

Let the basis of the class-MOC be denote by

$$\mathcal{O}^n = \{v(\tau), \zeta_2(\tau), ..., \zeta_n(\tau)\}. \tag{4.9}$$

The class-MOC is then used to construct a hyperplane "tube" $\mathcal{S}(\cdot)$ around Γ_0 which satisfies the transversality condition

$$f_0(\omega_0(\tau)) \notin \mathcal{S}(\tau), \quad \forall \tau \in \mathcal{I}_{T_0}, \tag{4.10}$$

where $\mathcal{S} : \mathcal{I}_{T_0} \to \mathbb{R}^{n-1}$. This is done by taking the $(n-1)$ basis vectors in $\mathcal{O}^n$ orthogonal to $v(\tau)$ to define a transverse projection operator,

$$Z(\tau) := [\zeta_2(\tau), ..., \zeta_n(\tau)] \in \mathbb{R}^{n \times (n-1)}. \tag{4.11}$$

Since $v(\tau)$ is given by (4.8), $Z(\tau)$ represents the operator projecting onto a moving transverse hyperplane which is orthogonal to the flow of the system at each $\omega_0(\tau)$. This transverse hyperplane is given by

$$\mathcal{S}(\tau) = \{x \in \mathbb{R}^n | v(\tau)^T (x - \omega_0(\tau)) = 0\}. \tag{4.12}$$

Thus, given any x in a sufficiently close neighborhood of $\omega_0(t)$, τ specifies the corresponding transversal hyperplane and ρ is the projected position on that hyperplane where $\rho = 0 \Leftrightarrow x = \omega_0(\tau)$. Figure 4.1 illustrates these hyperplanes.

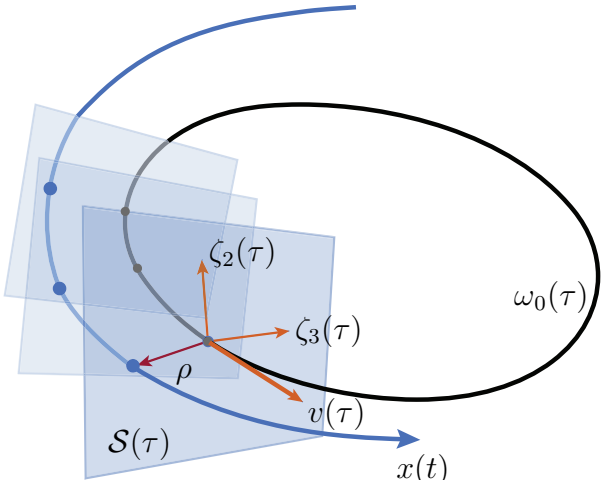

Figure 4.1: Illustration of the transverse coordinates. Example hyperplanes $\mathcal{S}(\tau)$ are indicated by the blue planes. The vectors ζ_2 and ζ_3 complete an orthonormal coordinate system with $v(\tau)$, as described in the constructive proof of Theorem 4.1.

The construction of $\mathcal{O}$ and the resulting projection $Z(\tau)$ provide the transformation law between x and the transverse coordinates (τ, ρ),

$$x = Z(\tau)\rho + \omega_0(\tau). \tag{4.13}$$

This transformation is only locally well-defined (see Definition 2.13). By applying the Implicit Function Theorem, the condition for the transformation to be well-defined results as follows.

Lemma 4.2 (Well-definedness condition)**.** *The transformation* (4.13) *is well-defined for all* $x \in \mathbb{R}^n$ *in the neighborhood of* Γ_0*, for which the condition*

$$\nu(\tau, \rho) := v(\tau)^T f_0(\omega_0(\tau)) + v(\tau)^T \frac{\partial Z(\tau)}{\partial \tau}\rho > 0, \tag{4.14}$$

is satisfied.

Proof. Consider the algebraic equation $F(x, \tau, \rho) = Z(\tau)\rho + \omega_0(\tau) - x$. Then the Jacobian with respect to the new coordinates τ, ρ is

$$J = \left[\frac{\partial F}{\partial \tau}, \frac{\partial F}{\partial \rho}\right], \tag{4.15}$$

where

$$\frac{\partial F}{\partial \tau} = \frac{d\omega_0(\tau)}{d\tau} + \frac{dZ(\tau)}{d\tau}\rho, \tag{4.16}$$

$$\frac{\partial F}{\partial \rho} = Z(\tau). \tag{4.17}$$

The inverse of J exists if $\det[J] \neq 0$. Since (4.17) has rank $n-1$ and $Z(\tau)$ builds an orthonormal system with $v(\tau)$, the following condition results from projecting (4.16) onto $v(\tau)$

$$v(\tau)^T \left(f_0(\omega_0(\tau)) + \frac{\partial Z(\tau)}{\partial \tau}^T \rho \right) \neq 0, \tag{4.18}$$

for the inverse of J to exist. From the Implicit Function Theorem well-definedness under condition (4.18) is concluded. The constraint to positive definiteness of (4.18) follows from $v(\tau)$ being defined by (4.8), which gives $v(\tau)^T f_0(\omega_0(\tau)) > 0$, $\forall \tau \in \mathcal{I}_{T_0}$, and the fact that at the origin of $\mathcal{O}^n$, $\rho = 0 \implies \frac{\partial Z(\tau)}{\partial \tau}^T \rho = 0$, such that finally (4.14) follows. □

Note that (4.14) is affine in ρ for a given τ.

Remark 4.2. At $\nu(\tau, \rho) = 0$ there exists a set of points x for which the transformation (4.13) is no longer well-defined. An intuition about this set of points can be obtained by the following consideration. For any given x, the corresponding coordinate τ of the transformation is decided from the $\omega_0(\tau)$ and related $v(\tau)$ which satisfy equation (4.12). If there is more than one $\omega_0(\tau)$ for which (4.12) is satisfied then the transformation $x \to (\tau, \rho)$ as in (4.13) is not unique, i.e., not well-defined. At these points x, equation (4.12) represents the orthogonal relation of the radius of a sphere to a tangent to its surface. For $n = 2$ this set of points x is singular and can be visualized by the intersection point of two neighboring hyperplanes.

4.3.2 An improved MOC for ROA analysis

The well-definedness condition stated in Lemma 4.2 poses a strict upper bound on the region which can be considered with the class-MOC. As we will see later this transfers to a strict upper bound on any inner estimate of the ROA which can be obtained from an analysis using the class-MOC, since the estimate cannot go beyond the region for which the transformation is well-defined.

Definition 4.3 (Well-defined "tube")**.** *The connected set in which the transformation to a MOC at a given location in* Γ_0 *indicated by* τ *is well-defined, is denoted by the* $\mathcal{V}_\tau$*, where*

$$\mathcal{V}_\tau := \{\rho \in \mathbb{R}^{n-1} \,|\, \rho = Z(\tau)^T \left(x - \omega_0(\tau)\right), \text{ (4.14) holds, } \tau \in \mathcal{I}^\circ_{T_0}\}. \tag{4.19}$$

The union $\mathcal{V} = \bigcup_{\tau \in \mathcal{I}^\circ_{T_0}} \mathcal{V}_\tau$ *has a tube-like structure and is referred to as well-defined tube with each* $\mathcal{V}_\tau$ *being called the well-defined region at* τ*.*

As defined above, $\mathcal{V}_\tau$ represents through (4.13) the set of all x located on a given hyperplane $\mathcal{S}(\tau)$ for which (4.14) holds.

Definition 4.4 (Well-defined MOC)**.** *If $\mathcal{V}_\tau \neq \varnothing$ for all $\tau \in \mathcal{I}^\circ_{T_0}$ then the MOC is referred to as well-defined MOC.*

Equation (4.14) and the transformation law (4.13) reveal the dependence of the size of $\mathcal{V}_\tau$ on $v(\tau)$. While in [Hal80] the existence of an MOC (the class-MOC) was shown for the particular choice of $v(\tau)$ as in (4.8), the results can in fact be generalized to a broader class of function $v(\tau)$, as is shown in the following.

Corollary 4.1. *A function $v : \mathcal{I}_{T_0} \to \mathbb{R}^n$ for which the properties stated in Lemma 4.1 hold, i.e., $v(\tau + T_0) = v(\tau)$, $\|v(\tau)\|_2 = 1$, $\forall \tau \in \mathcal{I}_{T_0}$ and $v(\tau)$ is Lipschitz continuous, and which additionally satisfies*

$$v(\tau)^T f_0(\omega_0(\tau)) > 0, \ \forall \tau \in \mathcal{I}_{T_0}, \tag{4.20}$$

allows for the construction of a well-defined MOC.

Proof. Lemma 4.1 guarantees the existence of a vector $\zeta^* \neq \pm v(\tau)$, $\forall \tau$. By the imposed properties on $v(\cdot)$, Theorem 4.1 proves the existence of an MOC. Thus, the construction of $\mathcal{O}^n$ as in (A.7) can directly be applied for any such $v(\tau)$. From (4.20) follows that the transversality condition (4.10) holds and thus the operator $Z(\tau)$ as given by (4.11) projects onto a transversal hyperplane representing the desired "tube" around Γ_0. Further, due to satisfying (4.20), the set $\mathcal{V}_\tau$ is non-empty for all τ and thus there exist a neighborhood in which the transformation (4.13) is well-defined for each $\tau \in \mathcal{I}^\circ_{T_0}$ as stated in Lemma 4.2. □

The regional constraints which condition (4.14) poses on the size of a ROA estimate, as well as the flexibility in choosing $v(\tau)$ motivate the aim of constructing a more suitable MOC than the class-MOC. The attribute "suitable" for a MOC is hereby subject to definition which can contain the following:

- provides a lower bound on the size of $\mathcal{V}_\tau$ for all τ which is open for modifications,
- minimizes the variation in size of $\mathcal{V}_\tau$ over τ,
- enables more direct knowledge of the size of $\mathcal{V}_\tau$ for each τ.

The first item can be accompanied with a maximization of the lower bound on the size of $\mathcal{V}_\tau$.

In [Man+11] the authors propose an optimization program to obtain a $v(\tau)$ for which ρ is maximized on each hyperplane while adhering to (4.14). This optimization program is, however, non-convex and requires a suitable initial guess. Also, there can be choices of $v(\tau)$ for which $\mathcal{V}_\tau$ for some τ become practically unbounded (namely when $\frac{\partial Z(\tau)}{\partial \tau}$ goes to zero). As this severely limits the size of $\mathcal{V}_\tau$ for other values of τ this can cause large

variations in the sizes of $\mathcal{V}_\tau$ which in general pose numerical issues in particular in the ROA analysis.

In the following we propose a novel construction of a MOC based on the choice of a tunable point x_c, which is the so called *center point*. We will therefore refer to this MOC as the *center point MOC* (cp-MOC). The cp-MOC allows explicit knowledge of the regions $\mathcal{V}_\tau$ for each τ and furthermore renders them adjustable to a certain, well-defined extend through different choices of x_c. As such, its applicability is constrained to a particular class of systems.

We first present the construction of the cp-MOC and the resulting regions $\mathcal{V}_\tau$, and then provide the description of the class of systems for which a cp-MOC can be constructed.

Construction of a well-defined cp-MOC

The vector function $v(\tau)$ from which the cp-MOC is constructed is obtained from the following algorithmic outline.

***Center point algorithm* (CPA):**

Step 1: Compute the normalized tangent vectors $v_t(\tau)$ to $\omega_0(\tau)$,

$$v_t(\tau) = \frac{f_0(\omega_0(\tau))}{\|f_0(\omega_0(\tau))\|}. \tag{4.21}$$

Step 2:

- $n = 2$: Choose a point x_c in the state space inside the area encircled by Γ_0.
- $n \geq 3$: Choose a point x_c in the state space which lies inside the encircled area obtained from an orthogonal projection of Γ_0 onto a 2-dimensional plane.

Step 3: Construct the normalized vectors $v_c(\tau)$ connecting each point in Γ_0 to the center point x_c

$$v_{cu}(\tau) = -\omega_0(\tau) + x_c, \tag{4.22}$$

$$v_c(\tau) = \frac{v_{cu}(\tau)}{\|v_{cu}(\tau)\|}. \tag{4.23}$$

Step 4:

- $n = 2$: Take $v(\tau) = [-v_{c_2}(\tau), v_{c_1}(\tau)]^T$, where $v_{c_1}(\tau), v_{c_2}(\tau)$ are the components of $v_c(\tau)$.

– $n \geq 3$: Construct a $(n-2)$-dimensional (τ-independent) subspace $\mathcal{N}_f \subseteq \mathbb{R}^{n-2}$ for which holds:

$$v_c(\tau) \notin \mathcal{N}_f, \quad v_t(\tau) \notin \mathcal{N}_f, \quad \forall \tau \in \mathcal{I}_{T_0}. \tag{4.24}$$

Compute $v(\tau) \in \mathbb{R}^n$ as the unit vector normal to the subspace generated by span $\{\mathcal{N}_f, v_c(\tau)\}$, for each $\tau \in \mathcal{I}_{T_0}$.

$$v(\tau): \ \begin{bmatrix} e_{f_1}, & \dots & e_{f_{n-2}}, & v_c(\tau) \end{bmatrix}^T v(\tau) = 0, \quad \tau \in \mathcal{I}_{T_0}. \tag{4.25}$$

As long as a subspace $\mathcal{N}_f$ can be found which satisfies the conditions (4.24) in Step 4, a vector function $v(\tau)$ can be computed from the CPA. However, not all $v(\tau)$ obtained from the CPA result in a well-defined MOC when used as a basis to construct a MOC as stated in Lemma 4.1 and Theorem 4.1. In particular, we find both the class of orbits Γ_0 and the choice of x_c in Step 2 to be constraining factors. In the following, these constraints are formalized.

Let

$$\Pi_{\mathcal{H}}: \ \mathbb{R}^n \to \mathbb{R}^2, \tag{4.26}$$

be an orthoganal projection onto a 2-dimensional plane $\mathcal{H} \subseteq \mathbb{R}^2$. Then, the set

$$\Gamma_0^{\mathcal{H}} = \{\omega_0^{\mathcal{H}} \in \mathbb{R}^2 \,|\, \omega_0^{\mathcal{H}}(\tau) = \Pi_{\mathcal{H}}\left(\omega_0(\tau)\right), \ \forall \tau \in \mathcal{I}_{T_0}\}, \tag{4.27}$$

denotes the projected orbit on $\mathcal{H}$.

Theorem 4.2. *If there exists a projection (4.26) and a point $x_c^{\mathcal{H}} \in \mathcal{H}$ such that there is a bijective map h,*

$$h: \frac{\omega_0^{\mathcal{H}}(\tau) - x_c^{\mathcal{H}}}{\|\omega_0^{\mathcal{H}}(\tau) - x_c^{\mathcal{H}}\|} \longrightarrow (1, \varphi), \quad \tau \in \mathcal{I}_{T_0}^{\circ}, \ \varphi \in [-\pi, \pi), \tag{4.28}$$

where $(1, \varphi)$ are the polar coordinates of a unit circle, and

$$\frac{d\varphi}{d\tau} \neq 0 \quad \forall \tau \in \mathcal{I}_{T_0}^{\circ}, \tag{4.29}$$

then the $v(\tau)$ obtained from the CPA with $x_c \in \Pi_{\mathcal{H}}^{-1}(x_c^{\mathcal{H}})$, $x_c < \infty$, results in a well-defined cp-MOC, i.e., $\mathcal{V}_\tau \neq \varnothing$, $\forall \tau \in \mathcal{I}_{T_0}^{\circ}$.

Proof. Let $v_{cu}^{\mathcal{H}} = -\omega_0^{\mathcal{H}}(\tau) + x_c^{\mathcal{H}}$ be the vectors connecting each element in $\Gamma_0^{\mathcal{H}}$ to $x_c^{\mathcal{H}}$. From the existence of the bijective map h onto the polar coordinates of a unit circle, i.e., $h\left(\frac{-v_{cu}^{\mathcal{H}}(\tau_i)}{\|v_{cu}^{\mathcal{H}}(\tau_i)\|}\right) = \varphi_i$ with a unique φ_i for each τ_i, it follows that

$$v_{cu}^{\mathcal{H}}(\tau_i) \nparallel v_{cu}^{\mathcal{H}}(\tau_j) \quad \forall \tau_i, \tau_j \in \mathcal{I}_{T_0}^{\circ}, \ i \neq j. \tag{4.30}$$

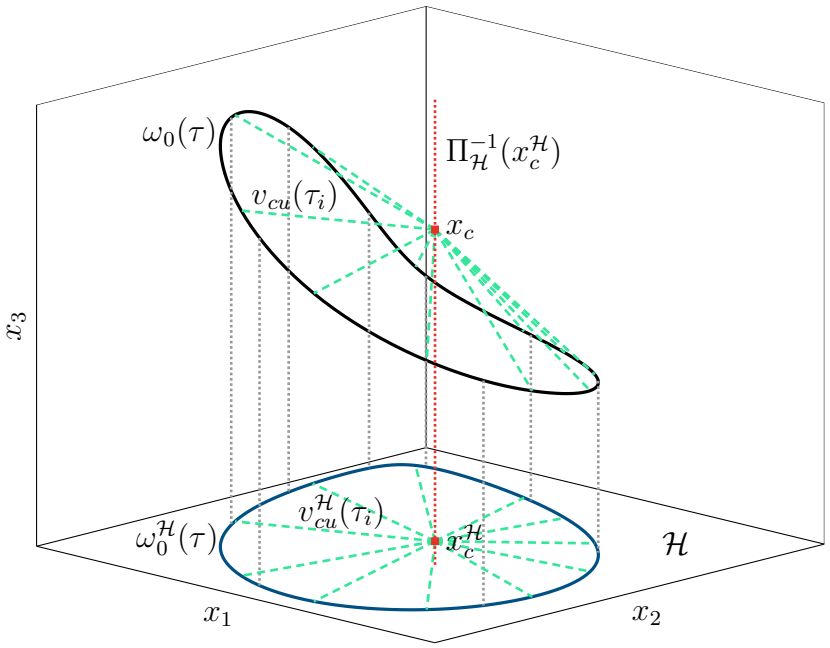

Figure 4.2: Illustration of the orthogonal projection of a 3-dimensional periodic orbit.

Let $f_0^{\mathcal{H}}$ denote the dynamics projected onto $\mathcal{H}$. From (4.30) and (4.29) follows that

$$f_0^{\mathcal{H}}(\omega_0^{\mathcal{H}}(\tau)) \nparallel \pm v_{cu}^{\mathcal{H}}(\tau), \quad \forall \tau \in \mathcal{I}_{T_0}^{\circ}, \tag{4.31}$$

as $f_0^{\mathcal{H}}(\omega_0^{\mathcal{H}}(\tau_i)) \parallel \pm {v_{cu}}^{\mathcal{H}}(\tau_i)$ for a $\tau_i \in \mathcal{I}_{T_0}^{\circ}$ otherwise either implies a symmetry in $\omega_0^{\mathcal{H}}(\tau)$ with respect to $v_{cu}^{\mathcal{H}}(\tau)$ and thus there exist τ_i and τ_j for which $\frac{-v_{cu}^{\mathcal{H}}(\tau_i)}{\|v_{cu}^{\mathcal{H}}(\tau_i)\|} = \frac{-v_{cu}^{\mathcal{H}}(\tau_j)}{\|v_{cu}^{\mathcal{H}}(\tau_j)\|}$ which contradicts (4.30); or it implies that there exists a saddle-point in the mapping at which however $\frac{d\varphi}{d\tau} = 0$ which contradicts (4.29).

From (4.31) follows that $f_0(\omega_0(\tau)) \nparallel \pm v_c(\tau)$, $\forall \tau \in \mathcal{I}_{T_0}^{\circ}$, where $v_c(\tau)$ as in (4.23) with x_c being any finite element in the set given by the inverse projection $\Pi_{\mathcal{H}}^{-1}(x_c^{\mathcal{H}})$. The function $v_c(\tau)$ then allows for the computation of a constant $(n-2)$-dimensional subspace $\mathcal{N}_f$ satisfying the conditions stated in Step 4 of the CPA, and the computation of $v(\tau)$ as in (4.25) for which results $v(\tau)^T f_0(\omega_0(\tau)) > 0$, $\forall \tau \in \mathcal{I}_{T_0}^{\circ}$, and thus $\mathcal{V}_\tau \neq \varnothing$, $\forall \tau \in \mathcal{I}_{T_0}^{\circ}$. □

Remark 4.3. Even though Theorem 4.2 shows that the cp-MOC can be constructed from any finite $x_c \in \Pi_{\mathcal{H}}^{-1}(x_c^{\mathcal{H}})$ for numerical reasons it is often beneficial to choose a $x_c \in \Pi_{\mathcal{H}}^{-1}(x_c^{\mathcal{H}})$ which lies in the neighborhood of Γ_0.

Note that Theorem 4.2 provides a sufficient condition for the cp-MOC to be well-defined. In practice, the well-definedness of a cp-MOC obtained from the CPA can be ascertained by checking the conditions of Corollary 4.1. Since $v(\tau)$ is continuous by construction, the remaining condition to check is (4.20). This is done in implementation by computing the zeros of the polynomial $v(\tau)^T f_0(\omega_0(\tau))$, $\tau \in \mathcal{I}_{T_0}^{\circ}$, after all steps up to Step 4 in the

CPA have been completed. If the polynomial has no zeros then the cp-MOC constructed from the obtained $v(\tau)$ is well-defined. If the polynomial has one or more zeros then the CPA can be recomputed for a different choice of x_c. Often, existing information on the shape of the orbit can be helpful in finding a suitable x_c from geometrical considerations. The cp-MOC allows to obtain an analytical expression for the sets $\mathcal{V}_\tau$, stated as follows.

Corollary 4.2. *For a cp-MOC, the set $\mathcal{V}_\tau$ for each $\tau \in \mathcal{I}^\circ_{T_0}$ is given by the open half space containing $\rho = 0$, which results from the subtraction of the $(n-2)$-dimensional hyperplane $\mathcal{S}_{\mathcal{V}_\tau}(\tau)$ generated by span$\left\{Z(\tau)^T \left(v_{c_u}(\tau) + ker\left(\frac{\partial v(\tau)}{\partial \tau}\right)\right)\right\}$ from the $(n-1)$-dimensional subspace $\mathcal{S}(\tau)$.*

Proof. As stated in Definition 4.3, for a $\tau \in \mathcal{I}^\circ_{T_0}$ the set $\mathcal{V}_\tau$ is given by all $\rho \in \mathbb{R}^{n-1}$ for which the well-definedness condition (4.14) is satisfied. Since (4.14) is an affine equation in ρ for a given τ, the hyperplane $\mathcal{S}_{\mathcal{V}_\tau}(\tau)$ is located where $\nu(\rho, \tau) = 0$. From this follows

$$
\begin{aligned}
& v(\tau)^T f_0(\omega_0(\tau)) + v(\tau)^T \frac{\partial Z(\tau)}{\partial \tau}\rho = 0, \\
\implies\ & v(\tau)^T f_0(\omega_0(\tau)) + \frac{\partial}{\partial \tau}\left(v(\tau)^T Z(\tau)\right)\rho - \frac{\partial v(\tau)^T}{\partial \tau} Z(\tau)\rho = 0, \\
\implies\ & v(\tau)^T f_0(\omega_0(\tau)) - \frac{\partial v(\tau)^T}{\partial \tau} Z(\tau)\rho = 0, \qquad \text{since } v(\tau)^T Z(\tau) = 0, \\
\implies\ & v(\tau)^T f_0(\omega_0(\tau)) - \frac{\partial v(\tau)^T}{\partial \tau}\left(x - \omega_0(\tau)\right) = 0, \qquad \text{from (4.13)}, \\
\implies\ & \frac{\partial v(\tau)^T}{\partial \tau} x = v(\tau)^T f_0(\omega_0(\tau)) + \frac{\partial v(\tau)^T}{\partial \tau}\omega_0(\tau), \\
& \qquad = \frac{\partial}{\partial \tau}\left(v(\tau)^T \omega_0(\tau)\right), \\
& \qquad = \frac{\partial}{\partial \tau}\left(v(\tau)^T \left(-v_{c_u}(\tau) + x_c\right)\right), \qquad \text{from (4.22)}, \\
& \qquad = \frac{\partial}{\partial \tau}\left(v(\tau)^T x_c\right), \qquad \text{since } v(\tau)^T v_{cu}(\tau) = 0 \text{ by construction}, \\
& \qquad = \frac{\partial v(\tau)^T}{\partial \tau} x_c, \qquad \text{since } x_c = \text{const}.
\end{aligned}
$$

The equality

$$
\frac{\partial v(\tau)^T}{\partial \tau} x = \frac{\partial v(\tau)^T}{\partial \tau} x_c, \tag{4.32}
$$

is satisfied by all

$$
x = x_c + \ker\left(\frac{\partial v(\tau)^T}{\partial \tau}\right). \tag{4.33}
$$

Inserting (4.33) into (4.13) and solving for ρ results in

$$\begin{aligned}\rho|_{\nu(\tau,\rho)=0} &= Z(\tau)^T \left(x_c - \ker\left(\frac{\partial v(\tau)^T}{\partial \tau}\right) - \omega_0(\tau) \right) \\ &= Z(\tau)^T \left(v_{c_u}(\tau) - \ker\left(\frac{\partial v(\tau)^T}{\partial \tau}\right) \right), \qquad \text{from (4.22).} \end{aligned} \tag{4.34}$$

Due to the linearity of $\nu(\tau,\rho)$ in ρ and $\rho = 0 \Rightarrow \nu(\tau,0) > 0$, the condition (4.14) holds for all ρ in the half space which contains $\rho = 0$ and is given by the subtraction of the hyperplane $\mathcal{S}_{\mathcal{V}_\tau}(\tau) := \rho|_{\nu(\tau,\rho)=0}$ from $\mathcal{S}(\tau)$. □

Remark 4.4. For $n = 2$, Corollary 4.2 results in the sets $\mathcal{V}_\tau$ being the 1-dimensional open half space containing $\rho = 0$, which is given by the intersection of $\mathcal{S}(\tau)$ with the center point x_c.

Figure 4.3 illustrates the hyperplanes obtained in a class-MOC and in a cp-MOC for a planar example. As stated in Remark 4.2, the regions $\mathcal{V}_\tau$ are limited by the point of intersection of two neighboring hyperplanes. The indicated hyperplanes for the class-MOC (left plot) show, that on the inward-pointing side of Γ_0, this results in significantly smaller regions at locations of large curvature of Γ_0 compared to locations of small curvature. In contrast, the hyperplanes for the cp-MOC reveal a unique intersection point at x_c which defines the limit of the regions $\mathcal{V}_\tau$ as described by Corollary 4.2. This illustration showcases the benefits of the cp-MOC consisting in more equally sized $\mathcal{V}_\tau$ for which the information about their size can be directly obtained. Moreover, the figure reveals how by changing the location of x_c the size of the sets $\mathcal{V}_\tau$ can be changed.

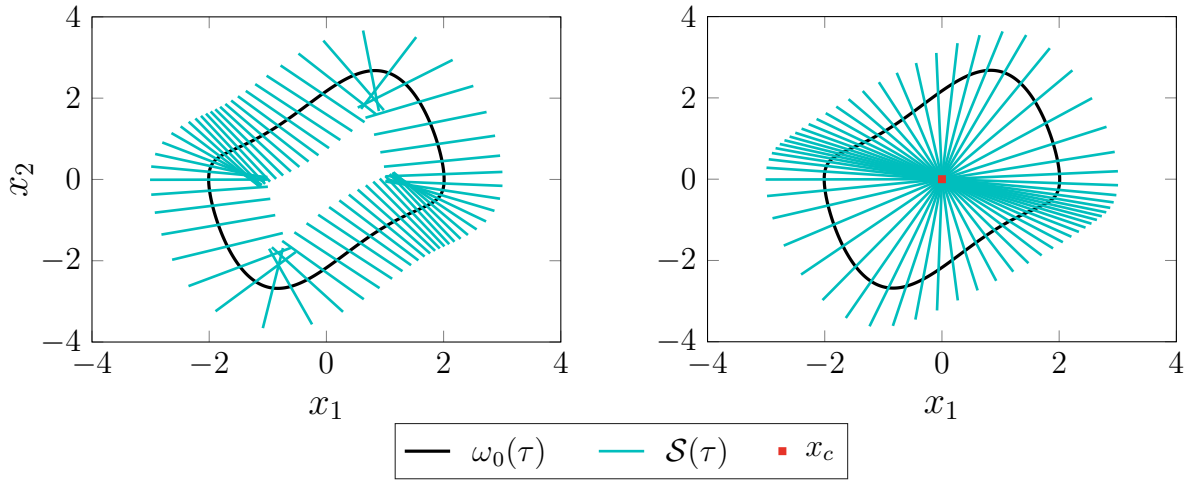

Figure 4.3: *Left plot:* Illustration of the hyperplanes $\mathcal{S}(\tau)$ given by the class-MOC for the limit cycle of the Van-der-Pol oscillator. *Right plot:* Illustration of the hyperplanes $\mathcal{S}(\tau)$ given by the cp-MOC with $x_c = [0,0]^T$ for the limit cycle of the Van-der-Pol oscillator.

4.3.3 Transverse coordinate dynamics

Consider the general dynamics (4.1) and let x satisfy the transformation equation (4.13) obtained from any well-defined MOC. The dynamics in the transverse coordinate (τ, ρ) are then obtained by considering

$$\frac{dZ(\tau)}{d\tau}\dot{\tau}\rho + Z(\tau)\dot{\rho} + f_0(\omega_0(\tau))\dot{\tau} = f(Z(\tau)\rho + \omega_0(\tau), \vartheta). \tag{4.35}$$

Projecting both sides of (4.35) onto $v(\tau)$ gives the 1-dimensional dynamics:

$$\dot{\tau} = \frac{v(\tau)^T f(\omega_0(\tau) + Z(\tau)\rho, \vartheta)}{v(\tau)^T f_0(\omega_0(\tau)) + v(\tau)^T \frac{\partial Z(\tau)}{\partial \tau}\rho}, \tag{4.36}$$

where (4.20) was used. Inspection of (4.35) reveals the denominator to be equal to the left hand side in (4.14). Let us thus define $\dot{\tau}(\tau, \rho) = \frac{\mu(\tau,\rho)}{\nu(\tau,\rho)}$, with

$$\mu(\tau, \rho) := v(\tau)^T f(\omega(\tau) + Z(\tau)\rho). \tag{4.37}$$

Further, projecting both sides of (4.35) onto $Z(\tau)$ gives the $n-1$-dimensional dynamics:

$$\dot{\rho} = \frac{dZ(\tau)}{d\tau}\dot{\tau}Z(\tau)\rho + Z(\tau)^T f(\omega_0(\tau) + Z(\tau)\rho, \vartheta) - Z(\tau)^T f_0(\omega_0(\tau))\dot{\tau}. \tag{4.38}$$

Note that in the case of class-MOC, $Z(\tau)^T f_0(\omega_0(\tau)) = 0$, which removes the third term in the right hand side of (4.38).

4.4 Region of attraction analysis of deterministic limit cycles

In this section an analysis method is presented with which an inner estimate for the ROA of the limit cycle of a deterministic system can be obtained. The approach is based on Lyapunov arguments which are formulated based on the transformation to transverse coordinates.

Consider the continuous time deterministic system

$$\dot{x} = f(x), \tag{4.39}$$

with $x \in \mathbb{R}^n$ and $f : \mathbb{R}^n \to \mathbb{R}^n$. As such, let the system (4.39) represent a nominal system $f_0(x)$ as defined in Section 4.2. Dropping the 0-subscript for the remainder of this section, the periodic orbit Γ of (4.39) follows from Definition 4.1 with $\vartheta = 0$,

$$\Gamma = \{x \in \mathbb{R}^n | x = \omega(t),\, t \in \mathcal{I}_T\}. \tag{4.40}$$

with periodic solution $\omega(t)$. Similarly, the notion of orbital stability and the definition of the ROA apply as in Definition 4.2 and equation (4.4) for the case of $\vartheta = 0$.

4.4.1 Lyapunov criteria for the ROA of a deterministic limit cycle

The Lyapunov arguments for the ROA of a periodic orbit (4.40) provided in the following theorem have been formulated in a similar form in [Man11]. In order to state the Lyapunov conditions the problem is considered for the system transformed to transverse coordinates using a MOC as presented in Section 4.3.

Theorem 4.3 ([Man11]). *Let $V : \mathcal{I}_T \times \mathbb{R}^{n-1} \to \mathbb{R}$ be a function piecewise continuously differentiable in τ and continuously differentiable in ρ, and let $\gamma > 0$ be a constant. If for the compact set $\mathcal{R} := \{(\tau, \rho) \in \mathcal{I}_T^\circ \times \mathbb{R}^{n-1} \mid V(\tau, \rho) \leq \gamma\}$ the following holds,*

$$V(\tau, \rho) > 0, \quad \forall (\tau, \rho) \in \mathcal{R}, \rho \neq 0, \tag{4.41}$$

$$V(\tau, 0) = 0, \quad \forall \tau \in \mathcal{R}, \tag{4.42}$$

$$\dot{V}(\tau, \rho) = \frac{\partial V(\tau, \rho)}{\partial \rho}\dot{\rho} + \frac{\partial V(\tau, \rho)}{\partial \tau}\dot{\tau} < 0, \quad \forall (\tau, \rho) \in \mathcal{R}, \rho \neq 0, \tag{4.43}$$

$$\nu(\tau, \rho) > 0, \quad \forall (\tau, \rho) \in \mathcal{R}, \tag{4.44}$$

where $\nu(\tau, \rho)$ is as defined in (4.14), then $\mathcal{R} \subseteq \mathcal{R}^*$, i.e., $\mathcal{R}$ is an inner estimate for the ROA of Γ.

A proof of this theorem can be found in [Man11]. In the following we restrict V to be polynomial in both τ and ρ. Using the transverse dynamics (4.38) and (4.36), condition (4.43) results in

$$\begin{aligned}\frac{\partial V(\tau, \rho)}{\partial \rho}\Bigg[\frac{dZ(\tau)}{d\tau}^T \dot{\tau} Z(\tau)\rho + Z(\tau)^T f(\omega(\tau) + Z(\tau)\rho)\dot{\tau} \\ - Z(\tau)^T f(\omega(\tau))\dot{\tau}\Bigg] + \frac{\partial V(\tau, \rho)}{\partial \tau}\dot{\tau} < 0.\end{aligned} \tag{4.45}$$

Equation (4.36) reveals that the left hand side in the condition (4.45) contains rational terms. Since the denominator term, $\nu(\tau, \rho)$, is, however, constrained to be positive in order for the transverse coordinate transformation to be well defined, multiplying both sides of condition (4.45) by $\nu(\tau, \rho)$ does not change its constraint on ρ and τ. This results in the polynomial inequality condition

$$\begin{aligned}\frac{\partial V(\tau, \rho)}{\partial \rho}\Bigg[\frac{dZ(\tau)}{d\tau}^T \mu(\tau, \rho) Z(\tau)\rho + Z(\tau)^T f(\omega(\tau) + \\ + Z(\tau)\rho)\nu(\tau, \rho) - Z(\tau)^T f(\omega(\tau))\mu(\tau, \rho)\Bigg] + \frac{\partial V(\tau, \rho)}{\partial \tau}\mu(\tau, \rho) < 0.\end{aligned} \tag{4.46}$$

With the modified condition (4.46) replacing (4.43), the constraints in Theorem 4.3 of are polynomial form in which they are accessible for computationally tractable algorithms presented in the following section.

4.4.2 Algorithms for a ROA estimate of the deterministic orbit

Considering a polynomial Lyapunov function V, the conditions (4.41), (4.42), (4.44) and (4.46) on the set $\mathcal{R}$ can be reformulated as semialgebraic set containment conditions. In the following we present an algorithmic outline which aims to maximize $\mathcal{R}$. It uses the results laid out in Section 2.1.3, in particular Lemma 2.1, to obtain computationally tractable relaxations of the set containment conditions in the form of *sum-of-squares* (SOS) constraints. This results in the following optimization problem in the shape of a generalized SOS program.

$$\max_{V,s_1,s_2} \quad \text{volume}\,(\mathcal{R}) \tag{4.47a}$$

subject to

$$V(\tau,\rho) - l(\rho) \in \Sigma[\tau,\rho], \tag{4.47b}$$

$$-\dot{V}(\rho,\tau) - (\gamma - V(\tau,\rho))s_1(\tau,\rho) - l(\rho) \in \Sigma[\tau,\rho], \tag{4.47c}$$

$$\nu(\rho,\tau) - (\gamma - V(\tau,\rho))s_2(\tau,\rho) \in \Sigma[\tau,\rho], \tag{4.47d}$$

$$s_1(\tau,\rho),\ s_2(\tau,\rho) \in \Sigma[\tau,\rho], \tag{4.47e}$$

where $l(\rho) = \epsilon\rho^T\rho$ with $\epsilon \ll 1$ enforces the inequation constraint of $\rho = 0$ in (4.41) and (4.46). The SOS multiplier s_1 and s_2 certify the inequality constraints to hold as stated in Theorem 2.2.

There are various possibilities for the choice of Lyapunov function V and the explicit form of the cost function in (4.47a), in particular regarding the implementation of the time-varying nature of V. These choices can vary significantly in their computational complexity. However, depending on the choice, the set $\mathcal{R}$ which is returned by the optimization program, will differ. As the aim is to maximize $\mathcal{R}$, a few selected options for Lyapunov functions and cost functions are presented in the following, ordered with increasing complexity. These options will further be referred to as *algorithmic options*.

Scaling the sublevel set of a fixed V (VSS-∂_{lin}):

This option was presented in [Man+11]. A Lyapunov function for an asymptotically orbitally stable periodic orbit Γ can be directly obtained from solving the periodic Lyapunov equation presented in [HC94] (and, in more general form, in [BCN91]). The periodic Lyapunov equation is a generalization of Lyapunov's Indirect Method to periodic solutions. It requires the linearization of the transverse dynamics (4.38) and (4.36) of system (4.1) around $\omega(\tau)$ (i.e., $\rho = 0$). The transverse linearization for a deterministic

system (4.39) results as

$$A_{\mathcal{S}}(\tau) = \left[\frac{d}{dt}Z(\tau)^T\right]Z(\tau) + Z(\tau)^T\frac{\partial f(\omega(\tau))}{\partial x}Z(\tau) - Z(\tau)^T f(\omega(\tau))\frac{v(\tau)^T\frac{\partial f(\omega(\tau))}{\partial x}Z(\tau) - v(\tau)^T\frac{\partial Z(\tau)}{\partial t}}{v(\tau)^T f(\omega(\tau))}. \tag{4.48}$$

The periodic Lyapunov equation is stated as

$$\dot{P}(\tau) + A_{\mathcal{S}}(\tau)^T P(\tau) + P(\tau)A_{\mathcal{S}}(\tau) + H(\tau) = 0, \tag{4.49}$$

where $H(\tau) \succ 0$ is a continuous T-periodic matrix. By solving (4.49), the unique periodic solution $P(\tau) \succ 0$ is obtained. The Lyapunov function

$$V(\tau, \rho) = \rho^T P(\tau)\rho, \tag{4.50}$$

can then be used in (4.47) with the objective function being the sublevel set size γ which is to be maximized,

$$\max_{\gamma, s_1, s_2} \quad \gamma. \tag{4.51}$$

Note that in this option the Lyapunov function is fixed to the result of (4.49) and is thus always a quadratic function.

Scaling the sublevel set of a quadratic V (VSS-$\partial(2)$):

This option is similar to an approach presented in [MAT13]. In this, the Lyapunov function is taken as a quadratic form with τ-varying Gram matrix

$$V(\tau, \rho) = \rho^T Q(\tau)\rho, \tag{4.52}$$

where $Q(\tau)$ is linear in τ. The objective function and maximization arguments are as follows, where in order to prevent the optimization from increasing γ by a direct rescaling of $Q(\tau)$, the trace of $Q(\tau)$ is fixed to a remain at a constant value $c(\tau) > 0$ for each $\tau \in \mathcal{I}_T^\circ$.

$$\max_{s_1, s_2, \gamma, Q} \quad \gamma \tag{4.53}$$

$$\text{subject to} \quad \text{tr}(Q(\tau)) = c(\tau), \quad \forall \tau \in \mathcal{I}_T^\circ. \tag{4.54}$$

The constraint (4.54) results in an additional linear constraint being added to (4.47).

Scaling the ellipse inside a variable-degree-V sublevel set (SE-$\partial(r)$):

As was the case for the optimization algorithm (3.22), higher degree Lyapunov functions have the potential to verify larger ROA estimates. In this algorithmic option, the Lyapunov function is thus taken as

$$V(\tau, \rho) = \text{v}(\rho)^T Q(\tau)\text{v}(\rho), \tag{4.55}$$

where $\mathrm{v}(\rho)$ is the monomial vector in ρ up to degree $r/2$ and with minimum monomial degrees of ≥ 1 (to satisfy (4.42)). In order to efficiently maximize the volume of $\mathcal{R}$ a fixed shape surrogate set is maximized which is constrained to lie inside of $\mathcal{R}$. This approach is similar to a method proposed in [JW03] for the maximization of estimates of *equilibrium point* ROAs. Here we propose a generalization of this approach to Lyapunov functions for periodic orbits. The surrogate set is given by the sublevel set of a quadratic function $b = \rho^T B_F \rho$,

$$\mathcal{B}_F = \{\rho \in \mathbb{R}^{n-1} \,|\, b(\rho) \leq \alpha\}, \tag{4.56}$$

where $B_F \in \mathbb{R}^{(n-1)\times(n-1)}$ is a fixed positive definite matrix prescribing the shape of the elliptical surrogate set. With the constraint

$$\mathcal{B}_F \subseteq \mathcal{R}, \tag{4.57}$$

added to the optimization program (4.47), and fixing the sublevel set of V to $\gamma = 1$, the objective function and maximization arguments result as

$$\max_{s_1, s_2, \alpha, Q} \quad \alpha. \tag{4.58}$$

Note that in this option the scaling factor of a single fixed shape ellipse is maximized while the ellipse is being constrained to lie inside of the τ-varying sublevel set of V. This simultaneously maximizes the sublevel set of V since Q enters the optimization as decision variable. The size of the verified set $\mathcal{R}$ can depend significantly on the choice of the ellipse shape. In general, the better the shape of the ellipse fits into the sublevel set the more efficient the optimization can potentially become.

Expanding the ellipse(s) inside a variable-degree-V sublevel set (EE-$\partial(r)$):

In order to circumvent the dependency of the verified set $\mathcal{R}$ on the choice of ellipse shape, the SE-$\partial(r)$ approach is extended in this option. This is done by using a surrogate set of a variable shape which is geometrically expanded inside of $\mathcal{R}$. Similarly to the procedure described in Section 2.1.5, the surrogate set is taken as the sublevel set of a quadratic function $b(\tau, \rho) = \rho^T B(\tau) \rho$,

$$\mathcal{B} = \{(\tau, \rho) \in \mathcal{I}_T^\circ \times \mathbb{R}^{n-1} \,|\, b(\tau, \rho) \leq 1\}, \tag{4.59}$$

with a fixed sublevel set scaling factor. The matrix $B(\tau) \in \mathbb{R}^{(n-1)\times(n-1)}$ is constrained to be positive definite and its entries enter as decision variables into (4.47). A convex objective function is then found by maximizing the geometric mean of the eigenvalues of B (cf. Section 2.1.5) and results, together with the maximization arguments, as

$$\max_{s_1, s_2, Q, B} \quad -\det\left(B(\tau)\right)^{1/(n-1)}. \tag{4.60}$$

As in SE-$\partial(r)$, the scaling factor of $\mathcal{R}$ is fixed to $\gamma = 1$, and the constraints

$$\mathcal{B} \subset \mathcal{R}, \quad B(\tau) \succ 0, \tag{4.61}$$

are added to the optimization program (4.47). A variation of this option will be included in the analysis, in which B is considered independent of τ. This allows to study the effect of a variably expanding ellipse compared to a fixed shape surrogate set. In terms of notation, the variant for the option with the τ-varying B is indicated by the subscript m, i.e., EE-$\partial(r)_m$ and the τ-independent B variant by s, i.e., EE-$\partial(r)_s$.

Remark 4.5. We emphasize on the fact that the list of algorithmic options considered here is not exhaustive. However, in terms of complexity and range of resulting estimate sizes we believe this list to reflect the range of possible objective function choices.

In the following, we focus on the implementation of the optimization program (4.47) under the EE-$\partial(r)_m$ option. By including (4.61) in the set containment conditions, the following SOS constraint is obtained.

$$-\left(1 - b(\tau, \rho)\right) s_3(\tau, \rho) + \left(1 - V(\tau, \rho)\right) \in \Sigma[\tau, \rho], \tag{4.62}$$

where $s_3(\tau, \rho)$ is an additional SOS multiplier.

With any of the above algorithmic options for V and the objective function, the generalized SOS program (4.47) has a convex objective function, however, the constraints contain bilinear terms in the decision variables. By alternating between fixing V while performing the optimization over s_1, s_2 and s_3, and then fixing s_1, s_2 and s_3 while optimizing over V the optimization problem can be efficiently solved in an iterative fashion where each of the iterative steps is an SOS program, and thus solvable as an *semidefinite program* (SDP) as described in Section 2.1.2.

Due to the dependency on the time-like variable τ the generalized SOS program (4.47) has a time-varying nature. Since this poses a significant computational complexity, accuracy of the solution can be traded in for computational efficiency by solving (4.47) for a N discrete τ values over the range of the full interval $[0, T]$ [TMT11]. This effectively chooses a set of fixed transversal hyperplanes on which the conditions of Theorem (4.3) are tested. Note that the finer the sampling of τ the lesser is the loss of accuracy but the higher are the computational cost due to the added constraints for each hyperplane. It then follows that the optimization problem (4.47) consists of a set of problems each evaluated for a discrete value of τ and with only ρ being left as the indeterminant. The τ-sampled polynomials are denoted with a superscript i in the following.

The sampling of τ results in the piecewise linear Lyapunov function

$$V^{(i)}(\rho) := \mathrm{v}(\rho)^T Q^{(i)} \mathrm{v}(\rho), \tag{4.63}$$

with explicit τ-derivative

$$\frac{\partial V^{(i)}(\rho)}{\partial \tau} = \mathrm{v}(\rho)^T \left(\frac{Q^{(i+1)} - Q^{(i)}}{\tau^{(i+1)} - \tau^{(i)}} \right) \mathrm{v}(\rho), \quad i = 1, ..., N-1. \tag{4.64}$$

By constraining $Q^{(i)} \succ 0$ the constraint (4.47b) is replaced. The τ-sampled optimization program for the algorithmic option EE-$\partial(r)_m$ then results as the following generalized SOS program.

$$\max_{s_1^{(i)}(\rho), s_2^{(i)}(\rho), s_3^{(i)}(\rho), i=1\ldots N-1} \quad -\sum_{i=1}^{N-1} \det\left(B^{(i)}\right)^{1/(n-1)} \tag{4.65a}$$

$$\text{subject to} \quad -\dot{V}^{(i)}(\rho) - \left(1 - V^{(i)}(\rho)\right) s_1^{(i)}(\rho) - l(\rho) \in \Sigma[\rho], \tag{4.65b}$$

$$\nu^{(i)}(\rho) - \left(1 - V^{(i)}(\rho)\right) s_2^{(i)}(\rho) \in \Sigma[\rho], \tag{4.65c}$$

$$-\left(1 - b^{(i)}(\rho)\right) s_3^{(i)}(\rho) + \left(1 - V^{(i)}(\rho)\right) \in \Sigma[\rho], \tag{4.65d}$$

$$s_1^{(i)}(\rho), s_2^{(i)}(\rho), s_3^{(i)}(\rho) \in \Sigma[\rho], \tag{4.65e}$$

$$Q^{(i)} \succ 0. \tag{4.65f}$$

The implementation of the iterative steps to solve (4.65) is shown in Algorithm 4.1. The iteration is initialized by solving the periodic Lyapunov equation (4.49) for the transverse linearization of the dynamics and scaling the result via bisection until SOS multipliers certifying (4.65b)-(4.65e) are found. Since this initial Lyapunov function is quadratic a feasible surrogate set size can be obtained by taking an even smaller scaled P. In Step 1, the Lyapunov function is kept fixed and for each $\tau^{(i)}$, a feasibility test consisting of (4.65b)-(4.65e) is computed to obtain the SOS multiplier for that $\tau^{(i)}$. Hereby, the problem for each $\tau^{(i)}$ sample is independent on the others such that $N-1$ feasibility tests are being performed in this step, which can be parallelized. In Step 2, the problem on each hyperplane depends on the neighboring ones due to the Lyapunov derivative. Thus, for each $\tau^{(i)}$ the multipliers are fixed and the constraints on V are added to a single large optimization program. In this second step the degree of the Lyapunov function can be increased to the desired order. Steps 1 and 2 are repeated until the maximum marginal increase of the expanding ellipses on the hyperplanes falls below a specified threshold (convCrit_B in Algorithm 4.1).

Remark 4.6. By substituting the appropriate cost function and adjusting the constraints as specified, Algorithm 4.1 can be used for any of the algorithmic options presented above.

4.4.3 Illustrative examples

In this section, the application of the ROA analysis is illustrated by two planar systems with the aim of comparing and highlighting the various features of the different MOCs presented in Section 4.3 and algorithmic options laid out in Section 4.4.2. An example of the application of the ROA analysis to a 3-dimensional controlled Airborne Wind Energy system will be provided in Chapter 5. The results presented here were computed from the scripts which are further presented in Chapter 6. In particular, the numerical criteria used for the comparisons are explained in Section 6.6.

Algorithm 4.1 Find Lyapunov function for deterministic orbit to maximize $\mathcal{R}$

Input: N, $\partial(s_1^{(i)})$, $\partial(s_2^{(i)})$, $\partial(s_3^{(i)})$, $\partial(V^{(i)})$, convCrit_B
Output: V, $\mathcal{R}$
procedure MAXROAESTIMATE
    $\dot{\rho}$, $\dot{\tau}$ $\xleftarrow{(4.38),(4.36)}$ $f(x)$, $\omega(t)$
    Initialization:
    $Q_{\text{ini}}(\tau) \leftarrow c \cdot P(\tau)$ solution of (4.49), bisect c such that (4.65b)-(4.65e) feasible
    ${Q_{\text{ini}}}^{(i)} \leftarrow Q_{\text{ini}}(\tau_i)$
    choose $B^{(i)}$ small enough such that (4.65d) is feasible
    Iteration:
    $k \leftarrow 0$
    repeat
        $k \leftarrow k + 1$
        for $i = 1 : N-1$ **do**
            Step 1: $s_1^{(i)}$, $s_2^{(i)}$, $s_3^{(i)} \leftarrow$ fix $Q^{(i)}$, $B^{(i)}$ solve (4.65b)-(4.65e)
        Step 2: $Q^{(i)}$, $B^{(i)}$, $_{i=1\ldots N-1} \leftarrow$ fix $s_1^{(i)}$, $s_2^{(i)}$, $s_3^{(i)}$, $_{i=1\ldots N-1}$ solve (4.65a)-(4.65d)
    until $\max\{\det(B^{(i)})_{k-1} - \det(B^{(i)})_k\}_{i=1}^{N-1} < \text{convCrit}_B$

Van-der-Pol oscillator

The Van-der-Pol oscillator dynamics,

$$\begin{aligned} \dot{x}_1 &= x_2, \\ \dot{x}_2 &= (1 - x_1^2)x_2 - x_1, \end{aligned} \tag{4.66}$$

have a unique stable limit cycle which encircles an unstable equilibrium point at $x_{\text{EP}} = [0, 0]^T$ [LS42]. Let Γ_{VDP} denote this limit cycle. The ROA of Γ_{VDP} thus includes all of $\mathbb{R}^2 \backslash \{x_{\text{EP}}\}$.

We use this example to investigate the effect of the choice of the MOC and the effect of different degrees of Lyapunov functions on the obtained ROA estimates $\mathcal{R}$. For this purpose we use the option EE-$\partial(r)_m$ in the Algorithm 4.1 and fix the multiplier to $\partial(s_1) = 6$, $\partial(s_2) = 2$ and $\partial(s_3) = 2$. Figure 4.4 shows the volume of the computed $\mathcal{R}$ as a function of τ for the four cases of a quadratic and a quartic Lyapunov function used under the class-MOC and the cp-MOC. The set $\mathcal{R}$ set were computed from 50 discrete values of $\tau \in [0, T]$ with $\tau_1 = \tau_{50}$, giving 49 distinct hyperplanes. As can be seen in the figure, the obtained ROA estimates are significantly larger for the cp-MOC than for the class-MOC. Further, consistently with the expectation, for both MOCs the quartic Lyapunov function returns on average a larger $\mathcal{R}$ than the quadratic.

Figure 4.5 provides a qualitative illustration of the computed $\mathcal{R}$ for each case, where the left plot shows the results obtained on a range of hyperplanes in the class-MOC

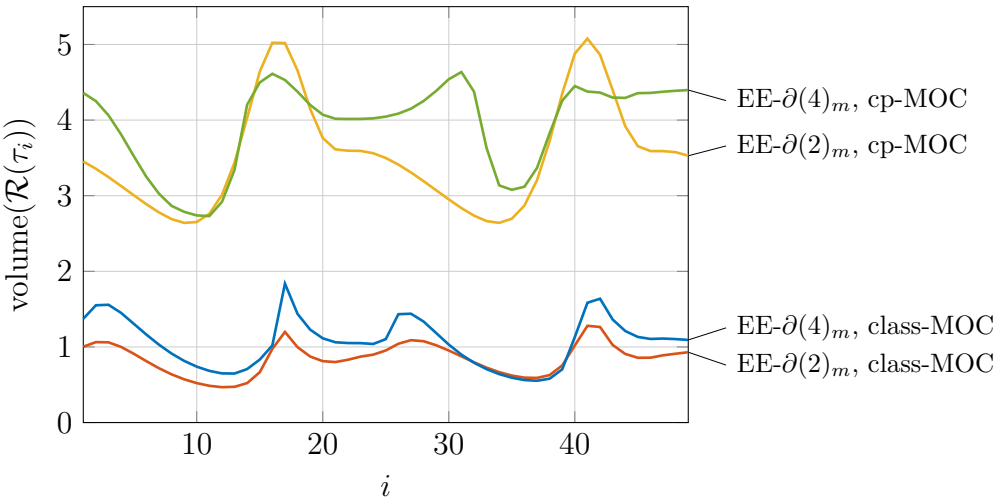

Figure 4.4: Comparison of $\mathcal{R}$ sizes obtained from Algorithm 4.1 for the algorithmic choice EE-$\partial(r)_m$ where both quadratic and quartic Lyapunov functions were used for both the class-MOC and the cp-MOC.

and the right plot shows the results on the same range of hyperplanes in the cp-MOC with $x_c = [0, 0]^T$. The results for a quadratic Lyapunov function are plotted on top of the results for a quartic Lyapunov function. This figure reveals the reason for the significantly smaller ROA estimates obtained with class-MOC, which is a consequence of Corollary 4.2: The intersection of neighboring hyperplanes which represents the limit point of the well-definedness of the transverse coordinate transformation (4.13), prevents the finding of larger sets $\mathcal{R}$. In the case of cp-MOC the hyperplanes all intersect in the single point x_c which allows much larger regions $\mathcal{R}$ to be found by Algorithm 4.1 in this example.

Dual-orbit system

This example consists in a modified version of the Liénard system given in [GG02].

$$\begin{aligned} \dot{x}_1 &= -x_2 + 3x_1(x_1^2 - 1/4)(x_1^2 - 1), \\ \dot{x}_2 &= x_1. \end{aligned} \tag{4.67}$$

The modifications contain a reduction of the system's order from 7 to 5 which entails the removal of a the third outermost stable LC, and the change of a parameter value. In the form considered here the system has two LCs of which one is encircling the other. The inner one is an attractive LC around the unstable equilibrium point $x_{\text{EP}} = [0, 0]^T$, which is further denoted by Γ^A_{dual}. The outer one is an unstable LC and is further indicated by Γ^U_{dual}. Figure 4.6 shows a phase portrait of the system in the neighborhood of the LCs. The true ROA of Γ^A_{dual} is given by the region encircled by Γ^U_{dual} (with exception of x_{EP}).

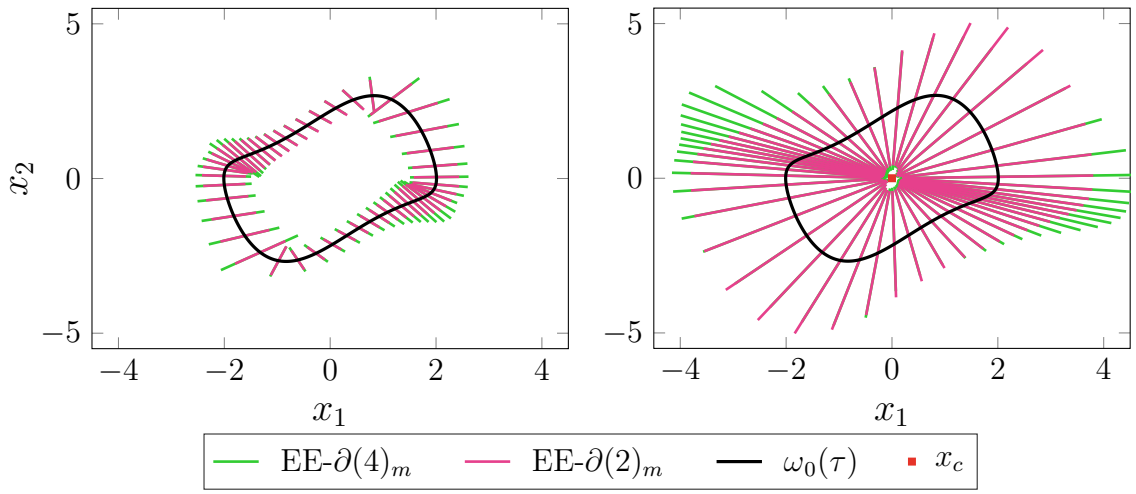

Figure 4.5: Illustration of the computed ROA estimates shown in Figure 4.4 for the Van-der-Pol oscillator (4.66). The results for the quadratic Lyapunov function are plotted on top of the results for the quartic. *Left plot:* ROA estimates for the class-MOC. *Right plot:* ROA estimates for the cp-MOC.

For this system all algorithmic options presented in Section 4.4.2 were used to compute a ROA estimate for both the class-MOC and cp-MOC. For the two options SE-$\partial(r)$ and EE-$\partial(r)$ which allow for higher order Lyapunov functions both the case of a quadratic and a quartic function was considered. The multiplier degrees were fixed for all options to $\partial(s_1) = 6$, $\partial(s_2) = 2$ and, where applicable, $\partial(s_3) = 2$. The aim of the comparison was to investigate the differences in the outcome among the algorithmic choices as well as to analyze the conservativeness of the results with respect to the true ROA.

The volumes for the computed $\mathcal{R}$ for each algorithmic option are shown as a function of τ in Figures 4.7 for the class-MOC and in Figure 4.8 for the cp-MOC. Each estimate was obtained for the same range of 50 discrete values of $\tau \in [0, T]$ with $\tau_1 = \tau_{50}$. Both figures reveal the tendency to obtain of larger sets $\mathcal{R}$ from higher degree Lyapunov functions and from cost functions which are more flexible in the adaption of the shape of the sublevel sets of both V and, where applicable, the surrogate set. Accordingly, $\mathcal{R}$ obtained from VSS-∂_{lin} is significantly smaller than all other estimates as its only flexibility consists in the uniform scaling of the Lyapunov sublevel set obtained for the linearized system. Allowing the shape of this sublevel set to vary results in significantly larger results, as the sets $\mathcal{R}$ obtained for VSS-$\partial(2)$ show. This option still only considers quadratic Lyapunov functions and the cost function is equal to the one in VSS-∂_{lin} while the computational complexity is significantly increased due to the constraints on Q and added decision variables.

For both cases of MOC the results from the algorithmic options involving quadratic Lyapunov functions (except for VSS-∂_{lin}) give very similar results. While for the class-MOC the use of a surrogate set in the options SE-$\partial(2)$, EE-$\partial(2)_s$ and EE-$\partial(2)_m$ results

in small increases compared to VSS-$\partial(2)$ these are negligibly small in the results for cp-MOC. The more significant benefit of using surrogate sets is clearly shown in the comparison of the results obtained for the quadratic Lyapunov function compared to the results of the quartic one. Except for SE-$\partial(4)$ for the class-MOC these results are significantly larger for the latter. Thereby it can be seen for both MOCs how a surrogate set which is allowed to shape more flexibly results on average in larger $\mathcal{R}$. The largest $\mathcal{R}$ obtained for the class-MOC is included in Figure 4.8 to facilitate a comparison of the results among both choices of MOC. As found in the previous example of the Van-der-Pol oscillator, also here the cp-MOC allows for larger regions to be obtained for all algorithmic options (except for VSS-∂_{lin}).

Figure 4.9 illustrates the obtained sets $\mathcal{R}$ for EE-$\partial(4)_m$ and VSS-$\partial(2)$ on the 49 chosen hyperplanes for the class-MOC (left plot) and the cp-MOC (right plot). The results for VSS-$\partial(2)$ were plotted on top of the results of EE-$\partial(4)_m$. The figure shows how both MOC enable the EE-$\partial(4)_m$ to obtain ROA estimates which are very close to the size of the true ROA towards its outer boundary. While due to the intersection of hyperplanes in the class-MOC case the estimates are not covering the neighborhood of x_{EP}, this limitation is not given for the cp-MOC for which the estimates are able to reach closer towards x_{EP}, which is also the chosen center point in this case. The plots further underline the finding that more flexible cost functions and higher order Lyapunov functions can result in significantly less conservative results.

Table 4.1 lists the number of iterations performed for each algorithmic option, choice of MOC and Lyapunov function degree. The comparison shows that there were significant differences in between the algorithmic options, inconsistent variations among different Lyapunov function degrees and comparably little variation between the two choices of MOC. Combining the volume plot results with the iteration numbers it can be seen that the larger sized ROA estimate obtained for the option EE-$\partial(r)_m$ comes at the cost of a significantly higher number of iterations than its less flexible counterpart EE-$\partial(r)_s$ needed for a slightly smaller sized ROA estimate.

Remark 4.7. Note that even though the estimates are only close to the hyperplane intersection point for a few values of τ for the class-MOC, the algorithm can not efficiently increase the estimates on the hyperplanes on which the estimates are still far from the intersection point. This is in despite of the flexibility of individually shaping the surrogate sets on each hyperplane which is given in the option EE-$\partial(4)_m$. Since in the cp-MOC it is often possible to design the hyperplanes in a way that the well-defined sets $\mathcal{V}_\tau$ are more similar in size this restriction can be diminished by choosing this MOC.

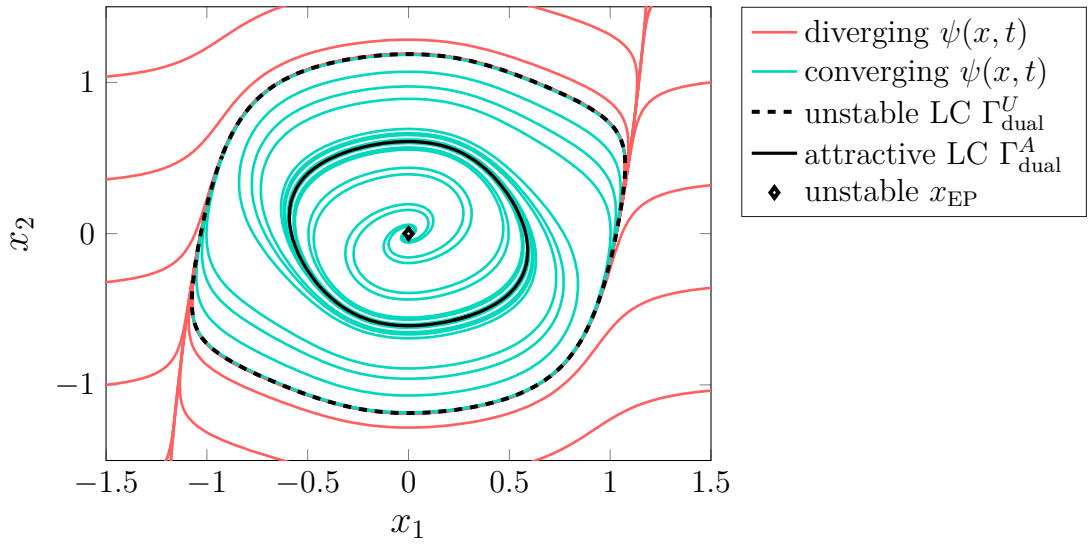

Figure 4.6: Phase portrait of the dual-orbit system (4.67) in the neighborhood of the attractive and unstable LCs. The green lines show examples of converging trajectories while the red lines represent diverging ones.

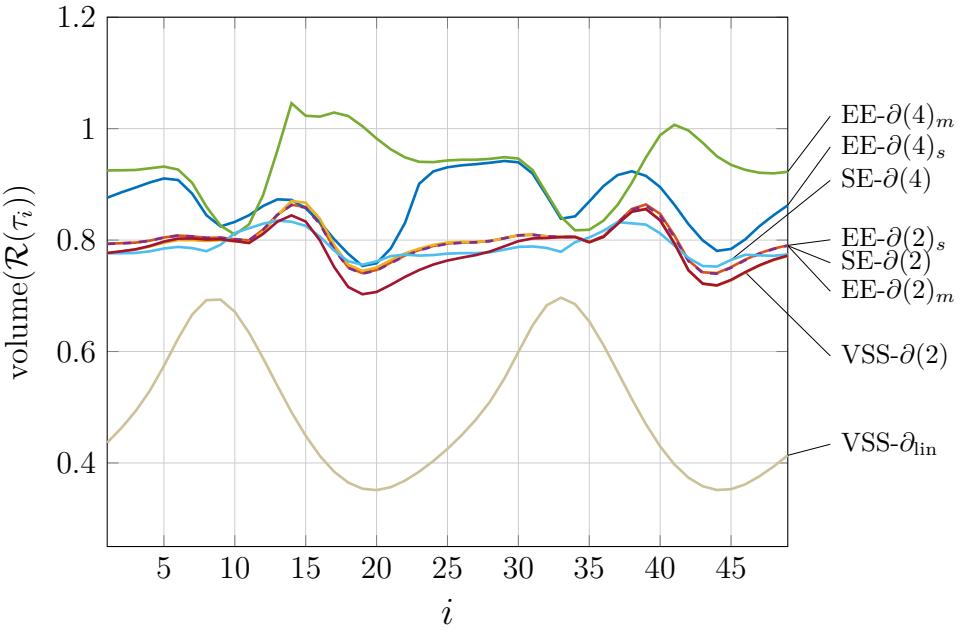

Figure 4.7: ROA estimates as a function of τ, obtained from the different algorithmic choices presented in 4.4.2 for the class-MOC.

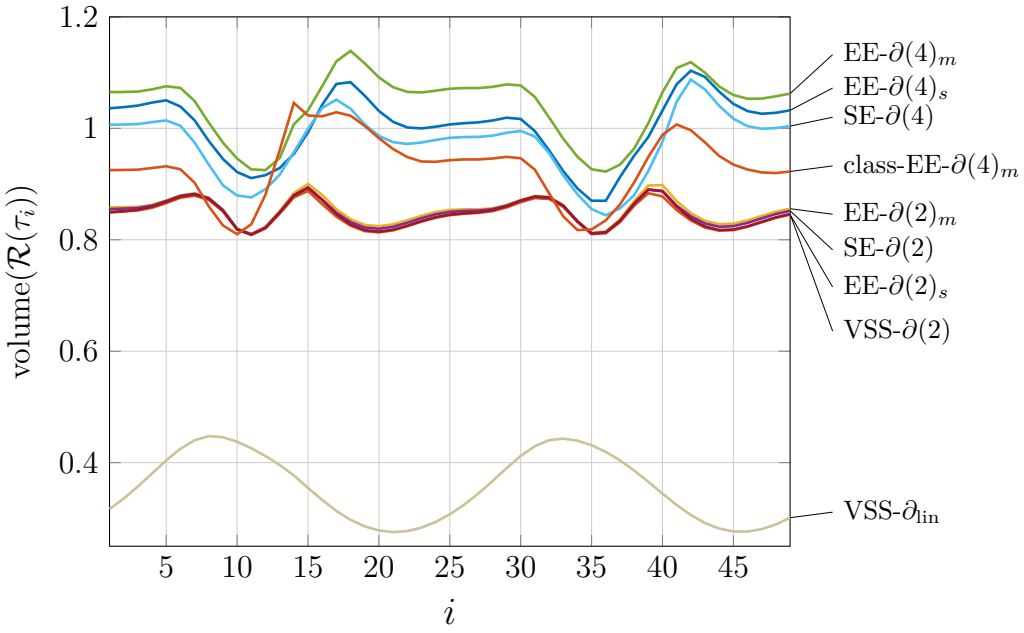

Figure 4.8: ROA estimates as a function of τ, obtained from the different algorithmic choices presented in 4.4.2 for the cp-MOC. For comparison, the EE-$\partial(4)_m$ result obtained for the class-MOC is included.

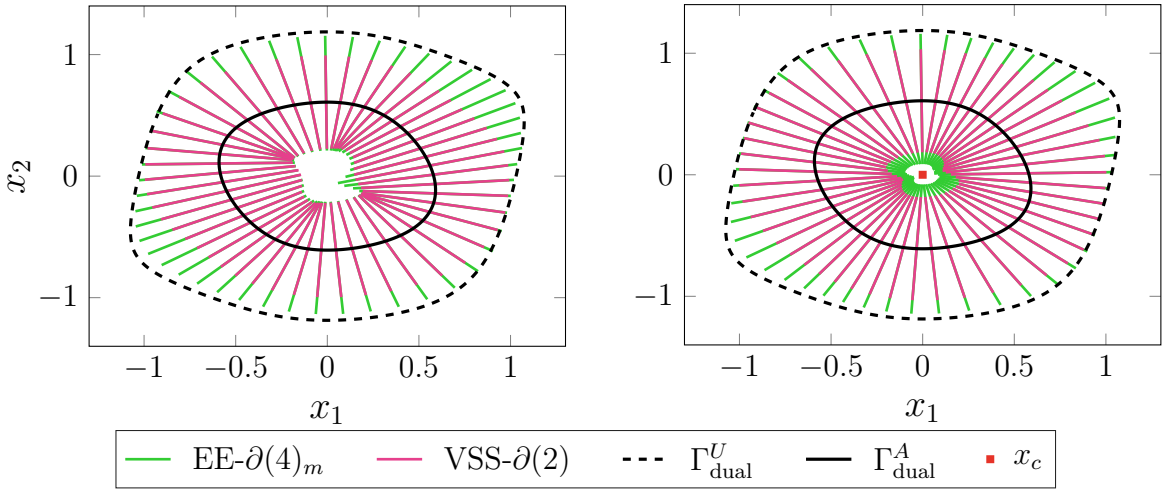

Figure 4.9: Illustration of selected ROA estimates shown in Figure 4.7 and Figure 4.8 for the dual-orbit system (4.67). The results for the quadratic Lyapunov function are plotted on top of the results for the quartic. *Left plot:* ROA estimates for the class-MOC. *Right plot:* ROA estimates for the cp-MOC.

Table 4.1: Comparison of iteration numbers obtained for the dual orbit example for each algorithmic option and MOC.

Algorithmic option	class-MOC		cp-MOC	
	$\partial(V)=2$	$\partial(V)=4$	$\partial(V)=2$	$\partial(V)=4$
EE-$\partial(r)_m$	23	51	20	49
EE-$\partial(r)_s$	10	9	8	8
SE-$\partial(r)$	39	32	39	33
VSS-$\partial(2)$	12	-	12	-
VSS-∂_{lin}	10	-	6	-

4.5 Region of contraction analysis of uncertain periodic orbits

We now consider the case of a parametric uncertainty affecting the system (4.1), i.e., $\vartheta \neq 0$. Since in this case the location of the periodic orbit depends on the realization of the uncertainty, Lyapunov methods can no longer be applied directly. In order to analyze the ROA of the uncertain orbit, contraction methods are employed instead. For this reason the ROA is also referred to as ROC, which we will adapt in the following.

Consider systems (4.1) where the uncertainty is parametric and affinely appearing in the dynamics

$$\dot{x} = f(x,\vartheta) = f_0(x) + \phi(x,\vartheta), \tag{4.68}$$

where x and $f_0(x)$ are as defined before and $\vartheta \in \Theta \subset \mathbb{R}^m$ is the uncertain parameter, $\phi : \mathbb{R}^n \times \mathbb{R}^m \to \mathbb{R}^n$ is Lipschitz continuous in x and ϑ, and further $\phi \in \mathcal{D}$ with

$$\mathcal{D} := \{\phi \,|\, \phi(x,\vartheta) = \tilde{\Phi}(x)\vartheta \;\; \forall x \in \mathbb{R}^n,\;\; \vartheta^L \leq \vartheta \leq \vartheta^U\}.$$

The constant vectors ϑ^L, $\vartheta^U \in \mathbb{R}^m$ denote the lower and upper bound of ϑ. Both $f_0(x)$ and the matrix $\tilde{\Phi} : \mathbb{R}^n \to \mathbb{R}^{n\times m}$ are known dynamics.

Before the contraction analysis of (4.68) is presented, a brief introduction to contraction methods for periodic orbits is provided.

4.5.1 Transverse Contraction Criteria

For the sake of this introduction to transverse contraction methods let us consider the deterministic system (4.39) and its periodic orbit Γ as presented in Section 4.4.

Consider a Riemannian metric function of the form

$$V_M(x,\delta_x) = \delta_x^T M(x) \delta_x, \tag{4.69}$$

where δ_x denotes a virtual displacement, i.e. a linear tangent differential form representing an incremental displacement of $x(t)$ at a fixed time. As presented, V_M has the meaning of a squared distance. Further, $M(x)$ is a Riemannian metric which implies $M(x) \succ 0$ for all x. Contraction analysis is concerned with the rate of change of this metric function.

With

$$\dot{\delta}_x = \frac{\partial f(x)}{\partial x}\delta_x, \tag{4.70}$$

we obtain from (4.69)

$$\frac{d}{dt}\left(\delta_x^T M(x)\delta_x\right) = \delta_x^T \left(\frac{\partial f(x)}{\partial x}^T M(x) + M(x)\frac{\partial f(x)}{\partial x} + \dot{M}(x)\right)\delta_x, \tag{4.71}$$

where $\dot{M}_{ij}(x) = \frac{\partial M_{ij}(x)}{\partial x} f(x)$ is the entry at the i-th row and j-th column of $\dot{M}(x)$. The following definition can be found in similar form in, e.g., [LS98].

Definition 4.5. *(Full contraction) A system (4.39) is called contracting in a region $\mathcal{K} \subseteq \mathbb{R}^n$ with respect to a positive definite metric $M(x)$ if*

$$\frac{\partial f(x)}{\partial x}^T M(x) + M(x)\frac{\partial f(x)}{\partial x} + \dot{M}(x) \leq -\eta_c M(x), \tag{4.72}$$

for all $x \in \mathcal{K}$ and a positive constant η_c.

If a system with a stable equilibrium point x_{EP} is contracting in a region $\mathcal{K} \subseteq \mathbb{R}^n$, where $x_{\text{EP}} \in \mathcal{K}$ then the distance between any two trajectories starting in the region $\mathcal{K}$ will eventually converge to zero. The negative rate of change of the distance happens in this case in the full state dimension.

In the case of the system having a stable periodic orbit, two neighboring trajectories will not converge to a single point but instead converge to the set Γ given by the periodic orbit. Since two points on a periodic orbit never converge to one point, such a system is not satisfying the full contraction criteria of Definition 4.5. Any two trajectories of this system are, however, contracting under a reparametrization of time. Also referred to as Zhukovsky stability, this reparametrization suggests a slowing down, respectively speeding up of one of the two trajectories such that the distance between them converges to zero. The existence of this reparametrization is sufficient to formulate a contraction condition for the convergence of trajectories to a limit cycle which requires the contraction condition (4.72) to only hold in a $n-1$-dimensional subspace transverse to the flow of the system. This is referred to as *transverse contraction*.

Theorem 4.4 (Transverse contraction, [MS14])**.** *Consider the system (4.39) on a subset $\mathcal{Z} \subset \mathbb{R}^n$. Let $\mathcal{Z}$ be compact, smoothly path-connected, and strictly forward invariant. If there exists a metric function $V_M(x, \delta_x)$ satisfying*

$$\frac{\partial V_M}{\partial x} f(x) + \frac{\partial V_M}{\partial \delta_x}\frac{\partial f(x)}{\partial x}\delta_x \leq -\eta_t V_M(x, \delta_x), \tag{4.73}$$

for all $\delta_x \neq 0$ *and a constant* $\eta_t > 0$*, such that the orthogonality condition* $\frac{\partial V_M}{\partial \delta_x} f(x) = 0$ *is satisfied, then the system* (4.39) *is called transverse contracting in* $\mathcal{Z}$*. For every two solutions* x_1 *and* x_2 *with initial conditions in* $\mathcal{Z}$ *there then exists a time reparametrizations* $\theta(t)$ *such that* $x_1(t) \to x_2(\theta(t))$ *as* $t \to \infty$*. Furthermore, if there are no attracting equilibrium points in* $\mathcal{Z}$ *any solution starting in* $x(0) \in \mathcal{Z}$ *converges to* $\omega(t)$*, the unique periodic orbit of the system, as* $t \to \infty$*.*

A proof of this theorem is included in the Appendix A.3.

Remark 4.8. Note that transverse contraction is a weaker form of full contraction. Thus, in order to eliminate the possibility of trajectories converging to an attracting equilibrium point inside $\mathcal{Z}$ its existence has to be excluded. In practice, this can be done by adding the constraint $f(x) \neq 0$, $\forall x \in \mathcal{Z}$, in case no prior information on the equilibrium point is available.

We call the largest region $\mathcal{Z}^* \subseteq \mathbb{R}^n$, for which the transverse contraction criteria stated in Theorem 4.4 are satisfied, the *true* region of contraction. Any subset $\mathcal{Z} \subset \mathcal{Z}^*$ on which the criteria are satisfied is referred to as (inner) estimate of the ROC, with the corresponding M being called the *contraction metric*.

For $V_M(x, \delta_x) = \delta_x^T M(x) \delta_x$, the orthogonality condition becomes

$$\frac{\partial V_M}{\partial \delta_x} f(x) = \delta_x^T M(x) f(x) = 0. \tag{4.74}$$

A computationally tractable criteria for transverse contraction to hold is provided by the following theorem.

Theorem 4.5 ([MS14])**.** *The system* (4.39) *is transverse contracting with rate* η_t *and a metric* $V_M(x, \delta_x) = \delta_x^T M(x, \delta_x) \delta_x$*, if and only if there exists a function* $\lambda(x) \geq 0$*, such that*

$$C(x) \frac{\partial f(x)}{\partial x}^T + \frac{\partial f(x)}{\partial x} C(x) - \dot{C}(x) + 2\eta_t C(x) - \lambda(x) S(x) \leq 0, \tag{4.75}$$

where $S(x) := f(x) f(x)^T$ *and* $C(x) := M(x)^{-1}$*.*

The proof is found in [MS14].

Equation (4.75) represents sufficient conditions for a region to be contracting, which can be tested in a computationally tractable way. In order to obtain a ROC estimate, Theorem 4.4 further requires positive invariance of the contracting region to hold. Consequently, (4.75) has to either be proven for all $x \in \mathbb{R}^n$ (which would show global contraction), or an additional invariance condition needs to be verified alongside condition (4.75). For full contraction, an invariance criteria is provided in [LS98], where (4.72) has to hold in a region which is a ball of constant radius with respect to the metric M (Theorem 2 in [LS98]). While in [TM14] (Theorem 2) it was shown how the same criteria

applies to a ball of constant radius with respect to the metric in the transverse subspace, this criteria can not directly be applied to (4.72) in a computationally tractable, i.e., convex, way. The reason for this is that the contraction condition is posed on the inverse of the metric while the invariance has to hold for a ball with respect to the metric, resulting in the search for a matrix with conditions on its entries and the entries of its inverse both of which are functions in x. Formulating convex criteria is thus not directly possible[4].

One solution is offered by imposing an additional invariance condition on the region for which contraction is analyzed. Since this increases the overall size of the problem, it is desirable to reduce the state dimension by formulating the contraction conditions only for the *transverse subspace*. This formulation can be obtained by using the transverse coordinate transformation presented in Section 4.3 and has been proposed in [MS14] and [TM14]. We use this contraction condition for the transverse subspace, extend it for uncertain systems and complete the analysis of a ROC by imposing suitable invariance conditions.

A ROC from consideration of the transverse subspace

Considering contraction conditions specifically for the transverse subspace reduces the state dimension by one and is thus leading to a significant reduction in computational complexity.

The $(n-1)$-dimensional subspace is given by all δ_x satisfying the orthogonality condition. In terms of the transverse coordinates defined in Section 4.3 this subspace is represented by the hyperplanes transverse to the system flow and will further be referred to as the *transverse subspace*. The system dynamics in this subspace are obtained by the transformation of the system into transverse coordinates as presented in Section 4.3.1.

In order to formulate the transverse contraction criteria the differential forms of the transverse coordinates need to be introduced. Referred to as transverse differential coordinates $(\delta_\tau, \delta_\rho)$, they represent virtual displacements in τ and ρ. Let

$$\begin{bmatrix} \delta_\tau \\ \delta_\rho \end{bmatrix} = \Theta(x,t)\delta_x, \tag{4.76}$$

where Θ is the transformation to transverse differential coordinates obtained from the Jacobian of an MOC $[v(\tau), Z(\tau)]^T$. By construction, δ_ρ lies in the subspace defined by all δ_x for which a Riemannian metric $M(x)$ can be found such that $\delta_x^T M(x) f(x) = 0$.

In [MS14] it is shown how to find a $M(x)$ which is also a contraction metric for the

[4]Unless the entries of the metric M are independent of x, in which case computationally tractable criteria could be obtained from the Schur complement.

transversal system. To this end, the time derivative of the differential forms is considered,

$$\frac{d}{dt}\begin{bmatrix}\delta_\tau \\ \delta_\rho\end{bmatrix} = \begin{bmatrix} 0 & * \\ 0 & A_{\mathcal{S}}(\tau,\rho)\end{bmatrix}\begin{bmatrix}\delta_\tau \\ \delta_\rho\end{bmatrix}, \tag{4.77}$$

where $A_{\mathcal{S}}(\tau,\rho)$ is the Jacobian of the transverse dynamics in (4.38), defined as

$$A_{\mathcal{S}}(\tau,\rho) = \frac{\partial f_{\mathcal{S}}(\tau,\rho)}{\partial \rho}, \tag{4.78}$$

where $f_{\mathcal{S}}(\tau,\rho) = \dot{\rho}$ for (4.39). The differential system (4.77) is linear in $[\delta_\tau, \delta_\rho]^T$. Using Lyapunov arguments, (4.77) is asymptotically stable and hence contracting if and only if there exists a positive symmetric matrix $M_{\mathcal{S}} \in \mathbb{R}^{(n-1)\times(n-1)}$ satisfying

$$A_{\mathcal{S}}(\tau,\rho)^T M_{\mathcal{S}}(\tau,\rho) + M_{\mathcal{S}}(\tau,\rho)A_{\mathcal{S}}(\tau,\rho) + \dot{M}_{\mathcal{S}}(\tau,\rho) < -\eta_{\mathcal{S}}\mathbb{I}, \tag{4.79}$$

for some $\eta_{\mathcal{S}} > 0$. Here,

$$\dot{M}_{\mathcal{S}ij}(\tau,\rho) = \frac{\partial M_{\mathcal{S}ij}}{\partial \rho}\dot{\rho} + \frac{\partial M_{\mathcal{S}ij}}{\partial \tau}\dot{\tau}, \tag{4.80}$$

where i, j denote the row and column of the matrix $M_{\mathcal{S}}$.

With the metric found in (4.79), the distance function

$$V_M(\tau,\rho,\delta_\tau,\delta_\rho) = \delta_p^T M(\tau,\rho)\delta_p, \qquad \delta_p := [\delta_\tau,\delta_\rho]^T, \tag{4.81}$$

can be defined. Imposing $\delta_\tau M(\tau,\rho)\delta_\rho = 0$ we can write

$$V_M(\tau,\rho,\delta_\tau,\delta_\rho) = \begin{bmatrix}\delta_\tau \\ \delta_\rho\end{bmatrix}^T \begin{bmatrix} M_v & 0 \\ 0 & M_{\mathcal{S}}(\tau,\rho)\end{bmatrix}\begin{bmatrix}\delta_\tau \\ \delta_\rho\end{bmatrix} \tag{4.82}$$

$$= \delta_\tau^2 + \delta_\rho^T M_{\mathcal{S}}(\tau,\rho)\delta_\rho, \tag{4.83}$$

where we assume w.l.o.g $M_v = 1$. This metric satisfies the transverse contraction criteria of Theorem 4.4 and represents the desired contraction metric M.

If the contraction condition (4.79) hold for all $x \in \mathcal{Y}$ where $\mathcal{Y} \subseteq \mathbb{R}^n$ is a compact connected set and where additionally $\mathcal{Y} \subseteq \mathcal{V}_\tau$ with $\mathcal{V}_\tau$ is as in Definition 4.3 is enforced, then $\mathcal{Y}$ is called a *transverse contracting region*.

Contraction in the Transverse Subspace - Uncertain System

From the results for deterministic system we now derive transverse contraction conditions for the uncertain system (4.68).

Defining

$$f^\phi(\tau,\rho) := \begin{bmatrix}(f_0(\tau,\rho) + \phi(\tau,\rho,\vartheta))_v \\ (f_0(\tau,\rho) + \phi(\tau,\rho,\vartheta))_{\mathcal{S}}\end{bmatrix} = \begin{bmatrix}\dot{\tau} \\ \dot{\rho}\end{bmatrix}, \tag{4.84}$$

and

$$A^{\phi}_{\mathcal{S}}(\tau,\rho,\vartheta) := \frac{\partial (f_0(\tau,\rho)+\phi(\tau,\rho,\vartheta)_{\mathcal{S}}}{\partial \rho}, \tag{4.85}$$

the contraction condition of (4.79) results in

$$A^{\phi}_{\mathcal{S}}(\tau,\rho,\vartheta)^T M_{\mathcal{S}}(\tau,\rho) + M_{\mathcal{S}}(\tau,\rho) A^{\phi}_{\mathcal{S}}(\tau,\rho,\vartheta) + \dot{M}^{\phi}_{\mathcal{S}}(\tau,\rho,\vartheta) < -\eta_{\mathcal{S}}\mathbb{I}, \tag{4.86}$$

for some $\eta_{\mathcal{S}} > 0$ and for all $\phi \in \mathcal{D}$. If (4.86) holds for all $(\tau,\rho) \in \mathcal{Y}$ with $\mathcal{Y} \subseteq \mathcal{V}_\tau$ then $\mathcal{Y}$ is a transverse contracting region for the uncertain system (4.68)

Note that in general the metric $M_{\mathcal{S}}(\tau,\rho)$ in condition (4.86) can also be dependent on ϑ. In numerical implementations this leads to potentially less conservative results at the exchange of (significantly) increased computational costs.

Since $\mathcal{D}$ has infinitely many elements, for each $x \in \mathcal{Y}$ condition (4.86) represents infinitely many constraints. We define

$$\hat{\mathcal{D}} := \{\hat{\phi} \,|\, \hat{\phi}(\tau,\rho) = \tilde{\Phi}(\tau,\rho)\vartheta_d, \text{ with } \vartheta_d \in \{\vartheta^L_d, \vartheta^U_d\}, \forall d\}, \tag{4.87}$$

where $\hat{\mathcal{D}}$ is a finite subset of $\mathcal{D}$. Thus containing only a finite number of elements, $\hat{\mathcal{D}}$ can now be used to express (4.86) as a finite number of constraints in ϑ. This is similar to an approach proposed by [TP09] for uncertain equilibrium points.

Proposition 4.1. *If*

$$\begin{aligned} &A^{\hat{\phi}}_{\mathcal{S}}(\tau,\rho)^T M_{\mathcal{S}}(\tau,\rho) + M_{\mathcal{S}}(\tau,\rho) A^{\hat{\phi}}_{\mathcal{S}}(\tau,\rho) + \dot{M}^{\hat{\phi}}_{\mathcal{S}} < -\eta_{\mathcal{S}}\mathbb{I}, \\ &\eta_{\mathcal{S}} > 0, \ \ \forall (\tau,\rho) \in \mathcal{Y} \subseteq \mathcal{V}_\tau, \end{aligned} \tag{4.88}$$

holds for all $\hat{\phi} \in \hat{\mathcal{D}}$, then (4.86) holds for all $\phi \in \mathcal{D}$.

Proof. Let $y \in \mathcal{Y}$ and $\phi \in \mathcal{D}$, then there exist $w_1(y), ..., w_n(y)$ with $0 \le w_i(y) \le 1$ such that $\phi(y)$ can be expressed as a convex combination of $(\vartheta^L, \vartheta^U)$, i.e. $\phi(y) = \tilde{\Phi}(y)(W\vartheta^L + (I-W)\vartheta^U)$, where W is diagonal with $W_{ii} = w_i$. Determined by W there exist nonnegative scalars $\mu_{\hat{\phi}}$ for $\hat{\phi} \in \hat{\mathcal{D}}$ with $\sum_{\hat{\phi}\in\hat{\mathcal{D}}} \mu_{\hat{\phi}} = 1$ such that

$$\phi(y) = \sum_{\hat{\phi}\in\hat{\mathcal{D}}} \mu_{\hat{\phi}} \hat{\phi}(y), \quad \forall \phi \in \mathcal{D}. \tag{4.89}$$

Consequently, using

$$\begin{aligned} (f_0(y) + \phi(y,\vartheta))_{\mathcal{S}} &= \left(f_0(y) + \sum_{\hat{\phi}\in\hat{\mathcal{D}}} \mu_{\hat{\phi}} \hat{\phi}(y) \right)_{\mathcal{S}} \\ &= \sum_{\hat{\phi}\in\hat{\mathcal{D}}} \mu_{\hat{\phi}} \left(f_0(y) + \hat{\phi}(y) \right)_{\mathcal{S}}, \end{aligned} \tag{4.90}$$

and

$$\frac{\partial \left(f_0(y) + \phi(y,\vartheta)\right)_{\mathcal{S}}}{\partial \rho} = \frac{\partial \left(f_0(y) + \sum_{\hat{\phi}\in\hat{\mathcal{D}}} \mu_{\hat{\phi}} \hat{\phi}(y)\right)_{\mathcal{S}}}{\partial \rho} = \sum_{\hat{\phi}\in\hat{\mathcal{D}}} \mu_{\hat{\phi}} \frac{\partial \left(f_0(y) + \hat{\phi}(y)\right)_{\mathcal{S}}}{\partial \rho},$$

we find

$$\begin{aligned} &A_{\mathcal{S}}^{\phi}(\tau,\rho,\vartheta)^T M_{\mathcal{S}}(\tau,\rho) + M_{\mathcal{S}}(\tau,\rho) A_{\mathcal{S}}^{\phi}(\tau,\rho,\vartheta) + \dot{M}_{\mathcal{S}}^{\phi}(\tau,\rho,\vartheta) \\ &= \sum_{\hat{\phi}\in\hat{\mathcal{D}}} \mu_{\hat{\phi}} \left(A_{\mathcal{S}}^{\hat{\phi}}(\tau,\rho)^T M_{\mathcal{S}}(\tau,\rho) + M_{\mathcal{S}}(\tau,\rho) A_{\mathcal{S}}^{\hat{\phi}}(\tau,\rho) + \dot{M}_{\mathcal{S}}^{\hat{\phi}}(\tau,\rho) \right) \\ &\leq -\sum_{\hat{\phi}\in\hat{\mathcal{D}}} \mu_{\hat{\phi}} \eta_{\mathcal{S}} \mathbb{I} = -\eta_{\mathcal{S}} \mathbb{I}, \end{aligned}$$

and (4.88) follows. □

This result also applies if the uncertainty parameter is time-varying as long as $\vartheta^L \leq \vartheta(t) \leq \vartheta^U$.

Equation (4.88) provides finitely many constraints for an uncertain system to be transverse contracting for all $(\tau,\rho) \in \mathcal{Y}$. In order to verify a transverse contracting region $\mathcal{Y}$ to be a ROC estimate $\mathcal{Z}$, it remains to provide a criteria for $\mathcal{Y}$ to be invariant.

Lemma 4.3. *Let*

$$\mathcal{Z} := \{(\tau,\rho) \in \mathcal{I}_{T_0} \times \mathbb{R}^{n-1} \mid z(\tau,\rho) \leq \gamma\}, \tag{4.91}$$

be a compact region with $\Gamma \subset \mathcal{Z}$, where $z : \mathcal{I}_{T_0} \times \mathbb{R}^{n-1} \to \mathbb{R}$ is a continuous function and $\gamma > 0$ a positive constant. If

$$\mathcal{Z} \subseteq \mathcal{V}_\tau, \tag{4.92}$$

$$\nabla z(\tau,\rho) f^{\hat{\phi}}(\tau,\rho) < 0, \ \ \forall (\tau,\rho) \in \hat{\mathcal{Z}}, \ \forall \hat{\phi} \in \hat{\mathcal{D}}, \tag{4.93}$$

where $\hat{\mathcal{Z}} := \{(\tau,\rho) \,|\, z(\tau,\rho) = \gamma\}$, then $\mathcal{Z}$ is a strictly positively invariant region of the uncertain system (4.68) for all $\phi \in \mathcal{D}$.

Proof. Let $\psi^{\hat{\phi}}(x_0,\cdot)$ denote the solution to (4.84) for $\phi = \hat{\phi}$ starting at x_0. The existence and uniqueness of solutions for all $x_0 \in \mathcal{Z}$ for a given $\hat{\phi} \in \hat{\mathcal{D}}$ is given by the Lipschitz continuity of (4.68), the compactness of $\mathcal{Z}$ and the well-definedness of the transformation (4.13) holding for all $(\tau,\rho) \in \mathcal{V}_\tau$ by definition, if every solution is contained in $\mathcal{Z}$. Assume there exists an initial condition $x_0 \in \mathcal{Z}$ for which there exists a $\hat{\phi} \in \hat{\mathcal{D}}$ such that $\psi^{\hat{\phi}}(x_0,t)$ leaves the set. Then there must exists a $t^\dagger$ such that $x(t^\dagger) = \psi^{\hat{\phi}}(x_0,t^\dagger)$, which satisfies $z(x(t^\dagger)) > \gamma$. Due to the continuity of the solutions and the function $z(x)$ there must then exist a $\tilde{t}$, where $0 < \tilde{t} < t^\dagger$ such that $z(\tilde{t}) = \gamma$ at which $\dot{z}(\tilde{t}) \geq 0$. This contradicts

(4.93) and thus every solution starting inside $\mathcal{Z}$ remains inside the region for all $\hat{\phi} \in \hat{\mathcal{D}}$ and $\mathcal{Z}$ is strictly forward invariant. Since this holds for all $\forall \hat{\phi} \in \hat{\mathcal{D}}$, by using the same reparametrization as in (4.89) and following the steps as in the proof of Proposition 4.1, it is shown to hold for all $\phi \in \mathcal{D}$. □

Using Lemma 4.3 together with Theorem 4.4, the following theorem summarizes the conditions on a ROC estimate.

Theorem 4.6. *Let the region $\mathcal{Z} \subset \mathbb{R}^n$ be given as in (4.91) and satisfy (4.92) and (4.93). If there exists a metric $M_{\mathcal{S}}(x)$ for which (4.88) holds for all $x \in \mathcal{Y}$ and $\hat{\phi} \in \hat{\mathcal{D}}$, and it further holds that $\mathcal{Z} \subseteq \mathcal{Y}$, then $\mathcal{Z} \subseteq \mathcal{Z}^*$, i.e., $\mathcal{Z}$ is an inner estimate of the true region of contraction.*

Theorem 4.6 can be used to formulate computationally tractable conditions for a region $\mathcal{Z}$ to be an ROC estimate. This is demonstrated in the following.

4.5.2 Algorithms for maximizing an inner estimate of the ROC and the uncertainty bounds

In this section an algorithm is presented to compute an ROC estimate for an uncertain polynomial system with an attracting periodic orbit. The algorithm implements the conditions on a region $\mathcal{Z}$ and a contraction metric $M_{\mathcal{S}}$ as stated in Theorem 4.6 in order to maximize an ROC estimate. Further, a modification is presented which, for a prescribed fixed size of $\mathcal{Z}$, maximizes the allowed bounds on the uncertainty variation.

Maximizing inner estimates of the ROC

By taking $z(\tau, \rho) = \mathrm{v}(\rho)^T Z(\tau) \mathrm{v}(\rho)$ with $Z(\tau) \succ 0$, $\mathcal{Z}$ as in (4.91) describes a γ-sized sublevel set in ρ for each $\tau \in \mathcal{I}_{T_0}$. This set is centered around the nominal periodic orbit Γ_0 as this orbit is the τ-parametrized origin of the transverse coordinate system. Let a contraction metric $M_{\mathcal{S}}$ of degree r be of the form

$$M_{\mathcal{S}}(\tau, \rho) = \begin{bmatrix} \sum_k a_k(\tau)\rho^k & \sum_k b_k(\tau)\rho^k & \dots \\ \sum_k b_k(\tau)\rho^k & \sum_k c_k(\tau)\rho^k & \\ \vdots & & \ddots \end{bmatrix}, \tag{4.94}$$

where $M_{\mathcal{S}} : \mathcal{I}_{T_0} \times \mathbb{R}^{n-1} \to \mathbb{R}^{(n-1)\times(n-1)}$ and each entry is a polynomial of degree r as defined in (2.1).

With (4.94), condition (4.88) represents for each $\hat{\phi} \in \hat{\mathcal{D}}$ a matrix inequality with both polynomial and rational entries. The rational terms are caused by the $\dot{\tau}$-dynamics which contain $\nu(\tau, \rho)$ in the denominator. Similarly, (4.93) contains rational terms caused by

the appearance of $\dot{\tau}$. Due to the problem being formulated in transverse coordinates the well-definedness condition $\nu(\tau,\rho) > 0$ has to hold for all $(\tau,\rho) \in \mathcal{Z}$, in order for $\mathcal{Z} \subseteq \mathcal{V}_\tau$ (4.92). Note that the condition (4.14) is independent of the uncertainty as it is concerned with the coordinate system transformation only. For this reason and since a polynomial inequality such as (4.88) and (4.93) does not change its feasible set when multiplied by a positive term, both sides of (4.88) and (4.93) are multiplied by $\nu(\tau,\rho)$ to obtain equivalent constraints now given in polynomial form only.

The aim of the algorithm is to maximize the size of $\mathcal{Z}$ by finding more suitable metrics. To this end, a computationally tractable measure for the volume of $\mathcal{Z}$ is needed. In general, the algorithmic options presented in Section 4.4.2 for efficiently maximizing the ROA volume can be extended to the ROC. Trading off potentially more conservative results for improved computational tractability we choose the objective function as the sublevel set size of a fixed shaped set $\mathcal{B}$, where we additionally allow the sublevel set size to vary among the hyperplanes. The surrogate set is then given by

$$\mathcal{B} = \{\rho \in \mathbb{R}^{n-1} \,|\, \rho^T B_F \rho \leq \alpha(\tau),\, \tau \in \mathcal{I}_{T_0}\}, \tag{4.95}$$

where the matrix $B_F \in \mathbb{R}^{(n-1)\times(n-1)}$, $B_F \succ 0$, has constant entries. Serving as a surrogate set, the constraint

$$\mathcal{B} \subseteq \mathcal{Z}, \tag{4.96}$$

is imposed. The polynomial inequality constraints (4.14), (4.93), (4.96), and the matrix polynomial constraint (4.88) need to be satisfied for all $\hat{\phi} \in \hat{\mathcal{D}}$ and $(\tau,\rho) \in \mathcal{Z}$. Formulating these constraints as set containment conditions and applying the Positivstellensatz 2.2, SOS and matrix SOS constraints are obtained. The matrix SOS constraints can be cast as SOS constraints by introducing a new set of indeterminants with no physical meaning, as described in 2.1.4. Since the coefficients in $Z(\tau)$ are decision variable we fix $\gamma = 1$ in (4.91). Let $J = \text{cardinality}(\hat{\mathcal{D}})$ with each element indexed by $j = 1, ..., J$. Further, let

$$G^{\hat{\phi}_j}(\tau,\rho) := \left(A_{\mathcal{S}}^{\hat{\phi}_j}(\tau,\rho)^T M_{\mathcal{S}}(\tau,\rho) + M_{\mathcal{S}}(\tau,\rho) A_{\mathcal{S}}^{\hat{\phi}_j}(\tau,\rho) + \dot{M}_{\mathcal{S}}^{\hat{\phi}_j} \;+ \eta_{\mathcal{S}}\mathbb{I}\right)\nu(\tau,\rho), \tag{4.97}$$

be the inequality constraint (4.88) in polynomial form by multiplication with $\nu(\tau,\rho)$ as explained above, and evaluated for the uncertainty element $\hat{\phi}_j \in \hat{\mathcal{D}}$. Then the following optimization program with both SOS and matrix SOS constraints results.

$$\max_{\alpha, M_{\mathcal{S}}, Z, q_j, m_j, s_1, s_2, j=1..J} \quad \alpha(\tau) \tag{4.98a}$$

$$\text{subject to} \quad M_{\mathcal{S}}(\tau,\rho) \in \Sigma^{(n\text{-}1)\times(n\text{-}1)}[\tau,\rho], \tag{4.98b}$$

$$\nu(\tau,\rho) - \left(1 - \mathrm{v}(\rho)^T Z(\tau)\mathrm{v}(\rho)\right) s_1(\tau,\rho) \in \Sigma[\tau,\rho], \tag{4.98c}$$

$$-\left(\alpha(\tau) - \rho^T B_F \rho\right) s_2(\tau,\rho) + \left(1 - \mathrm{v}(\rho)^T Z(\tau)\mathrm{v}(\rho)\right) \in \Sigma[\tau,\rho], \tag{4.98d}$$

$$s_1(\tau,\rho),\ s_2(\tau,\rho) \in \Sigma[\tau,\rho], \tag{4.98e}$$

$$Z(\tau) \succ 0, \tag{4.98f}$$

$$\text{for each } j \in J: \ -G^{\hat{\phi}_j}(\tau,\rho) - \left(1 - \mathrm{v}(\rho)^T Z(\tau)\mathrm{v}(\rho)\right) m_j(\tau,\rho) \in \Sigma^{(n\text{-}1)\times(n\text{-}1)}[\tau,\rho], \tag{4.98g}$$

$$m_j(\tau,\rho) \in \Sigma^{(n\text{-}1)\times(n\text{-}1)}[\tau,\rho], \tag{4.98h}$$

$$-\left(\frac{\partial z(\tau,\rho)}{\partial \rho} f_{\mathcal{S}}^{\hat{\phi}_j}(\tau,\rho) + \frac{\partial z(\tau,\rho)}{\partial \tau} f_v^{\hat{\phi}_j}(\tau,\rho)\right) \nu(\tau,\rho) - q_j(\tau,\rho)\left(1 - \mathrm{v}(\rho)^T Z(\tau)\mathrm{v}(\rho)\right) \in \Sigma[\tau,\rho]. \tag{4.98i}$$

Constraint (4.98b) prescribes $M_{\mathcal{S}} \succ 0$ for all $(\tau,\rho) \in \mathcal{I}_{T_0} \times \mathbb{R}^{n-1}$ which, due to its structure, is not a stricter constraint than $M_{\mathcal{S}} \succ 0$ for all $(\tau,\rho) \in \mathcal{Z}$. Constraints (4.98c) and (4.98d) enforce the well-definedness condition, respectively the set containment of the surrogate set in $\mathcal{Z}$, with the help of SOS multipliers constrained as such in (4.98e). For each $j \in J$ an additional set of constraints (4.98g)-(4.98h) are added to the optimization program which enforce contraction for all $(\tau,\rho) \in \mathcal{Z}$ and each element in $\hat{\mathcal{D}}$, as well as invariance of $\mathcal{Z}$. The multipliers m_j in (4.98h) are matrix SOS multiplier which certify the matrix SOS constraint in (4.98g) to hold. Their structure is similar to the structure of the metric $M_{\mathcal{S}}$ displayed in (4.94). The multipliers $q_j(\tau,\rho)$ are indefinite polynomials which certify the equality constraint $z(\tau,\rho) = 1$ to hold in (4.98i).

In order to circumvent the increased complexity given by the τ-dependency, the constraints in problem (4.98) can be sampled for a N discrete values of τ over the full interval $[0,T]$, similarly to as it was done for the optimization problem (4.65). With a τ-sampling, the metric $M_{\mathcal{S}}$ has the structure

$$M_{\mathcal{S}}^{(i)}(\rho) = \begin{bmatrix} \sum_k a_k^i \rho^k & \sum_k b_k^i \rho^k & \cdots \\ \sum_k b_k^i \rho^k & \sum_k c_k^i \rho^k & \\ \vdots & & \ddots \end{bmatrix}, \tag{4.99}$$

and the following derivative with respect to τ

$$\frac{\partial M_{\mathcal{S}}^{(i)}(\rho)}{\partial \tau} = \frac{M_{\mathcal{S}}^{(i+1)}(\rho) - M_{\mathcal{S}}^{(i)}(\rho)}{\tau^{(i+1)} - \tau^{(i)}}. \tag{4.100}$$

The function $z(\tau,\rho)$ can be taken, e.g., as piecewise linear in τ, similar to (4.63).

This results in the following optimization problem which is now a generalized SOS program in the indeterminant ρ, with matrix SOS constraints.

$$\max_{\alpha^{(i)},M_{\mathcal{S}}^{(i)},Z^{(i)},q_j^{(i)},m_j^{(i)},s_1^{(i)},s_2^{(i)},i=1..N-1,j=1..J} \quad \sum_i^{N-1} \alpha^{(i)} \tag{4.101a}$$

$$\text{subject to} \qquad M_{\mathcal{S}}^{(i)}(\rho) \in \Sigma^{(n\text{-}1)\times(n\text{-}1)}[\rho], \tag{4.101b}$$

$$\nu^{(i)}(\rho) - \left(1 - \mathrm{v}(\rho)^T Z^{(i)} \mathrm{v}(\rho)\right) s_1^{(i)}(\rho) \in \Sigma[\rho], \tag{4.101c}$$

$$-\left(\alpha^{(i)} - \rho^T B_F \rho\right) s_2^{(i)}(\rho) + \left(1 - \mathrm{v}(\rho)^T Z^{(i)} \mathrm{v}(\rho)\right) \in \Sigma[\rho], \tag{4.101d}$$

$$s_1^{(i)}(\rho),\ s_2^{(i)}(\rho) \in \Sigma[\rho], \tag{4.101e}$$

$$Z^{(i)} \succ 0, \tag{4.101f}$$

$$\text{for each } j \in J: \ -G^{\hat{\phi}_j,(i)}(\rho) - \left(1 - \mathrm{v}(\rho)^T Z^{(i)} \mathrm{v}(\rho)\right) m_j^{(i)}(\rho) \in \Sigma^{(n\text{-}1)\times(n\text{-}1)}[\rho], \tag{4.101g}$$

$$m_j^{(i)}(\rho) \in \Sigma^{(n\text{-}1)\times(n\text{-}1)}[\rho], \tag{4.101h}$$

$$-\left(\frac{\partial z^{(i)}(\rho)}{\partial \rho} f_{\mathcal{S}}^{\hat{\phi}_j,(i)}(\rho) + \frac{\partial z^{(i)}(\rho)}{\partial \tau} f_v^{\hat{\phi}_j,(i)}(\rho)\right) \nu^{(i)}(\rho) - \\ -q_j^{(i)}(\rho)\left(1 - \mathrm{v}(\rho)^T Z^{(i)} \mathrm{v}(\rho)\right) \in \Sigma[\rho]. \tag{4.101i}$$

After introducing the auxiliary indeterminants for the matrix SOS conditions, the optimization problem has $(3J+6)(N\text{-}1)$ SOS constraints in $2(n-1)$ indeterminants. The solution of the resulting generalized SOS program is then obtained iteratively by fixing one term while optimizing over the other and vice versa. More details on the algorithmic implementation are provided after presenting the alternative optimization of maximizing the allowed uncertainty.

Remark 4.9. By taking $z(\tau,\rho) = \rho^T M_{\mathcal{S}}(\tau,\rho)\rho$ the number of decision variables can be reduced at the exchange of constraining the invariant region to a ball with respect to the metric.

Remark 4.10. The sublevel set size $\alpha(\tau)$ can be kept constant among the hyperplanes which is advisable if numerical issues occur in the computations.

Maximizing allowed parameter variation for a given $\mathcal{Z}$

In this section we present a modified problem in which the size of $\mathcal{Z}$ is fixed to a desired value and the question on the allowed magnitude variation of the parameteric uncertainty for the fixed set is answered.
In general the size of the ROC and the size of the uncertainty polytope $\hat{\mathcal{D}}$ trade off; the larger the uncertainty the smaller the ROC. An optimization over both the volume $\hat{\mathcal{D}}$ and the ROC estimate is thus not considered. In order to prevent the algorithm from maximizing $\hat{\mathcal{D}}$ by diminishing the volume of the ROC estimate, the size of $\mathcal{Z}$ is kept fixed for this case. Note that this makes the use of a surrogate set obsolete. Also, condition

(4.101c) needs to be tested for the fixed set $\mathcal{Z}$ only and can then be omitted. To allow for an increased flexibility of the generalized SOS program to certify the prescribed ROC estimate for larger uncertainties, the coefficients of the metric $M_{\mathcal{S}}$ can, however, optionally enter as decision variables. We consider the uncertainty to be symmetric around zero such that $\vartheta^L = -\vartheta^U$. The optimization program then results as follows.

$$\max_{\vartheta^U, M_{\mathcal{S}}^{(i)}, q_j^{(i)}, m_j^{(i)}, i=1..N-1, j=1..J} \quad \vartheta^U \tag{4.102a}$$

$$\text{subject to} \quad (4.101b), (4.101g)\text{-}(4.101i), \quad Z^{(i)} = Z_{\text{fix}}^{(i)}. \tag{4.102b}$$

Algorithms to maximize $\mathcal{Z}$ and ϑ^U

Algorithm 4.2 outlines the implementation of the generalized SOS program (4.101). The program is initialized by computing an initially feasible metric. This is obtained from solving the Lyapunov inequality (4.79) for the deterministic Jacobian $A_{\mathcal{S}}$ evaluated at $\rho = 0$, which gives a metric with constant entries. The region $\mathcal{Z}$ is initialized by using the sampled Lyapunov inequality result which is scaled until feasible SOS multiplier in (4.101) are found. The surrogate set is scaled to a sufficiently small size to satisfy (4.101d). Through a two step iteration the bilinear terms are efficiently circumvented and convex problems are obtained instead. In Step 1, the $M_{\mathcal{S}}$, Z and α are fixed and the corresponding constraints are solved to obtain the multipliers. Note that in this step the problem for each hyperplane and $\hat{\phi} \in \hat{\mathcal{D}}$ is independent of the others and can be solved as separate optimization problems which allows parallelization. In Step 2, the constraints on $M_{\mathcal{S}}^{(i)}$ and $Z^{(i)}$ for each hyperplane and each $\hat{\phi}$ are added to a single optimization problem maximizing for α. The algorithm terminates after the maximum relative increase in the $\alpha^{(i)}$ falls below a specified threshold.

Algorithm 4.3 describes the implementation of the generalized SOS program (4.102). Since this problem requires a desired size for the ROC estimate $\mathcal{Z}$, a feasible Z as well as an initial $M_{\mathcal{S}}$ need to be provided. These can be obtained by first computing Algorithm 4.2 for the case of very small uncertainty bounds and terminating it at the desired size of $\mathcal{Z}$. Since the decision variables in the program (4.102) appear bilinearly in not only $M_{\mathcal{S}}$ and the multiplier but additionally in $M_{\mathcal{S}}$ and the uncertainty bounds, the problem is here convexified by an iterative three-step algorithm. In the first step, multipliers are obtained from parallelizable feasibility problems while $M_{\mathcal{S}}$ and ϑ^U are kept fixed, similar to Step 1 in Algorithm 4.2. In the second step, a single large optimization problem is solved in which ϑ^U is maximized while keeping both the multipliers and $M_{\mathcal{S}}$ fixed. In Step 3, a single large feasibility test is performed in which a more suitable metric is obtained. These steps are repeated until the relative increase in each uncertainty bound has fallen below a specified threshold.

Algorithm 4.2 Find contraction metric to maximize $\mathcal{Z}$ for given uncertainty bounds

Input: N, $\partial(s_1^{(i)})$, $\partial(s_2^{(i)})$, $\partial(q_j^{(i)})$, $\partial(m_j^{(i)})$, $\partial(M_{\mathcal{S}}^{(i)})$, convCrit$_\alpha$, ϑ^L, ϑ^U, B_F
Output: $M_{\mathcal{S}}$, maximized $\mathcal{Z}$
procedure MAXIMIZEROCESTIMATE
    $A_{\mathcal{S}}^{\hat{\phi}_j}(\tau,\rho)$, $\xleftarrow{(4.85),(4.38),(4.36)}$ $f(x,\vartheta)$, $\omega(t)$, ϑ^L, ϑ^U
    Initialization:
    $A_{\mathcal{S}}(\tau,\rho)$, $\xleftarrow{(4.85),(4.38),(4.36)}$ $f_0(x)$, $\omega(t)$
    ${M_{\mathcal{S}\text{ini}}}^{(i)} \leftarrow M_{\mathcal{S}0}(\tau)$, zero-degree solution of (4.79) with $A_{\mathcal{S}}|_{\rho=0}$, sampled at $\tau^{(i)}$
    ${Z_{\text{ini}}}^{(i)} \leftarrow c \cdot {M_{\mathcal{S}\text{ini}}}^{(i)}$ bisect on c such that (4.101c),(4.101e)-(4.101i) feasible
    $\alpha_{\text{ini}} \leftarrow$ value of α by bisection such that (4.101d)-(4.101e) is feasible
    Iteration:
    $k \leftarrow 0$
    repeat
        $k \leftarrow k+1$
        Step 1:
        for $i = 1 : N-1$ **do**
            $s_1^{(i)} \leftarrow$ fix $Z^{(i)}$ solve (4.101c),(4.101e)
            $s_2^{(i)} \leftarrow$ fix $\alpha^{(i)}$, $Z^{(i)}$, solve (4.101d),(4.101e)
            for $j = 1 : J$ **do**
                $m_j^{(i)} \leftarrow$ fix $M_{\mathcal{S}}^{(i)}$, $Z^{(i)}$, solve (4.101g),(4.101h)
                $q_j^{(i)} \leftarrow$ fix $Z^{(i)}$, solve (4.101i)
        Step 2:
        $M_{\mathcal{S}}^{(i)}$, $\alpha^{(i)}$, $Z^{(i)}$, $_{i=1\ldots N-1} \leftarrow$ fix $m_j^{(i)}, q_j^{(i)}$, $s_1^{(i)}, s_2^{(i)}$, $_{i=1\ldots N-1,\, j=1\ldots J}$ solve (4.101a)-(4.101d), (4.101f)-(4.101g),(4.101i)
    until $\max(\alpha_{k+1}^{(i)} - \alpha_k^{(i)}) <$ convCrit$_\alpha$

Algorithm 4.3 Find contraction metric to maximize uncertainty bounds for a fixed $\mathcal{Z}$

Input: N, $\partial(q_j^{(i)})$ $\partial(m_j^{(i)})$, $\partial(M_{\mathcal{S}}^{(i)})$, $\text{convCrit}_{\vartheta^U}$
Output: $M_{\mathcal{S}}$, $\mathcal{Z}$, ϑ^L, ϑ^U
procedure MAXIMIZEUNCERTAINTYBOUNDS
    $A_{\mathcal{S}}^{\hat{\phi}_j}(\tau, \rho, \hat{\phi}_j)$, $\xleftarrow{(4.85),(4.38),(4.36)}$ $f(x, \vartheta)$, $\omega(t)$
    Initialization:
    ${M_{\mathcal{S}}}_{\text{ini}}^{(i)}$, $Z_{\text{ini}}^{(i)} \leftarrow M_{\mathcal{S}}^{(i)}$, $Z^{(i)}$, desired size $\mathcal{Z}$ from Algorithm 4.2 for $\vartheta^L, \vartheta^U \ll 1$
    Iteration:
    $k \leftarrow 0$
    repeat
        $k \leftarrow k + 1$
        Step 1:
        for $i = 1 : N\text{-}1$ **do**
            for $j = 1 : J$ **do**
                $m_j^{(i)} \leftarrow$ fix $M_{\mathcal{S}}^{(i)}$, ϑ_j^L, ϑ_j^U, solve (4.101g),(4.101h)
                $q_j^{(i)} \leftarrow$ fix ϑ_j^L, ϑ_j^U, solve (4.101i)
        Step 2:
        ϑ^L, $\vartheta^U \leftarrow$ fix $M_{\mathcal{S}}^{(i)}$, $m_j^{(i)}$, $q_j^{(i)}$, $_{j=1\ldots J, i=1\ldots N-1}$ solve (4.102a), (4.101g),(4.101i)
        Step 3:
        $M_{\mathcal{S}}^{i}$, $_{i=1\ldots N-1} \leftarrow$ fix ϑ^L, ϑ^U, $m_j^{(i)}$, $_{j=1\ldots J, i=1\ldots N-1}$ solve (4.101b), (4.101g)
    until $\max(\vartheta_{k+1}^U - \vartheta_k^U) <$ $\text{convCrit}_{\vartheta^U}$

4.5.3 Illustrative example

The results presented here were computed from the collection of scripts which are further presented in Chapter 6. In particular, the numerical criteria used for the comparisons are explained in Section 6.6.

The following planar example of a third order polynomial system is considered which is a modified version of the system presented in [GG05].

$$\begin{aligned} \dot{x}_1 &= x_2(x_1 + x_2 + 8) + (x_1^2 + x_2^2 - 1)(1 - x_1) + \vartheta x_2, \\ \dot{x}_2 &= -x_1(x_1 + x_2 + 3). \end{aligned} \tag{4.103}$$

The system has a stable LC encircling an unstable equilibrium point and it further has a stable equilibrium point in the outside neighborhood of the LC. The location of both equilibrium points as well as the LC depend on the realization of the uncertainty. The change in location can be observed in Figure 4.10 which shows the phase portrait of the system for $\vartheta = 1$ (left plot) and the phase plot for $\vartheta = -1$ (right plot) for illustration.

Algorithm 4.2 was applied to the system for the nominal case with $\vartheta = 0$ and for the case of $\vartheta \in \{-0.3, 0.3\}$. Both cases were computed in the class-MOC and cp-MOC

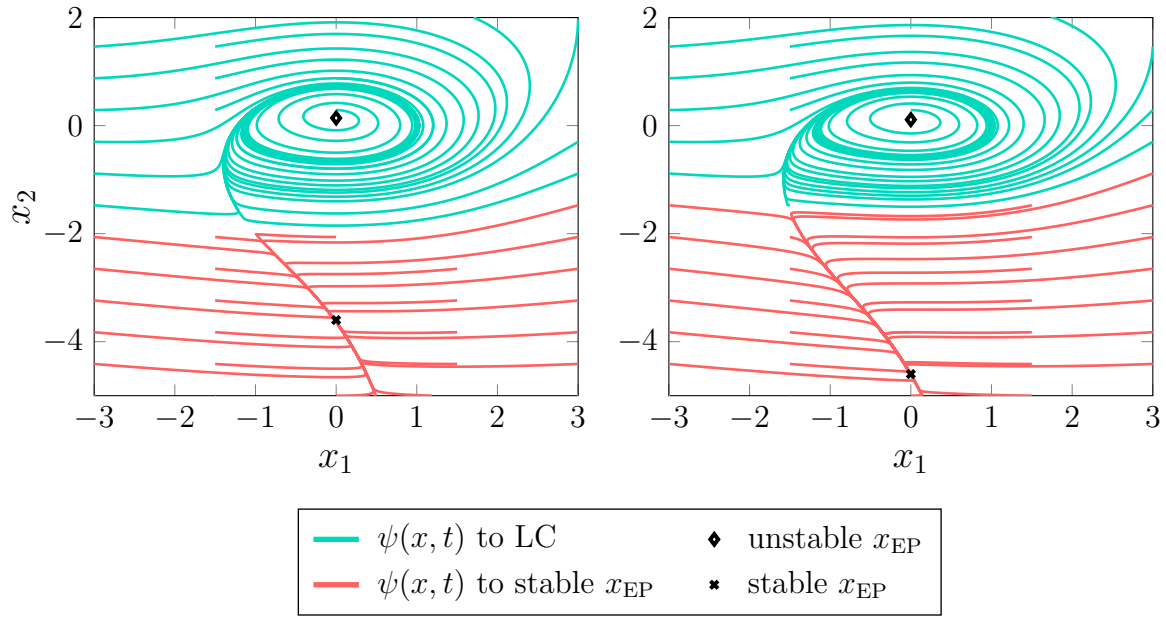

Figure 4.10: Phase portraits of the dynamics (4.103). *Left plot:* For the case of $\vartheta = 1$. *Right plot:* For the case of $\vartheta = -1$.

with $x_c = [0, 0]^T$ for comparison, where 50 discrete values of τ resulting in 49 distinct hyperplanes were chosen.

Figure 4.11 illustrates the results for the uncertain case in a planar plot. Additionally, Algorithm 4.3 was used to compute the maximum bounds $\{\vartheta^L, \vartheta^U\}$ for a prescribed region in the cp-MOC. In Figure 4.12 the results are shown in form of the volume obtained on each hyperplane. The maximized uncertainty was obtained as $\{\vartheta^L = -0.71, \vartheta^U = 0.71\}$. It can be seen in Figure 4.12 that the prescribed region $\mathcal{Z}$ for the uncertainty maximization is distinctly smaller than the ROC estimate obtained for the fixed uncertainty case, which however enabled the algorithm to obtain larger uncertainty bounds. This is consistent with the results of $\mathcal{Z}$ obtained for the nominal case which are larger than the regions with uncertainty. Finally, both Figure 4.12 and Figure 4.12 show how the results for the cp-MOC significantly exceed the results for the class-MOC.

The multiplier degrees in the Algorithm 4.2 were set to $\partial(s_1) = 2$, $\partial(s_2) = 2$, $\partial(m) = 4$, $\partial(q) = 4$, and the metric degree was chosen as $\partial(M) = 2$. The invariant region was chosen as ball with respect to the metric, as mentioned in Remark 4.9. For Algorithm 4.2, the multiplier degrees were kept at $\partial(m) = 4$ and $\partial(q) = 4$.

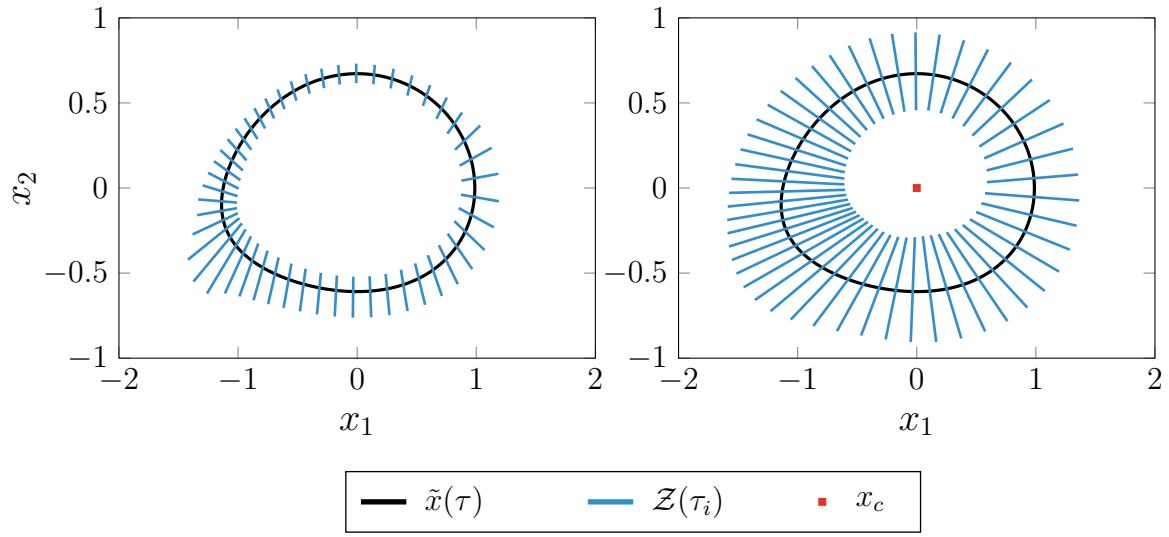

Figure 4.11: Illustration of the sets $\mathcal{Z}$ obtained from Algorithm 4.2 for the uncertain system with $\vartheta \in \{-0.3, 0.3\}$. *Left plot:* Results for the class-MOC. *Right plot:* Results for the cp-MOC.

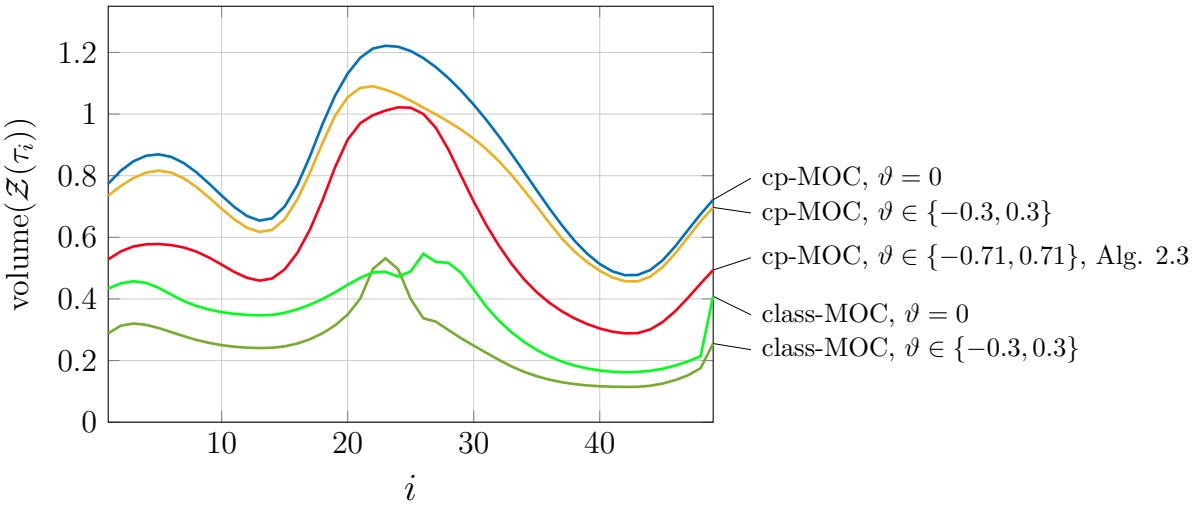

Figure 4.12: Comparison of the sizes of $\mathcal{Z}$ as a function of τ resulting from Algorithm 4.2 for the nominal case and for $\vartheta \in \{-0.3, 0.3\}$ each computed for the class-MOC and the cp-MOC. Additionally, results from Algorithm 4.3 are shown in which, for the fixed sized $\mathcal{Z}$, a maximum uncertainty of $\vartheta \in \{-0.71, 0.71\}$ was obtained. In each case the metric degree was 2.

4.6 On the contraction analysis of stochastic periodic orbits

As the last class of systems with limit cycle behavior, we now consider continuous time second order processes,

$$\dot{x}(t,\xi) = f(x(t,\xi),\kappa(\xi)), \tag{4.104}$$

where $x \in \mathbb{R}^n$ is the random state variable, $\kappa(\xi) \in \mathcal{L}_2(\Theta,\mu;\mathbb{R}^m)$ is a vector of $\mathcal{L}_2$-bounded uncertain parameters, ξ is the one-dimensional stochastic germ as defined in Section 2.2.1, and $f : \mathbb{R}^n \times \mathbb{R}^m \to \mathbb{R}^n$ is a polynomial function in x and κ. The initial state is random as well, $x(0) = x_{\text{ini}}(\xi)$. We further assume the support Θ of the stochastic germ $\xi \in \mathcal{L}_2(\Theta,\mu)$ to be finite, as stated in Assumption 3.1. The system (4.104) has an uncertainty-dependent periodic orbit set Γ as as given in equation (4.3) which is asymptotically orbitally stable as defined in Definition 4.2. Thus, for each realization of $\xi^\dagger \in \Theta$ trajectories starting in a neighborhood of Γ converge to a limit cycle $\Gamma_{\xi^\dagger} \subset \Gamma$ as $t \to \infty$, where $\Gamma_{\xi^\dagger}$ is defined as in (4.2). Based on these properties, the true region of attraction of the periodic orbit set is then defined as in 4.4 where the uncertainty is now generated by the random variable $\xi \in \Theta$. Since we apply contraction criteria for the analysis of the set (4.4), we refer to it as ROC with the true ROC set indicated by $\mathcal{Z}^*$, similar to the notation in Section 4.5.

As in Chapter 3, let the PCE of the stochastic system (4.104) be denoted by

$$\dot{\bar{x}} = \bar{f}(\bar{x}), \tag{4.105}$$

where $\bar{x} \in \mathbb{R}^{n(p+1)}$ is the vector of PCE coefficients of the state $x \in \mathbb{R}^n$, and $\bar{f} : \mathbb{R}^{n(p+1)} \to \mathbb{R}^{n(p+1)}$ specifies the PCE coefficient dynamics.

4.6.1 PCE for limit cycle systems

It has been previously shown [PB06] that the PCE of a stochastic system with limit cycle is able to accurately represent the *short-time* statistical variations of the system's trajectories. However, the PCE fails to accurately reproduce the *spatial* statistical properties (such as the location of the mean limit cycle, or the variance of particular solutions of interests such as peak amplitude values [MKB03]) of the periodic solution for *long* time spans, even for high truncation orders. Several modified PCE approaches have been proposed to obtain more accurate long-term representations of the purely spatial variations of a limit cycle. For example, an equation-free approach essentially resulting in studying the dynamics on Poincaré maps-like hyperplanes was proposed in [XKG05]. In [LLC10] the authors present a multi-element approach which results in a grid of local expansions. Alternatively, a better suited basis for oscillatory responses can be used, such as Wiener-Haar wavelets proposed in [PB06], or Fourier polynomials which were

introduced in [MKB03].
For the purpose of the analysis presented here, the exact spatial statistics of the periodic orbit are not required to be known. This allows us to leverage short-time accuracy of the PCE in order to represent the statistical behavior of the trajectories in the vicinity of a periodic solution. As for the periodic solution itself we take advantage of the fact that the *qualitative* behavior is still accurately captured by the PCE. That is, the PCE dynamics are able to discriminate between the existence or not of a periodic attractor, while we do not attempt to use it to characterize other properties, e.g., the mean or variance of amplitude and/or frequency.

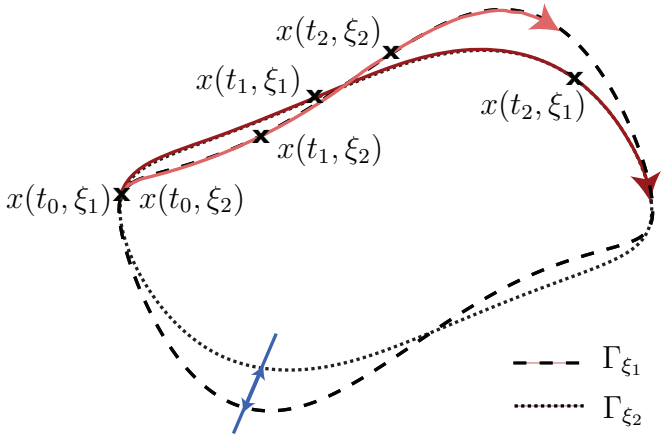

Figure 4.13: Illustration of two trajectories starting from the same initial point for two different realizations of the uncertainty, ξ_1 and ξ_2. Both follow a limit cycle corresponding to their uncertainty. The state of both trajectories at the same time t_1 and t_2 is indicated. The mean and variance of those states for each fixed time clearly differ from a purely spatial mean and variance at a fixed location, here indicated by the hyperplane in blue.

More precisely, we find the following.

Lemma 4.4. *If the system (4.104) has a stochastic periodic solution $\omega(t, \xi)$, then the PCE coefficient system (4.105) also has a periodic solution $\bar{\omega}(t)$.*

Proof. The PCE coefficients of a random process are obtained from the projection (2.19), in particular

$$\begin{aligned}\bar{f}(\bar{x}(t)) &= \gamma^{-1}\langle f(x(t,\xi),\kappa(\xi)),\Phi_j(\xi)\rangle \\ &= \gamma^{-1}\int_\Theta f(x(t,\xi),\kappa(\xi))\Phi_i(\xi)d\mu(\xi).\end{aligned}$$

Since the polynomial basis $\{\Phi_i(\xi)\}_{i=0}^{\infty}$ is time invariant, the projection of a variable or process which is periodic for all ξ in the domain of integration onto a member $\Phi_i(\xi)$ of the basis is a linear combination of periodic quantities and thus is also periodic. □

Similarly to the notation for the stochastic system, we define for the PCE system the set containing the periodic solution as

$$\bar{\Gamma} = \{\bar{x} \in \mathbb{R}^{n(p+1)} \,|\, \bar{x} = \bar{\omega}(t),\ t \in \mathcal{I}_{T_{\bar{\omega}}}\}, \tag{4.106}$$

with period $\mathcal{I}_{T_{\bar{\omega}}}$ of the PCE orbit. For small t, the solution of (4.105) represents the *spatial* statistics of the periodic solutions $\omega(t, \xi)$ but for $t \gg 0$ the PCE solutions converge to a periodic behavior which differs from the spatial statistics of $\omega(t, \xi)$. This can be intuitively understood by considering that PCE represents the 'full' statistics, which includes spatial and *temporal* statistics. Trajectories starting from the same initial condition in the set Γ but with a different realization of the uncertainty will, in general, not only vary in the exact location of the periodic solution but also in the speed with which they travel the orbit, i.e., their frequency. Considering, for example, the mean of the spatial variability over all trajectories after a certain time t has passed, one clearly sees that, in general, they differ significantly from the spatial variability one would expect to find from, e.g., Poincaré maps-like or hyperplane considerations. An illustration of the temporal and spatial variation is provided in Figure 4.13.

Note, that the reverse of Lemma 4.4 does not necessarily hold when the expansion (2.18) is truncated. For the truncated system we thus impose Assumption 3.2, which in this context implies the assumption that the truncated PCE system represents the properties under consideration, i.e. short-time accuracy of statistics and periodicity of solutions, accurately.

4.6.2 Regions of transverse contraction

The aim in the following is to obtain inner estimates of the true ROC, $\mathcal{Z}^*$, by means of PCE representations. The first step towards this goal is to establish a connection between the stochastic orbital stability of the stochastic orbit and the deterministic orbital stability of the PCE orbit.

Proposition 4.2. *Let $K \subset \mathbb{R}^n$ be a region such that $\Gamma \subset K$, and further $\bar{\Gamma} \subset \bar{K} \subset \mathbb{R}^{n(p+1)}$, where*

$$\bar{K} = \{\bar{x} \in \mathbb{R}^{n(p+1)} \,|\, \bar{x}_i = \gamma_i^{-1}\langle x, \Phi_i\rangle, x \in K\}. \tag{4.107}$$

Then the orbit Γ defined in (4.3) is stochastically asymptotically orbitally stable in K if the PCE orbit $\bar{\Gamma}$ is asymptotically orbitally stable in the region $\bar{K}$.

Proof. Asymptotic orbital stability of $\bar{\Gamma}$ in $\bar{K}$ implies that any solution starting at $\bar{x}_{\text{ini}}$ in the neighborhood of $\bar{\Gamma}$ eventually converges to it, i.e., $\bar{\psi}(\bar{x}_{\text{ini}}) \to \bar{\Gamma}$ as $t \to \infty$, where $\bar{\psi}(\bar{x}_{\text{ini}}, \cdot)$ denotes the flow (4.105). Further, $x_{\text{ini}}(\xi) = \sum_{i=0}^{p} \bar{x}_{\text{ini}i}\Phi_i(\xi)$ from the PCE representation (2.18). Let $\bar{\psi}(\cdot, \cdot)$ be the flow of the PCE system (4.105). Assume, that $\exists\, x_{\text{ini}}(\xi)$ for which $\psi(x_{\text{ini}}(\xi), t) \not\to \Gamma$ as $t \to \infty$. Then $\lim_{t\to\infty} \psi(x_{\text{ini}}(\xi), t) =$

$\lim_{t\to\infty} \sum_{i=0}^{p} \bar{\psi}(\bar{x}_{\text{ini}}, t)_i \Phi_i(\xi) = \sum_{i=0}^{p} \bar{\omega}_i(t)\Phi_i(\xi) = \omega(\xi, t)$, which is in contradiction with the assumption. The statement of the proposition thus follows. □

Leveraging Proposition 4.2, the stochastic orbital stability of the periodic orbit Γ can be investigated by analyzing the orbital stability of the PCE orbit. The problem is addressed by first finding regions in which a PCE system is converging to $\bar{\Gamma}$ and then retrieving from them the region in which the stochastic system converges to Γ. That is, an inner estimate of $\mathcal{Z}^*$ (4.4) is computed.

Transverse contraction criteria

Since, just as in Section 4.5, the location of both stochastic and PCE orbit are in general unknown, Lyapunov arguments cannot be applied for the stability analysis. Instead, we again employ contraction methods. In this case, however, we do not consider a transformation to transverse coordinates but keep the full state dimension and focus on the contraction condition given in Theorem 4.5. Since the aim is to investigate contraction of the stochastic system by contraction of its PCE, we first consider a Riemannian metric function in the $\bar{x}$ coordinates:

$$V_M(\bar{x}, \delta_{\bar{x}}) = \delta_{\bar{x}}^T M(\bar{x}, \delta_{\bar{x}})\delta_{\bar{x}}, \tag{4.108}$$

where $\delta_{\bar{x}}$ is a virtual displacement, i.e., an infinitesimal displacement of $\bar{x}$ at fixed time, and $V_M(\bar{x}, \delta_{\bar{x}})$ measures the squared distance with respect to the metric $M \succ 0$.

Since the PCE system $\bar{f}(\bar{x})$ is deterministic, transverse contraction criteria for the system in a positively invariant region $\bar{Z}$ with $\bar{\Gamma} \subset \bar{Z}$ are given by Theorem 4.4. Thus, if the PCE system is transverse contracting in an invariant region $\bar{Z}$, then every trajectory starting in $\bar{Z}$ eventually converges the unique limit cycle $\bar{\Gamma} \subset \bar{Z}$. The largest such region $\bar{Z}$ is then defined as:

$$\bar{\mathcal{Z}}^* = \{\bar{x}_{\text{ini}} \in \mathbb{R}^{n(p+1)} \mid \lim_{t\to\infty} \operatorname{dist}(\bar{\psi}(\bar{x}_{\text{ini}}, t), \bar{\Gamma}) = 0\}, \tag{4.109}$$

where $\bar{\psi}(\cdot, \cdot)$ is the flow of the PCE system (4.105).

The PCE system's transverse contracting behavior can be tested by condition (4.75), and conditions on the positive invariance of a region are stated in Lemma 4.3. By invoking both previous results, conditions on a region $\bar{\mathcal{Z}}$ to be an inner estimate of the true ROC $\bar{\mathcal{Z}}^*$ are obtained as follows.

Theorem 4.7. *Let $B : \mathbb{R}^{n(p+1)} \to \mathbb{R}$ be a continuously differentiable function and let $\bar{\mathcal{Z}} = \{\bar{x} \in \mathbb{R}^{n(p+1)} | B(\bar{x}) \leq \beta\}$ where β is a positive scalar such that $\bar{\Gamma} \subset \bar{\mathcal{Z}}$. If*

- *there exists a metric function $V_M(\bar{x}, \delta_{\bar{x}}) = \delta_{\bar{x}}^T M(\bar{x}, \delta_{\bar{x}})\delta_{\bar{x}}$, a convergence rate η_t and a function $\lambda(\bar{x}) \geq 0$, such that*

$$C(\bar{x})\frac{\partial \bar{f}(\bar{x})}{\partial \bar{x}}^T + \frac{\partial \bar{f}(\bar{x})}{\partial \bar{x}}C(\bar{x}) - \dot{C}(\bar{x}) + 2\eta_t C(\bar{x}) - \lambda(\bar{x})S(\bar{x}) \leq 0, \quad \forall \bar{x} \in \bar{\mathcal{Z}}, \tag{4.110}$$

where $S(\bar{x}) := \bar{f}(\bar{x})\bar{f}(\bar{x})^T$, $C(\bar{x}) := M(\bar{x})^{-1}$ *and* $\dot{C}(\bar{x}) = -M^{-1}(\bar{x})\dot{M}(\bar{x})M^{-1}(\bar{x})$, *and*

- *the derivative of* B *with respect to time on the boundary of* $\bar{\mathcal{Z}}$ *is negative, i.e.*

$$\nabla B(\bar{x})\bar{f}(\bar{x}) < 0, \ \forall \bar{x} \in \hat{\bar{\mathcal{Z}}}, \tag{4.111}$$

where $\hat{\bar{\mathcal{Z}}} := \{\bar{x} \,|\, B(\bar{x}) = \beta\}$,

then the region $\bar{\mathcal{Z}}$ *is transversely contracting and positively invariant. Thus,* $\bar{\mathcal{Z}} \subseteq \bar{\mathcal{Z}}^*$, *i.e.* $\bar{\mathcal{Z}}$ *is an inner estimate of th ROC of the system* (4.105), *and all trajectories starting inside* $\bar{\mathcal{Z}}$ *converge to* $\bar{\Gamma}$.

Applied to PCE systems, a proof of the first property is given by the proof of Theorem 4.5, and the proof for the second property is presented by the proof of Lemma 4.3.

Retrieving $\mathcal{Z}$ from $\bar{\mathcal{Z}}$

In order to retrieve an inner estimate $\mathcal{Z}$ of the true ROC of the stochastic system we use an approach similar to the one proposed in Section 3.2.3 for a ROA estimate of stochastic equilibrium points. More precisely, with a set $\bar{\mathcal{Z}}$ obtained for the PCE system from Theorem (4.7), a set $\mathcal{Z} \subseteq \mathcal{Z}^*$ of the stochastic orbit is obtained from the following condition.

Lemma 4.5. *Let* $\bar{\mathcal{Z}}$ *be an inner estimate of the ROC of the PCE system. Then the set*

$$\mathcal{Z} = \{x_{ini} \in \mathbb{R}^n \,|\, x_{ini}(\xi) = \sum_{i=0}^{p} \bar{x}_{ini,i}\Phi_i(\xi), \ \forall \bar{x}_{ini} \in \bar{\mathcal{Z}}\}, \tag{4.112}$$

is an inner estimate of the ROC of the stochastic system.

This Lemma results directly from the PCE representation (2.18) and from Proposition 4.2 applied to the sets given by the regions $\bar{\mathcal{Z}}$ and $\mathcal{Z}$.

The region $\mathcal{Z}$ as given by equation (4.112) is a stochastic region. An explicit expression for this region can be obtained by fixing the variance of the initial states to a desired value, and representing the region $\mathcal{Z}$ as the set of the mean values which are contained in $\bar{\mathcal{Z}}$ with that fixed variance, as described in Section 3.2.3.

4.6.3 Algorithm for computing PCE ROC

In this section we propose an optimization program to compute an ROC estimate $\bar{\mathcal{Z}}$ for (4.105) by verifying the conditions of Theorem 4.7. The optimization program consists of two parts. In the first part, the region in which the system is contracting is maximized by testing condition (4.110). This contracting region will be denoted by $\bar{\mathcal{Z}}_C$. In the second part, the largest invariant set inside of the contracting region is extracted in order to obtain a transversely contracting *and* invariant region $\bar{\mathcal{Z}}$.

Part 1: Maximizing the contracting region

In order to obtain a region $\bar{\mathcal{Z}}_C$ in which the system is transversely contracting, a metric has to be found which satisfies condition (4.110). Let the region $\bar{\mathcal{Z}}_C$ be given by the sublevel set β of a polynomial function $z(\bar{x}) = \mathrm{v}(\bar{x})^T Z \mathrm{v}(\bar{x})$, i.e., $\bar{\mathcal{Z}}_C := \{\bar{x} \,|\, z(\bar{x}) \leq \beta\}$, where $\mathrm{v}(\bar{x})$ is the vector of monomials. The optimization program both aims at finding a contraction metric M which satisfies the transverse contraction condition (4.110) for all $\bar{x} \in \bar{\mathcal{Z}}_C$, as well as maximize the region $\bar{\mathcal{Z}}_C$ itself. Since the condition (4.110) is in matrix polynomial form, we can employ a similar approach as in Section 4.5.2 and formulate set containment constraints in order to test the condition in a generalized SOS program.

In order to maximize the contracting region estimate the program optimizes over the sublevel set size β, while at the same time optimizing over the shape of the region given by Z. To prevent an increase of β by simple rescaling of Z the trace of Z is bounded by a constant value $a > 0$.

$$\max_{C(\bar{x}),\lambda(\bar{x}),s_1(\bar{x}),s_2(\bar{x}),Z} \quad \beta \tag{4.113a}$$

$$\text{subject to} \quad C(\bar{x}) - l \in \Sigma^{n\times n}[\bar{x}], \tag{4.113b}$$

$$-J(\bar{x}) - \eta C(\bar{x}) + \lambda(\bar{x})S(\bar{x}) - s_1(\bar{x})(\beta - z(\bar{x})) - s_2(\bar{x})(b(\bar{x}) - \epsilon) \in \Sigma^{n\times n}[\bar{x}], \tag{4.113c}$$

$$s_1(\bar{x}), s_2(\bar{x}) \in \Sigma^{n\times n}[\bar{x}], \tag{4.113d}$$

$$\lambda(\bar{x}) \in \Sigma[\bar{x}], \tag{4.113e}$$

$$Z \succ 0, \quad \mathrm{tr}(Z) \leq a, \tag{4.113f}$$

where $J(\bar{x}) := C(\bar{x})\frac{\partial \bar{f}(\bar{x})}{\partial \bar{x}}^T + \frac{\partial \bar{f}(\bar{x})}{\partial \bar{x}} C(\bar{x}) - \dot{C}(\bar{x})$, $b(\bar{x}) = \bar{f}^T \bar{f}$ and $\epsilon \ll 1$ is a small fixed constant. The last term in constraint (4.113c) serves to exclude equilibrium points at which the dynamics are zero and at which thus (4.110) does not hold. The matrix SOS multipliers $s_1(\bar{x})$ and $s_2(\bar{x})$ certify the matrix SOS constraints, and $l = \epsilon \bar{x}^T \bar{x}$ enforces strict positivity of $C(\bar{x})$.

Using the variable $y \in \mathbb{R}^{n(p+1)}$ as auxiliary indeterminants for the matrix SOS constraints as described in Section 2.1.4, we obtain a generalized SOS program with bilinear terms in the coefficients of the multiplier s_1 and β/Z. As in the algorithms presented in the previous sections, we solve the generalized SOS program (4.113) as a series of convex problems by the iterative procedure of fixing one bilinearly appearing variable while optimizing over the other and vice versa. This is done until the result for β converges. This iterative procedure can be initialized with a unit matrix Z and a bisection on β. More details are shown in the algorithmic outline in Algorithm 4.4.

Part 2: Finding an invariant region

In the second part, the set $\bar{\mathcal{Z}}$ is obtained as the largest invariant region inside of the contracting region estimate $\bar{\mathcal{Z}}_C$ obtained in Part 1. In order to obtain $\bar{\mathcal{Z}}$, con-

dition (4.111) can be directly tested on the boundary of the region $\bar{\mathcal{Z}}_C$. More generally, using a polynomial function $r(\bar{x}) = \mathrm{v}(\bar{x})^T R \mathrm{v}(\bar{x})$, a maximized invariant region $\bar{\mathcal{Z}} = \{\bar{x} \,|\, r(\bar{x}) \leq \beta_{\text{inv}}\} \subseteq \bar{\mathcal{Z}}_C$ can be obtained by applying Positivstellensatz arguments to the set containment condition on the invariant set. Setting $\partial(r) = \partial(z)$ and $\beta_{\text{inv}} = \beta$, where β is obtained in Part 1, the following feasibility problem in the form of a generalized SOS program is formulated. The aim of the program is to start from the largest possible set inside $\bar{\mathcal{Z}}_C$, e.g., the set $\bar{\mathcal{Z}}_C$ itself, and decreasing its size in the direction of decreasing derivatives at the boundary of the set until condition (4.111) is satisfied.

$$
\begin{aligned}
\text{find} \quad & R, q(\bar{x}), s(\bar{x}), \varepsilon && && \text{(4.114a)}\\
\text{subject to} \quad & -\left(\nabla r(\bar{x})\bar{f}(\bar{x}) - \varepsilon \bar{x}^T\bar{x}\right) - q(\bar{x})(\beta - r(\bar{x})) && \in \Sigma[\bar{x}], && \text{(4.114b)}\\
& -(\beta - r(\bar{x}))s(\bar{x}) - (z(\bar{x}) - \beta)) && \in \Sigma[\bar{x}], && \text{(4.114c)}\\
& s(\bar{x}) && \in \Sigma[\bar{x}], && \text{(4.114d)}\\
& \varepsilon < 0. && && \text{(4.114e)}
\end{aligned}
$$

The SOS polynomial $s(\bar{x})$ certifies the set containment $\bar{\mathcal{Z}} \subseteq \bar{\mathcal{Z}}_C$ in (4.114c), and the indefinite polynomial multiplier $q(\bar{x})$ results from the equality constraint in (4.93) imposed in (4.114b). The variable ε is used to enforce the program to find an invariant region $\bar{\mathcal{Z}}$. Since this invariant region is characterized by inwards pointing dynamics at the boundary (i.e. negative time derivative of the boundary), an invariant region is found as soon as a negative value for ε has been reached. In practice, the constraint (4.114e) is removed and the program (4.114) is solved as a minimization problem for ε. It is initialized with a feasible positive ε and proceeds with an iteration over the bilinearities in s and R until a $\varepsilon < 0$ is found by the minimization. Algorithm 4.5 outlines the procedure.

Remark 4.11. If program (4.114) cannot find a region for which ε is negative the reasons can be the following: Either, the contracting region $\bar{\mathcal{Z}}_C$ obtained in Part 1 is too small to contain an invariant region, or the invariant region inside $\bar{\mathcal{Z}}_C$ has a shape which cannot be fitted with a sublevel set of the polynomial function r. In the first case, a larger region can be searched for by increasing the polynomial degree of the metric and/or SOS multipliers in Part 1. In the second case, the polynomial degree of both z and r can be increased.

4.6.4 Comments on the implementation and examples

We use Algorithms 4.4 and 4.5 on the following stochastic system previously considered in a deterministic version in [GH13],

$$
\begin{aligned}
\dot{x}_1 &= -x_1 + x_2,\\
\dot{x}_2 &= x_1 - (2 + \kappa(\xi))x_2.
\end{aligned}
\tag{4.115}
$$

Algorithm 4.4 Part 1: Maximize the contracting region $\bar{\mathcal{Z}}_C$

Input: p, $\partial(s_1)$, $\partial(s_2)$, $\partial(\lambda)$, $\partial(C)$, $\partial(z)$, η, convCrit_β
Output: β, $\bar{\mathcal{Z}}_C$
procedure MAXCONTRACTINGREGION
    $\bar{f}(\bar{x}) \xleftarrow{\text{PCE}} f(x, a)$
    Initialization:
    $Z_{\text{ini}} \leftarrow \mathbb{I}$
    $a \leftarrow$ trace of Z_{ini}
    $\beta \leftarrow$ bisection on β with Z_{ini} until (4.113b)-(4.113e) feasible
    Iteration:
    $k \leftarrow 0$
    repeat
        $k \leftarrow k + 1$
        Step 1:
            s_1, s_2, λ, $C \leftarrow$ fix Z, β, solve (4.113b)-(4.113e)
        Step 2:
            Z, $\beta \leftarrow$ fix s_1, s_2, λ, C, solve (4.113a), (4.113c), (4.113f)
    until $\beta_k - \beta_{k-1} < \text{convCrit}_\beta$

Algorithm 4.5 Part 2: Find an invariant region $\bar{\mathcal{Z}} \subseteq \bar{\mathcal{Z}}_C$

Input: $\partial(s)$, $\partial(h)$, $\partial(r)$
Output: ε, $\bar{\mathcal{Z}}_C$
procedure FINDINVARIANTREGION
    Initialization:
    R_{ini}, $\beta_{\text{inv}} \leftarrow Z$, β results from Algorithm Part 1 (4.4)
    $\varepsilon \leftarrow$ bisection on ε until (4.114b)-(4.114d) feasible
    Iteration:
    $k \leftarrow 0$
    repeat
        $k \leftarrow k + 1$
        Step 1:
            s, $q \leftarrow$ fix R, ε, solve (4.114b)-(4.114d)
        Step 2:
            R, ε, $\leftarrow$ fix s, q, solve (4.114b)-(4.114d) while minimizing ε
    until $\varepsilon < 0$

The stochastic parameter κ is normally distribution with mean $\Lambda = 0$ and variance $\sigma^2 = 0.2$, i.e., the random variable ξ has standard normal distribution. As a basis for the PCE the Hermite polynomials are chosen as these give optimal convergence in the $\mathcal{L}_2$-sense for normal distributions. A truncation order $p = 2$ was used to capture the significant PCE modes. For a metric inverse with $\partial(C) = 2$, SOS multiplier degrees $\partial(s_1) = 2$, $\partial(s_2) = 0$, $\partial(\lambda) = 0$, $\partial(s) = 2$, $\partial(q) = 2$, a quadratic invariant and contracting region with R being the identity matrix $\mathbb{I}^{6\times 6}$ was found with a radius $\beta = 5$.

Due to the increased state dimension coming from the PCE and the matrix SOS constraints (which lead to a doubling of the number of indeterminants), a tractable implementation of Algorithm 4.4 for a more meaningful example has not yet been possible. In particular, we found that the degrees of the metric inverses, which would be necessary to find contracting regions sufficiently large to fit an invariant region, become prohibitively high for polynomial systems with degrees larger than one. A possible remedy under the current solver capabilities could be found by considering more flexible metrics and regions. For example, Algorithms 4.4 and 4.5 could be used to test for composite metrics, similar to an approach taken for composite Lyapunov functions in [TP08], or locally piecewise constructed metrics, similar to an approach for piecewise affine metrics in [GH13].

4.7 Conclusion

In this chapter we consider systems with limit cycles and propose methods to analyze the ROA, respectively ROC, of the orbits. For deterministic systems and systems affected by affine parametric uncertainty we use MOCs for the analyses. Based on the classical MOC of [Hal80] we propose an improved MOC, the cp-MOC, for which we present the construction algorithm, derive the class of systems for which it provides a well-defined transformation, and derive formal results on the well-defined range of the transformation. Lyapunov conditions for an inner estimate of the ROA of a deterministic LC and contraction conditions for an inner estimate of the ROC of the uncertain LC are formulated based on the MOCs. The implementation of the conditions under various algorithmic options into computationally efficient optimization programs is presented and illustrated by examples. For stochastic orbits we use the PCE framework to pose contraction conditions. Orbital stability of the stochastic limit cycle is connected to the orbital stability of the PCE limit cycle in order to employ deterministic contraction criteria to obtain an inner estimate of the stochastic ROA. An implementation of the conditions is presented in the form of generalized SOS programs.

CHAPTER 5

Region of Attraction Analysis for Airborne Wind Energy Systems

Airborne Wind Energy (AWE) denotes an emerging technology aiming at extracting power from high-altitude winds with tethered aircrafts, also referred to as *kites*.

One of the challenges the AWE technology is currently facing lies in guaranteeing reliability of the system. This guarantee implies the system being able to behave as desired at all times and within a specified range of operating conditions. Among other concerns, such as material durability, air space traffic regulations, etc., this challenge particularly addresses the development of the controllers dedicated to the autonomous operation of the kites. While there have been successful demonstrations of control designs for kite systems in the past [Fag+14; ES15; Ron+15; WHS17], the question of their reliability remains open.

In this chapter we consider the application of the methods presented in Chapter 4 to Airborne Wind Energy systems. A brief introduction to the field with emphasis on the pumping cycle operation is given in Section 5.1. In our analysis we focus on the power generating phase of flexible wing kites in which the kite is flying in crosswind conditions. In Section 5.2 a simplified and feedback controlled model previously employed for the control of the kite in the power generating phase is presented. The kite is stabilized with a state feedback control designed for the system in transverse coordinates to follow an optimized periodic reference trajectory. We demonstrate the control design for the example of a *Linear Quadratic Regulator* (LQR). Considering first the nominal closed loop system, the Lyapunov criteria for an inner estimate of the ROA of a periodic orbit presented in Section 4.4 are applied to obtain an inner estimate of the regions in which the controller is able to stabilize the kite. Allowing for two parameters to be affected by additive uncertainty we then apply the contraction criteria presented in Section 4.5 to obtain regions in which the uncertain system is contracting. The results of both analyses are presented in Section 5.3. The verified regions are validated by simulation for which we present an implementation of the transverse controller design in Section 5.4.

5.1 Introduction to AWE

The physical concept of generating power by exploiting the high forces acting on kites flying in crosswind conditions was first formalized in [Loy80]. Since the beginning of this century the concept has motivated many startups and research institutes to enter the race of developing and commercializing the technology. Promising larger wind power harvesting capabilities while requiring significantly less material compared to conventional wind turbines, the technology has started off on various different paths, with substantially varying protoypes and target application areas.

Soft wings are developed by Skysails Power[1] for ship propulsion and off-grid power production, by Kitepower[2] with focus on wind farms, and by Inuit WindSled[3] to propel sledges in Antarctica. Enerkite[4] uses ultralight semi-rigid wings for a mobile energy production station. Propelled and fully actuated tethered aircrafts are developed by Kitemill[5], Twingtec[6], Windlift[7], Ampyx[8] and Makani/Shell[9] for electricity generation at remote locations, where the latter two also target off-shore large scale power production. A rigid box-wing kite is being desigend by Skypull[10]. Multi-kite systems for wind farms are researched by Kiteswarms[11].

While almost all of the prototypes are based on the principle of generating power mechanically on the ground, a few, most prominently Makani, are focused on aircrafts with power generating mechanisms on board, e.g., in the form of suitably sized turbines. Moreover, a further crucial difference between the various AWE systems consists in their start and landing concepts, which are posing major challenges for the fully autonomous operation [FS17; RS18].

AWE technologies can be defined more broadly to consists of approaches which aim to exploit the power of high-altitude winds using other physical mechanisms than crosswind generated forces. For example, the company Altaeros Energies[12] develops wind turbines which are made buoyant by being embedded in a Helium-filled inflatable shell. Winds at altitudes as high as 600 meters above ground are targeted.

To this point in time the benefits of each prototype seem to be in a trade off with their disadvantages. While kite systems connected to the ground by multiple tethers

[1] https://www.skysails-power.com
[2] http://www.kitepower.eu
[3] https://www.greenland.net/windsled/
[4] https://www.enerkite.de
[5] https://www.kitemill.com
[6] http://www.twingtec.ch
[7] https://www.windlift.com
[8] https://www.ampyxpower.com
[9] https://www.makanipower.com
[10] https://www.skypull.technology
[11] https://www.kiteswarms.com
[12] http://www.altaeros.com

offer higher safety and more actuation degrees (for flexible wings) than a single line, each additional line contributes with a significant increase in drag force which decreases the efficiency of the system [Zan+13; Dun18]. Flexible wings compared to rigid wings have the advantage of being light weight, low-cost, less invasive to the environment under system failure and more easy to transport [ADS13]. On the down side, fully autonomous take-off is often still a challenge for flexible wings. Current approaches include passive launching through a high tower [Bau+18] and a combination of a tower and an assisting multicopter [RS18]. This challenge is more easily tackled by rigid kites which allow for actuation and propulsion by small scale onboard propellers. Vertical drone-like take-offs [Van13], linear launching techniques [FS17; Fag+18], as well as rotational launches [Gee+12] have been investigated in this regard. In general, rigid wings can achieve higher aerodynamic efficiencies and offer more rigorous control possibilities due to the larger number of actuators compared to their flexible counterparts [Cos+15]. The onboard propulsion system also enables a more steady energy generation by regulating velocity variations over the flight pattern. A comprehensive overview of the different prototypes, their characteristics and their development can be found in [ADS13; Che+15; Sch18], with further references to each of the here mentioned aspects, and others more.

In this work we consider two-line flexible wing kites in crosswind flight with mechanical ground based power generation. Note that the ROA analysis presented here can also directly be applied to periodic motions of other kites systems in case an appropriate model is available. The power generation mechanism is presented in the following.

5.1.1 Power generation through pumping cycles

Most kite systems are based on a mechanical mechanism to generate power in which the kite is performing so called pumping cycles. A pumping cycle consists of two phases, which are illustrated in Figure 5.1. In Phase 1 the kite is controlled in crosswind conditions with the aim of maximizing the forces acting on the aerodynamic surfaces. These forces are used to pull on the tethers which are connected to the kite on one end and wound around drums on the ground at the other end. Pulling on the tethers leads to a turning motion of the drums which consequently drives a generator and produces power. In this phase the kite is flying either figures of eight or circular shaped trajectories, which are spiraling away from the ground station. After the tethers are fully reeled out the kite enters Phase 2 of the pumping cycle. In this phase the aim is to minimize the forces acting on the kite in order to rewind the tethers around the drums with the least power necessary. Depending on the type of kite this is achieved in different ways.

Kites with limited actuation, such as flexible wing kites, are often flown out of the crosswind conditions and are pulled back in a long side-way leading arc (see, e.g., [ES15; Woo+18]). Control pods, such as used by Kitepower, enable an active change in the angle

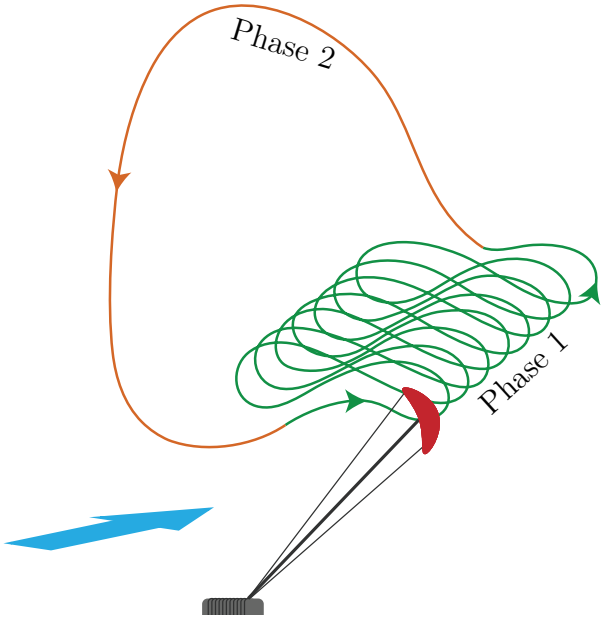

Figure 5.1: Illustration of the two phase pumping cycle. During Phase 1 the kite flies in crosswind conditions (wind direction is indicated by the blue arrow) and generates power by slowly unreeling the lines from a winch on the ground. In Phase 2 the tethers are reeled back while maneuvering the kite away from crosswind conditions to reduce the forces acting on it and thus minimize the power loss in this phase.

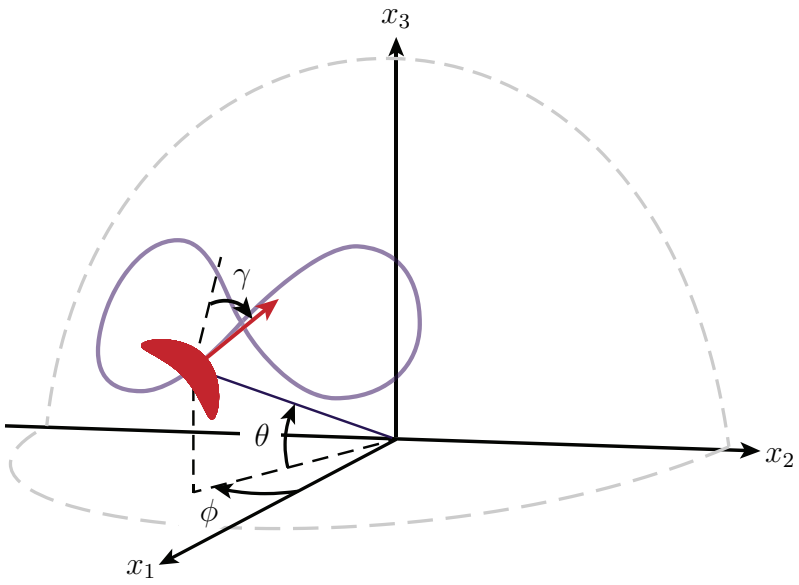

Figure 5.2: Illustration of the coordinate system. The kite system is modeled in the dynamics of the elevation angle θ, the azimuth angle ϕ and the heading angle γ. Note that γ is defined on the tangential plane at the kite's location and $\gamma = 0$ when the kite points local north on this plane.

of attack of their kites which allows for a so called depowering. In depowering mode the lift forces on the kite are reduced to a minimum such that the kite can be effectively reeled in by following the shortest and fastest path [JS14]. Rigid kites usually have more actuation possibilities which allows for active manipulation of their aerodynamic surfaces. They can thus be pulled back via the shortest path while the loads from aerodynamic forces significantly reduced (see, e.g., [Lic+19]).

The objective of flying pumping cycles is to maximize the net energy generated by the system over time, where the net energy generation is the difference between the energy generated in Phase 1 and the energy needed in Phase 2. The goal of maximizing the net power has given rise to a variety of optimization problems proposed in the literature, most of which focus on optimizing the flight path flown by the kite in the power generation phase [ZFM15; CFB17]. The overall power generated can also be maximized by aiming for the total energy produced over one hour or one day.

The power generation phase of the pumping cycle, Phase 1, is a widely studied aspects in the AWE literature [ADS13; Fag+14; ES15; WHS17; Sch18; Fag+18]. Many different control strategies have been proposed to both autonomously operate the kite as well as to optimize its flight path [CFB17; Lic+19; Sta+19]. The automatic control of kites is a particularly challenging task due to the dynamics being highly nonlinear and time-varying, and due to the exposure to substantial disturbances caused by the volatility of winds. Among the first successfully implemented control strategies is the so called switching-point strategy. This consists in a switching-based heading angle control approach in which the kite alternatingly targets two fixed points in the downwind window and by doing so arrives at a figure of eight flight path [ES13; Fag+14]. Model-based controllers were proposed in, e.g., [IHD07; CFM10; Woo+15], and experimentally tested in, e.g., [WHS17; Sta+19] using Nonlinear Model Predictive Control. While these control approaches have shown their prowess during many flight hours, a formal guarantee for these methods to control the kite reliably in a prescribed range of operating conditions is still an open question. For the commercialization of the technology, guarantees for the reliable operation in all flight phases including starting and landing are necessary. This provides the motivation for this work, where we aim at obtaining these guarantees for a controlled kite model in the crosswind flight phase.

5.2 Flight control for the power generating phase

The flight pattern in the power generation phase can be decomposed into a radial and a tangential motion. The radial motion is prescribed by the reel out velocity. It is in general a significantly slower motion compared to the tangential motion. The latter is perpendicular to the radial direction and tangential to the sphere to which the motion

is constrained for a given fixed line length. The tangential motion describes a periodic figure which is usually of a circular or a figure of eight shape. Due to the radial motion being significantly slower than the tangential, the overall motion of the kite in the power generation phase can be approximated as a periodic motion.
Circular as well as figure eight paths have been proposed for the flight path shape in the power generation phase. Both figures have shown to result in similar power outputs when optimized under the same conditions [Lic+19]. While the circular figure represents a geometrically simpler figure to track and optimize it requires a swivel mechanism to prevent the line from twisting. For a multi-line system, such as the two line flexible kite system considered here, a figure of eight path is the common choice for this reason.

A figure eight path can be obtained from the zero sets of polynomials in algebraic geometry which are called lemniscates (e.g., [Law72]). These lemniscates provide an analytic expression of the path. Since often the aim is to optimize the flight path with respect to a maximum of the aerodynamic forces, a figure eight trajectory can also be obtained as the numerical solution of an optimization problem. Using an optimization framework offers the benefit of simultaneously solving an optimal control problem and obtaining a feasible feedforward input for the optimized trajectory. In this work a figure eight trajectory is obtained from solving an optimization problem. This requires a model of the system, which is therefore introduced first.

5.2.1 Unicycle-type system model

Due to the system varying on a fast time scale, a controller is required to work at a high sampling rate. Real-time feasibility thus poses a challenge to model based control which results in the need for low complexity models that still capture the key characteristics of the dynamics. For flexible kites, simplified dynamics given by a first order kinematic model in three states were previously employed successfully in kite control applications [Woo+15; ES15; CFB17]. This model is similar to unicycle dynamics and thus referred to as unicycle, or unicycle-like model. The states are $x = (\theta, \phi, \gamma)$, where θ denotes the elevation angle, ϕ the azimuth angle, and γ the orientation angle of the kite. Figure 5.2 illustrates this configuration. The model is the following,

$$\begin{aligned} \dot{\theta} &= \frac{v_k}{L}\cos(\gamma), \\ \dot{\phi} &= \frac{v_k}{L}\cos(\theta)^{-1}\sin(\gamma), \\ \dot{\gamma} &= v_k G u, \end{aligned} \tag{5.1}$$

where L is the line length, and

$$v_k = v_w E\,\cos(\theta)\,\cos(\phi), \tag{5.2}$$

is the wind velocity, and $E = C_L/C_D$ is the glide ratio with C_L denoting the lift coefficient and C_D the drag coefficient. Further, G is the steering gain and u is the control input.

Flexible kite system are usually steered by changing the difference in length of the two lines connected to the right and left tip of the wing. This line length difference is then taken as the input. In this model the tether is implicitly assumed to be a rigid rod of zero mass.

In the stability analysis the parameters of the system are assumed to be affected by uncertainty. In particular, we consider the following additive uncertainties:

1. uncertainty in wind speed: $v_w = v_{w_0} + \vartheta_{v_w}$,
2. uncertainty in steering gain: $G = G_0 + \vartheta_G$.

Here, v_{w_0}, G_0 denote the nominal values and ϑ_{v_w}, ϑ_G the respective disturbances. Both parameters are usually difficult to identify and vary with flight conditions.

5.2.2 Reference trajectory optimization

Optimizations of the reference trajectory for kites have been proposed in several studies [HD07; WLO08; HD10; Lic+19]. In most of these an optimal control problem is solved to obtain a control policy for steering the kite on a power optimal reference flight trajectory while adhering to various constraints.

We consider the following optimization problem in order to obtain an example of a desirable periodic trajectory for the kite to follow. The optimization problem is implemented in ACADO [HFD11]. The objective function consists in the tether force $F(x(t), u(t))$ resulting from an aerodynamic equilibrium with the lift and drag forces, which is maximized over the time needed to fly one cycle of the periodic pattern, T.

$$\max_{x(t),u(t),x_0,T,t\in[0,T]} \quad \frac{1}{T}\int_0^T F(x(t),u(t))dt \tag{5.3}$$

subject to

$$\dot{x} = f(x(t), u(t)), \tag{5.4}$$
$$c_x^L \leq x(t) \leq c_x^U, \tag{5.5}$$
$$c_u^L \leq u(t) \leq c_u^U, \tag{5.6}$$
$$c_{\dot{u}}^L \leq \dot{u}(t) \leq c_{\dot{u}}^U, \tag{5.7}$$
$$x(0) = x(T) = x_0, \tag{5.8}$$

where (5.4) encodes the open-loop unicylce-like dynamics given in (5.1). The constraints in (5.5) restrict the pose of the kite to remain within favorable crosswind flight conditions. They include a minimum height constraint for safety and further prevent looping such that the flight path is forced to be a figure of eight shaped trajectory. This shape is further enforced to be flown in an upward direction by not allowing the orientation angle to take values $|\gamma| \geq 180°$. The input constraints in (5.6) restrict the turning rate of the kite

such that it complies with the limits of the physical system. In order to obtain a smooth feedforward signal the derivative of the input is constrained as well with (5.7). Finally, the constraint in (5.8) imposes the periodicity of the trajectory. The trajectory $\tilde{x}(t)$ and open-loop inputs $\tilde{u}(t)$ obtained from the optimization problem (5.3) thus represent a controlled periodic orbit, which is denoted by $\tilde{\Gamma} = \{(\tilde{x}(t),\, \tilde{u}(t)) \,|\, t \in [0, T]\}$.

5.2.3 Transverse state feedback controllers for the kite system

In order to stabilize the kite around the reference orbit $\tilde{\Gamma}$ various control strategies can be used. Since the main objective is to apply the above presented ROA analysis tools, the controller presented here serves to formulate the closed-loop system. We thus choose the LQR controller, which was previously used to stabilize the kite in [Woo+15]. The ROA analysis considers the system under the transformation to transverse coordinates. This requires the controller to be implemented for the transverse dynamics which results in state feedback gains for the transverse states. LQR controller for transverse dynamics have previously been used in, e.g., [Man+11]. The controller requires a linearization of the transverse dynamics around $\tilde{\Gamma}$,

$$\dot{\rho} = A_{\mathcal{S}}(\tau)\rho + B_{\mathcal{S}}(\tau)u_{\mathcal{S}},$$

where $u_{\mathcal{S}} = K_{LQR}(\tau)\rho$ is the transverse component of the input provided by the feedback control, and $A_{\mathcal{S}}(\tau), B_{\mathcal{S}}(\tau)$ are obtained from linearizing the transverse dynamics around $\tilde{x}(\tau), \tilde{u}(\tau)$ (i.e., $\rho = 0$),

$$\begin{aligned} A_{\mathcal{S}}(\tau) = &\left[\frac{d}{dt}Z(\tau)\right]^T Z(\tau) + Z(\tau)^T \frac{\partial f(\tilde{x}(\tau), \tilde{u}(\tau))}{\partial x} Z(\tau) \\ &- Z(\tau) f(\omega(\tau)) \frac{v(\tau)^T \frac{\partial f(\omega(\tau))}{\partial x} Z(\tau) - v(\tau)^T \frac{\partial Z(\tau)}{\partial t}^T}{v(\tau)^T f(\omega(\tau))}, \end{aligned} \tag{5.9}$$

$$B_{\mathcal{S}}(\tau) = Z(\tau)^T \frac{\partial f(\tilde{x}(\tau), \tilde{u}(\tau))}{\partial u}. \tag{5.10}$$

The feedback gains $K_{LQR}(\tau)$ are computed by solving the periodic LQR problem

$$\min_{\rho} \quad J(\tau, \rho) = \rho^T(T) Q_T \rho(T) + \int_0^T \left(\rho^T(\tau) Q \rho(\tau) + u_{\mathcal{S}}^T(\tau) R u_{\mathcal{S}}(\tau)\right) d\tau, \tag{5.11}$$

where $Q_T \succ 0$, $Q \succeq 0$, $R \succ 0$ are the weighting matrices. The optimal solution to problem (5.11) is

$$J_{\text{opt}}(\rho, \tau) = \rho^T P(\tau) \rho, \tag{5.12}$$

where $P(\tau)$ is the positive definite solution of the periodic Riccati equation [BCN91] for a $H \succ 0$,

$$-\dot{P}(\tau) = A_{\mathcal{S}}T(\tau)P(\tau) + P(\tau)A_{\mathcal{S}}(\tau) - P(\tau)B_{\mathcal{S}}(\tau)R^{-1}B_{\mathcal{S}}T(\tau)P(\tau) + H. \tag{5.13}$$

The LQR transverse state feedback gain then result in

$$K_{LQR}(\tau) = -R^{-1}B_{\mathcal{S}}(\tau)^T P(\tau), \tag{5.14}$$

which leads to the stabilizing input of the system being given by

$$u(x) = \tilde{u}(\tau) + u_{\mathcal{S}}(Z(\tau)^T(x - \tilde{x}(\tau)), \tau). \tag{5.15}$$

The feedback stabilized system (5.1) with (5.15) can then be regarded as an autonomous system and as such is amenable to the analysis methods described in Chapter 4.

5.3 Stability analysis of the feedback controlled kite system

In this Section an analysis of the region in the state space, in which the transverse feedback controller presented in Section 5.2.3 is able to stabilize the system, is presented. Due to the periodic nature of the problem the analysis methods presented in Chapter 4 are employed. The unicycle-like model of the kite (5.1) is considered where (5.3) was used to compute an optimized reference trajectory $\tilde{x}(\tau)$. The system parameters were set to $L = 60$ m, $E = 5.7$, $v_{w_0} = 6$ m/s, and $G_0 = 1.25$. The parameter G_0 was obtained from a rough approximation of the steering gain derived from first principles as proposed in [Fag+14]. For τ-discretization, 50 evenly spaced discrete values of τ were chosen over the period $[0, T]$, where $T = 5$s. This results in 49 distinct hyperplanes.

Since the verification methods in Chapter 4 require the system to be in polynomial form, the closed-loop system is approximated by a third-order Taylor series around $\tilde{x}(\tau)$. For the results shown here it is important to keep in mind that the analysis is performed on an approximation of the system. It thus remains to validate that the obtained ROA and ROC estimates are also ROA and ROC estimates for the real system. This will be presented, together with the implementation of the controller, in Section 5.4.

5.3.1 Center point MOC for the kite trajectory

The kite system provides an example for the cp-MOC for a three dimensional system. Figure 5.3 illustrates 8 randomly selected hyperplanes $\mathcal{S}(\tau_i)$ in the cp-MOC for the reference trajectory. The plots show how all hyperplanes intersect in a 1-dimensional subspace consisting in a line through the center point which was chosen at $x_c = [0.3, 0, 0]^T$. The rotation in the left plot was chosen such that the line points out of the plane, which reveals the $\phi - \gamma$ coordinates of x_c.

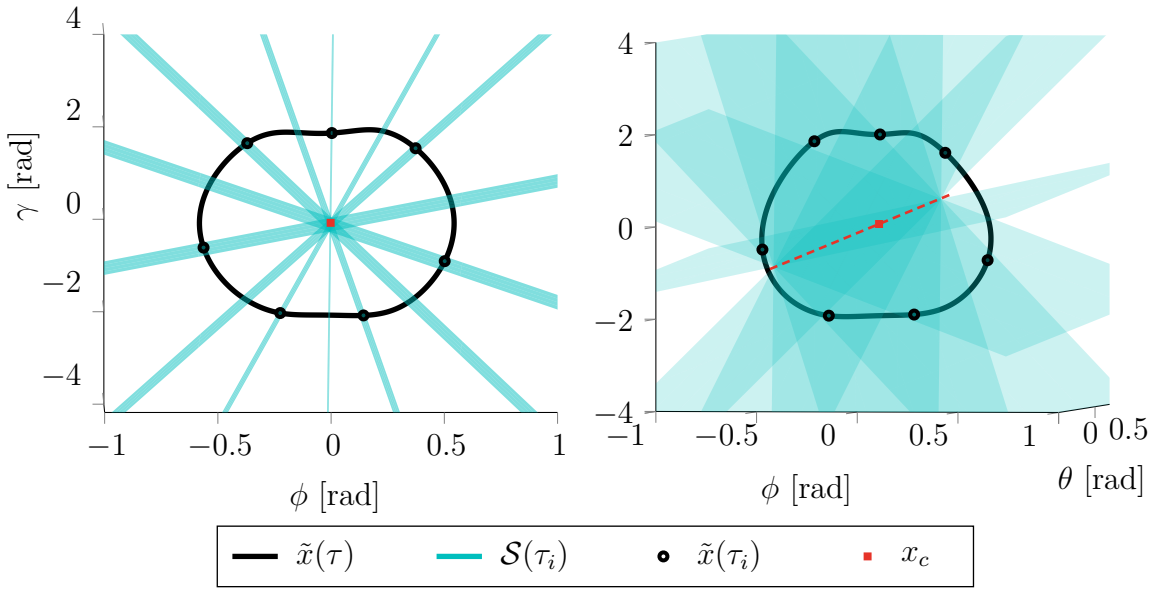

Figure 5.3: Illustration of the hyperplanes in the cp-MOC from two different angles. In the right plot, the red dashed line indicates the 1-dimensional subspace given by the intersection of the hyperplanes.

5.3.2 ROA analysis of the deterministic system

In the first analysis, the deterministic system is considered where the model parameters take their nominal values. The ROA analysis methods presented in Section 4.4 are then applied to obtain an inner estimate of the ROA of the periodic feedback-stabilized reference trajectory.

As a second objective, the deterministic kite dynamics are used to compare the different algorithmic options presented in 4.4.2 on a 3-dimensional system. The results presented here were computed from the scripts which are described in Chapter 6. In particular, the numerical criteria used for the comparisons are explained in Section 6.6.

Figure 5.4 presents the results for each algorithmic option and for each choice of MOC presented in Section 4.3.1. For the options amenable to higher order Lyapunov functions both the results for a quadratic and a quartic function are shown. The volume of the set $\mathcal{R}$ was numerically obtained by fitting a 80-sided polygon into the verified sublevel set of $V(\tau, \rho)$, which for 3-dimensional system is a planar region on each hyperplane.

The comparison of the least complex algorithmic option, VSS-∂_{lin} shows a significantly larger result for the cp-MOC than for the class-MOC. Furthermore, while for the class-MOC the remaining results for a quadratic V are of relatively small size and very similar to each other, they are found to be much larger sized and differ more widely for the cp-MOC. Interestingly, for the cp-MOC and both degrees of V, the computationally most complex option, EE-$\partial(r)_m$, perform worst overall (in the terms of the size of

estimated ROA), while the second most complex, EE-$\partial(r)_s$ performs the best overall. For EE-$\partial(r)_m$, the numerical results reveal issues which prevented continued iterations in Algorithm 4.1 to obtain larger estimates. There are several reasons which can cause these numerical issues some of which are discussed in Section 6.5.

In contrast, the results for the class-MOC show the overall largest sized $\mathcal{R}$ for the option EE-$\partial(r)_m$, albeit the difference to the second largest is marginal in the case of $\partial(V) = 2$. In particular, for both degrees of V, a spike is observed around $i = 14$. For these hyperplanes, the curvature of the reference trajectory is very small, which leads to the well-defined regions, $\mathcal{V}_\tau$, to be very large. Due to the flexibility of EE-$\partial(r)_m$ to adjust the objective function individually to each hyperplane, the algorithm was able to take advantage of these particularly large sets $\mathcal{V}_\tau$ in this case.

The small sizes of the results for SE-$\partial(r)$ for all MOCs and Vs show the potentially detrimental effect of a surrogate set which is fixed in shape and could not be pre-adjusted to the shape of the sublevel set of $V(\tau_i, \rho)$ due to lack of information.

The iteration numbers for each case are listed in Table 5.1. In particular the comparison with the iteration number for the 2-dimensional dual orbit example in Section 4.4.3 shows that the option EE-$\partial(r)_s$ was again among the options requiring a comparably low number of iterations. While the option EE-$\partial(r)_m$ for the class-MOC and quartic Lyapunov function gave the largest ROA estimates the number of iterations required is also significantly higher than for most other options. For the class-MOC the iteration numbers for the option SE-$\partial(r)$ were again very high, like in the dual orbit example They were acceptable for the cp-MOC, however, the obtained estimates are comparably small. This highlights the disadvantage of this algorithmic option that originates from fixing the shape of the surrogate set.

Figures 5.5 and 5.6 illustrate the region $\mathcal{R}$ obtained from EE-$\partial(4)_s$ on each of the selected 49 hyperplanes in a 3-dimensional plot for both the choice of the class-MOC and the cp-MOC. The plots highlight the significantly larger regions obtained with the cp-MOC choice of moving coordinate system. Figure 5.6 reveals that the algorithm was able to verify the stability of the system on regions extending close to the boundaries of the well-defined regions $\mathcal{V}_\tau$. The plots show how the intersecting sets for the class-MOC are at a much closer distance to the trajectory $\tilde{x}(\tau)$ around the extreme values of ϕ while for the cp-MOC all hyperplanes intersect in a single line which goes through the center point, as shown in Section 5.3.1.

5.3.3 ROC analysis of the system with parametric uncertainty

In the second analysis the model is considered with parametric uncertainty as described in Section 5.2.1. The ROC analysis methods presented in Section 4.5 are applied to obtain robustly contracting regions of the periodic feedback-stabilized reference trajectory, $\mathcal{Z}$, for two cases of uncertainty. The class-MOC was used for the transverse coordinate

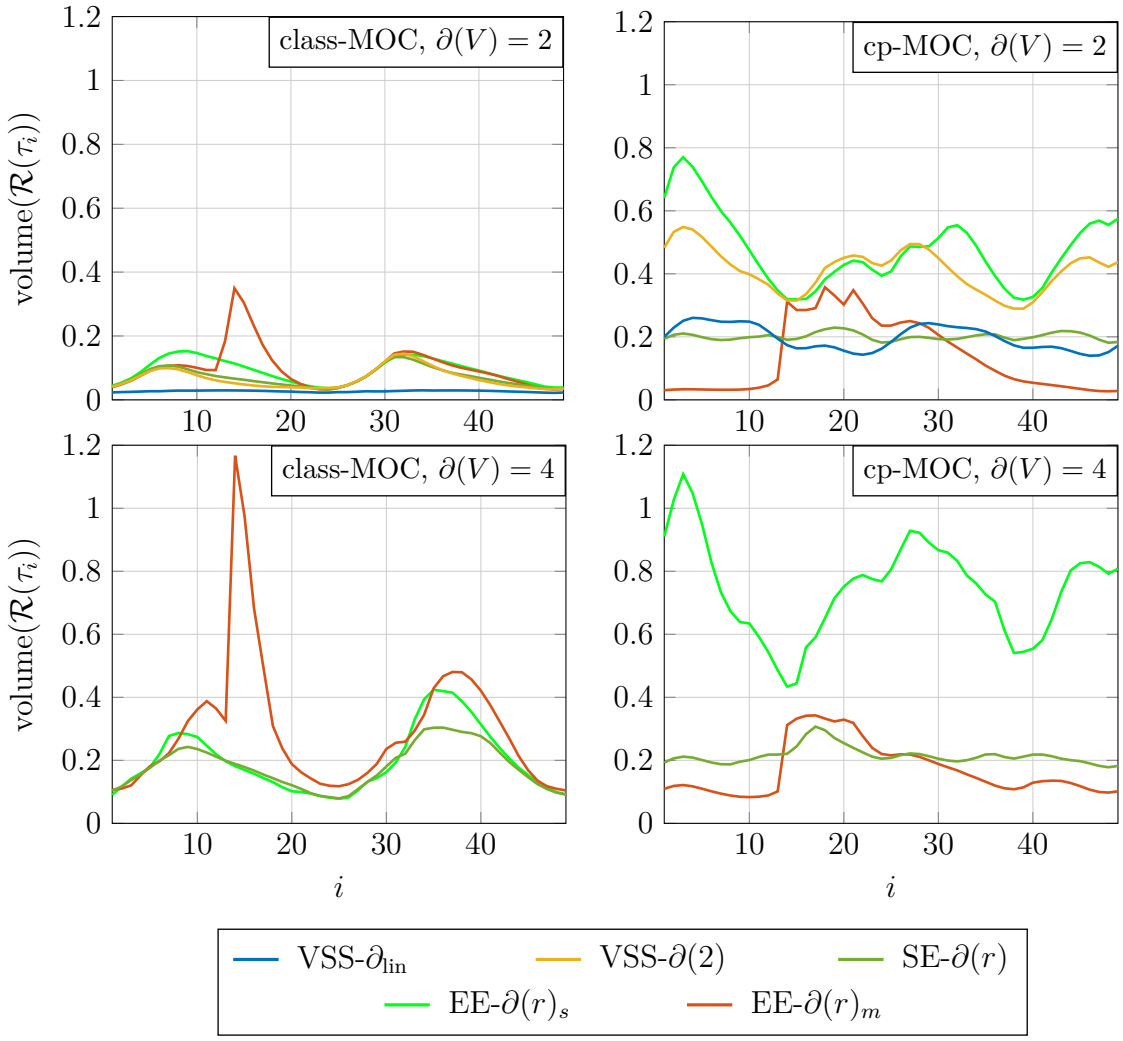

Figure 5.4: Results for the volume of $\mathcal{R}$ on each of the 49 selected distinct hyperplanes $\mathcal{S}(\tau_i), i = 1, ..., 49$, obtained from the different algorithmic options in Section 4.4.2 and from both presented options of MOC in Section 4.3.1. A quadratic and a quartic (where applicable) Lyapunov function were used.

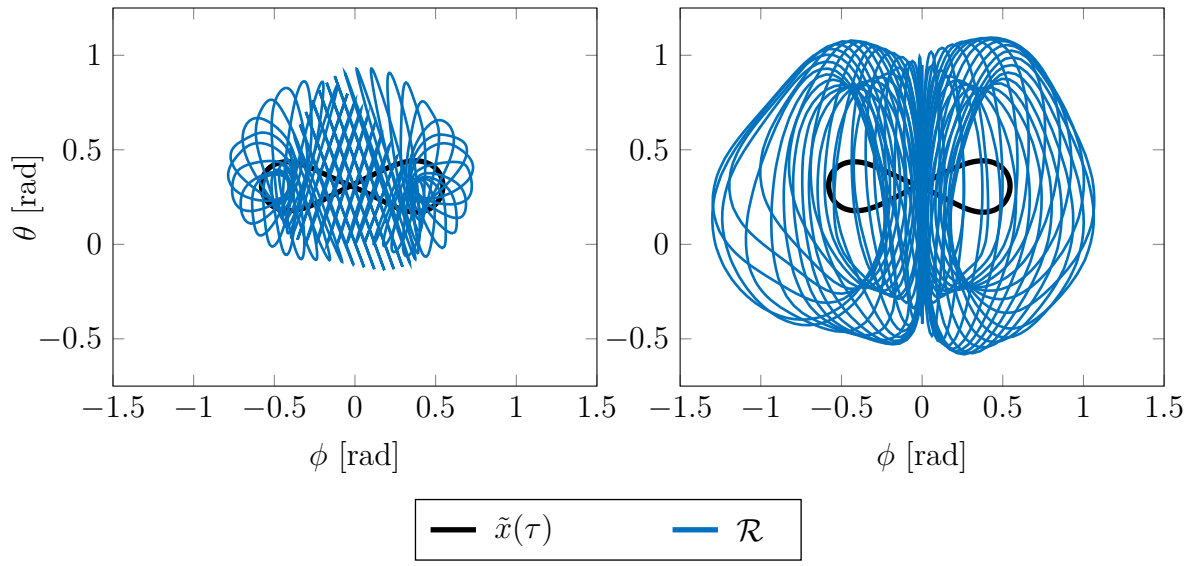

Figure 5.5: Results for $\mathcal{R}$ obtained from EE-$\partial(4)_s$, plotted on each corresponding hyperplane. The ϕ-θ plane of the 3-dimensional plot is shown. *Left plot:* Results for the class-MOC. *Right plot:* Results for the cp-MOC.

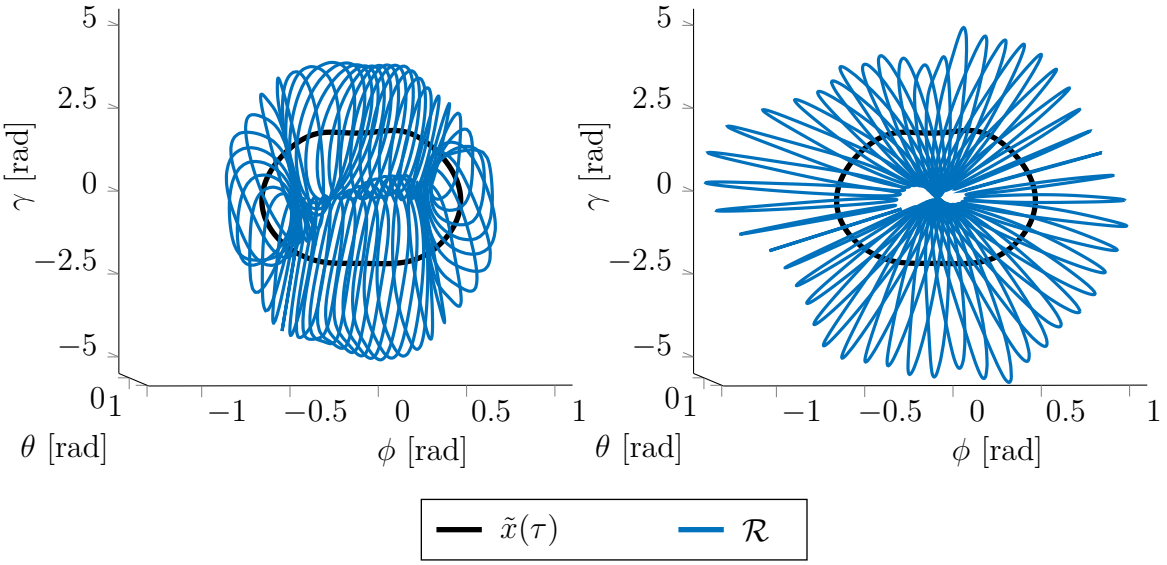

Figure 5.6: Rotated view of the plots in Figure 5.5.

Table 5.1: Comparison of iteration numbers obtained for the deterministic kite example for each algorithmic option and MOC.

Algorithmic option	class-MOC		cp-MOC	
	$\partial(V)=2$	$\partial(V)=4$	$\partial(V)=2$	$\partial(V)=4$
EE-$\partial(r)_m$	19	44	11	10
EE-$\partial(r)_s$	10	18	15	19
SE-$\partial(r)$	54	27	18	15
VSS-$\partial(2)$	8	-	12	-
VSS-∂_{lin}	7	-	14	-

transformation in this analysis.

In order to obtain less conservative results for the stabilizing regions of the controller we modify the algorithms to compute an ROC estimate presented in Section 4.5.2. The modification consists in using $z(\tau,\rho) = \rho^T M_{\mathcal{S}}(\tau,\rho)\rho$ (Remark 4.9), and removing the invariance constraint on the region $\mathcal{Z}$ in (4.93). This reduces the number of decision variables and multiplier entering Algorithm (4.2) significantly, allowing for larger regions to be tested. The modifications are motivated by the fact that, due to using a Taylor approximation of the dynamics, an a-posteriori validation needs to be performed in which the convergence of simulated trajectories starting at the boundary of $\mathcal{Z}$ is tested. Validating convergence of controlled trajectories thus offers a replacement for the invariance condition.

Robustly contracting regions $\mathcal{Z}$ for both cases of uncertainty where computed. For the case of uncertainty in the steering gain G the region $\mathcal{Z}$ was maximized for two different fixed magnitudes of the uncertainty given by $\pm 20\%$ and $\pm 40\%$ of the nominal value. Additionally, the contracting region for the nominal system was computed. Figure 5.7 displays the results obtained for each uncertainty bound which showcase the tendency of a diminishing contracting region size with an increase in uncertainty.

The allowed variation in the wind speed was then maximized by using Algorithm 4.3 for a contracting region size fixed to 75% of the nominal $\mathcal{Z}$. We observe that the results for the maximized lower and upper uncertainty bounds to arrived at the limits of typical operating conditions of 4-10 m/s which were set as stopping criteria for the iteration. Simulations of the dynamics show, that uncertainty in the wind speed in this range does not affect the location of the trajectories of the system and only affects how fast the trajectories evolve.

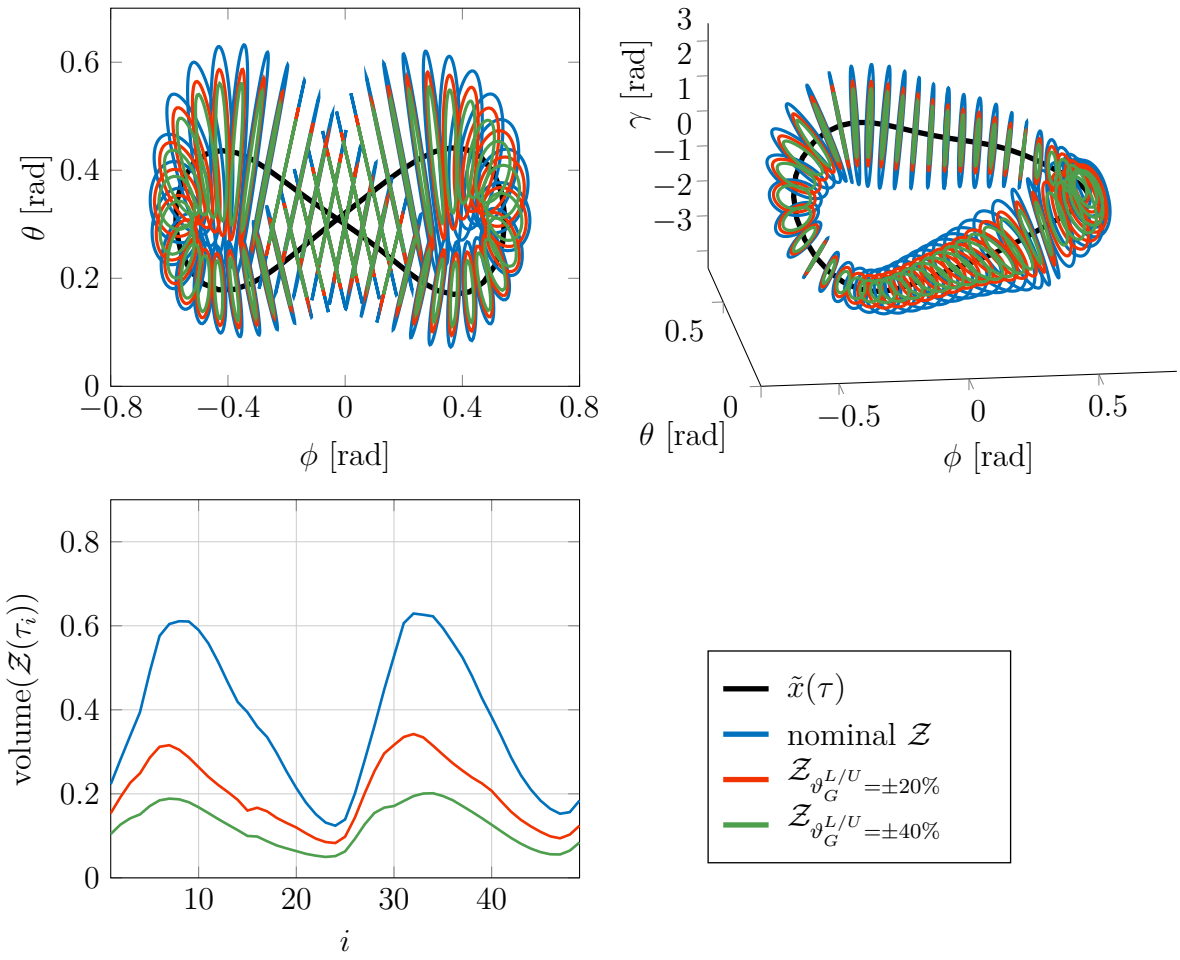

Figure 5.7: Results for $\mathcal{Z}$ obtained for different magnitudes of uncertainty in the steering gain, plotted on each corresponding hyperplane in the class-MOC. *Left plot:* Plot of the results in the ϕ-θ plane. *Right plot:* Rotated plot of the results in the full 3-dimensional space.

5.4 Simulation results

5.4.1 Transverse controller implementation

The feedback-law obtained from the transverse LQR approach removes the time dependence of the reference from the problem of stabilizing the kite. The feedback gains only depend on the location of the kite with respect to the hyperplanes $\mathcal{S}(\tau)$. This turns the time-sensitive problem of trajectory tracking into the often simpler problem of path-following. However, due to the dependence of the problem on the hyperplanes, the question of how to find the appropriate hyperplane from a given location x of the system arises. More precisely, the inverse of the transformation to transverse coordinates is required for the implementation of the controller.

For any given value of τ, the corresponding hyperplane and coordinates of every state x on that hyperplane are given by the transformation laws (4.12) and (4.13) which are analytic equations. The inverse of the transformation implies the problem of finding, for a given state x of the system, the unique hyperplane it is corresponding to. In the following a numerically implementable solution is proposed. Let

$$\mathcal{T}_\tau := \{\tau \in [0, T) \,|\, v(\tau)^T (x - \tilde{x}(\tau)) = 0\}, \tag{5.16}$$

be the set containing all τ for which the given x lies on the $\mathcal{S}(\tau)$ as defined by the condition (4.12). The set $\mathcal{T}_\tau$ is obtained from computing the zeros of $v(\tau)^T(x - \tilde{x}(\tau))$. For each $\tau \in \mathcal{T}_\tau$ the state can then be transformed into transverse coordinates ρ via the corresponding projection operator $Z(\tau)$.

By precomputing the ROA estimate offline with Algorithm 4.1 for the deterministic case, or Algorithm 4.2 for the uncertain case, information on the size of the stabilizing region of the feedback gains for a given hyperplane is available from the set $\mathcal{R}$, respectively $\mathcal{Z}$. For each pair (τ, ρ) obtained from $\mathcal{T}_\tau$, the condition

$$\rho^T Q(\tau)\rho \leq 1 \;\text{ (in the case of } \mathcal{R}), \qquad \rho^T M_{\mathcal{S}}(\tau, \rho)\rho \leq 1 \;\text{ (in the case of } \mathcal{Z}), \tag{5.17}$$

is checked. If the given state x is inside $\mathcal{R}/\mathcal{Z}$, condition (5.17) is satisfied by a unique pair (τ, ρ). The uniqueness is hereby guaranteed by the well-definedness condition (4.14) which is imposed as a constraint in the ROA/ROC estimate optimization algorithms. Keeping the non-intersecting hyperplanes interpretation of well-definedness condition in mind, the importance of this constraint on the application is evident. If the state is outside of $\mathcal{R}/\mathcal{Z}$, then the corresponding hyperplane might still be found, however, there is no guarantee that the controller is still stabilizing the system.

5.4.2 Simulation of the controlled system - validation of the ROA and ROC estimates

The results for the attracting regions of the deterministic system and the contracting regions of the uncertain system presented in Section 5.3 are validated by simulating the closed loop system from a range of initial conditions on the boundary of the respective sets. The feedback controller was thereby implemented as described in Section 5.4.1. For the simulation of the uncertain system the simulation was performed for each of the dynamics obtained from using an extreme value of the uncertainty. Regarding the ROA estimate, the largest sized estimate, i.e. the $\mathcal{R}$ obtained from EE-$\partial(4)_s$, was validated. Note that a validation consisting of taking a fine range of initial conditions on the boundary between neighboring hyperplanes simultaneously allows to validate the attractive region in between the selected hyperplanes.

Figure 5.8 shows a sample simulation of the closed loop kite dynamics starting inside the contracting regions. The left plot shows the trajectory of the system with a $+40\%$ perturbation of the nominal steering gain, and the right plot shows the result for -40%. We observe that the system converges to different periodic orbits depending on the value of the uncertainty.

Both the sets $\mathcal{R}$ and $\mathcal{Z}$ were validated as converging regions. Since invariance was not imposed on $\mathcal{Z}$ the simulation revealed that some trajectories exit the region before reentering and converging to their respective periodic trajectory.

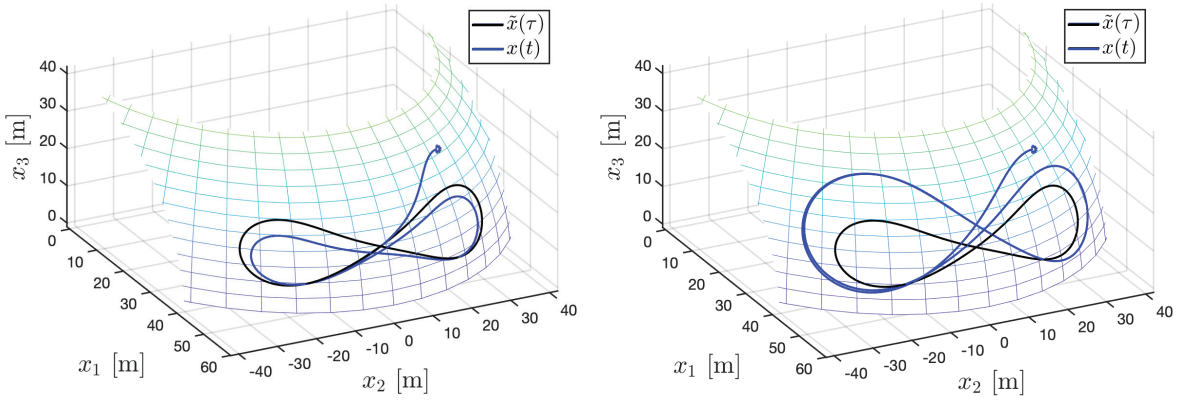

Figure 5.8: Simulation of the the kite dynamics given in (5.1) with different realizations of the uncertain steering gain. *Left plot:* $G = 1.4 \cdot G_0$. *Right plot:* $G = 0.6 \cdot G_0$.

5.5 Conclusion

In this chapter we present the application of the analysis methods of Chapter 4 to feedback-stabilized autonomous kite power systems. The kite is considered to be in the power generating phase of the flight cycle for which a model and a power optimized trajectory is presented. We use a feedback controller based on a periodic transverse LQR and present details on the implementation of the resulting transverse controller. A ROA estimate of the trajectory of the stabilized deterministic kite model, and a ROC estimate of the trajectory of the stabilized kite model with two different parametric uncertainties is computed. The obtained regions are verified by simulation of the controlled system from a range of initial conditions on the boundary of the regions. A transverse controller implementation is proposed which is based on the MOC and the ROA, respectively ROC estimates.

CHAPTER 6

ROA Analysis Tools

In this chapter we provide an overview of the collection of scripts in which the analysis methods presented in this thesis have been implemented in a generalized form. The scripts are available open source and can be downloaded at `https://github.com/evaahbe/roa-analysis-tools.git`.

The aim of these scripts is to offer transparency on the details of the implementation and a comprehensive tool to start off from when engaging in the ROA analysis for a system of interest. Since any of the presented methods test sufficient conditions, it is difficult if not impossible to generalize an implementation to the extent of a 'plug-and-play'-like utility for arbitrary systems, even with the restriction to polynomial systems. A successful analysis therefore often hinges on an informed tuning of the involved parameters and problem specific adjustments. The scripts facilitate this step by providing easy access to the tunable parameters, and by implementing all involved analysis steps in a generalized way with the aim of minimizing the need for user interaction.

Remark 6.1. The scripts were not written with the aim of computational efficiency nor with any warranty of merchantability. Please also note the licence provided in the directory.

The file directory is self sufficient and offers access to all functions and auxiliary files involved in the computations. Note, however, that since the scripts use the SOS toolbox of Yalmip [Lof09], the installation of Yalmip [Loe04] and the specification of an SDP solver software (e.g., Mosek [MOS17], SeDuMi [Stu99]) are required.

Remark 6.2. All numerical examples presented in this thesis have been computed in Matlab version 2018b/2019b, using Yalmip version R20180612 and Mosek version 8.0.

The list of tools included in the scripts is as follows.

- ROA analysis of an equilibrium point of a PCE system (Algorithm 3.1).
- Optimization program to retrieve stochastic ROA from PCE ROA with user specified variance (Algorithm 3.2).

- Control design aiming at ROA maximization for stochastic systems with equilibrium points (Algorithm 3.3).
- ROA analysis of a deterministic limit cycle (Algorithm 4.1).
- ROC and maximum uncertainty analysis of an uncertain limit cycle (Algorithm 4.3).

All relevant fields in the scripts which require user input, are commented with explanations. In the following we provide details on the general structure of the scripts and offer some guidance on the parameter tuning. This chapter aims to complement the explanations provided both in the previous chapters and the comments provided directly in the scripts, and is not a complete documentation.

6.1 General structure

The scripts are divided into two subdirectories of which one contains the files on the analysis of equilibrium points and the other the files on limit cycle analysis. The scripts are coordinated through the following main files

- Equilibrium point:
  - `main_ROA_EP.m` – ROA analysis of PCE equilibrium point, stochastic ROA retrieval
  - `main_ROA_CDEP.m` – Controller design and ROA analysis for a PCE equilibrium point, stochastic ROA and controller retrieval
- Limit Cycle:
  - `main_ROA_LC.m` – ROA analysis of a deterministic LC, periodic Riccati gains
  - `main_ROC_LC.m` – ROC analysis and maximized uncertainty bounds of an uncertain LC, periodic Riccati gains

The main files enable to choose from the different features presented for each analysis method in this work, as well as plotting the results. Further details on the implemented features will be provided in the following Sections.

The `systemFiles..` directories contains the files implementing the systems treated in this thesis, as well as template files which enable the user to implement a system of interest.

Upon successful termination of an analysis the results are saved to a `.mat` file in the corresponding directory `resultsFiles...`.

In between the iterations of an analysis the intermediate results are saved to a `.mat` file named `intermediateResults...`, which is automatically deleted once the final results file has been created. This intermediate results file enables the tuning of parameters and inspection of results in between iterations.

Remark 6.3. The only files requiring user action and input are the main file together with the system file folder. Each field which requires input is commented as to what input it represents.

During the run of an analysis, the iteration number, successful accomplishment of a step and, depending on the kind of analysis, intermediate results to inform on the progress are shown in the command window.

6.2 Equilibrium point analysis

The subdirectory `EquilibriumPointAnalysis` contains the following folders.

- `systemFilesEP` - contains the system files of the equilibrium point examples in this thesis, as well as the template files folder
- `PCEprojection` - functions for obtaining the PCE of a stochastic system, files are provided for normal and uniform distributions
- `verificationROAPCE` - contains function for the PCE ROA verification steps and function for the stochastic ROA recovery
- `verificationROAPCE_CD` - contains function for the control design with PCE ROA maximization
- `resultsFilesPCEstoch`, `resultsFilesPCEstoch_CD` - folders in which final results are saved as `.mat` file
- `plottingFilesEP` - plotting files to illustrate obtained ROA in $\bar{x}_0$ coordinates (max. dimension for plotting is 2)

The files which necessarily require user input are presented in the next two subsections.

6.2.1 System files

Details on the system of interest need to be provided by filling out the indicated fields in all files in the `template_EP` (for autonomous systems), respectively `template_CD` (for controlled systems) folder. These files contain:

- `initializeTemplate.m` - system parameters and details on uncertainty, feedback vector, input constraints, etc.
- `dynamics_TEMPLATE.m` - differential equations representing true system dynamics
- `poly_dynamics_TEMPLATE.m` - polynomial differential equations approximating true system dynamics (in case true system is not polynomial)
- `dynamics_TEMPLATE_INT.m` - true (closed loop) system dynamics (includes considered feedback vector $h(x)$ if applicable), needed for integration purposes only

The number of states, inputs (where applicable), or random parameters is not limited and needs to be specified together with the details on the distribution in the initialization file. Note that in the current implementation the random variables can be either normally distributed or uniformly but not both.

For the control design a feedback vector $h(x)$ has to be specified, and the type of desired analysis (nominal open-loop, stochastic open-loop, stochastic closed-loop, stochastic closed-loop with input constraints) needs to be indicated.

Further, an initial guess for the equilibrium point of the system is needed in terms of its nominal location. Since the equilibrium point is then obtained by simulation of the system the initial guess is only required to be close to the desired equilibrium point in case the system has multiple equililibria. The PCE coefficients of the equilibrium set are then retrieved automatically.

6.2.2 Main file

Once the system files are set up the main file enables the interaction of the user with the tunable parameters and analysis options.

The main file can be used to execute either of the three analysis parts separately:

1. Computation of the PCE ROA.
2. Retrieval of stochastic ROA for a specified variance.
3. Plotting of the results.

Note, however, that parts 2 and 3 naturally require the results files of the the previous step to exist. In particular for part 2 it might be desirable to run the ROA retrieval for several different fixed variances for which the PCE ROA needs to be computed only once.

At the beginning of a new PCE ROA analysis, the parameter `numsets.initVscale` needs to be tuned which scales the initial Lyapunov function. This is done by manually

bisecting on the value (usually towards smaller values) and running the script, until the first multiplier test turns out successful. Similarly, at the beginning of a new stochastic ROA retrieval analysis the parameter `numsetsRE.initQ0scale`, which scales the Q_0 matrix (see Section 3.2.4), needs to be tuned.

In addition to these parameters, in the main file for the control design, the parameter `numsets.initKvals` can be tuned, which represents a small initial value for the gain matrix K. It can be either left as zero, initialized with a small scalar or initialized as matrix of appropriate shape with small entries. Tuning this initial value can be a bit tricky as simply taking a zero might eliminate terms in the first multiplier steps, rendering the obtained multipliers ill-equipped to account for these terms in later steps. Any non-zero value, however, has to be feasible. The parameter `numsets.initt` initializes the value of the auxiliary variable c needed to enforce input constraints (see Section 3.3.4) and is best set to a small, positive value.

The tuning of the multipliers is discussed below in Section 6.4.

6.3 Limit cycle analysis

The subdirectory contains the following folders.

- `systemFilesLC` - contains the system files of the LC examples in this thesis, as well as the template files folder
- `initialLyapunov` - functions to compute periodic Riccati / Lyapunov equation solution
- `MOCfiles` - contains all files needed for transformation to the MOCs
- `verificationROA` - functions containing the verification of the ROA estimate for each algorithmic option
- `verificationROC` - functions for the verification of the ROC estimate and maximization of the uncertainty
- `resultsFilesROA`, `resultsFilesROC` - folders in which final results are saved as `.mat` file
- `plottingFiles` - plotting files for the ROA/ROC results for 2 or 3 dimensional systems.

The files which necessarily require user input are presented in the next two subsections.

6.3.1 System files

As for the equilibrium point, details on the system of interest need to be provided by filling out the indicated fields in all files in the `template_LC` folder.

The list of files contains the following.

- `initializeTemplate.m` - system parameters and details on uncertainty, feedback vector, input constraints, etc.
- `dynamics_TEMPLATE.m` - differential equations representing true system dynamics
- `poly_dynamics_TEMPLATE.m` - polynomial approximation of true system equations (in case true system is not polynomial)
- `deriv_dynamics_TEMPLATE.m` - dynamic derivative equations of the true system
- `linear_dynamics_TEMPLATE.m` - Jacobian matrix of the true system
- `uncertain_dynamics_TEMPLATE.m` - differential equations including the uncertain parameters (only needed for ROC analysis)
- `uncertain_poly_dynamics_TEMPLATE.m` - polynomial approximation of true uncertain system equations (only needed for ROC analysis and non-polynomial systems)

In the initialization file, the `.mat` data file containing the finely spaced numerical values of the trajectory of the periodic orbit needs to be indicated. Note that in the limit cycle analyses systems with inputs can be considered. For these, the trajectory data file needs to also contain the corresponding feedforward input values, if applicable. For the choice of analysis using the cp-MOC, the center point x_c has to be indicated in the field `sys.xc`.

The derivative dynamics are used for a more precise spline interpolation and the file containing the Jacobian is used for computing the initial Lyapunov function, respectively Riccati gains.

6.3.2 Main file

As for the equilibrium point analysis, the main files enable the interaction of the user with the tunable parameters and algorithmic options.

In the field `verimethod` the desired algorithmic option among the ones presented in Section 4.4.2 can be indicated, where

1. `SSSfixV` - VSS-∂_{lin}

2. `SSSdeg2V` - VSS-$\partial(2)$
3. `SESSdegdV` - SE-$\partial(r)$
4. `EEdegdV` - EE-$\partial(r)$

and the parameter `numsets.tvball` lets the user choose between EE-$\partial(r)_s$ (=0) and EE-$\partial(r)_m$ (=1). In the ROC analysis `roc.numsets.tvalpha` lets the user keep α either fixed (= 0) or make it varying (= 1).

With `sys.trafo`, the MOC can be selected, where 1 = class-MOC and 2 = cp-MOC. The number of hyperplanes is indicated in `sys.Nhp`.

The parameter `pinit.initVscale` which scales the initial Lyapunov function needs to be tuned as described in Section 6.2.2.

Where applicable, the parameter `ellipsemat` represents the surrogate set matrix B_F and lets the user define the fixed shape of the surrogate set.

The tuning of the multipliers is discussed in the following.

6.4 Multiplier tuning

There are no general theoretical limitations on the maximum nor on the minimum degree of any of the multiplier resulting from the Positivstellensatz 2.2. However, as the computational tractability of the analysis decreases with increasing maximum polynomial degree, it is desirable to keep the multiplier degrees as low as possible, while still being feasible.

In [JW+05] a recommendation for the choice of the multiplier degrees was provided. Therein, each term in a constraint should have the same maximum even degree, or smaller uneven degree (clearly, in order for a SOS decomposition to exist the highest degree of a constraint has to be is even). We have found that this recommendation provides an often suitable starting point for the tuning.

As an example, consider equation (3.22c). With $\partial(V) = 4$, $\partial(f) = 3$ and $\partial(l) = 2$ fixed, the degree for the Lyapunov derivative results as $\partial(\dot{V}) = 6$. The multiplier degree could thus be chosen as $\partial(s_1) = 2$. Choosing a higher degree can often lead to the verification of larger estimates, however, it trades off with an increased computational cost. It is still highly recommended to test for larger degrees and reduce back to lower ones when computational time becomes unacceptable or estimates start decreasing (usually due to numerical issues).

Further, numerical issues in the solvers can arise if coefficients of the multiplier have to be set to zero in order for the problem to be feasible. For these cases it is best to 'assist' the solver by manually setting these coefficients to zero or by directly removing the terms from the multiplier polynomial.

As example, consider the Lyapunov function constraints which include $V(0) = 0$ and positivity of $V(x)$ for all x inside the ROA. To satisfy these constraints, there can be no homogeneous or linear terms in the Lyapunov function polynomial. Consequently, in equation (3.22c) the coefficients of the homogeneous and linear terms in the s_1 multiplier polynomial need to be zero. Initializing the s_1 directly without these terms does not only prevent this source of numerical issues but also decreases computational cost due to a reduced amount of constraints.

6.5 Issues in practice

The causes for infeasibility can be plenty and in the following is a (non-exhaustive) list of comments to keep in mind. In particular the initialization of the iteration is the part of the analysis which often requires the most user interaction and can become tedious.

- The numerical solution of the limit cycle trajectory should be smooth and finely gridded. In particular in the case it has an input solution, the derivative of the input should be smooth to prevent numerical issues.
- For the maximization of an ROC estimate for fixed uncertainty (Algorithm 4.2), depending on the size of the uncertainty, there might not be an initial $\mathcal{Z}$ of any size. This is because the ROC conditions require invariance of the region, which means that for any uncertainty realization the periodic orbit needs to lie within $\mathcal{Z}$. The initial Lyapunov function which is computed for the nominal system might not result in any region large enough to include all limit cycle realizations. A workaround here is simply to start the iteration with a small uncertainty for which the first step is feasible and then increase the uncertainty in small steps at each next iteration, thus allowing the algorithm to find better suited Lyapunov functions.
- The inital Lyapunov function in the LC analysis is the periodic solution of a periodic equation which is initialized with a positive definite matrix H. In order to obtain a periodic solution the time-varying equation should be propagated for some periods until it is converged to the periodic behavior (default is 8).
- The contraction analysis computations can become very long, depending on the amount of the iterations and multiplier degrees needed. Due to the way how Yalmip allocates memory some speed up can be gained by stopping and restarting the script after every couple of iterations (the scripts have been designed for this purpose, such that stopping and restarting by continuing from where the computations can be done without requiring further interaction).
- The iteration might terminate after many steps due to an encountered infeasibility (usually in the multiplier step). While for feasibility tests the SDP solvers usually

return values well within the feasible set, in the case of an optimization problem it is known that they might not return strictly feasible certificates due to termination criteria and floating-point implementations [Lof09]. In this case the Lyapunov function step can be rerun as a feasibility test for a fixed, slightly decreased value of the result from the previous optimization.

6.6 General comparison criteria for ROA estimates

In the following we present some remarks on conducting comparisons with SOS programs which are in particular relevant for the illustrative examples shown in this thesis.

The conditions treated in the analysis methods are sufficient conditions, which implies that even if a solution (i.e. a Lyapunov function) has been found there might still exist one which can certify larger results. There are still various comparisons which can be performed in a meaningful way among different approaches, for example among the various algorithmic options in Section 4.4.2. This is done by keeping as many parameters fixed in between the various options as possible. Due to the various algorithmic options differing as much as including a varying set of multipliers, a 'ceteris paribus' study is not fully possible. However, to come as close as possible, the following actions can be taken for the comparison, and have been implemented for the examples presented in this work.

- Keep all multiplier degrees constant in between algorithmic options and options of the MOCs, in particular also in between changes of the Lyapunov function degree.
- Set the convergence criteria to be of comparable relative size for the different parameters among the algorithmic options.
- Keep the accuracy of the SDP solver fixed among options.
- To allow for a meaningful comparison of iterations to convergence, take the same size for the initial ROA estimate and surrogate set size (where applicable), or sizes as similar to each other as possible.

In particular the last item of the list requires a pre-run of the analysis to find the largest common or comparable ROA estimate and surrogate set size. For a selected MOC the size can be kept constant among algorithmic options by keeping the parameter `pinit.initVscale` fixed and the initial surrogate set a function of it. However, since the initial Lyapunov candidate depends on the choice of MOC, finding a same initial size is more difficult for inter-MOC comparisons.

In most applications the highest priority is the maximization of the size of the ROA estimate, while computational time (as long as it is acceptable) can be considered as secondary priority. This gives rise to another possibility of comparison which consists

in exploring the parameter space for each algorithmic option and choice of MOC for the largest possible result. Due to the large parameter space this comparison is not recommended unless criteria can be found to significantly reduce the parameter options by apriori discarding unproductive choices.

CHAPTER 7

Conclusions and Outlook

In this thesis we considered attractive equilibrium points and limit cycles of various classes of continuous systems. Among these are, firstly, stochastic autonomous and controlled systems with finite second moment and uncertainty dependent equilibrium points, and secondly, systems with limit cycles which are either deterministic, affected by affine parametric uncertainty or stochastic systems with finite second moment.

For the finite second moment stochastic systems, also referred to as second order random processes, we use the framework of *Polynomial Chaos Expansion* (PCE) to obtain a deterministic representation of the system. We derive connections between the moment boundedness of the stochastic system and the asymptotic stability of the PCE system and provide corresponding notions of the *region of attraction* (ROA). These are then used to formulate optimization problems in the form of *sum-of-squares* (SOS) programs which result in inner estimates of the ROA. The comparison with ROA estimates obtained for the examples from existing literature shows that the proposed approach provides estimates, which are comparable to literature results obtained with less general methods. Further, the approach allows the user to obtain information on the ROA of the system with defined statistical properties, such that if a particular uncertainty on the initial condition is known, the corresponding ROA estimate can be obtained.

The proposed method is then extended to serve in the design of a stochastic state feedback control law for second order random processes, which aims at maximizing the ROA. The control design is able to optionally account for input constraint. The examples show how the design procedure is successful in not only counteracting the detrimental effects of the uncertainty on the ROA but significantly increasing the ROA beyond the size of the nominal estimates. The comparison of different nonlinear state feedback vectors h with linear controllers (Linear Quadratic Regulator) proposed in existing literature reveals that improvements on the ROA are mainly due to the fact that a nonlinear control design formulation is employed, rather than due to the adoption of a polynomial basis for h.

For the stability analysis of deterministic and uncertain limit cycles we used a *moving orthonormal coordinate system* (MOC) to formulate Lyapunov and contraction condi-

tions which provide criteria for inner estimates of the ROA, respectively *region of contraction* (ROC). We first derived a novel construction for an MOC, to which we refer to as *center point MOC* (cp-MOC). We demonstrate its advantages over the existing 'classical' approach [Hal80] both by deriving a formal characterization of the well-definedness properties, and by showing how the obtained ROA estimates can result significantly larger for the cp-MOC than the classical. By comparing various algorithmic options for the computational implementation of the Lyapunov conditions we show how modifications to the existing approaches can lead to larger estimates. The contraction criteria are completed with an invariance condition and an extension to account for bounded parametric uncertainty to result in an inner estimate of the ROC. The stability as well as the contraction conditions are implemented and tested in generalized SOS optimization programs. Finally, the stability analysis of stochastic orbits is approached by connecting the periodic and contracting properties of the stochastic system to the corresponding behaviors of its PCE system. Transverse contraction criteria are formulated which certify an inner estimate of the ROC for the ROC system.

The application of the ROA and ROC methods for limit cycles to feedback-stabilized autonomous kite power systems is demonstrated by a commonly employed flight control model. Along with the analysis we present the implementation of a transverse controller both formally and in simulation.

The scripts containing a generalized implementation of the analysis methods presented in this work have been made available to the public, and essential details on their functionality have been provided in this thesis.

7.1 Future research directions

7.1.1 Computational efficiency of SOS programs

The computational tractability of solving an SOS program depends crucially on the size of the problem. The problem size scales exponentially in the number of states and polynomial degrees (polynomial, if scaled in either state or in polynomial degree alone).

In particular for the analysis of PCE systems, computational cost can often become an issue. While the PCE does not alter the polynomial degrees it still leads to a $(p+1)$-fold increase of the number of states. Depending on the number of modes needed to represent the system with a sufficient accuracy, the number of states can quickly become prohibitively large for low-dimensional stochastic systems. In a similar way, the analysis of the contraction region can arrive at an unacceptable slow-down for computations of a low number states due to the doubling of the indeterminants in the matrix SOS constraints.

Since the analysis of contraction regions for stochastic limit cycles combines both

the $(p+1)$-fold increase and the doubling from the matrix constraints, the dimensional increase is still too large in order for this method to be applied in a appropriate way (sufficiently high expansion order and tractability).

Research on more efficient *semidefinite program* (SDP)-solvers is ongoing and this limitation is likely to be alleviated in the future. One immediate remedy is offered by the DSOS/SDSOS framework introduced in [AM19a], which can solve SOS programs tractably for up to 50 states. While potentially resulting in more conservative estimates these relaxations promise a significant speed up of SOS programs.

Recently, there has been a focus of studies in the SDP community on exploiting structure of an SDP in order to facilitate its solving. In particular, reformulations leading to sparsity in the constraint matrix have been shown promising speed ups and enhanced capabilities in terms of state dimension [WKK06; MHA19]. The SOS programs in this thesis are solved using the SOS toolbox of YALMIP [Lof09]. The toolbox includes a pre- and post-processing of the SOS constraints which aims at increasing computational efficiency by removing superfluous constraints, redundancies and introducing reformulations of some problem parts. While the processing steps might decrease solver time, due to the way Yalmip is allocating memory for the symbolic variables, using Yalmip can over all slow down the analysis significantly. Extending the computational implementations proposed here by both a more efficient SOS toolbox and by using more sophisticated SDP reformulations which are able to recognize and exploit problem dependent structure, could allow the methods to be efficiently applied to system (most of all PCE systems) with dimensions currently still out of reach. In particular the latter would not only require the progress in solver capabilities but an increased insight into the numerical structure of the SOS constraints dealt with in this thesis. The effects of the precise formulation of the cost function, multiplier degrees and the system dynamics on the size of the obtained ROA estimate could be investigated rigorously from a better understanding of the influence of structure. In particular, investigating the possibility of a dependency of cost function on system dynamics with the aim of finding optimal pairings could be interesting.

Usually, the improvement of the objective value is found to be strongly increasing in the beginning and then flattening out upon converging. One observation, which was made during the many runs of the analyses was that sometimes, instead, these improvements would start 'creeping', i.e., increasing by about the same absolute value for many iterations. Clearly, the efficiency of the programs presented here highly depends on the number of iterations needed for convergence. Understanding and, consequently, being able to influence the convergence rate would represent worthwhile future research direction for these methods.

Finally, a potentially interesting new implementation in terms of computational efficiency and capabilities could be presented by recent results on SDP free approaches to solving SOS programs [PY19].

7.1.2 PCE for stability analysis and control

While the prowess of the ROA analysis methods for PCE has been demonstrated here for various systems, increased state dimensionality and expansion order are clearly a challenge and are ultimately limiting the application at this point. Besides the previously discussed need of increasing SDP solver capabilities, another possibility could be offered by reducing the dimensionality of the problem by decreasing the truncation order. For this to be possible, rigorous results of the truncation error on the stability representation of the PCE system would be needed. Alternatively, ways to include terms representing a strict upper bound on the truncation error could be explored. This would also allow to eliminate Assumption 3.2. Approaches presented in this regard for linear systems in [Wan+18] could be interesting to start off from.

It seems to be an undisputed fact in the PCE community that second order random processes include most processes of the real world. This was postulated in [XK03] and has been widely referred to ever since. However, the question arises: In general, how can one actually *verify* that a given (nonlinear) process is a second order random process? Research on this topic revealed that there does not seem to exist a general answer to that question yet. Finding rigorous criteria could thus be of potentially high interest.

The control design proposed in this work offers a range of possibilities for extensions and future investigations. Firstly, the input constraints are still quite conservative in terms of the resulting size of the ROA estimate. One way to potentially decrease their conservatism is to extend the control law to allow for saturation and alter the conditions on the ROA and input in the SOS program accordingly. A similar approach has been proposed in [Ted+10; MAT13]. This might, however, increase the computational cost due to the larger number of constraints and associated multipliers. Further, performance criteria could be considered, such as convergence time to the equilibrium point.

During the course of this PhD, research was conducted with the aim of applying PCE to analyze the stability of stochastic orbits. While some results are presented in Chapter 4, another direction, namely using PCE on the system in *transverse* coordinates has shown some promise but eventually stalled due to numerical issues. Using PCE for stochastic orbits has received quite some interest in particular from the aerospace community [PB04; BPM06] and current developments in numerical toolboxes for PCE such as proposed in [Mue+20] could offer new chances for the analysis in transverse coordinates.

7.1.3 Optimizing the transverse controller and the MOC

Algorithms 4.1 and 4.2 can be directly extended to systems with affine input for a control design which aims at maximizing the ROA/ROC of the limit cycle. The transverse coordinate transformation does not alter the affine appearance of the control gain and

a third step optimizing for K similar to as in Algorithm 3.3 can be introduced. For the initialization of the problem the feedback gain resulting from the periodic Riccati equation (5.13) can be used as presented in Section 5.2.3.

As shown in Section 4.3, the location of the center point can be chosen from a problem dependent set. There could be a potential for more efficient algorithms in terms of the verified ROA estimate, by including an optimization for the center point location and the particular choice of the $(n-2)$ dimensional subspace $\mathcal{N}_f$. An optimization could, for example, take the system dynamics and the shape of the limit cycle into consideration and maximize the smallest well-defined region.

While the testing of the stability conditions on a finite number of hyperplanes provides for many applications a sufficient certification of stability (in particular when combined with simulations), for some problems it might still be desirable to obtain a formal certificate of stability also in between the chosen hyperplanes. Since the continuous problem poses a significant increase in computational complexity of the SOS programs, a computationally less demanding criteria would be desirable. An interesting approach in this direction could be to find an upper bound on the change in the dynamics from one hyperplane to the other, possibly similar to an approach in [FP19] used for collocation methods. Due to the hyperplanes representing $(n-1)$-dimensional subspaces, obtaining these bounds could, however, require significant extension. Coming from a different direction, an other approach could be to find criteria on the minimum finite amount of hyperplanes necessary to guarantee for the systems behavior in between. Ideas in this regard have also been mentioned in [TMT11].

On the practical side, the transverse controller implementation described in Section 5.4.1 calls for an extension of the control approach. Reliability of the feedback controller for any state of the system *inside* the ROA/ROC was provided, however the ROA/ROC estimate might not be large enough to cover the whole state space in which the system can potentially be. In order to reliably stabilize the system also in these regions, the control design could be extended to include a set of feedback-stabilized *auxiliary* trajectories which lead the system back to the periodic orbit. These trajectories would be chosen such that all their respective ROA/ROC combined cover the full state space of interest. This approach would be similar to a control design based on stability funnels proposed in [Ted+10] for trajectory tracking of robotic systems.

APPENDIX A

Appendix

A.1 Proof of Theorem 3.2

This proof is mostly following the proofs for Lyapunov's direct method which are standard in the literature and can be found in, e.g., [Kha02].

System (3.1) is by definition continuous in x and t. The projection (2.18) consists in the projection of a continuous function onto a constant basis and is thus continuous. It follows that the PCE representation (3.4) of the system (3.1) continuous. Assume without loss of generality $\bar{x}_{\text{EP}} = 0$. Consider any $r > 0$ for which $B_r = \{\bar{x} \in \mathbb{R}^{n(p+1)} \,|\, \|\bar{x}\| \leq r\} \subset \bar{D}$. Let $\alpha = \min_{\|\bar{x}\|=r} V(\bar{x})$. Then $\alpha > 0$ by (3.12). Take $\beta \in (0, \alpha)$ and let

$$\Omega_\beta = \{\bar{x} \in B_r \,|\, V(\bar{x}) \leq \beta\}. \tag{A.1}$$

From this follows that $\Omega_\beta \subset B_r$. Since

$$\dot{V}(\bar{x}(t)) < 0 \Longrightarrow V(\bar{x}(t)) < V(\bar{x}(0)) \leq \beta, \forall t > 0, \tag{A.2}$$

any trajectory starting in Ω_β at $t = 0$ remains strictly inside Ω_β for all $t > 0$. From local existence and uniqueness theorems for Lipschitz bounded continuous functions[1] it follows that since Ω_β is compact, (3.4) has a unique solution defined for all $t \geq 0$ whenever $\bar{x}(0) \in \Omega_\beta$. As $V(\bar{x})$ is continuous and $V(0) = 0$, there is a $\delta > 0$ such that

$$\|\bar{x}\| \leq \delta \Longrightarrow V(\bar{x}) < \beta. \tag{A.3}$$

Thus, $B_\delta \subset \Omega_\beta \subset B_r$. Since $V(\bar{x}(t))$ is monotonically decreasing and bounded from below by zero,

$$V(\bar{x}(t)) \to c \geq 0, \quad \text{as } t \to \infty. \tag{A.4}$$

The bound $c = 0$ is shown by contradiction. Suppose $c > 0$. By continuity of $V(\bar{x})$ there is a $d > 0$ such that $B_d \subset \Omega_c$. The limit $V(\bar{x}(t)) \to 0$ implies that the trajectory $\bar{x}(t)$ remains outside of B_d for all $t \geq 0$.Let $-\gamma = \max_{d \leq \|\bar{x}\| \leq r} \dot{V}(\bar{x})$, which exists because the

[1] See, e.g., Theorem 3.1, Theorem 3.3. in [Kha02]

continuous function $\dot{V}(\bar{x})$ has a maximum over the compact set $d \leq \|\bar{x}\| \leq r$. By (3.13), $-\gamma < 0$. It follows that

$$V(\bar{x}(t)) = V(\bar{x}(0) + \int_0^t \dot{V}(\bar{x}(\tau))d\tau \leq V(\bar{x}(0)) - \gamma t. \tag{A.5}$$

Since the right hand side will eventually become negative, the inequality contradicts the assumption that $c > 0$.

Choosing $\beta = \beta$ results in the properties of Ω_β to hold for Ω_{V_β}. Since thus any trajectory starting in Ω_{V_β} remains in Ω_{V_β} for all $t \geq 0$ and converges to 0 as $t \to \infty$, from (3.11) it directly follows that $\Omega_{V_\beta} \subseteq \bar{\mathcal{R}}$.

A.2 Proof of Theorem 4.1

The proof is shown here as found in [Hal80].

Suppose $n \geq 3$. If $v(\tau) = f_0(\omega_0(\tau))\|f_0(\omega_0(\tau))\|_2^{-1}$, then the hypotheses on ω_0 imply that v is periodic of period T_0 and Lipschitz. Let $e_1 = \zeta^*$ be a constant unit vector (the existence of which is assured by Lemma 4.1) such that $e_1 \neq \pm v(\tau)$, $0 \leq \tau \leq T_0$. Adjoin to e_1 any constant vectors $e_2, ...e_n$ such that $\{e_1, e_2, ...e_n\}$ is an orthonormal basis for $\mathbb{R}^n$. The moving orthonormal system along Γ_0 is then obtained in the following manner: let S be the $(n-2)$-dimensional subspace of $\mathbb{R}^n$ orthogonal to the plane formed by e_1 and $v(\tau)$. Rotate the coordinate system about S in the positive sense until e_1 coincides with $v(\tau)$. If $\zeta_1, \zeta_2, ..., \zeta_n$ are the rotated positions of $e_1, e_2, ...e_n$, then the moving orthonormal system is given by

$$\{v(\tau), \zeta_2(\tau), ..., \zeta_n(\tau)\}, \quad 0 \leq \tau \leq T_0, \tag{A.6}$$

where $\zeta_1(\tau) = v(\tau)$.

If $\gamma_j(\tau)$, $j = 1, 2, ..., n$ are the direction angles of $v(\tau)$, $e_j \cdot v(\tau) = \cos(\gamma_j(\tau)$, $j = 1, 2, ..., n$, then one can show that the vectors ζ_j are given by

$$\zeta_j(\tau) = \eta_j - \frac{\eta_j' v(\tau)}{1 + \eta_1 v(\tau)}(\eta_1 + v(\tau)), \quad j = 2, 3, ..., n. \tag{A.7}$$

The derivation of (A.7) is omitted for brevity and can be found in [Hal80].

The proof then continues by treating the case $n = 2$. For this case the moving orthonormal system is directly constructed as

$$\{v(\tau), \zeta_2(\tau)\}, \quad \zeta(\tau) = \pm[-v_2(\tau), v_1(\tau)]^T, \tag{A.8}$$

where $v_1(\tau), v_2(\tau)$ are the components of $v(\tau)$. The proof completes with the conclusion that equations (A.6)-(A.8) for the *classical MOC* (class-MOC) along Γ_0 clearly imply that the system is $\mathcal{C}^{p-1}(\mathbb{R}, \mathbb{R}^n)$ if ω_0 is $\mathcal{C}^p(\mathbb{R}, \mathbb{R}^n)$.

A.3 Proof of Theorem 4.5

The proof shown here is taken after the proof presented in [MS14].

With the given metric, Theorem 4.4 gives the following condition for transverse contraction to hold.

$$\delta_x \left(\frac{\partial f(x)}{\partial x}^T M(x) + M(x) \frac{\partial f(x)}{\partial x} + \dot{M}(x) + 2\eta_t M(x) \right) \delta_x \leq 0, \tag{A.9}$$

for all δ_x satisfying the transversality condition $\delta_x^T M(x) f(x) = 0$. Reformulating this constraint in terms of $\chi := M(x)\delta_x$, i.e., $\delta_x = M^{-1}(x)\chi$ and defining $C(x) = M^{-1}(x)$, an equivalent condition for all δ_x satisfying the transversality condition is given as

$$\chi^T \left(C(x) \frac{\partial f(x)}{\partial x}^T + \frac{\partial f(x)}{\partial x} C(x) - \dot{C}(x) + 2\eta_t C(x) \right) \chi \leq 0, \tag{A.10}$$

since $\dot{C}(x) = -M^{-1}(x)\dot{M}(x)M^{-1}(x)$. Further, the transversality condition results as $\chi^T f(x) = 0$. Define a matrix function $P(x) := f(x)f(x)^T$ which is rank-one and positive-semidefinite.This implies, that the set $\{\chi \,|\, \chi^T f(x) = 0, \{\chi \,|\, \chi^T P(x)\chi = 0\}$, and $\{\chi \,|\, \chi^T P(x)\chi \leq 0\}$ are the same. Transverse contraction with rate η_t is then defined by the existence of a positive-definite matrix function $C(x) > 0$ such that the following implication holds.

$$\chi^T P(x)\chi \leq 0 \Rightarrow \chi^T \left(C(x) \frac{\partial f(x)}{\partial x}^T + \frac{\partial f(x)}{\partial x} C(x) - \dot{C}(x) + 2\eta_t C(x) \right) \chi \leq 0. \tag{A.11}$$

By the S-procedure losslessness theorem [Yak97], (A.11) is true if and only if there exists a $\lambda(x) \geq 0$ such that the condition in the theorem, (4.75), holds.

Bibliography

[AWS18a] E. Ahbe, T. A. Wood, and R. S. Smith. "Stability verification for periodic trajectories of autonomous kite power systems". In: *IEEE European Control Conference*. 2018, pp. 46–51.

[AC17] E. Ahbe and K. Caldeira. "Spatial distribution of generation of Lorenz's available potential energy in a global climate model". In: *Journal of Climate* 30.6 (2017), pp. 2089–2101.

[AIS20a] E. Ahbe, A. Iannelli, and R. S. Smith. "Local contraction analysis of stochastic systems with limit cycles". In: *IEEE Conference on Decision and Control*. 2020, to appear.

[AIS20b] E. Ahbe, A. Iannelli, and R. S. Smith. "Region of attraction analysis of nonlinear stochastic systems using Polynomial Chaos Expansion". In: *Automatica* (2020), to appear.

[Ahb+20] E. Ahbe, P. Listov, A. Iannelli, and R. S. Smith. "Feedback control design maximizing the region of attraction of stochastic systems using Polynomial Chaos Expansion". In: *IFAC World Congress*. 2020, to appear.

[AS17] E. Ahbe and R. S. Smith. *Airborne Wind Energy Trajectory Analysis Application*. 2017. URL: https://github.com/evaahbe/AWE_tool.

[Ahb+19] E. Ahbe, T. Stastny, M. Dangel, R. Siegwart, and R. S. Smith. "Experimental Validation of Path-Tracking Model Predictive Control for Fixed-Wing Power Kites". In: *Book of Abstracts of the International Airborne Wind Energy Conference (AWEC 2019)*. 2019, p. 46.

[AWS17] E. Ahbe, T. A. Wood, and R. S. Smith. "Stability Certificates for a Model-Based Controller for Autonomous Power Kites". In: *Book of Abstracts of the International Airborne Wind Energy Conference (AWEC 2017)*. 2017, p. 86.

[AWS18b] E. Ahbe, T. A. Wood, and R. S. Smith. "Transverse contraction-based stability analysis for periodic trajectories of controlled power kites with model uncertainty". In: *IEEE Conference on Decision and Control*. 2018, pp. 6501–6506.

[AH17] A. Ahmadi and G. Hall. "Sum of squares basis pursuit with linear and second order cone programming". In: *Contemporary Mathematics*. Vol. 685. 2017, pp. 27–53.

[AHA19] A. A. Ahmadi, G. Hall, and A. A. Ahmadi. "On the Construction of Converging Hierarchies for Polynomial Optimization Based on Certificates of Global Positivity". In: *Mathmatics of Operations Research, Articles in Advance* August (2019), pp. 1–16.

[AM19a] A. A. Ahmadi and A. Majumdar. "DSOS and SDSOS Optimization: More Tractable Alternatives to Sum of Squares and Semidefinite Optimization". In: *SIAM Journal on Applied Algebra Geometry* 3.2 (2019), pp. 193–230.

[AM19b] A. A. Ahmadi and A. Majumdar. "DSOS and SDSOS optimization: More tractable alternatives to sum of squares and semidefinite optimization". In: *SIAM Journal on Applied Algebra and Geometry* 3.2 (2019), pp. 193–230.

[ADS13] U. Ahrens, M. Diehl, and R. Schmehl. *Airborne Wind Energy*. Springer, Berlin, 2013, p. 611.

[APS08] E. M. Aylward, P. A. Parrilo, and J.-J. E. Slotine. "Stability and robustness analysis of nonlinear systems via contraction metrics and SOS programming". In: *Automatica* 44 (2008), pp. 2163–2170.

[Bau+18] F. Bauer, C. M. Hackl, K. Smedley, and R. M. Kennel. "Crosswind kite power with tower". In: *Airborne Wind Energy: Advances in Technology Development and Research*. Springer Nature Singapore, 2018, pp. 441–462.

[BM16] V. A. Bavdekar and A. Mesbah. "Stochastic Nonlinear Model Predictive Control with Joint Chance Constraints". In: *IFAC-PapersOnLine* 49.18 (2016), pp. 270–275.

[BPM06] P. S. Beran, C. L. Pettit, and D. R. Millman. "Uncertainty quantification of limit-cycle oscillations". In: *Journal of Computational Physics* 217.1 (2006), pp. 217–247.

[Ber+16] F. Berkenkamp, R. Moriconi, A. P. Schoellig, and A. Krause. "Safe learning of regions of attraction for uncertain, nonlinear systems with Gaussian processes". In: *IEEE Conference on Decision and Control*. 2016, pp. 4661–4666.

[BCN91] S. Bittanti, P. Colaneri, and G. D. Nicolao. "The Periodic Riccati Equation". In: *The Riccati Equation*. Ed. by S Bittanti, A Laub, and J. Williams. Springer, Berlin, 1991, pp. 127–162.

[BCR98] J. Bochnak, M. Coste, and M.-F. Roy. *Real Algebraic Geometry*. Springer, 1998.

[BS19] J. Bouvrie and J.-J. Slotine. "Wasserstein contraction of stochastic nonlinear systems". In: *ArXiv* (2019), pp. 1902.08567v2, 1–6.

[BV04] S. Boyd and L. Vandenberghe. *Convex Optimization*. Cambridge University Press, 2004.

[CM47] R. H. Cameron and W. T. Martin. "The Orthogonal Development of Non-Linear Functionals in Series of Fourier-Hermite Functionals". In: *The Annals of Mathematics* 48.2 (1947), pp. 385–392.

[CGW01] F. Camilli, L. Gruene, and F. Wirth. "A generalization of Zubov's method to perturbed systems". In: *SIAM Journal on Control and Optimization* 40.2 (2001), pp. 496–515.

[CL06] F. Camilli and P. Loreti. "A Zubov's method for stochastic differential equations". In: *Nonlinear Differential Equations and Applications* 13.2 (2006), pp. 205–222.

[CFM10] M. Canale, L. Fagiano, and M. Milanese. "High altitude wind energy generation using controlled power kites". In: *IEEE Transactions on Control Systems Technology* 18.2 (2010), pp. 279–293.

[CSB11] A. Chakraborty, P. Seiler, and G. J. Balas. "Nonlinear region of attraction analysis for flight control verification and validation". In: *Control Engineering Practice* 19.4 (2011), pp. 335–345.

[CF06] X. Chen and C. Fengde. "Stable periodic solution of a discrete periodic Lotka-Volterra competition system with a feedback control". In: *Applied Mathematics and Computation* 181.2 (2006), pp. 1446–1454.

[Che+15] A. Cherubini, A. Papini, R. Vertechy, and M. Fontana. "Airborne Wind Energy Systems: A review of the technologies". In: *Renewable and Sustainable Energy Reviews* 51 (2015), pp. 1461–1476.

[Che04a] G. Chesi. "Computing output feedback controllers to enlarge the domain of attraction in polynomial systems". In: *IEEE Transactions on Automatic Control* 49.10 (2004), pp. 1846–1850.

[Che+05] G. Chesi, A. Garulli, A. Tesi, and A. Vicino. "LMI-based computation of optimal quadratic Lyapunov functions for odd polynomial systems". In: *International Journal of Robust and Nonlinear Control* 15.1 (2005), pp. 35–49.

[Che04b] G. Chesi. "Estimating the domain of attraction for uncertain polynomial systems". In: *Automatica* 40 (2004), pp. 1981–1986.

[Che09] G. Chesi. "Estimating the domain of attraction for non-polynomial systems via LMI optimizations". In: *Automatica* 45 (2009), pp. 1536–1541.

[Che11] G. Chesi. *Domain of Attraction Analysis and Control via SOS Programming*. London, U.K.: Springer, 2011, p. 278.

[CA15] H. D. Chiang and L. F. Alberto. *Stability Regions of Nonlinear Dynamical Systems: Theory, Estimation, and Applications*. Cambridge University Press, 2015.

[CHW88] H. D. Chiang, M. W. Hirsch, and F. F. Wu. "Stability Regions of Nonlinear Autonomous Dynamical Systems". In: *IEEE Transactions on Automatic Control* 33.1 (1988), pp. 16–27.

[CH95] C. C. Chung and J. Hauser. "Nonlinear control of a swinging pendulum". In: *Automatica* 31.6 (1995), pp. 851–862.

[Cos+15] S. Costello, C. Costello, G. Francois, and D. Bonvin. "Analysis of the maximum efficiency of kite-power systems". In: *Journal of Renewable and Sustainable Energy* 7.5 (2015), pp. 1–26.

[CFB17] S. Costello, G. Francois, and D. Bonvin. "Real-Time Optimizing Control of an Experimental Crosswind Power Kite". In: *IEEE Transactions on Control Systems Technology* 26.2 (2017), pp. 507–522.

[CMS01] E. Cruck, R. Moitie, and N. Seube. "Estimation of basins of attraction for uncertain systems with affine and Lipschitz dynamics". In: *Dynamics and Control* 11.3 (2001), pp. 211–227.

[Deb+05] B. J. Debusschere, H. N. Najm, P. P. Pébayt, O. M. Knio, R. G. Ghanem, and O. P. Le Maître. "Numerical challenges in the use of polynomial chaos representations for stochastic processes". In: *SIAM Journal on Scientific Computing* 26.2 (2005), pp. 698–719.

[Dun18] S. Dunker. "Tether and Bridle Line Drag in Airborne Wind Energy Applications". In: *Airborne Wind Energy: Advances in Technology Development and Research*. Ed. by S. R. Green Energy and Technology. Springer, Singapore., 2018, pp. 29–56.

[EGHA17] A. El-Guindy, D. Han, and M. Althoff. "Estimating the region of attraction via forward reachable sets". In: *Proceedings of the American Control Conference*. AACC, 2017, pp. 1263–1270.

[ES13] M. Erhard and H. Strauch. "Control of Towing Kites for Seagoing Vessels". In: *IEEE Transactions on Control Systems Technology* 21.5 (2013), pp. 1629–1640.

[ES15] M. Erhard and H. Strauch. "Flight control of tethered kites in autonomous pumping cycles for airborne wind energy". In: *Control Engineering Practice* 40 (2015), pp. 13–26.

[FK12] L. Fagiano and M. Khammash. "Nonlinear stochastic model predictive control via regularized polynomial chaos expansions". In: *IEEE Conference on Decision and Control*. 2012, pp. 142–147.

[FKN11] L. Fagiano, M. Khammash, and C. Novara. "On the guaranteed accuracy of Polynomial Chaos Expansions". In: *IEEE Conference on Decision and Control*. 2011, pp. 728–733.

[FS17] L. Fagiano and S. Schnez. "On the take-off of airborne wind energy systems based on rigid wings". In: *Renewable Energy* 107 (2017), pp. 473–488.

[Fag+14] L Fagiano, A. U. Zgraggen, M Morari, and M Khammash. "Automatic crosswind flight of tethered wings for airborne wind energy: modeling, control design and experimental results". In: *IEEE Transactions on Control Systems Technology* 22.4 (2014), pp. 1433–1447.

[Fag+18] L. Fagiano, E. Nguyen-Van, F. Rager, S. Schnez, and C. Ohler. "Autonomous Takeoff and Flight of a Tethered Aircraft for Airborne Wind Energy". In: *IEEE Transactions on Control Systems Technology* 26.1 (2018), pp. 151–166.

[FKS13] J. Fiala, M. Kočvara, and M. Stingl. "PENLAB: A MATLAB solver for nonlinear semidefinite optimization". In: *ArXiv preprint* (2013), pp. 1311.5240v1, 1–14.

[FG04] R. V. Field and M. Grigoriu. "On the accuracy of the polynomial chaos approximation". In: *Probabilistic Engineering Mechanics* 19.1 (2004), pp. 65–80.

[FB08] J. Fisher and R. Bhattacharya. "Stability analysis of stochastic systems using Polynomial Chaos". In: *American Control Conference*. 2008, pp. 4250–4255.

[FB09] J. Fisher and R. Bhattacharya. "Linear quadratic regulation of systems with stochastic parameter uncertainties". In: *Automatica* 45.12 (2009), pp. 2831–2841.

[FP19] F. A. Fontes and L. T. Paiva. "Guaranteed constraint satisfaction in continuous-time control problems". In: *IEEE Control Systems Letters* 3.1 (2019), pp. 13–18.

[FS14] F. Forni and R. Sepulchre. "A Differential Lyapunov Framework for Contraction Analysis". In: *IEEE Transactions on Automatic Control* 59.3 (2014), pp. 614–628.

[FS12] L. B. Freidovich and A. S. Shiriaev. "Transverse Linearization for Underactuated Nonholonomic Mechanical Systems with Application to Orbital Stabilization". In: *Distributed Decision Making and Control*. Springer-Verlag London Limited, 2012. Chap. 11, pp. 245–258.

[GTK14] A. Gajduk, M. Todorovski, and L. Kocarev. "Stability of power grids: An overview". In: *European Physical Journal: Special Topics* 223.12 (2014), pp. 2387–2409.

[GG02] A. Gasull and H. Giacomini. "A new criterion for controlling the number of limit cycles of some generalized liénard equations". In: *Journal of Differential Equations* 185.1 (2002), pp. 54–73.

[Gee+12] K. Geebelen, H. Ahmad, M. Vukov, S. Gros, J. Swevers, and M. Diehl. "An experimental test set-up for launch/recovery of an Airborne Wind Energy (AWE) system". In: *Proceedings of the American Control Conference*. 2012, pp. 4405–4410.

[GTV85] R. Genesio, M. Tartaglia, and A. Vicino. "On the Estimation of Asymptotic Stability Regions: State of the Art and New Proposals". In: *IEEE Transactions on Automatic Control* 30.8 (1985), pp. 747–755.

[GS91] R. G. Ghanem and P. D. Spanos. "Spectral Stochastic Finite-Element Formulation for Reliability Analyisis". In: *Journal of Engineering Mechanics* 117.10 (1991), pp. 2351–2372.

[GG05] H. Giacomini and M. Grau. "On the stability of limit cycles for planar differential systems". In: *Journal of Differential Equations* 213 (2005), pp. 368–388.

[Gie04] P. Giesl. "Necessary conditions for a limit cycle and its basin of attraction". In: *Nonlinear Analysis, Theory, Methods and Applications* 56.5 (2004), pp. 643–677.

[Gie09] P. Giesl. "On the determination of the basin of attraction of periodic orbits in three- and higher-dimensional systems". In: *Journal of Mathematical Analysis and Applications* 354.2 (2009), pp. 606–618.

[GH13] P. Giesl and S. Hafstein. "Construction of a CPA contraction metric for periodic orbits using semidefinite optimization". In: *Nonlinear Analysis* 86 (2013), pp. 114–134.

[Gon05] J. M. Gonçalves. "Regions of Stability for Limit Cycle Oscillations in Piecewise Linear Systems". In: *IEEE Transactions on Automatic Control* 50.11 (2005), pp. 1877–1882.

[GH18] S. Gudmundsson and S. Hafstein. "Probabilistic basin of attraction and its estimation using two Lyapunov functions". In: *Complexity* 2018 (2018), pp. 1–9.

[Hal80] J. K. Hale. *Ordinary Differential Equations*. R.E. Krierger Pub. Co., New York, 1980.

[Hal19] G. Hall. “Engineering and Business Applications of Sum of Squares Polynomials”. In: *ArXiv preprint* 1906.07961 (2019), pp. 1–36.

[HC94] J. Hauser and C. C. Chung. “Converse Lyapunov functions for exponentially stable periodic orbits”. In: *System & Control Letters* 23 (1994), pp. 27–34.

[HS19] S. Heim and A. Spröwitz. “Beyond Basins of Attraction: Quantifying Robustness of Natural Dynamics”. In: *IEEE Transactions on Robotics* 35.4 (2019), pp. 939–952.

[Hil93] D. Hilbert. “Ueber die vollen Invariantensysteme”. In: *Mathematische Annalen* 42 (1893), pp. 313–337.

[HD07] B Houska and M Diehl. “Optimal control for power generating kites”. In: *Proceedings of the 9th European Control Conference* October (2007), pp. 3560–3567.

[HD10] B. Houska and M. Diehl. “Robustness and stability optimization of power generating kite systems in a periodic pumping mode”. In: *IEEE International Conference on Control Applications* (2010), pp. 2172–2177.

[HFD11] B. Houska, H. J. Ferreau, and M. Diehl. “ACADO toolkit-An open-source framework for automatic control and dynamic optimization”. In: *Optimal Control Applications and Methods* 32.3 (2011), pp. 298–312.

[HT06] F. S. Hover and M. S. Triantafyllou. “Application of polynomial chaos in stability and control”. In: *Automatica* 42.5 (2006), pp. 789–795.

[IML19a] A. Iannelli, A. Marcos, and M. Lowenberg. “Nonlinear Robust Approaches to Study Stability and Postcritical Behavior of an Aeroelastic Plant”. In: *IEEE Transactions on Control Systems Technology* 27.2 (2019), pp. 703–716.

[IML19b] A. Iannelli, A. Marcos, and M. Lowenberg. “Robust estimations of the Region of Attraction using invariant sets”. In: *Journal of the Franklin Institute* 356.8 (2019), pp. 4622–4647.

[ISM18] A. Iannelli, P. Seiler, and A. Marcos. “An equilibrium-independent region of attraction formulation for systems with uncertainty-dependent equilibria”. In: *IEEE Conference on Decision and Control*. 2018, pp. 725–730.

[ISM19] A. Iannelli, P. Seiler, and A. Marcos. “Region of attraction analysis with Integral Quadratic Constraints”. In: *Automatica* 109 (2019), p. 108543.

[IHD07] A Ilzhöfer, B Houska, and M Diehl. “Nonlinear MPC of kites under varying wind conditions for a new class of large scale wind power generators”. In: *International Journal of Robust and Nonlinear Control* 17.17 (2007), pp. 1590–1599.

[JW+05] Z. Jarvis-Wloszek, R. Feeley, W. Tan, K. Sun, and A. Packard. "Controls applications of sum of squares programming". In: *Positive Polynomials in Control*. Springer, Berlin, Heidelberg, 2005, pp. 3–22.

[JW03] Z. W. Jarvis-Wloszek. "Lyapunov Based Analysis and Controller Synthesis for Polynomial Systems using Sum-of-Squares Optimization". PhD thesis. University of California, Berkeley, 2003.

[JS14] C. Jehle and R. Schmehl. "Applied Tracking Control for Kite Power Systems". In: *Journal of Guidance, Control, and Dynamics* 37.4 (2014), pp. 1211–1222.

[JKE10] L. Jin, R. Kumar, and N. Elia. "Reachability analysis based transient stability design in power systems". In: *International Journal of Electrical Power and Energy Systems* 32.7 (2010), pp. 782–787.

[JP19] M. Jones and M. M. Peet. "Using SOS for optimal semialgebraic representation of sets: Finding minimal representations of limit cycles, chaotic attractors and unions". In: *Proceedings of the American Control Conference*. American Automatic Control Council, 2019, pp. 2084–2091.

[KBF16] M. Kamgarpour, C. Beyss, and A. Fuchs. "Reachability-based Control Synthesis for Power System Stability". In: *IFAC-PapersOnLine* 49.27 (2016), pp. 238–243.

[Kha02] H. Khalil. *Nonlinear systems*. 3rd. Prentice Hall, Upper Saddle River, 2002.

[Kha12] R. Khasminskii. *Stochastic stability of differential equations*. 2nd. Springer, 2012.

[KB13] K.-K. K. Kim and R. D. Braatz. "Generalised polynomial chaos expansion approaches to approximate stochastic model predictive control". In: *International Journal of Control* 86.8 (2013), pp. 1324–1337.

[Kim+13] K.-K. K. Kim, D. E. Shen, Z. K. Nagy, and R. D. Braatz. "Wiener's Polynomial Chaos for the analysis and control of nonlinear dynamical systems with probabilistic uncertainties". In: *IEEE Control Systems Magazine* October (2013), pp. 58–67.

[Koz69] F. Kozin. "A survey of stability of stochastic systems". In: *Automatica* 5.1 (1969), pp. 95–112.

[Las01] J. B. Lasserre. "Global Optimization with Polynomials and the Problem of Moments". In: *SIAM Journal on OptimizationP* 11.3 (2001), pp. 796–817.

[Law72] J. D. Lawrence. *A catalog of special plane curves*. New York:Dover, 1972, p. 218.

[LK10] O. Le Maitre and O. Knio. *Spectral methods for uncertainty quantification*. Springer, 2010.

[LLC10] J. Le Meitour, D. Lucor, and J.-C. Chassaing. "Prediction of stochastic limit cycle oscillations using an adaptive Polynomial Chaos method". In: *Journal of Aeroelasticity and Structural Dynamics* 2.1 (2010), pp. 3–22.

[Leo06] G. A. Leonov. "Generalization of the Andronov-Vitt theorem". In: *Regular and Chaotic Dynamics* 11.2 (2006), pp. 281–289.

[LS42] N. Levinson and O. K. Smith. "A general equation for relaxation oscillations". In: *Duke mathmatical Journal* 9 (1942), pp. 382–403.

[LX09] J. Li and D. Xiu. "A generalized polynomial chaos based ensemble Kalman filter with high accuracy". In: *Journal of Computational Physics* 228.15 (2009), pp. 5454–5469.

[Lic+19] G. Licitra, J. Koenemann, A. Bürger, P. Williams, R. Ruiterkamp, and M. Diehl. "Performance assessment of a rigid wing Airborne Wind Energy pumping system". In: *Energy* 173 (2019), pp. 569–585.

[LN00] M. Loccufier and E. Noldus. "New trajectory reversing method for estimating stability regions of autonomous nonlinear systems". In: *Nonlinear Dynamics* 21.3 (2000), pp. 265–288.

[Loe04] J. Loefberg. "YALMIP : A Toolbox for Modeling and Optimization in MATLAB". In: *Proceedings of the CACSD Conference*. 2004.

[Lof09] J. Lofberg. "Pre- and Post-Processing Sum-of-Squares Programs in Practice". In: *IEEE Transactions on Automatic Control* 54.5 (2009), pp. 1007–1011.

[LS98] W. Lohmiller and J.-J. E. Slotine. "On Contraction Analysis for Non-linear Systems". In: *Automatica* 34.6 (1998), pp. 683–696.

[Loy80] M. Loyd. "Crosswind kite power". In: *Journal of Energy* 4.3 (1980), pp. 106–111.

[Luc+17] S. Lucia, J. A. Paulson, R. Findeisen, and R. D. Braatz. "On stability of stochastic linear systems via polynomial chaos expansions". In: *Proceedings of the American Control Conference* (2017), pp. 5089–5094.

[LSK04] D. Lucor, C. H. Su, and G. E. M. Karniadakis. "Generalized polynomial chaos and random oscillators". In: *International Journal for Numerical Methods in Engineering* 60.3 (2004), pp. 571–596.

[Lya92] A. M. Lyapunov. "The General Problem of the Stability of Motion (in Russian)". PhD thesis. University Kharkov, 1892.

[MAT13] A. Majumdar, A. A. Ahmadi, and R. Tedrake. "Control Design along Trajectories with Sums of Squares Programming". In: *IEEE International Conference on Robotics and Automation*. 2013, pp. 4054–4061.

[MAT14] A. Majumdar, A. A. Ahmadi, and R. Tedrake. "Control and verification of high-dimensional systems with DSOS and SDSOS programming". In: *IEEE Conference on Decision and Control*. IEEE, 2014, pp. 394–401.

[MHA19] A. Majumdar, G. Hall, and A. A. Ahmadi. "A Survey of Recent Scalability Improvements for Semidefinite Programming with Applications in Machine Learning, Control, and Robotics". In: *ArXiv preprint* 1908.05209 (2019), pp. 1–32.

[MT17] A. Majumdar and R. Tedrake. "Funnel Libraries for Real-Time Robust Feedback Motion Planning". In: *The International Journal of Robotics Research* 36.8 (2017), pp. 947–982.

[Man11] I. R. Manchester. "Transverse Dynamics and Regions of Stability for Nonlinear Hybrid Limit Cycles". In: *IFAC Proceedings Volumes*. Vol. 44. 1. IFAC, 2011, pp. 6285–6290.

[MS14] I. R. Manchester and J.-J. E. Slotine. "Transverse contraction criteria for existence, stability, and robustness of a limit cycle". In: *Systems & Control Letters* 63 (2014), pp. 32–38.

[Man+11] I. R. Manchester, M. M. Tobenkin, M. Levashov, and R. Tedrake. "Regions of Attraction for Hybrid Limit Cycles of Walking Robots". In: *IFAC Proceedings Volumes*. IFAC, 2011, pp. 5801–5806.

[Meg13] A. Megretski. *SPOT: systems polynomial optimization tools*. 2013. URL: https://github.com/spot-toolbox/spotless.

[MKB03] D. R. Millman, I. P. King, and P. S. Beran. "A stochastic approach for predicting bifurcation of a pitch and plunge airfoil". In: *21st AIAA Applied Aerodynamics Conference* June (2003).

[MCT14] J. Moore, R. Cory, and R. Tedrake. "Robust Post-Stall Perching with a Simple Fixed-Wing Glider using LQR-Trees". In: *Bioinspiration & biomimetics* 9.025013 (2014), pp. 1–15.

[MOS17] MOSEK ApS. *The MOSEK optimization toolbox for MATLAB manual. Version 8.0*. 2017.

[Mue+20] T. Muehlpfordt, F. Zahn, V. Hagenmeyer, and T. Faulwasser. "PolyChaos.jl – A Julia Package for Polynomial Chaos in Systems and Control". In: *IFAC PapersOnLine*. 2020, to appear.

[Müh+18] T. Mühlpfordt, R. Findeisen, V. Hagenmeyer, and T. Faulwasser. "Comments on truncation errors for Polynomial Chaos Expansions". In: *IEEE Control Systems Letters* 2.1 (2018), pp. 169–174.

[NB03] Z. K. Nagy and R. D. Braatz. "Recent advances in the optimal control of batch processes". In: *Recent Research Developments in Chemical Engineering* 5.1 (2003), pp. 99–127.

[Pap+13] A. Papachristodoulou, J. Anderson, G. Valmorbida, S. Prajna, P. Seiler, and P. A. Parrilo. *SOSTOOLS: Sum of squares optimization toolbox for MATLAB*. 2013.

[PP02] A. Papachristodoulou and S. Prajna. "On the Construction of Lyapunov Functions using the Sum of Squares Decomposition". In: *IEEE Conference on Decision and Control*. Vol. 3. 2002, pp. 3482–3487.

[PP05a] A. Papachristodoulou and S. Prajna. "A Tutorial on Sum of Squares Techniques for Systems Analysis". In: *Proceedings of the American Control Conference*. 2005, pp. 2686–2700.

[PP05b] A. Papachristodoulou and S. Prajna. "Analysis of non-polynomial systems using the sum of squares decomposition". In: *Positive polynomials in control*. 2005, pp. 23–43.

[PY19] D. Papp and S. Yildiz. "Sum-of-squares optimization without semidefinite programming". In: *SIAM Journal on Optimization* 29.1 (2019), pp. 822–851.

[Par00] P. A. Parrilo. "Structured semidefinite programs and semialgebraic geometry methods in robustness and optimization". PhD thesis. California Institute of Technology, 2000.

[Par04] P. A. Parrilo. "Sum of Squares Programs and Polynomial Inequalities". In: *SIAG/OPT Views-and-News: A Forum for the SIAM Activity Group on Optimization* 15.2 (2004), pp. 7–15.

[PL03] P. A. Parrilo and S. Lall. "Semidefinite Programming Relaxations and Algebraic Optimization in Control". In: *European Journal of Control* 9.2-3 (2003), pp. 307–321.

[PB06] C. L. Pettit and P. S. Beran. "Spectral and multiresolution Wiener expansions of oscillatory stochastic processes". In: *Journal of Sound and Vibration* 294.4 (2006), pp. 752–779.

[PB04] C. L. Pettit and P. S. Beran. "Polynomial chaos expansion applied to airfoil limit cycle oscillations". In: *45th AIAA/ASME/ASCE/AHS/ASC Structures, Structural Dynamics & Materials Conference* 3 (2004), pp. 1975–1985.

[PTS09] Q.-C. Pham, N. Tabareau, and J.-J. E. Slotine. "A contraction theory approach to stochastic incremental stability". In: *IEEE Transactions on Automatic Control* 54.4 (2009), pp. 816–820.

[Poi99] H. Poincaré. *Les Méthodes Nouvelles de la Mécanique Céleste*. Gauthier-Villars: Paris, 1899, 3 vols.

[PPW04] S. Prajna, A. Papachristodoulou, and F. Wu. "Nonlinear Control Synthesis by Sum of Squares Optimization : A Lyapunov-based Approach". In: *5th Asian Control Conference*. IEEE, 2004, pp. 157–165.

[Put93] M. Putinar. "Positive Polynomials on Compact Semi-algebraic Sets". In: *Indiana University Mathematics Journal* 42.3 (1993), pp. 969–984.

[RS18] S. Rapp and R. Schmehl. "Vertical takeoff and landing of flexible wing kite power systems". In: *Journal of Guidance, Control, and Dynamics* 41.11 (2018), pp. 2386–2400.

[RH05] P. B. Reddy and I. A. Hiskens. "Limit-induced stable limit cycles in power systems". In: *IEEE Russia Power Tech* 603 (2005), pp. 1–5.

[Rez00] B. Reznick. "Some Concrete Aspects of Hilbert's 17th Problem". In: *Contemporary mathematics* 253 (2000), pp. 251–272.

[Ron+15] N. Rontsis, S. Costello, I. Lymperopoulos, and C. N. Jones. "Improved path following for kites with input delay compensation". In: *IEEE Conference on Decision and Control*. IEEE, 2015, pp. 656–663.

[SH06] C. W. Scherer and C. W. Hol. "Matrix sum-of-squares relaxations for robust semi-definite programs". In: *Mathematical Programming* 107.1-2 (2006), pp. 189–211.

[Sch18] R. Schmehl. *Airborne Wind Energy: Advances in Technology Development and Research*. Springer Nature Singapore, 2018.

[SB10] P. Seiler and G. J. Balas. "Quasiconvex Sum-of-Squares Programming". In: *IEEE Conference on Decision and Control*. 2. 2010, pp. 3337–3342.

[Sta+19] T. Stastny, E. Ahbe, M. Dangel, and R. Siegwart. "Locally power-optimal nonlinear model predictive control for fixed-wing airborne wind energy". In: *American Control Conference*. 2019, pp. 2191–2196.

[ST12] J. Steinhardt and R. Tedrake. "Finite-time regional verification of stochastic non-linear systems". In: *The International Journal of Robotics Research* 31.7 (2012), pp. 901–923.

[Ste74] G. Stengle. "A Nullstellensatz and a Positivstellensatz in Semialgebraic Geometry". In: *Math. Ann* 207 (1974), pp. 87–97.

[Stu99] J. F. Sturm. "Using SeDuMi 1.02, a MATLAB toolbox for optimization over symmetric cones". In: *Optimization Methods and Software* 11.12 (1999), pp. 625–653.

[Sul15] T. J. Sullivan. *Introduction to Uncertainty Quantification*. Springer, 2015.

[TP06] W. Tan and A. Packard. "Stability region analysis using sum of squares programming". In: *Proceedings of the American Control Conference*. 2006, pp. 2297–2302.

[TP08] W. Tan and A. Packard. "Stability Region Analysis Using Polynomial and Composite Polynomial Lyapunov Functions and Sum-of-Squares Programming". In: *IEEE Transactions on Automatic Control* 53.2 (2008), pp. 565–571.

[TBM17] J. Z. Tang, A. M. Boudali, and I. R. Manchester. "Invariant funnels for underactuated dynamic walking robots: New phase variable and experimental validation". In: *IEEE International Conference on Robotics and Automation*. 2017, pp. 3497–3504.

[TM14] J. Z. Tang and I. R. Manchester. "Transverse contraction criteria for stability of nonlinear hybrid limit cycles". In: *IEEE Conference on Decision and Control*. 2014, pp. 31–36.

[Ted+10] R. Tedrake, I. R. Manchester, M. Tobenkin, and J. W. Roberts. "LQR-trees : Feedback Motion Planning via Sums-of-Squares Verification". In: *The International Journal of Robotics Research* 29.8 (2010), pp. 1038–1052.

[TVG96] A. Tesi, F. Villoresi, and R. Genesio. "On the stability domain estimation via a quadratic Lyapunov function: Convexity and optimality properties for polynomial systems". In: *IEEE Transactions on Automatic Control* 41.11 (1996), pp. 1650–1657.

[TMT11] M. M. Tobenkin, I. R. Manchester, and R. Tedrake. "Invariant Funnels around Trajectories using Sum-of-Squares Programming". In: *IFAC Proceedings Volumes*. Vol. 44. 1. IFAC, 2011, pp. 9218–9223.

[TP09] U. Topcu and A. Packard. "Local Stability Analysis for Uncertain Nonlinear Systems". In: *IEEE Transactions on Automatic Control* 54.5 (2009), pp. 1042–1047.

[TPS08] U. Topcu, A. Packard, and P. Seiler. "Local stability analysis using simulations and sum-of-squares programming". In: *Automatica* 44 (2008), pp. 2669–2675.

[Top+10] U. Topcu, A. K. Packard, P. Seiler, and G. J. Balas. "Robust region-of-attraction estimation". In: *IEEE Transactions on Automatic Control* 55.1 (2010), pp. 137–142.

[TD14] A Trofino and T. J. M. Dezuo. "LMI stability conditions for uncertain rational nonlinear systems". In: *International Journal of Robust and Nonlinear Control* 24.July 2013 (2014), pp. 3124–3169.

[Ura67] M. Urabe. *Nonlinear autonomous oscillations: Analytical theory.* Academic Press, 1967, Vol. 34.

[VA17] G. Valmorbida and J. Anderson. "Region of attraction estimation using invariant sets and rational Lyapunov functions". In: *Automatica* 75 (2017), pp. 37–45.

[Van13] D. Vander Lind. "Analysis and Flight Test Validation of High Performance Airborne Wind Turbines". In: *Airborne Wind Energy*. Springer, Berlin, 2013, pp. 473–490.

[WKK06] H. Waki, S. Kim, and M. Kojima. "Sums of Squares and Semidefinite Program Relaxations for Polynomial Optimization Problems with Structured Sparsity". In: *SIAM Journal on Optimization* 17.1 (2006), pp. 218–242.

[Wan+18] Y. Wan, D. E. Shen, S. Lucia, R. Findeisen, and R. D. Braatz. "Robust Static H-infinity Output-Feedback Control Using Polynomial Chaos". In: *Proceedings of the American Control Conference* (2018), pp. 6804–6809.

[Wie38] N. Wiener. "The Homogeneous Chaos". In: *American Journal of Mathematics* 60.4 (1938), pp. 897–936.

[Wig03] S. Wiggins. *Introduction to Applied Nonlinear Dynamical Systems and Chaos*. Vol. 53. 9. Springer-Verlag New York, 2003, pp. 122–151.

[WLO08] P. Williams, B. Lansdorp, and W. Ockels. "Optimal crosswind towing and power generation with tethered kites". In: *Journal of Guidance, Control, and Dynamics* 31.1 (2008), pp. 81–93.

[Woo+17] T. A. Wood, E. Ahbe, H. Hesse, and R. S. Smith. "Predictive Guidance Control for Autonomous Kites with Input Delay". In: *IFAC World Congress* 50.1 (2017), pp. 13276–13281.

[Woo+18] T. A. Wood, H. Hesse, M. Polzin, E. Ahbe, and R. S. Smith. "Modeling, Identification, Estimation and Adaptation for the Control of Power-Generating Kites". In: *IFAC PapersOnLine* 51.15 (2018), pp. 981–989.

[WHS17] T. A. Wood, H. Hesse, and R. S. Smith. "Predictive Control of Autonomous Kites in Tow Test Experiments". In: *IEEE Control System Letters* 1.1 (2017), pp. 110–115.

[Woo+15] T. A. Wood, H. Hesse, A. U. Zgraggen, and R. S. Smith. "Model-based flight path planning and tracking for tethered wings". In: *IEEE Conference on Decision and Control*. 2015, pp. 6712–6717.

[WYL14] M. Wu, Z. Yang, and W. Lin. "Domain-of-attraction estimation for uncertain non-polynomial systems". In: *Communications in Nonlinear Science and Numerical Simulation* 19.9 (2014), pp. 3044–3052.

[WM04] S. J. Wu and X. Z. Meng. "Boundedness of nonlinear differential systems with impulsive effect on random moments". In: *Acta Mathematicae Applicatae Sinica* 20.1 (2004), pp. 147–154.

[Xiu10] D. Xiu. *Numerical Methods for Stochastic Computations*. Princeton University Press, 2010.

[XK02] D. Xiu and G. E. M. Karniadakis. "The Wiener-Askey Polynomial Chaos for stochastic differential equations". In: *SIAM Journal on Scientific Computing* 24.2 (2002), pp. 619–644.

[XK03] D. Xiu and G. E. M. Karniadakis. "Modeling uncertainty in flow simulations via generalized polynomial chaos". In: *Journal of Computational Physics* 187.1 (2003), pp. 137–167.

[XKG05] D. Xiu, I. G. Kevrekidis, and R. Ghanem. "An equation-free, multiscale approach to uncertainty quantification". In: *Multiphysics Modeling* May/June (2005), pp. 16–23.

[Xiu+02] D. Xiu, D. Lucor, C. H. Su, and G. E. M. Karniadakis. "Stochastic modeling of flow-structure interactions using generalized polynomial chaos". In: *Journal of Fluids Engineering, Transactions of the ASME* 124.1 (2002), pp. 51–59.

[Yak97] V. A. Yakubovich. "S-procedure in nonlinear control theory". In: *Vestnick Leningrad Univ. Math.* 4 (1997), pp. 73–93.

[Zan+13] M. Zanon, S. Gros, J. Andersson, and M. Diehl. "Airborne wind energy based on dual airfoils". In: *IEEE Transactions on Control Systems Technology* 21.4 (2013), pp. 1215–1222.

[ZFM15] A. U. Zgraggen, L. Fagiano, and M. Morari. "Real-time optimization and adaptation of the crosswind flight of tethered wings for airborne wind energy". In: *IEEE Transactions on Control Systems Technology* 23.2 (2015), pp. 434–448.

[Zub61] V. I. Zubov. "Methods of AM Lyapunov and their application". In: *No. AEC-TR-4439. ERDA Div. Phys. Res.* (1961).